

https://dspace.org/

Geological storage of CO2: The effect of impurity gases in CO2 streams on the sorption behaviour of CO2 in coal

Koutsouvelis, Nicolas Spiros

2015-05-08
http://hdl.handle.net/10539/17696

Downloaded from a DSpace repository. https://dspace.org/

GEOLOGICAL STORAGE OF CO_2: THE EFFECT OF IMPURITY GASES IN CO_2 STREAMS ON THE SORPTION BEHAVIOUR OF CO_2 IN COAL

Nicolas Spiros Koutsouvelis

A dissertation submitted to the Faculty of Engineering and the Built Environment, University of the Witwatersrand, Johannesburg, in fulfilment of the requirements for the degree of Master of Science in Engineering

Johannesburg, 2014

DECLARATION

I declare that this dissertation is my own unaided work. It is being submitted to the Master of Science in the University of the Witwatersrand, Johannesburg. It has not been submitted before for any degree or examination to any other University.

……

____ day of _____ year _____

ABSTRACT

Due to the continued dominance of fossil fuels in global industry, CO_2 capture and geological storage (CCS) is a vital technology in efforts to combat climate change. Capture technologies are implemented to purify CO_2 streams from industrial sources, and these streams are injected deep underground in specialised geological storage media. However, impurity gases could still comprise greater than 5% of the captured stream and be co-stored with the CO_2. The presence of impurities underground could be detrimental or beneficial to CO_2 storage; but as yet, the influence of many impurities is unclear.

Coal seams, which have been classified as 'unmineable', are unconventional CO_2 storage media that hold importance in areas where saline aquifers are not readily available. The major storage mechanism in this medium is sorption, which must be quantified experimentally for storage capacity estimations. An important impurity in CCS is SO_2, which has very strong sorbing properties and the potential to affect coal storage capacity. In this study, the effect of different concentrations of SO_2 on CO_2 sorption in a typical South African coal was investigated via laboratory-scale volumetric adsorption experiments.

After sorption experiments of binary CO_2-SO_2 mixtures, with SO_2 concentration from 0% to 6.7%, were run for 48 hours at 85 bar and 40°C, it was clear that SO_2 sorbed very strongly to the coal and its sorption is preferential to that of CO_2. The results show that SO_2 interacts with CO_2, and can potentially enhance or inhibit CO_2 sorption, depending on the model used to describe the density of the CO_2-SO_2 mixture. The effect of SO_2 is seen to be significant even at low concentrations (< 2% SO_2), and it is recommended that its effect is taken into account when storage capacity estimations on coal seams are carried out.

ACKNOWLEDGEMENTS

I would like to acknowledge and sincerely thank my supervisor, Prof Nicola Wagner, who was influential in every aspect of this research. I am very grateful for her commitment to the project and for helping beyond her duties as a supervisor

My co-supervisors, Dr Willem Augustyn and Craig Sheridan, played integral roles in shaping the project and the realisation of its goals. Their contributions and continual efforts are valued most highly.

I would like to acknowledge Nonhlanhla Mguni, Prof Nicola Wagner, Patience Moyo and Andrew Odeh for their contribution in the laboratory towards coal characterisation. Kasturie Premlall, Major Mabuza and Muzi Shongwe are also thanked for their efforts in the experimentation carried out at the Tshwane University of Technology (TUT). The helpfulness of senior students, Tshifiwa Maphala, Rosalind dos Santos and Mulanga Maphada, with respect to equipment training and advice is also acknowledged. The workshop staff, Rhoderick Mcrae-Samuel, Phathu Sikhwari and Theo Prasinos, is thanked kindly for all the help they provided throughout.

I gratefully acknowledge the funding available from the Norwegian Agency for Development Cooperation (NORAD) Energy and Petroleum (EnPe) agreement between the University of the Witwatersrand (Wits) and the Norwegian University of Science and Technology (NTNU). The generous funding made it possible meet all needs of the project.

CONTENTS

DECLARATION 1
ABSTRACT 2
ACKNOWLEDGEMENTS 3
CONTENTS 4
LIST OF FIGURES 7
LIST OF TABLES 13
LIST OF SYMBOLS 15
NOMENCLATURE 16
CHAPTER 1: Introduction 17
1.1 Background 17
1.2 Motivation 21
1.3 Aims and Objectives 23
1.4 Dissertation Outline 24
CHAPTER 2: Literature Review 25
2.1 CO_2 Capture and Geological Storage (CCS) Fundamentals 25
2.1.1 Climate Change and CCS as a Mitigation Technique 25
2.1.2 The CCS System 27
2.2 CO_2 Purity for CCS 35
2.2.1 Impurities in Capture and Transport 35
2.2.2 Impurities in Geological Storage 38
2.3 Components 46
2.3.1 Coal 47
2.3.2 Gases 49
2.4 CO_2 Storage Capacity and Sorption in Coal 57
2.4.1 Storage Capacity 57
2.4.2 Sorption Theory 59
2.5 Chapter Summary 61
CHAPTER 3: Methodology 63
3.1 Sample Preparation and Characterisation 63
3.1.1 Sample Preparation 63
3.1.2 Proximate Analysis 64

3.1.3 Ultimate and C-S Analyses 65
3.1.4 Petrographic Analysis 65
3.1.5 Brunauer, Emmett and Teller Analysis 65
3.1.6 Sample Volume Determination 66
3.2 Sorption Experiments 66
3.2.1 Equipment 67
3.2.2 Procedure 78
3.3 Post-Sorption Analysis 80
3.4 Chapter Summary 81
CHAPTER 4: Results and Discussion 82
4.1 Coal Characterisation 82
4.1.1 Proximate Analysis 82
4.1.2 Ultimate and C-S Analyses 83
4.1.3 Petrographic Analysis 83
4.1.4 BET Analysis 84
4.1.5 Sample Volume 85
4.2 Sorption Capacity 86
4.2.1 Free Volume 87
4.2.2 Density Calculations 87
4.2.3 Pressure versus Run Time 92
4.2.4 Gas Composition Analysis 96
4.2.5 Fourier Transform Infrared Spectroscopy 98
4.2.6 The Effect of Impurities on Sorption 103
4.3 Summary of Key Findings 119
CHAPTER 5: Conclusions and Recommendations 122
5.1 Conclusions 122
5.2 Recommendations 126
REFERENCES 130
APPENDICES 139
Appendix A: Material Safety Data Sheets (MSDS) 139
A.1 Bituminous Coal 140
A.2 CO_2 143

A.3 SO_2 145
Appendix B: Equipment 149
B.1 Leak Tests 149
B.2 Volumetric Adsorption System at TUT 152
Appendix C: Experimental Procedures 154
C.1 Sample Degassing 154
C.2 Free Volume Determination 155
C.3 VAS 156
C.4 Mixing System 160
C.5 GC 165
Appendix D: Sorption Experiment Calculations and Results 166
D.1 Free Volume Determination 166
D.2 Density 170
D.3 VAS Results 176
D.4 Gas Analysis 187
D.5 Adsorption Modelling 206
Appendix E: Sample Characterisation 208
E.1 Sample Volume Calculations 208
E.2 Petrography Report 209
E.3 BET Isotherm and Summary Report 211

LIST OF FIGURES

Figure 1.1: Proposed contribution of various technologies to reduce global CO_2 emissions (IEA, 2010). 19
Figure 1.2: Location of unmineable coal seams for potential CO_2 storage in South Africa (black circles). Collectively the storage potential of unmineable coal seams in South Africa is between 0.3 and 1.4 $GtCO_2$ (Viljoen et al., 2010). 20
Figure 2.1: Schematic illustration of the overall CCS process (modified from Total, 2007) 27
Figure 2.2: Principles of (a) Post-combustion; (b) Pre-combustion; and (c) Oxy-fuel combustion capture processes (adapted from Mondal et al. (2012))..... 29
Figure 2.3: (a) Vertical and (b) horizontal seismic sections through the developing CO_2 plume at the Sleipner gas field, North Sea (British Geological Survey, 2012). From (a) it is evident that the CO_2 is effectively stopped from rising upwards by the caprock and rather expends downwards over time through the porous aquifer region. From (b) the lateral migration of the CO_2 plume over time is apparent. The successful storage of CO_2 at Sleipner creates a strong case in favour of the safety of CO_2 storage. 32
Figure 2.4: Schematic representation of CO_2 trapping mechanisms (Viljoen et al., 2010). After the CO_2 is injected into the storage site, it migrates slowly between the porous rock (see right) where it is trapped residually, dissolves into the formation water, sorbs, and reacts to become an immobile part of the storage medium..... 32
Figure 2.5: Adsorption of various components on coal (Bachu, 2008a) 41
Figure 2.6: Excess sorption curves for coals pretreated with different materials plotted against pressure (Sakurovs et al., 2011). Note: W0 is the maximum sorption capacity for the coal calculated according to a modified Dubinin-Radushkevich equation fitted to excess sorption data. 43
Figure 2.7: Phase diagram of CO_2 (IPCC, 2005)..... 50
Figure 2.8: CO_2 density as a function of pressure and temperature (IPCC, 2005) 51
Figure 2.9: Phase diagram of SO_2 (Hogenboom et al., 1996)..... 53
Figure 2.10: Schematic sorption process. A – Adsorption; B – Absorption; C – Chemisorption; (1) – Fluid sorbate molecules; (2) – Solid sorbent; (3), (4) and (5) – Sorbed molecules in sorbed phase 60
Figure 3.1: Schematic diagram of VAS internals housed in a temperature controlling oven. Valves, pressure indicators, cells, sorbent and sorbate are represented. 68
Figure 3.2: Complete VAS as viewed in the Laboratory at Wits..... 71
Figure 3.3: Mixing System as viewed in the Laboratory at Wits 74
Figure 3.4: Temperature Program for GC method..... 77
Figure 3.5: Calibration Curve produced for SO_2 77
Figure 3.6: Vacuum setup for sample degassing. 78
Figure 3.7: Schematic diagram of VAS pressure vessels indicating volumes of interest, i.e. the volume between V1 and V2 (Volume A) and the volume between V2 and V3 (Free Volume)..... 79

Figure 3.8: Schematic diagram of VAS pressure vessels indicating volumes of interest, i.e. the volume between V1 and V2 (Volume A) and the volume between V2 and V3 (Free Volume)\..... 155
Figure 4.1: Density of relevant CO_2-SO_2 mixtures as a function of pressure at 40°C calculated using Amagat's Law 89
Figure 4.2: Density of different CO_2-SO_2 mixtures as a function of pressure at 40°C as predicted according to the Patel-Teja model..... 91
Figure 4.3: Sample cell pressure and temperature throughout a volumetric sorption experiment with a sorbate containing 0.16 mol% SO_2 and 99.84 mol% CO_2..... 93
Figure 4.4: Sample cell pressure and temperature throughout a volumetric sorption experiment with a sorbate containing 0.95 mol% SO_2 and 99.05 mol% CO_2..... 93
Figure 4.5: Sample cell pressure and temperature throughout a volumetric sorption experiment with a sorbate containing 2.52 mol% SO_2 and 97.48 mol% CO_2..... 94
Figure 4.6: Initial pressure of sample cell versus initial SO_2 concentration of mixture..... 96
Figure 4.7: Comparison of the SO_2 concentration of each mixture determined before and after the sorption experiments. Error bars indicate the level of experimental deviation obtained from repeat concentration measurements on the GC..... 97
Figure 4.8: FTIR Spectrum produced for coal sample without sorption treatment 99
Figure 4.9: FTIR Spectrum produced for coal sample treated with pure CO_2 at 85 bar and 40°C for 48 hours. The peak indicating the CO_2 retained by the coal is circled..... 99
Figure 4.10: FTIR Spectrum produced for coal sample treated with 0.16% SO_2 (balance CO_2) at 85 bar and 40°C for 48 hours. The peak indicating the CO_2 retained by the coal is circled. 100
Figure 4.11: FTIR Spectrum produced for coal sample treated with 3.20% SO_2 (balance CO_2) at 85 bar and 40°C for 48 hours. The peak indicating the CO_2 retained by the coal is circled. 100
Figure 4.12: FTIR Spectrum produced for coal sample treated with 6.69% SO_2 (balance CO_2) at 85 bar and 40°C for 48 hours. The peak indicating the CO_2 retained by the coal is circled. 101
Figure 4.13: Excess sorption in a typical South African coal when exposed to CO_2 mixtures with differing initial sorbate concentrations of SO_2. The temperature is 40°C and the initial pressure is approximately 85 bar. The mixture density was calculated using Amagat's Law and the standard deviation at 0% SO_2 is shown via error bars. 106
Figure 4.14: Sample cell pressure and temperature throughout a volumetric sorption experiment with a sorbate containing 3.72 mol% SO_2 and 96.28 mol% CO_2..... 108
Figure 4.15: Excess sorption as a function of initial sorbate SO_2 concentration, at approximately 85 bar and 40°C, observed up until 6.69 mol% SO_2. The Henry's law adsorption model is fitted to the SO_2 sorption. The mixture

density used in excess sorption calculations was calculated using Amagat's Law. 109
Figure 4.16: Percentage of SO_2 and CO_2 in the sorbed phase as a function of its initial concentration of the sorbate. Note: the outlying points at 3.20% SO_2 are excluded from the trendline functions. 112
Figure 4.17: Excess sorption in a typical South African coal when exposed to CO_2 mixtures with differing initial sorbate concentrations of SO_2. The temperature is 40°C and the initial pressure is approximately 85 bar. The mixture density was calculated using the Patel-Teja EOS. 114
Figure 4.18: The initial and final sorbate densities determined by the Patel-Teja EOS corresponding to each sorption experiment run for different initial concentrations of SO_2 116
Figure 4.19: Percentage CO_2 sorbed, calculated as 100 x (Moles CO_2 sorbed)/(Moles CO_2 fed), as a function of the initial SO_2 concentration in the mixture. This is compared for scenarios where the mixture density was determined using Amagat's law and the Patel-Teja EOS..... 118
Figure B.1: Pressure stability test with empty reactor after fittings and reactor seal were replaced 149
Figure B.2: Pressure stability test with empty sample cell after pneumatic valves were tightened..... 150
Figure B.3: Pressure stability test with empty sample cell with new seal design, polished reactor sealing surface under different levels of reactor bolt tightening 151
Figure B.4: Pressure stability test for sample cell assembled from Swagelok parts using a copper seal..... 152
Figure B.5: VAS located at TUT. Labelled components:..... 153
Figure D.1: Schematic diagram of VAS pressure vessels indicating volumes of interest, i.e. the volume between V1 and V2 (Volume A) and the volume between V2 and V3 when a sample is loaded into the sample cell (Free Volume) 166
Figure D.2: Behaviour of pressure and temperature in VAS cells during volume determination experiment when sample cell is empty..... 168
Figure D.3: Behaviour of pressure and temperature in VAS cells during volume determination experiment when sample cell contains a sample 169
Figure D.4: Density of CO_2 as a function of pressure at 40°C. Data points were determined by the Span Wagner EOS obtained from the NIST database while an almost perfect fit polynomial was applied in this pressure range using MS Excel. 170
Figure D.5: Density of SO_2 as a function of pressure at 40°C. Data points were obtained from the NIST database and an almost perfect fit polynomial was applied in this pressure range using MS Excel. 171
Figure D.6: Density of relevant CO_2-SO_2 mixtures as a function of pressure at 40°C calculated using Amagat's Law 172
Figure D.7: Density of different CO_2-SO_2 mixtures as a function of pressure at 40°C as predicted according to the Patel-Teja model..... 176
Figure D.8: Patel-Teja EOS pure component densities of SO_2 and CO_2 compared with respective densities obtained from the NIST database 176

Figure D.9: Sample cell pressure (black) and temperature (red) recorded during VAS experiment. Mixture concentration and sorption calculated are shown. Pure CO_2 – 1. 177
Figure D.10: Sample cell pressure (black) and temperature (red) recorded during VAS experiment. Mixture concentration and sorption calculated are shown. Pure CO_2 – 2. 178
Figure D.11: Sample cell pressure (black) and temperature (red) recorded during VAS experiment. Mixture concentration and sorption calculated are shown. Pure CO_2 – 3. 178
Figure D.12: Sample cell pressure (black) and temperature (red) recorded during VAS experiment. Mixture concentration and sorption calculated are shown. Low SO_2 – 1. 179
Figure D.13: Sample cell pressure (black) and temperature (red) recorded during VAS experiment. Mixture concentration and sorption calculated are shown. Low SO_2 – 2. 179
Figure D.14: Sample cell pressure (black) and temperature (red) recorded during VAS experiment. Mixture concentration and sorption calculated are shown. Medium SO_2 – 1. 180
Figure D.15: Sample cell pressure (black) and temperature (red) recorded during VAS experiment. Mixture concentration and sorption calculated are shown. Medium SO_2 – 2. 180
Figure D.16: Sample cell pressure (black) and temperature (red) recorded during VAS experiment. Mixture concentration and sorption calculated are shown. Medium SO_2 – 3. 181
Figure D.17: Sample cell pressure (black) and temperature (red) recorded during VAS experiment. Mixture concentration and sorption calculated are shown. High SO_2 – 1. 181
Figure D.18: Sample cell pressure (black) and temperature (red) recorded during VAS experiment. Mixture concentration and sorption calculated are shown. High SO_2 – 2. 182
Figure D.19: Sample cell pressure (black) and temperature (red) recorded during VAS experiment. Mixture concentration and sorption calculated are shown. High SO_2 – 3. 182
Figure D.20: Sample cell pressure (black) and temperature (red) recorded during VAS experiment. Mixture concentration and sorption calculated are shown. High SO_2 – 4. 183
Figure D.21: Calibration Curve produced for SO_2. SO_2 Concentration = 0.006938 x SO_2 Peak Area 188
Figure D.22: Chromatograms of 5 gas sample runs of a CO_2-SO_2 mixture with a high level of SO_2 (High SO_2 - Mixture 4) before sorption. The entire chromatogram (top) and SO_2 peak close-up (bottom) are shown. 188
Figure D.23: Chromatograms of five gas sample runs of High SO_2 - Mixture 4 after sorption. The entire chromatogram (top) and SO_2 peak close-up (bottom) are shown. 189
Figure D.24: Comparison of representative SO_2 peaks before and after sorption. High SO_2 - Mixture 4. 190

Figure D. 25: Chromatograms of 5 gas sample runs of a CO_2-SO_2 mixture (High SO_2 - Mixture 3) with a high level of SO_2 before sorption. The entire chromatogram (top) and SO_2 peak close-up (bottom) are shown. 190
Figure D.26: Chromatograms of five gas sample runs of a CO_2-SO_2 mixture (High SO_2 - Mixture 3) after sorption. The entire chromatogram (top) and SO_2 peak close-up (bottom) are shown. 191
Figure D.27: Comparison of representative SO_2 peaks before and after sorption. High SO_2 - Mixture 3..... 192
Figure D. 28: Chromatograms of four gas sample runs of a CO_2-SO_2 mixture with a high level of SO_2 (High SO_2 - Mixture 2) before sorption. The entire chromatogram (top) and SO_2 peak close-up (bottom) are shown. 192
Figure D.29: Chromatograms of five gas sample runs of a CO_2-SO_2 mixture (High SO_2 - Mixture 2) after sorption. The entire chromatogram (top) and SO_2 peak close-up (bottom) are shown. 193
Figure D.30: Comparison of representative SO_2 peaks before and after sorption. High SO_2 - Mixture 2..... 194
Figure D.31: Chromatograms of four gas sample runs of a CO_2-SO_2 mixture with a high level of SO_2 (High SO_2 - Mixture 1) before sorption. The entire chromatogram (top) and SO_2 peak close-up (bottom) are shown. 194
Figure D.32: Chromatograms of five gas sample runs of a CO_2-SO_2 mixture (High SO_2 - Mixture 1) after sorption. The entire chromatogram (top) and SO_2 peak close-up (bottom) are shown. 195
Figure D.33: Comparison of representative SO_2 peaks before and after sorption. High SO_2 - Mixture 1..... 196
Figure D.34: Chromatograms of five gas sample runs of a CO_2-SO_2 mixture with a mid level of SO_2 (Medium SO_2 - Mixture 3) before sorption. The entire chromatogram (top) and SO_2 peak close-up (bottom) are shown. 196
Figure D.35: Chromatograms of five gas sample runs of a CO_2-SO_2 mixture (Medium SO_2 - Mixture 3) after sorption. The entire chromatogram (top) and SO_2 peak close-up (bottom) are shown. 197
Figure D.36: Comparison of representative SO_2 peaks before and after sorption. Medium SO_2 - Mixture 3. 198
Figure D. 37: Chromatograms of five gas sample runs of a CO_2-SO_2 mixture with a mid level of SO_2 (Medium SO_2 - Mixture 2) before sorption. The entire chromatogram (top) and SO_2 peak close-up (bottom) are shown. 198
Figure D.38: Chromatograms of five gas sample runs of a CO_2-SO_2 mixture (Medium SO_2 - Mixture 2) after sorption. The entire chromatogram (top) and SO_2 peak close-up (bottom) are shown. 199
Figure D.39: Comparison of representative SO_2 peaks before and after sorption. Medium SO_2 - Mixture 2. 200
Figure D. 40: Chromatograms of five gas sample runs of a CO_2-SO_2 mixture with a mid level of SO_2 (Medium SO_2 - Mixture 1) before sorption. The entire chromatogram (top) and SO_2 peak close-up (bottom) are shown. 200
Figure D.41: Chromatograms of five gas sample runs of a CO_2-SO_2 (Medium SO_2 - Mixture 1) mixture after sorption. The entire chromatogram (top) and SO_2 peak close-up (bottom) are shown. 201
Figure D.42: Comparison of representative SO_2 peaks before and after sorption. Medium SO_2 - Mixture 1. 202

Figure D.43: Chromatograms of four gas sample runs of a CO_2-SO_2 mixture with a low level of SO_2 (Low SO_2 - Mixture 2) before sorption. The entire chromatogram (top) and SO_2 peak close-up (bottom) are shown. 202
Figure D.44: Chromatograms of five gas sample runs of a CO_2-SO_2 mixture (Low SO_2 - Mixture 2) after sorption. The entire chromatogram (top) and SO_2 peak close-up (bottom) are shown. 203
Figure D.45: Comparison of representative SO_2 peaks before and after sorption. Low SO_2 - Mixture 2. 204
Figure D.46: Chromatograms of four gas sample runs of a CO_2-SO_2 mixture with a low level of SO_2 (Low SO_2 - Mixture 1) before sorption. The entire chromatogram (top) and SO_2 peak close-up (bottom) are shown. 204
Figure D.47: Chromatograms of five gas sample runs of a CO_2-SO_2 mixture (Low SO_2 - Mixture 1) after sorption. The entire chromatogram (top) and SO_2 peak close-up (bottom) are shown. 205
Figure D.48: Comparison of representative SO_2 peaks before and after sorption. Low SO_2 - Mixture 1. 206
Figure D.49: Comparison of sorption isotherm models fit to CO_2 sorption data 207
Figure E.1: Schematic diagram of stereopycnometer (Quantachrome Instruments, 2009) 208
Figure E.2: Complete results and calculations for stereopycnometer sample volume calculations for three identically prepared 2 g coal samples 209
Figure E.3: Low pressure isotherm plot produced for coal parameter calculations 211

LIST OF TABLES

Table 2.1: Estimated Component Concentrations in Flue Gas and Purified CO_2 Streams (Last and Schmick, 2011) 37
Table 2.2: An Illustrative Calculation on the Component Concentrations of streams resulting from CO_2 capture processes (Mikunda and de Coninck, 2011) 37
Table 2.3: Coal Seam Temperature and Pressure as a Function of Depth (reconstructed from work by Zhang, 2008) 49
Table 2.4: Important Physical States of CO_2 (NIST, 2011; Span and Wagner, 1994) 50
Table 2.5: General Physical Properties of CO_2 (IPCC, 2005) 51
Table 2.6: Important Physical States of SO_2 (NIST, 2011; Hasenberg, 2008; Hogenboom et al., 1996) 52
Table 2.7: Difference between adsorption and chemisorption (Ruthven, 1984) .. 59
Table 4.1: Composition of Coal as determined from Proximate Analysis 82
Table 4.2: Major Elemental Composition of Coal Sample 83
Table 4.3: Petrographic Composition of Coal 83
Table 4.4: Summarised BET Results specifying the modelling methods used for calculation 84
Table 4.5: The volume determined for three identically prepared 2 g coal samples 85
Table 4.6: Sample cell system volume 87
Table 4.7: SO_2 experimental peak areas and calculated concentrations 97
Table 4.8: Characteristic infrared absorption frequencies of S-containing functional groups (Table of IR Absorption Frequencies, unknown) 103
Table 4.9: Excess sorption calculated for three samples runs with pure CO_2 105
Table B.1: Main differences between the VAS units at Wits and TUT 153
Table C.1: VAS run parameters 158
Table D.1: Experimental and calculated values for system volume determination 169
Table D.2: Critical properties of CO_2 and SO_2 173
Table D.3: Initial and final number of moles present in the sorption experiment with 2 g of coal when the initial SO_2 concentration is 1.25%. The excess sorption is calculated from these values according to mass balance principles. Two alternative density prediction methods are used in calculating these values. 185
Table D.4: Summarised average results table for initial concentration of High SO_2 - Mixture 4 189
Table D.5: Summarised average results table for final concentration of High SO_2 - Mixture 4 189
Table D. 6: Summarised average results table for initial concentration of High SO_2 - Mixture 3 191
Table D.7: Summarised average results table for final concentration of High SO_2 - Mixture 3 191
Table D.8: Summarised average results table for initial concentration of High SO_2 - Mixture 2 193

Table D.9: Summarised average results table for final concentration of High SO_2 - Mixture 2 193
Table D.10: Summarised average results table for initial concentration of High SO_2 - Mixture 1..... 195
Table D.11: Summarised average results table for final concentration of High SO_2 - Mixture 1 195
Table D.12: Summarised average results table for initial concentration of Medium SO_2 - Mixture 3..... 197
Table D.13: Summarised average results table for final concentration of Medium SO_2 - Mixture 3..... 197
Table D. 14: Summarised average results table for initial concentration of Medium SO_2 - Mixture 2 199
Table D.15: Summarised average results table for final concentration of Medium SO_2 - Mixture 2..... 199
Table D. 16: Summarised average results table for initial concentration of Medium SO_2 - Mixture 1 201
Table D.17: Summarised average results table for final concentration of Medium SO_2 - Mixture 1..... 201
Table D.18: Summarised average results table for initial concentration of Low SO_2 - Mixture 2..... 203
Table D.19: Summarised average results table for final concentration of Low SO_2 - Mixture 2 203
Table D.20: Summarised average results table for initial concentration of Low SO_2 - Mixture 1..... 205
Table D.21: Summarised average results table for final concentration of Low SO_2 - Mixture 1 205
Table D.22: Summary of adsorption isotherm models fit to experimental data (Foo and Hameed (2010)) 206
Table D.23: Sorption isotherm model parameters 207
Table E.1: Detailed Petrographic Report 210
Table E.2: Conditions of BET Experiment..... 212
Table E.3: Summary Report of coal parameters calculated by specified numerical methods..... 212

LIST OF SYMBOLS

A	Area of the coal seam
a_i , b_i , c_i	Parameters used in the Patel-Teja Equation of State
f_a	Ash mass fraction
f_m	Moisture mass fraction
G_C	Coal gas content (dry, ash free)
h	Effective thickness of the coal seam
M_{CO_2}	Theoretical CO_2 storage capacity
m	Mass
$N_{(i)sorbed}$	Excess sorption (moles of component i sorbed per mass of sample)
n	Number of moles
$\widetilde{n_C}$	Bulk coal density
P	Pressure
R	Universal gas constant
R^2	Coefficient of determination
T	Temperature
V1, V2, V3	Valves 1, 2 and 3, respectively
V	Molar Volume
v_i	Volume of i
x_i	Mole fraction of component i
ξ_{ij}	Binary interaction parameter
$\rho_{CO_2(std)}$	Mass-based CO_2 density at standard conditions
ρ_i	Molar density of component i

NOMENCLATURE

AAD	Absolute Average Deviation
BET	Brunauer, Emmett and Teller
CCS	Carbon dioxide Capture and Geological Storage
COORAL	CO_2 Purity for Capture and Storage
ECBMR	Enhanced Coal Bed CH_4 Recovery
EGR	Enhanced Gas Recovery
EnPe	Energy and Petroleum
EOR	Enhanced Oil Recovery
EOS	Equation of State
FTIR	Fourier Transform Infrared Spectroscopy
GC	Gas Chromatography
IEA	International Energy Agency
IEAGHG	International Energy Agency's Greenhouse Gas Research and Development Program
IMPACTS	The impact of the quality of CO_2 on transport and storage behaviour
IPCC	Intergovernmental Panel on Climate Change
MEA	Monoethanolamine
MSDS	Material Safety Data Sheets
NIST	National Institute of Standards and Technology
NORAD	The Norwegian Agency for Development Cooperation
NTNU	Norwegian University of Science and Technology
PR	Peng-Robinson
SRK	Soave Redlich Kwong
STP	Standard Temperature and Pressure
TCD	Thermal Conductivity Detector
TGA	Thermogravimetric Analyser
TUT	Tshwane University of Technology
VAS	Volumetric Adsorption System
VLE	Vapour-Liquid Equilibrium
Wits	University of the Witwatersrand
XRD	X-Ray Diffraction Analysis

CHAPTER 1: Introduction

In this chapter the reader is introduced to the project by means of the following sections: Background, Motivation, Research Objectives, and Dissertation Outline. The aim of this chapter is to describe the context of project, give it meaning, and clarify what it hopes to achieve.

1.1 Background

A cause of global concern is the rapid increase of CO_2 levels in the atmosphere in recent times. The CO_2 concentration has increased from a pre-industrial value of 280 ppm to 395 ppm in 2013 (Tans and Keeling, 2013; Intergovernmental Panel on Climate Change (IPCC), 2007). This rise is mainly due to vast increases in anthropogenic CO_2 emissions, two thirds of which stem from fossil fuel usage, causing the CO_2 to accumulate in the atmosphere (IPCC, 2007). Carbon dioxide is a greenhouse gas and plays an important role in the climate control mechanisms of the earth. It is widely accepted among climate experts that increasing levels of CO_2 in the atmosphere can have adverse effects on the world's climate, and if the CO_2 concentration of 450 ppm is exceeded, the global average temperature will rise by more than 2°C (International Energy Agency (IEA), 2010). Many governments are backing plans to limit the increase in global temperature to less than 2°C by increasing funding for research and development into low-carbon energy, implementation of new and more effective policies, as well as national emissions reduction targets (IEA, 2010).

Many alternatives to fossil fuel-based technologies, such as renewable energy technologies, exist. However, they struggle to replace CO_2-intensive fossil fuel based technologies due to these technologies being well-established, reliable and the cheapness of fossil fuels (IPCC, 2005). All major economies of the world are underpinned by fossil fuels, while South Africa, being the 13^{th} highest CO_2 emitter world-wide, is as dependent on coal as any country in the world (Beck *et al*., 2011). Even though fossil fuel dependence is expected to increase in South Africa in the next 50 to 60 years, the South African government has pledged to demonstrate a responsible approach towards reducing its CO_2 emissions (Beck *et*

al., 2011). In fact, at the climate change negotiations in Copenhagen, South Africa announced that it would take mitigation actions to reduce national CO_2 emissions equating to a deviation of 42% below the "business as usual" emissions growth trajectory by 2025 (Beck *et al*., 2011). This commitment and other similar commitments worldwide highlight the importance of technologies and concepts aimed at CO_2 reduction; one such concept is CO_2 Capture and Geological Storage (CCS).

The implementation of CCS potentially allows for fossil fuel-dependent processes to operate without releasing CO_2 into the atmosphere. This is done by separating the CO_2 from the waste/flue gas stream of the CO_2 producing facility and pumping it underground, where it will be safely trapped in the long term (IPCC, 2005). Thus, CCS can play a vital role in helping to transit to renewable energy, providing valuable time for its development (IPCC, 2005). While the application of CCS to CO_2 producing facilities will add significant cost to their operations, these costs are still very competitive when compared with other technologies that would reduce CO_2 emissions in the energy sector. For instance, it is predicted that the electricity prices will increase by 210% by 2050 if CCS and nuclear energy are not utilised in the schemes to achieve the global CO_2 emissions reduction targets specified by the IEA; as opposed to an 80% increase in the electricity price if they are included (Courtright and Howard, 2009). This statistic, along with Figure 1.1, which indicates the predicted contributions of different technologies to reducing CO_2 production, reveals the important role CCS has to play in achieving emissions reduction targets. The importance of CCS is further emphasised in a press release by the National Grid in the UK (2013) where it is stated that: "Global energy demand is likely to double in the next twenty years, and CCS is the only technology that can turn high carbon fuels into genuinely low carbon electricity and keep costs low for consumers".

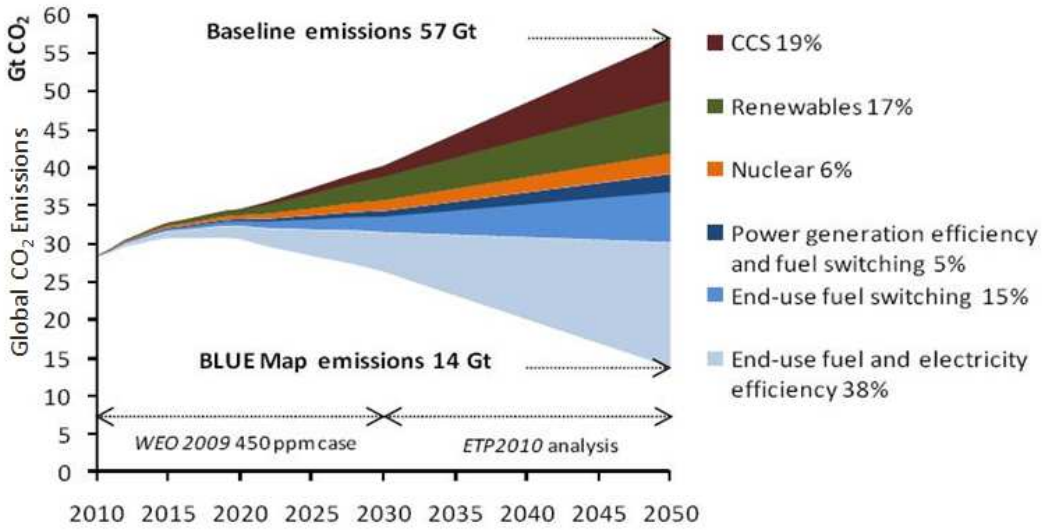


Figure 1.1: Proposed contribution of various technologies to reduce global CO_2 emissions (IEA, 2010).
These target emission levels would stabilise the atmospheric CO_2 concentration at 450 ppm in 2050, thereby limiting the global average temperature increase to 2℃. The 'BLUE Map scenario' necessitates emissions to be decreased to 14 $GtCO_2$, while 'business as usual' would produce 57 $GtCO_2$ by 2050. CCS contributes significantly in these plans accounting for 19% of the CO_2 emissions to be reduced.

One of the most significant barriers to CCS deployment, though, is the cost, the largest of which owes to the CO_2 capture stage of CCS (Daniels *et al.*, 2012). Capture refers to the process of separating CO_2 from any other components so that a relatively pure stream of CO_2 is obtained. Carbon dioxide emission streams are usually mostly comprised of N_2 (>70%) but can also contain a wide range of minor components, including Ar, H_2O, H_2, H_2S, SO_x, NO_x, O_2, CO, etc. (Last and Schmick, 2011). Separating CO_2 from the bulk of the gas can be done according to a large number of processes. For example, the scrubbers can be used to remove N_2 from a power plant flue gas (post combustion), or N_2 can be separated from the air using cryogenic distillation upstream to the power plant combustion process (oxyfuel combustion) (IPCC, 2005). Purification processes, such as desulphurisation, are also implemented to remove any other unwanted impurities to prepare the CO_2 stream for the transport and storage phases of CCS (IPCC, 2005). The type of impurities and their concentration in the final stream sent to storage is thus a function of the CO_2 production process, capture process, and purification processes implemented.

In order for CO_2 storage to be successful, it is important that suitable storage sites be identified. Potential sites for CO_2 storage include depleted oil and gas fields, saline aquifers, and unmineable coal seams (Bachu, 2008a). The storage options in South Africa are largely in offshore saline aquifer formations, which comprise 98% of the storage capacity estimations provided by Viljoen *et al*. (2010). However, concerns have been raised about the high operational costs of offshore storage facilities, as well as about costs of CO_2 transport to these sites which are located far from the large point sources of CO_2 (Viljoen *et al*., 2010). Onshore unmineable[1] coal seams are therefore also considered as a potential storage option. Even though unmineable coal seams only comprise a small fraction of the total storage capacity in South Africa, they comprise a large fraction of the onshore capacity (approximately 50%). They are also advantageously located in close proximity to large CO_2 sources (Viljoen *et al*., 2010). See Figure 1.2 for location of the unmineable coal seams in South Africa.

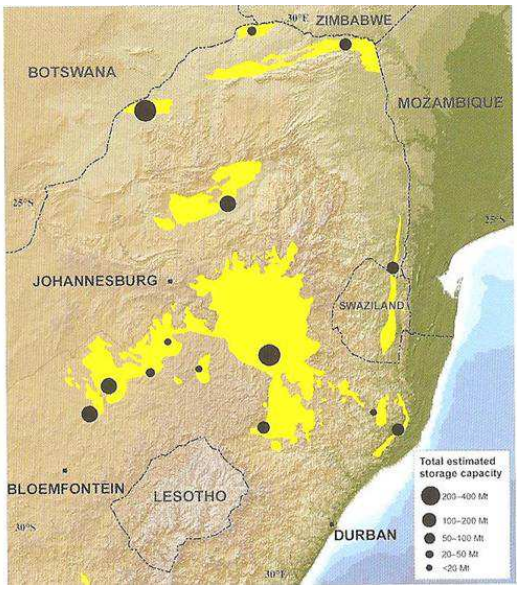


Figure 1.2: Location of unmineable coal seams for potential CO_2 storage in South Africa (black circles). Collectively the storage potential of unmineable coal seams in South Africa is between 0.3 and 1.4 $GtCO_2$ (Viljoen et al., 2010).

[1] 'Unmineable' coal seams are coal seams that have been defined as too deep and/or too thin to be economically mined with current conventional mining methods (Viljoen *et al*., 2010). This implies that coal that is defined as unmineable now might not always be considered unmineable as mining technology advances. The likely future fate of a coal seam, considering its mining potential and potential for enhanced coal bed CH_4 recovery (ECBMR), is a key determinant of its suitability for CO_2 storage (IPCC, 2005; Viljoen *et al*., 2010).

An important property that makes coal storage possible is the ability for coal to adsorb CO_2 under the high pressure conditions underground. In fact, coal's affinity for CO_2 is so high that the CO_2 that is adsorbed onto the coal can potentially free CH_4 from the coal (Reeves and Schoeling, 2000). If this CH_4 could be recovered, it could offset some of the costs associated with CCS and make this storage option more attractive (IPCC, 2005). The adsorption, or sorption (collectively adsorption, absorption and chemisorption), capacity of the coal is an important parameter used to estimate a coal seams' 'storage capacity' (Bachu *et al*., 2007). The storage capacity is an estimation of the amount of CO_2 that can be stored in the site, and is important to know when assessing the feasibility of a CCS venture.

From the background covered, it is evident that CCS plays an important role in global and local plans to combat climate. Impurity gases in CO_2 streams are significant contributors to the cost of capture, which is the phase of CCS that is influential in holding this technology back from being implemented widely at a commercial scale. Impurities will always be present in a CO_2 stream to be stored. Unmineable coal seams are relevant potential CO_2 storage media, and determining the sorption capacities in coals is important for reliable storage capacity estimations.

1.2 Motivation

Coal is an unconventional storage medium for CO_2 and the storage capacity in this medium needs to be better understood (NORAD, 2011). Laboratory sorption studies are essential for estimating the storage capacity in unmineable coal seams, and they are in short supply in South Africa (Viljoen *et al*., 2010). Most sorption studies in coal only consider pure CO_2 in their experimental setups, with some studies considering N_2 and CH_4 in addition to CO_2 and mixtures of these three components, due to their importance in CH_4 recovery processes. A whole host of impurities can, however, exist in captured CO_2 streams (Li, H. *et al*., 2011), with some minor components, such as SO_2 and H_2S, having very strong sorbing properties (Bachu, 2008a). The influence of many of these minor component impurities is unknown, and it is proposed that they could affect CO_2 sorption

directly through competition or react with the coal and change its characteristics for CO_2 sorption (Sakurovs *et al*., 2011).

Due to shortage of sorption data, storage capacity estimations have assumed that any gases injected with the CO_2 will not affect its sorption behaviour (Bachu, 2008b). Very few studies have been conducted to test the reliability of this assumption when realistic amounts of minor component impurities are present in the gas streams. If this knowledge was obtained, the accuracy of storage capacity estimations for coal seams could be improved. In addition to more accurate storage capacity estimations being possible, the influence of the quality of the CO_2 changing over time, as may be the case in reality, can be determined if underground impurity effects are better understood (NORAD, 2011).

Some potential ways of reducing the cost of CO_2 capture would be if fewer processes were implemented to purify the CO_2 stream, or if the purity specifications on a CO_2 stream could be relaxed so that less stringent operating conditions were required. Oxyfuel combustion is a good example of such a case as the flue gas stream is already captured, i.e. rich in CO_2, but also contains a wide range of minor component impurities, including significant amounts of SO_2 if coal is the combustion medium (Mikunda and de Coninck, 2011). It has been proposed that the co-injection of combustion impurities that are difficult to separate out, with the CO_2 could be economically advantageous (Crandell *et al*., 2009; Li, Q. *et al*., 2011). In addition, this would prevent pollutants such as H_2S and SO_2 being emitted into the atmosphere, and companies could save large amounts of money that are spent on obtaining permits for the rights to emit these gases (Crandell *et al*., 2009). However, the long term effects of these gases underground is largely unknown and it is essential to determine these effects before the co-injection of impurities can be considered (Crandell *et al*., 2009; Heeschen *et al*., 2011).

It is also desirable to know the effects of impurities on underground storage from the perspective of defining the allowable CO_2 purity for storage (Heeschen *et al*., 2011). Even though regulations governing the injection of CO_2 have been proposed, no clear specifications on the purity for the injected CO_2 have been defined (Crandell *et al*., 2009; Mikunda and de Coninck, 2011). Indeed, the

Directive 2009/31/EC of the European parliament and council (2009) only defines qualitatively that a stream to be injected for storage must consist "overwhelmingly of CO_2". Several projects, including the IMPACTS[2] and COORAL[3] projects, which aim to determine the effects of impurities in aid of providing quantitative specifications for injected CO_2 streams, are currently underway (Lilliestrale, 2013; Ruetters, 2013).

Thus, there is a lot of motivation for the present study, stemming from the importance of laboratory sorption studies for coal seam capacity determination and the significance of impurities in CCS. While the effects of many impurities require clarification, SO_2 is selected as the impurity of focus for this study. This selection is made primarily due to the properties of SO_2. Of the common impurities that could exist in captured CO_2 streams, SO_2 is one of the most highly reactive and polar molecules, and is known to have very strong sorption properties to coal. It is therefore deemed that it would be valuable to pinpoint the effects of a molecule with these 'extreme' properties. If the study is successful in identifying whether the effects of SO_2 are favourable or unfavourable to the storage of CO_2 in coal, it would provide motivation to broaden the experimentation to other impurities. More generally, the study carries novelty as many effects of impurities are unknown, and, if they were known, there is potential for significant financial repercussions[4].

1.3 Aims and Objectives

The primary aim of the project is to deduce if, and if so, to what extent, the sorption of CO_2 in coal is affected by the presence of SO_2 at high pressure and moderate temperature conditions relevant to CO_2 storage. It is desired to know if a trend exists between the level of SO_2 in the captured CO_2 stream and the sorption capacity of the coal. Thus the aim is to analyse different concentrations of SO_2 that are both equal to and above realistic SO_2 levels of captured CO_2 streams. The

[2] IMPACTS - The impact of the quality of CO_2 on transport and storage behaviour
[3] COORAL - CO_2 Purity for Capture and Storage
[4] Note: The study does not investigate the financial repercussions; but the potential for financial consequences resulting from knowing impacts of certain impurities on storage capacity serves as motivation for the study.

aims of the project are to be realised experimentally through the following objectives:

- Determine the amount of sorption that takes place in a representative South African coal sample when in contact with pure CO_2 for 48 hours at a pressure approaching 90 bar using volumetric adsorption apparatus.
- Determine the equivalent amount of sorption that takes place if the only variable changed experimentally is the purity level of the CO_2 that is contacted with the coal. SO_2 is the impurity considered and the sorption is quantified for different concentrations of binary CO_2-SO_2 mixtures where the SO_2 concentration falls between 0.1% and 10%.
- Compare the amount of sorption for the pure CO_2 and CO_2-SO_2 mixture cases and make deductions on the effect of SO_2 of the sorption capacity of the coal. As far as possible, make recommendations on whether the presence of SO_2 is favourable for CO_2 storage in coal.
- Develop an experimental method to achieve the above objectives by modifying the experimental volumetric adsorption setup at Wits to include a CO_2-SO_2 mixture producing system and GC sampling system for gas analysis.

1.4 Dissertation Outline

This dissertation is structured conventionally. Chapter 1 is the introductory chapter and sets the scene for the project. Chapter 2 provides an in depth literature review covering major areas relevant to the study as well as important findings of previous research. Chapter 3 outlines the methodology of the project so that the experimental work used to produce results in Chapter 4 can be fully appreciated. Chapter 4 presents and discusses all the findings of the project which are split into suitable subsections. Chapter 5 then concludes on the important findings of Chapter 4, and provides recommendations for future work.

CHAPTER 2: Literature Review

The literature review conducted has been split into sections that provide important and relevant insight into the project. Section 2.1 outlines the fundamentals of CCS, including its place in society and descriptions of the three major CCS stages. Section 2.2 describes the role of impurities in CCS, as well as the findings of projects conducted that are similar to this one. Section 2.3 describes important properties and aspects of coal and the gases considered in the study. Section 2.4 explains the concept of storage capacity and describes the process of sorption. Finally, Section 2.5 summarises the most important findings of the literature review.

2.1 CO_2 Capture and Geological Storage (CCS) Fundamentals

2.1.1 Climate Change and CCS as a Mitigation Technique

Atmospheric greenhouse gases are responsible for the retention of a fraction of the long-wave radiation that is reflected off the earth's surfaces (IPCC, 2007). The greenhouse gas's function in the earth's energy/radiation balance is important in maintaining the climate of the earth (IPCC, 2007). One of the most important greenhouse gases is CO_2, and its atmospheric concentration has risen by about 35% since the industrial era. This increase is known to be due to human activities, largely through the combustion of fossil fuels (IPCC, 2007). In order to mitigate the serious consequences of climate change, measures have been put in place in order to stabilise the concentration of atmospheric CO_2 (IPCC, 2007). A broad portfolio of measures and actions has been proposed, and no single technology option will provide all the emission reductions required (Bachu, 2008a; IPCC, 2005). Among the CO_2 mitigation techniques conceived is CO_2 capture and geological storage, which is an important option as demonstrated by Figure 1.1.

CCS has a great potential and can decrease the cost of mitigating climate change when compared to scenarios where only other mitigation technologies, such as renewable energy, are employed (IPCC, 2005). This is based on projections predicting that fossil fuels will remain the dominant source for primary energy

production into the middle of the century at least (IPCC, 2005). CCS is a technology that would ideally be used to capture CO_2 from large point sources, such as power plants or large industrial processes, and store it permanently and safely underground (IPCC, 2005). Thus, CCS would enable fossil fuel energy plants, and other CO_2 producing industries, to operate at low greenhouse gas emission levels (IPCC, 2005). CCS is potentially compatible with most current fossil fuel-dependent energy infrastructures and can thus increase flexibility in achieving the necessary greenhouse gas emission reduction targets (IPCC, 2005).

Although there are many costs and challenges in CCS, such as decreased efficiencies when implementing capture in power plants and difficulty in guaranteeing long term storage of CO_2 (Bolland, 2012; Valdelievre, 2012), many components in CCS are mature technologies; i.e. technologies now in operation with multiple replications worldwide (IPCC, 2005). For instance, CO_2 is typically removed in many industries with the aim of purifying other streams, and CO_2 is injected into oil reservoirs to enhance oil recovery (IPCC, 2005). In the majority of cases, however, these technologies are not used to complete a full CCS chain or implemented with the intent of reducing CO_2 emissions. Indeed, only five large-scale commercial applications of CCS are in operation worldwide (Ringrose, 2012), with only one commercial scale application of CO_2 capture to a coal-fired power plant nearing completion (Monea, 2013).

It is apparent that a great deal of work is necessary on many different fronts to optimise the process chains of CCS, particularly with its application to power generation processes. However, this is a highly promising, important technology that can grow and become established as additional financial incentives for development and industrial application are made available, so that its vital role in in mitigating climate change is fulfilled.

2.1.2 The CCS System

CO_2 capture and geological storage is a three stage[5] technology with each stage defined briefly as follows (Rutherford, 2012):

- Capture: CO_2 is 'captured' (i.e. separated from other components to form a stream rich in CO_2) from point-source emission facilities.
- Transport: The captured CO_2 is then compressed and transported to the injection site of a selected storage medium.
- Geological Storage: The CO_2 is injected into deep subsurface geological formations where it is trapped or 'stored' for significant periods of time.

For further clarity, the overall CCS process is illustrated schematically in Figure 2.1. The current project focusses mainly on the 'storage' element of CCS, more specifically, the storage in unmineable coal seams. However, all stages of CCS are directly linked and one must have an understanding of the system as a whole to fully appreciate any one element. Thus, in this literature review section, each stage of CCS is briefly outlined, highlighting areas of importance and understanding in capture and transport stages, with a more detailed summary provided in the storage section.

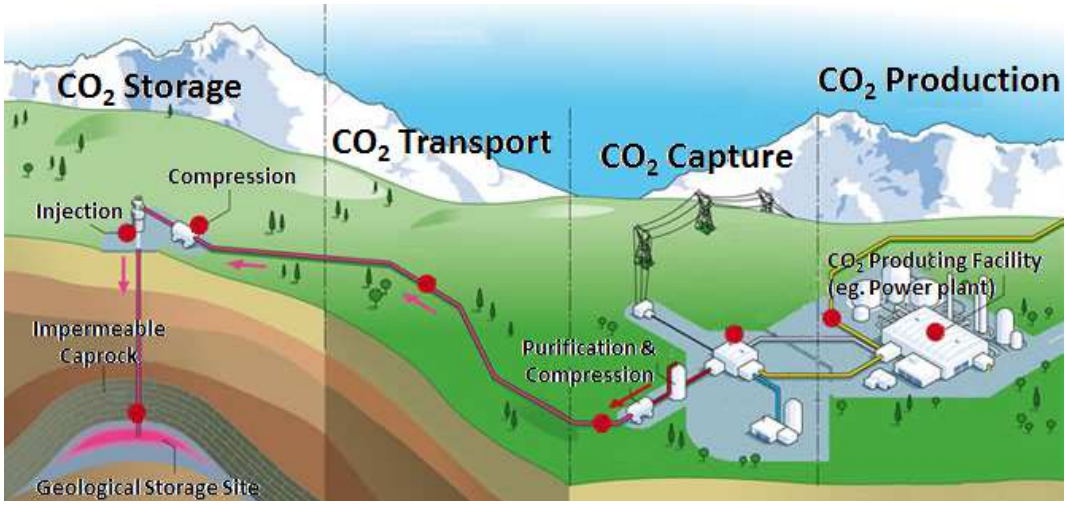


Figure 2.1: Schematic illustration of the overall CCS process (modified from Total, 2007)

[5] Some consider a fourth phase of CCS to be 'monitoring', whereby the long and short term progress of fluid underground is tracked after it is injected (IPCC, 2005).

a) CO_2 Capture

A number of different industries produce CO_2, but seldom is it produced in a very pure stream. For instance, less than 2 % of industries produce a high purity CO_2 stream (> 95 %), while the CO_2 streams produced from fossil fuel combustion using air are very diluted (~ 14 %) (Last and Schmick, 2011; IPCC, 2005). In principle, it is possible to compress and inject low-purity CO_2 streams into geological storage sites, but this has several disadvantages. The main disadvantage is that compression and injection of large impure streams is associated with high energy and other costs, and is generally considered impractical (Ottiger *et al.*, 2008; IPCC, 2005). It is thus necessary to separate out other gaseous components and produce a high purity CO_2 stream for injection. This CO_2 purification/separation process is termed 'capture'.

CO_2 capture encompasses a wide range of technology types and systems. Liquid solvent absorption, membranes, solid sorbents and cryogenic distillation are all technologies used to separate CO_2 from other process gases (Mondal *et al.*, 2012; Pires *et al.*, 2011; IPCC, 2005). Of these technologies, solvent absorption is the most mature, with many applications in industry – ammonia and natural gas industries, for example (Mondal *et al.*, 2012; IPCC, 2005). Membrane technologies have some advantages but suffer setbacks when applied industrially; adsorption technologies are mostly employed in small scale applications; while distillation, although employed commercially, is very energy intensive and requires a relatively high CO_2 feed concentration to be economical (Mondal *et al.*, 2012; Bolland, 2012; Gottlicher and Pruschek, 1997).

It is of great interest to apply CO_2 separation technologies to fossil fuel-driven energy production facilities. Three systems making use of capture technologies have been developed for these facilities. These systems are: post-combustion capture, pre-combustion capture, and oxy-fuel capture systems (Mondal *et al.*, 2012; Pires *et al.*, 2011; IPCC, 2005). Post-combustion involves the removal of CO_2 from the flue gas produced by conventional fossil fuel combustion (Mondal *et al.*, 2012; IPCC, 2005). Pre-combustion is designed for integrated gasification combined cycle (IGCC) power plants. The important steps for this capture process

are coal gasification, or analogous natural gas reforming, and water-gas shift stages (IPCC, 2005). The CO_2 would be separated from H_2 once the syngas, resulting from gasification/reforming, undergoes a water-gas shift reaction (Mondal *et al.*, 2012; IPCC, 2005); H_2 would be used as a carbon-free fuel. Lastly, oxy-fuel capture is similar to post-combustion capture in that the CO_2 stream requires purification after combustion. However, the fuel is combusted in pure O_2 that has been cryogenically separated from air, which in turn makes the downstream purification of CO_2 easier (Mondal *et al.*, 2012). For greater clarity of the processes described above, Figure 2.2 is offered. All systems have their advantages and disadvantages and the reader is referred to IPCC (2005) or any other reputable source on the subject for more information.

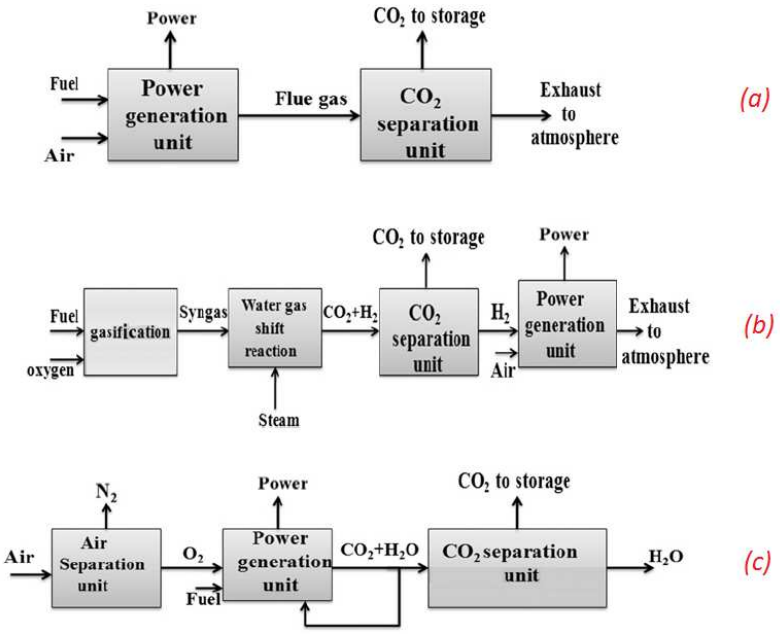


Figure 2.2: Principles of (a) Post-combustion; (b) Pre-combustion; and (c) Oxy-fuel combustion capture processes (adapted from Mondal et al. (2012))

All capture processes will reduce a power plant's net efficiency, i.e. the plant will require more fuel to generate each kilowatt-hour of electricity (Valdelievre, 2012; IPCC, 2005). Thus, capture technology would only be feasible with high efficiency power plants, such as supercritical or ultra-supercritical technology when considering coal-powered plants (Valdelievre, 2012; IPCC, 2005). It is important to note that the decrease in efficiency will depend on the type and system of capture applied as well as the need for additional treatment systems to

remove low levels of sulphur, nitrogen oxides or other minor components (Last and Schmick, 2011; IPCC, 2005).

b) Transport

After point-source CO_2 has been conditioned to the desired purity, it is necessary to transport it to the injection site of a selected storage medium. There may a large distance between these two sites, and thus a reliable and safe means of CO_2 transport is vital. Pipelines are the most common method for transporting CO_2 and are a mature technology as technical requirements are similar to those applied to the transport of other gases (Pires *et al.*, 2011; IPCC, 2005).

CO_2 is compressed to its supercritical form (80 – 150 bar) for transport as this helps to improve efficiency and prevent two-phase flow (Pires *et al.*, 2011). It is also important to remove impurities such as water and hazardous gases (such as H_2S) to low levels to prevent corrosion and reduce health risks, if an incident were to occur in a populated area, respectively (Pires *et al.*, 2011; IPCC, 2005).

c) Geological Storage

The geological storage or sequestration of CO_2 refers to isolating industrially produced CO_2 from the atmosphere by trapping it in subsurface geological formations for a significant period of time (Bachu *et al.*, 2007). An acceptable 'significant period of time' is difficult to define; however it is suggested that 400 to 1000 years be the minimum time before minor atmospheric leaks are tolerable (Beck, 2012), with a storage period in the order of centuries to millennia suggested by other sources (De Silva and Ranjith, 2011; Bachu *et al.*, 2007).

In order to achieve the desired objectives of successful storage, the geological formations in which the CO_2 is to be stored must be carefully chosen. It is suggested that the formations satisfy the following storage criteria (Bachu, 2008a):

- Capacity – The geological formation must be able to accept the intended amount of CO_2 physically and trap it by any relevant mechanisms.
- Injectivity – The storage medium must be porous and able to take in CO_2 at the rate supplied by the CO_2 producer(s).

- Confinement – Barriers impermeable to CO_2 (such as caprock) must be present to prevent the migration and leakage of the buoyant and mobile CO_2 to the surface, shallow, potable groundwater, or any other subsurface places.

To help visualise the process and clarify public misconceptions of CO_2 being stored underground in large cavities, the storage process is described briefly here. It has been mentioned earlier in this section that it is common practice to compress CO_2 for pipeline transport to high pressures in the order of 100 bar where it exists in its supercritical state. In this state, CO_2 has properties common to both a liquid and a gas, most importantly it can exist with a density approaching that of a liquid (Bachu, 2008a). The supercritical CO_2 is injected via a borehole drilled through impermeable caprock into a dense storage system, generally greater than 800 m below the surface, where it remains pressurised in a supercritical state. This 'storage system' consists of: a dense medium, such as rock or coal; tiny pores or channels in the dense medium; and a fluid (formation waters) that fills the pores. When the CO_2 is injected it undergoes the following chain of processes as simplified from descriptions by Viljoen *et al.* (2010) and IPCC (2005): The CO_2 migrates downward according to the pressure gradients created by the injection process, displacing the fluid in the pores. It then travels laterally with natural hydraulic gradients (hydrodynamic trapping) and is driven up by buoyant forces against the caprock (structural or stratigraphic trapping). The CO_2 cannot rise to the surface due to the impermeability of the caprock, while lateral flow of CO_2 with the formation waters within the storage system can continue for potentially thousands to millions of years. In this extended time period, the CO_2 undergoes a number of other slow trapping or transformational mechanisms to become part of the storage system. These slower mechanisms depend on the specific storage medium system and can include processes such as: i) Residual trapping - CO_2 is trapped in the pore spaces due to capillary action; ii) Solubility trapping - CO_2 dissolves into the formation waters; iii) Mineral trapping – dissolved CO_2 reacts with the storage medium to form new carbonate minerals; and iv) Sorption trapping - CO_2 is adsorbed or absorbed into an organic material.

Figures 2.3 and 2.4 display the migration patterns and trapping mechanisms of CO_2 respectively.

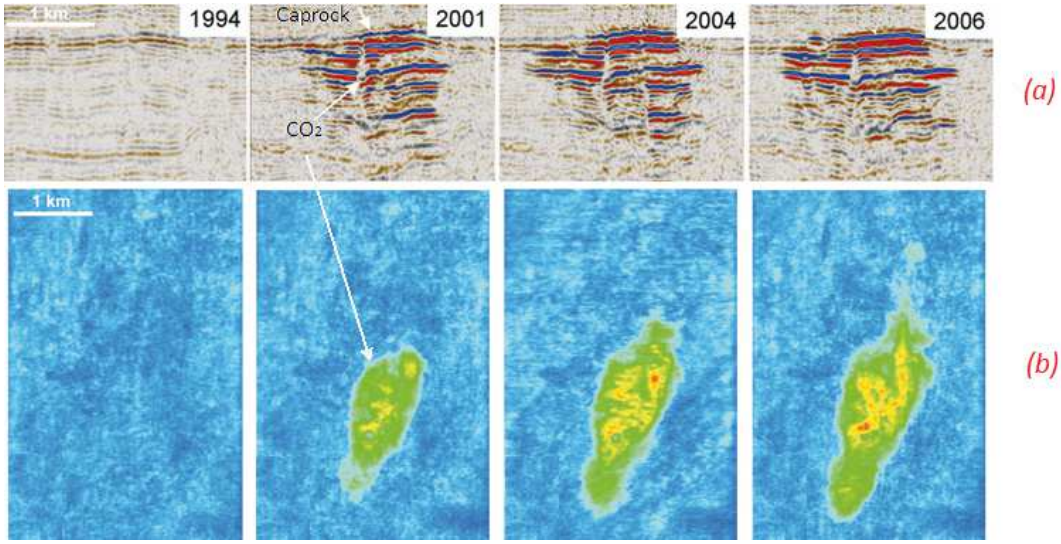


Figure 2.3: (a) Vertical and (b) horizontal seismic sections through the developing CO_2 plume at the Sleipner gas field, North Sea (British Geological Survey, 2012). From (a) it is evident that the CO_2 is effectively stopped from rising upwards by the caprock and rather expends downwards over time through the porous aquifer region. From (b) the lateral migration of the CO_2 plume over time is apparent. The successful storage of CO_2 at Sleipner creates a strong case in favour of the safety of CO_2 storage.

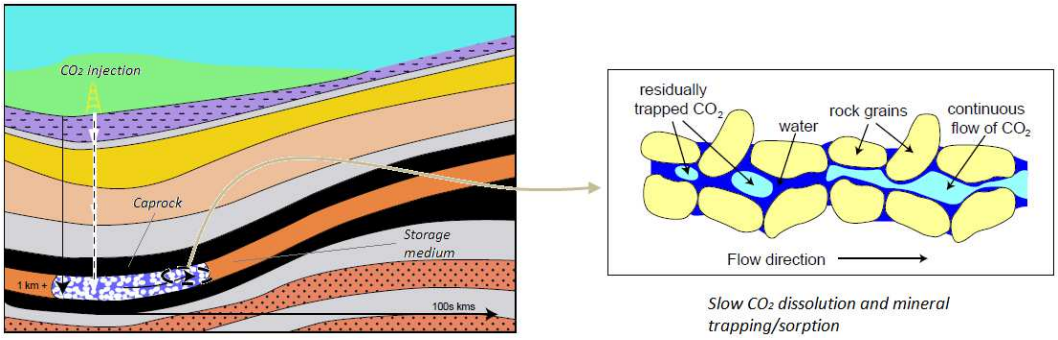


Figure 2.4: Schematic representation of CO_2 trapping mechanisms (Viljoen et al., 2010). After the CO_2 is injected into the storage site, it migrates slowly between the porous rock (see right) where it is trapped residually, dissolves into the formation water, sorbs, and reacts to become an immobile part of the storage medium.

It is clear that only special structures will be feasible for geological storage. Three main types of feasible storage formations that have received extensive consideration are (IPCC, 2005): (i) oil and gas reservoirs, (ii) deep saline formations/saline aquifers, and (iii) unmineable coal beds. The first storage option listed refers to structures in which hydrocarbons, such as gas and oil, are naturally trapped (Viljoen *et al.*, 2010). These resources are often recovered for their

economic value and reservoirs that have been depleted or are almost depleted are ideal candidates for CO_2 storage (Li *et al.*, 2006). An important process in this field is enhanced oil recovery (EOR). This process uses the injection of CO_2 into partially depleted oil reservoirs to increase the pressure in the well and force up additional oil that would not have been conventionally recovered (Viljoen *et al.*, 2010; Li *et al.*, 2006). EOR, as well as the analogous enhanced gas recovery (EGR), are economically viable and widely practiced in oil and gas industries (Li *et al.*, 2006). These geological storage sites have successfully stored hydrocarbon fluids underground for geological timeframes, and thus have great potential for CO_2 storage (Viljoen *et al.*, 2010).

Saline aquifers are formations consisting of water-permeable rocks that are saturated with brine. These systems mainly consist of sandstone saturated with formation waters unsuitable for human consumption or agriculture, and are generally located at depths below 800 m (Viljoen *et al.*, 2010; IPCC, 2005). Saline aquifers have the highest potential capacity for CO_2 storage globally and the storage process can be successfully and safely applied today, as indicated by the Sleipner project operating commercially in Norway (De Silva and Ranjith, 2011; Michael *et al.*, 2009).

Unmineable coal seams, although unconventional, are one of the main onshore storage options in South Africa (Viljoen *et al.*, 2010). They are the type of geological storage medium that is most relevant to the study in this project and thus will be discussed more thoroughly in the following subsection than the others.

Unmineable coal seam storage. Coal contains fractures, called cleats, that contribute to making coal seams porous, which is a key factor for a potential storage medium (IPCC, 2005) (for more information on coal structure, see Section 2.3.1). However, the main contributing attribute of coal to its feasibility as a CO_2 storage medium is its ability to sorb large volumes of CO_2, largely by adsorption in the coals' many micropores (Bachu, 2008a; Reeves, 2001). Coal sorption typically consists of the following three mechanisms as described by Aydin *et al.* (2010): (i) internal surface adsorption; (ii) molecular structure absorption; (iii) and

pore and natural fracture absorption. It is usually difficult to discern between these three mechanisms in practice (Pini *et al.*, 2010), and thus the term 'sorption' is used to describe any single or combination, of some or all, of these mechanisms. The reader is referred to Section 2.4 for more information on coal sorption.

It is important to note that the porosity of a coal seam decreases with increasing depth, and thus it is debateable whether CO_2 should be stored deeper than 800 m (Viljoen *et al.*, 2010; IPCC, 2005). The global storage capacity estimates for unmineable coal seam storage are given broadly in IPCC (2005) as 3 – 200 $GtCO_2$. Favourable attributes of coal seams for storage are: a simple structure with minimal faulting or folding; laterally continuous coal seams that are vertically isolated exist; frequently located near large point sources of CO_2 (IPCC, 2005; Reeves, 2001). However, doubt has been cast over the use of a valuable mineral as a storage site for CO_2 (Viljoen *et al.*, 2010; IPCC, 2005).

The term 'unmineable' is used to describe a coal bed that is currently considered too deep or too thin to be economically mined with conventional mining methods (Viljoen *et al.*, 2010). Thus, CO_2 storage can only be considered in coal seams that satisfy this criterion as once CO_2 is injected into a coal seam, depressurising that coal for mining purposes will release the CO_2 into the atmosphere (IPCC, 2005). Also, one cannot be certain that coal that is not economical to mine now will not become economical with the advancement of technology. Conflict between mining and CO_2 storage are, therefore, possible and the predicted, likely future fate of a coal seam is a key determinant for its suitability for storage (IPCC, 2005).

A counter-argument in the favour of coal seam storage could be the possibility of enhanced coal bed CH_4 recovery (ECBMR) upon the injection of CO_2 (Reeves, 2001). In the coalification process significant amounts of CH_4 are generated and retained in the free and sorbed phase if a sealing structure is present (Pini *et al.*, 2009), and this coal bed CH_4, if recovered, could be exploited for energy production (Ottiger *et al.*, 2008). Since coal has a strong affinity for CO_2, CO_2 injected into a coal seam would be preferentially adsorbed into the coal and CH_4, that was previously adsorbed, subsequently released into the free phase (Bachu,

2008a). Thus ECBMR proposes the net storage of CO_2 and concomitant enhanced recovery of valuable CH_4 (Ottiger *et al*., 2008). This process is attractive from an economical point of view as the production of CH_4 could offset some of the costs of CCS (Reeves, 2001). However, ECBMR is still in the early stages of its development with integrated research and commercial-scale field demonstration projects operating in the San Juan Basin (Reeves, 2001). It is a widely held opinion that the storage of CO_2 in unmineable coal seams should only be considered for high gas content coal beds and if CH_4 can be successfully recovered (Viljoen *et al.*, 2010).

2.2 CO_2 Purity for CCS

In this section, the role of gaseous impurities, i.e. non-CO_2 substances that exist as gases at STP, in the CCS system is explored. Particular emphasis is placed on condensable impurities with interest lying on the storage element, particularly with coal seam storage. However, research in this specific area does not stand alone and thus all gaseous impurities, including non-condensable impurities, in all three storage opportunities along with brief capture and transport considerations are included in the discussion where deemed relevant. This section is therefore divided into the following subsections: Impurities in Capture and Transport (Section 2.2.1), and Impurities in Geological Storage (Section 2.2.2). The last section listed operates as a review of the literature most relevant for the current project and reports relevant findings in the field.

2.2.1 Impurities in Capture and Transport

Impurity gases in CO_2 emission streams can originate from a number of different sources (Last and Schmick, 2011). As a sample case, one can consider a coal-fired power plant. The combustion process in this plant transforms the various non-carbon components of coal through reaction or vaporisation into the vapour phase flue gas. For instance, sulphur or nitrogen containing minerals in coal can react with oxygen to form SO_x or NO_x, respectively. The CO_2 in the flue gas stream can also be diluted by inert or excess gases such as Ar, H_2 or N_2. Thus, it is clear that CO_2 stream composition is a complex function of process type, process variations,

feedstocks, operating conditions, and a great deal of other factors, even before capture processes are implemented.

As mentioned in Section 2.1.2, it is necessary to use capture processes to recover CO_2 as a relatively pure stream ranging, from 85 % to greater than 99 % (International Energy Agency's Greenhouse Gas Research and Development Program (IEAGHG), 2011). Since the emphasis for CO_2 capture is placed on recovery of CO_2 rather than selective removal of other specific components, other purification technologies exist for the removal of specific substances. For example, SO_x emissions are regulated in some countries for environmental reasons, and this component may be removed via a wet desulphurisation process upstream or downstream of the CO_2 capture, or even possibly within the CO_2 capture, depending on the scenario (Mikunda and de Coninck, 2011). The type of capture process implemented also plays a role in which impurities are more significantly present. Wang *et al.* (2012) reports that among the three commonly investigated capture processes, the highest level of impurities would be present in oxy-fuel combustion, which is also possibly the most promising capture process (Bolland, 2012). In a report by the IEAGHG (2011) it is stated that SO_2 and NO_x will be captured at levels as high as 0.5 – 3 % from oxy-fuel combustion for transport and storage.

To illustrate the variability in CO_2 stream impurities, the following tables from Last and Schmick (2011), and Mikunda and de Coninck (2011) are offered respectively below (Tables 2.1 and 2.2). It should be noted that the impurity concentrations in these tables are examples indicating variability and are not binding to define the various processes.

Table 2.1: Estimated Component Concentrations in Flue Gas and Purified CO_2 Streams (Last and Schmick, 2011)

Component	Relative Proportions in Flue Gas (%[v])	Relative Proportions in Separated CO_2 Stream Without Wet Flue Gas Desulfurization Scrubber (%[w])	Relative Proportions in Separated CO_2 Stream with Wet Flue Gas Desulfurization Scrubber (%[w])	Relative Proportions in Separated CO_2 Stream with Low NO_x Burners, Selective Catalytic Reduction, and Wet Flue Gas Desulfurization Scrubber (%[w])	Estimated Concentrations in Separated CO_2 Stream, Assuming Amine Adsorption (%[v])[1]
CO_2	13.5	97.45	99.8	99.8	93.2
SO_2	0.016	2.3	0.12575	0.12575	Trace
SO_3	0.00325	0.0295	0.01535	0.01535	Trace
N_2	74.7				0.17
NO_2	0.0025	0.00585	0.0046	0.00185	
NO_x	0.06				Trace
HCl	0.00525	0.0422	0.000575	0.000575	
O_2	4				0.01
H_2O	7.7				6.5
Hydrocarbons	Trace				Trace
Metals	Trace				Trace
Hg(2+)	Trace	0.0000142	0.00000145	0.00000145	

Table 2.2: An Illustrative Calculation on the Component Concentrations of streams resulting from CO_2 capture processes (Mikunda and de Coninck, 2011)

Component	Post combustion capture at subcritical pulverized coal plant (MEA)	Pre-combustion capture at coal IGCC plant (Selexol)	Oxy-fuel combustion at supercritical pulverised coal plant (Stack gas)	Cement plant (MEA)	Refinery stack (MEA)
Argon, Ar	22 ppmv	178 ppmv	3.7%	11 ppmv	38 ppmv
Arsenic, As	0.0055 ppmv	0.0033 ppmv	0.0085 ppmv	0.0029 ppmv	
Methane, CH_4		112 ppmv		0.026 ppmv	
Chlorine, Cl	0.85 ppmv	17.5 ppmv	0.14%	0.41 ppmv	0.4 ppmv
Carbon monoxide, CO		0.13%		1.2 ppmv	
Carbon dioxide, CO_2	99.7%	98.1%	88.4%	99.8%	99.6%
Carbonyl sulphide, COS		1.7 ppmv			
Hydrogen, H_2		1.5%			
Water, H_2O	640 ppmv	376 ppmv	640 ppmv	640 ppmv	640 ppmv
Hydrogen sulphide H_2S		0.17%			7.9 ppmv
Mercury, Hg	0.00069 ppmv	0.00068 ppmv	0.0035 ppmv	0.00073 ppmv	
Nitrogen, as N_2	0.18%	195 ppmv	2.8%	893 ppmv	0.29%
Ammonia, NH_3		38 ppmv			
Nitric oxides as NO_2	1.5 ppmv	11 ppmv	721 ppmv	0.86 ppmv	2.5 ppmv
Oxygen, O_2	61 ppmv		3.6%	35 ppmv	121 ppmv
Selenium, Se	0.017 ppmv	0.01 ppmv	0.026 ppmv	0.0088 ppmv	
Sulphur oxides, as SO_2	0.84 ppmv		1.3%	0.097 ppmv	1.3 ppmv

Note: MEA (Monoethanolamine) and Selexol are the solvents used in the respective processes.

The amount and type of impurities predicted from capture processes varies considerably (IEAGHG, 2011; Li, H. *et al*., 2011). Impurities gases can be categorised into non-condensable gases, such as N_2, O_2, Ar, and H_2, and condensable gases, such as SO_x, NO_x, H_2S, and H_2O (IEAGHG, 2011; Li, H. *et al*., 2011). Other impurities include particulate matters and heavy metals (IEAGHG, 2011). It is also not uncommon to expect trace amounts of substances associated with solvent absorption columns (such as MEA or NH_3) to occur in a captured gas stream (Sakurovs *et al*., 2011).

Some main considerations with regard to impurities in CO_2 pipeline transport are, corrosion, pressure requirements and compression work, and health and safety considerations when toxic components are present (de Visser *et al*., 2008). de Visser *et al*. (2008) report that there is a lack of standards governing impurity levels permitted for CO_2 transport, and they advise some safe impurity regulations for transport. Though, they do note that some industries operate above, and even greatly above, these levels, particularly with regard to H_2S.

It is thus evident that a wide range of impurities with a fair amount of uncertainty with regard to acceptable levels are generated in the steps preceding geological storage. If it were determined that it was safe and feasible to store certain hazardous substances, for example SO_2, with the CO_2 streams, then this could have far reaching economic consequences with regard to purification or overall process selection, and potentially make certain CCS projects more attractive (Li, H. *et al*., 2011). On the other hand if geological storage forced stricter regulations to be imposed, detrimental effects on a CCS project could be encountered.

2.2.2 Impurities in Geological Storage

From Section 2.2.1, one can see that a great deal of impurity level variability exists in the processes preceding storage in the CCS chain. At each stage of CCS upstream of storage, varying regulations on the various impurity levels exist (Mikunda and de Coninck, 2011; de Visser *et al*., 2008). However, due to the uncertainties regarding the interactions of impurities and geological storage systems, whether long term or short term, no legislation quantifying the permitted impurity levels in a stream injected for storage currently exists in Europe (Mikunda and de Coninck, 2011). The composition of the injected CO_2 stream has, thus far, been left to the responsibility of the competent authority on a case-by-case basis (Mikunda and de Coninck, 2011).

This section looks at the non-CO_2 component effects in storage systems, particularly with regard to storage capacity (The reader is referred to Section 2.4 for an explanation on storage capacity). As always, emphasis is placed on impurity sorption effects on coal; however, this area of research is limited and insight into impurity effects in aquifer or gas/oil reservoirs could also be valuable.

a) Impurity Effects on Coal Storage

It was mentioned in Section 2.1.2 that the utilisation of coal seams as a CO_2 storage medium will depend a lot on its potential for ECBMR. Thus, a growing body of research into the competitive sorption-desorption interactions between CH_4 and CO_2, and the influence of N_2 exists (Pini *et al*., 2010; Wang *et al*., 2009; Ottiger *et al*., 2008; Reeves, 2001; Chaback *et al*., 1996). High pressure sorption studies are important to estimate the storage capacity of coal, to describe the sorption-desorption dynamics, and to correctly model the recovery of gas (Pini *et al*., 2010; Chaback *et al*., 1996). CH_4 and CO_2 are the main components of any ECBMR operation and N_2 has been successfully used as an alternative to or together with CO_2 (Pini *et al*., 2010; Reeves, 2001). Pini *et al*. (2010), Wang *et al*. (2009), Ottiger *et al*. (2008), and Chaback *et al*. (1996) all produced sorption isotherms experimentally for pure CO_2, CH_4 and N_2, as well as for their binary and, in some cases, ternary mixtures on different coals at pressures relevant to storage. Either gravimetric or volumetric experimental setups coupled to gas chromatographs (GC's) were used, and the experimental sorption isotherms were modelled by varying theory or correlations (for example, the Langmuir model). It must be noted that sorption isotherms are an indication of the storage capacity of coal and an explanation of sorption isotherms and measures of storage capacity is offered in Section 2.4.

Reeves (2001) presented a paper that described the fundamental reservoir mechanisms of CO_2 sequestration and enhanced CH_4 recovery. This paper also reported the field performances of two ECBMR pilot plants (Allison and Tiffany Units) in the San Juan basin. The final report by Reeves and Koperna (2008) relayed technical findings from field validation studies for these same pilot units, laboratory experiments, and theoretical model development aimed at advancing industry's understanding of coal bed CH_4 reservoir behaviour in the presence of multicomponent mixtures (CO_2, CH_4, and N_2). Selected important findings, from the literature mentioned thus far in this subsection, with regard to the behaviour of a CO_2-CH_4-N_2 system on various coals in CCS conditions, are listed below.

- The mechanisms of CO_2 sequestration and enhanced CH_4 recovery from coal by the presence of CO_2 and/or N_2 is a complex mix of physical and chemical interactions that must achieve equilibrium simultaneously in the sorbed state, as well as in the gaseous state (Reeves, 2001).
- CO_2 adsorbs to coal more strongly than CH_4, which in turn adsorbs more strongly than N_2 (Ottiger *et al*., 2008; Pini *et al*., 2010). CO_2, CH_4, and N_2 exist in the sorption phase in an approximate ratio of 4:2:1 respectively (Reeves, 2001).
- CO_2 is preferentially adsorbed in the sorption phase and thus 'pushes' CH_4 to the gas phase. N_2 on the other hand overwhelms the gas phase creating a disequilibrium and 'pulls' or strips the CH_4 from the sorption into the gas phase (Reeves, 2001). Thus, we can see how these components work to enhance CH_4 recovery and flue gas injection has been considered attractive (Reeves and Schoeling, 2000).
- An optimum ratio of N_2:CO_2 is proposed to exist in an ECBM recovery project, when accounting for the economics of separating N_2 from the recovered CH_4 stream (Reeves and Schoeling, 2000).
- Increased sorption of N_2 at elevated pressures is also seen to decrease the sorption of CO_2 (Wang *et al*., 2009).
- An additional advantage of including N_2 in the injected stream (as present in flue gas) involves coal-seam porosity. Coal swells and therefore decreases in permeability under high CO_2 pressure (Ottiger *et al*., 2008; Reeves and Schoeling, 2000). In response to this unfavourable observation, it has been proposed that the presence of N_2 in flue gas might keep the coal permeability high enough to exploit the coal seam in a more efficient way (Ottiger *et al*., 2008)
- The extended Langmuir isotherm model gas been found to be a useful tool in modelling laboratory experimental data in multicomponent systems with regard to accuracy and mathematical simplicity (Pini *et al*., 2010; Chaback *et al*., 1996; Wang *et al*., 2009). This model was shown to be inaccurate in modelling field studies, however, and thus an improved model, the Simplified Local-density Adsorption model with the Peng-

Robinson equation of state (SLD-PR model), was developed for rigorous application to CO_2-CH_4-N_2 systems (Reeves and Koperna, 2008). The SLD-PR model is capable of generating accurate isotherms based solely on information provided by coal characterisation (Reeves and Koperna, 2008).

The focus of the research above is on the major components of an ECBMR system with little or no attention being paid to minor, non-CO_2 components. This is the case even though flue gas streams, that contain a wide range of minor component impurities, have been recommended for ECBMR. Gases such as SO_2 and H_2S, although only existing in small amounts in CO_2 streams before or after capture, have been shown to have even stronger affinities to coal than CO_2 (Bachu, 2008a) – see Figure 2.5. Bachu (2008a) claims that, in the presence of multiple gases, it is expected that the amount of each gas in the sorbed state would be approximately in proportion to the respective affinities of each to coal. IPCC (2005) also mentions that the strong affinities of SO_2 and H_2S to coal would reduce the storage capacity for CO_2, on the basis that these impurities will be preferentially adsorbed. The limited experimentation conducted on CO_2-impurity mixtures and their combined sorption properties at coal-seam storage conditions warrants greater research into this subject.

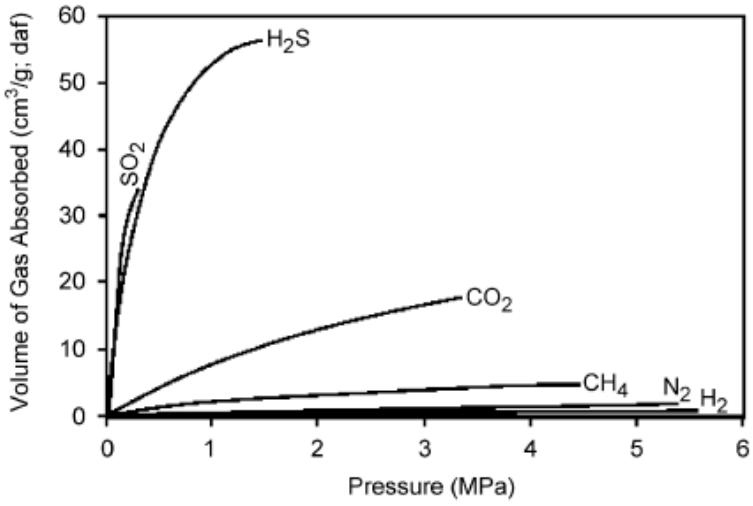


Figure 2.5: Adsorption of various components on coal (Bachu, 2008a)

There are many potential effects CO_2-stream impurities can have on coal sorption. It is proposed that minor impurity gases could compete and affect CO_2 sorption

directly. Or they could react with the coal potentially changing its structure and characteristics, affect its swelling or influence the saline coal environment which could influence the CO_2 sorption indirectly (Sakurovs *et al*., 2011). Sakurovs *et al*. (2011) also claim that even though these impurities exist in low concentrations (ranging from trace amounts to 8% (Last and Schmick, 2011)), strong sorption characteristics give them the potential to accumulate near the injection site, thus increasing the potential for additional effects.

Only two experimental studies that aim to deduce the effects of minor components on CO_2 sorption of coal have been found, namely, Sakurovs *et al*. (2011) and Mazumder *et al*. (2006). Sakurovs *et al*. (2011) conducted a relatively long-term experiment exposing a moistened Australian bituminous coal to an intensified impurity environment of substances common to various captured CO_2 streams. Pure SO_2, H_2S, NO_2, NH_3, a number of potential amine capture agents, as well as CO_2 itself, were trapped with coal samples in sealed containers for up to two years at 3 bar and 55°C. At the end of the two year duration, they evacuated the samples and measured the treated-coal's CO_2 sorption behaviour by producing sorption isotherms up to 170 bar using a gravimetric method. The coals' mineralogy was also determined before and after treatments by X-ray diffraction (XRD) analysis and He density analysis. Their main finding was that SO_2 markedly reduced the coal's CO_2 sorption capacity by 25 % by modifying the microporous structure of the coal. It is proposed that this reduction was caused by SO_2 changing the coal mineralogy by attacking the clay minerals and turning them to sulphates, as opposed to the coal's pores being blocked. Other conclusive findings were that H_2S also reduced the sorption capacity slightly, while NH_3, CO_2 and NO_2 had no significant effect (see Figure 2.6). They conclude that if SO_2 is present in a stream proposed for storage, its effect needs to be taken into account when predicting the sorption potential of the coal. Sakurovs *et al*. (2011) deduced that the strong effects observed, particularly on the coal's mineralogy, indicate that SO_2 should be avoided as an impurity if CO_2 is to be injected into an organic rich environment such as a coal seam.

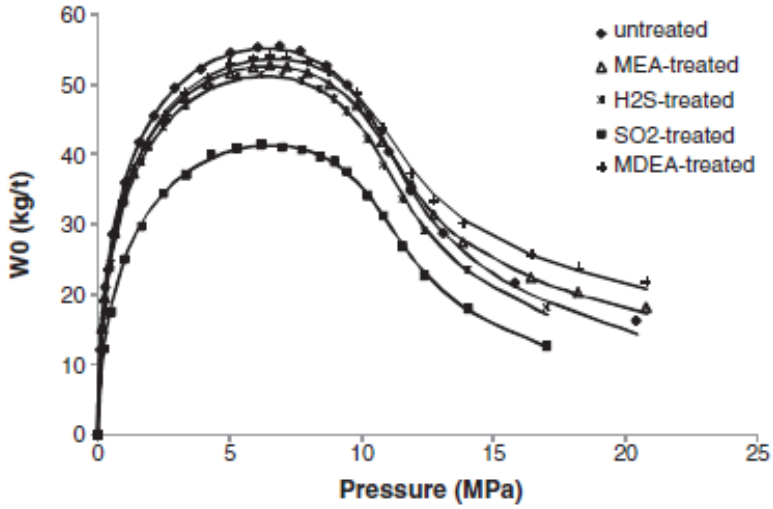


Figure 2.6: Excess sorption curves for coals pretreated with different materials plotted against pressure (Sakurovs et al., 2011). Note: W0 is the maximum sorption capacity for the coal calculated according to a modified Dubinin-Radushkevich equation fitted to excess sorption data.

The second experimental study found that considered minor component sorption on coal is one by Mazumder *et al*. (2006). This experiment compared the sorption behaviour of pure CO_2 to that of a seven-component, custom class, industrial flue gas mixture on a Polish, Selesia Basin coal (both wet and dry samples were tested). The flue gas in question had the following composition: 11 % CO_2, 0.01 % CO, 9 % H_2, 3 % CH_4, 3 % O_2, 0.1 % SO_2, balance 73.89% N_2. Sorption isotherms were produced using a volumetric method that produced measurements up to 110 bar, and stepwise desorption of the flue gas was tracked using a GC (for greater detail refer to Mazumder *et al*. (2006)). The main findings of the paper in the interest of non-CO_2 component effects were:

- The sorption capacity of coal is much higher for pure CO_2 than for flue gas. This is mainly due to the extra components (majority non-condensables) reducing the partial pressure of the main sorbing component - CO_2.
- There is indication that O_2 reacts or chemisorbs to the coal, although the authors question the reliability of results for this component.
- Measured SO_2 results are considered unreliable in this experiment due to lack of repeatability.

- CO_2 and CH_4 are strongly sorbed with CO_2 being most strongly sorbed as expected. Both N_2 and H_2 sorb very little to coal, however H_2 shows increased sorption with the presence of moisture. This is explained by the dissolution of H_2 in water.
- Good correspondence of the CO_2 sorption in the flue gas to pure CO_2 sorption indicates that the sorption of CO_2 is not hindered by the addition of other gases, other than the dilution effect of pressure.

It is thus evident that the research in this area is very limited even though there is considerable interest surrounding ECBMR applications, particularly in North America (Reeves and Koperna, 2008).

b) General and Aquifer Impurity Effects

While not much literature involving impurity interactions on coal has been encountered, a larger body of research, though still at an early developmental stage, is available on aquifer interactions and physical stream effects. The IPCC (2005) reports that gas impurities in CO_2 streams would increase the volume needed for storing a given amount of CO_2. i.e. space will be taken up in the free phase by other gases which will affect the capacity for CO_2 storage. The International Energy Agency's Greenhouse Gas Research and Development Program (IEAGHG) (2011) reports that the presence of impurities can significantly affect the phase and pressure-temperature behaviour of the fluid. Thus, common equations of state, such as the Peng-Robinson equation, are imperative to gas-mixture calculations in CO_2 storage in all media (IEAGHG, 2011).

The IEAGHG (2011) investigates the physical effects of possible impurities from, and in the range of, oxy-fuel capture processes. Topics of phase behaviour, physical storage capacity, permeation flux, buoyancy and rising velocity, and dissolution of CO_2 in formation water are addressed (IEAGHG, 2011). Some selective findings are that non-condensable impurities such as Ar, N_2, H_2 and O_2 decrease the mixture density and viscosity, lower permeability, increase the buoyancy of the CO_2 plume, and decrease the solubility of CO_2 in the formation water.

An important finding in the IEAGHG (2011) that is repeated in a paper by Wang *et al*. (2012) has to do with the influence of the non-condensable as well as condensable (SO_2 and H_2S) impurities on the physical storage capacity. Wang *et al*. (2012) derived an equation quantifying the effect of impurities on storage capacity, as a function of density and stream composition. This equation revealed that the non-condensable impurities decrease the storage capacity of CO_2 and, at a certain pressure, a maximum reduction in the storage capacity exists. It is naturally important to avoid this maximum storage capacity reduction. The effect of condensable impurities is seen to be more complex. Both SO_2 and H_2S have pressures at which the storage capacity is affected 'optimally'. For a CO_2 stream with 5% H_2S, the optimal point is the pressure at which a minimum reduction of storage capacity is observed. However, SO_2 is actually seen to increase storage capacity of CO_2 at certain pressures. At the optimal point for 3% SO_2 in a CO_2 stream, the storage capacity of CO_2 is predicted to increase by as much as 5%.

The effects of impurities in saline aquifer systems are an area in which there is a great deal of active research. The CO_2 Purity for Capture and Storage (COORAL) project is a German research project dedicated to investigating the influence of impure CO_2 in CCS since 2009 (Ruetters, 2013). This project has developed a base of specific research into the impurity effects in saline aquifer systems. It is proposed that impurities can have reactive effects with caprock and affect the mineral sequestration of CO_2 (IEAGHG, 2011). The IEAGHG (2011) perform thermochemical evaluations for SO_2, NO_x, H_2S, O_2, CO_2, and H_2 on minerals important to caprock integrity and sandstone. Important findings are that the dissolution of sandstone (represented by quartz) is not affected thermodynamically by SO_2 or NO_x but these components could dissolve several caprock minerals. However, the effect on the caprock minerals decreases with decreasing concentration of the gases.

Mikunda and de Coninck (2011) review in-depth research conducted into the interactions of impurities in saline aquifer systems over extended periods of time. They assess impurity effects on geochemical trapping, dissolved gas-rock interactions, injectivity, and impacts of certain geological formations. Many

articles reviewed in this study with regard to condensable impurities reveal consistent findings, through flow and reaction simulations, that impurities such as SO_2, NO_2, and H_2S decrease the pH of the brine through the formation of strong acids. These acidic conditions increase the rate of geochemical reactions which affects the porosity and permeability of the rock.

The injection of impure CO_2 streams into geological storage media on a commercial scale can be seen in acid gas injection. The injection of acid gas (2 % to 86 % mixtures of H_2S in CO_2) into saline aquifers and depleted hydrocarbon reservoirs has become common practice in Western Canada since 1990 (Bachu and Gunter, 2005; IPCC, 2005). This technology was introduced with the aim of disposing of H_2S (a waste gas from natural gas recovery), while CO_2 is co-injected as it is uneconomical to separate the two components (IPCC, 2005). This technology has proven successful with 41 active applications in 2003 and 5.5 Mt of acid gas being disposed of, with no incidents (Bachu and Gunter, 2005). The apparent success of this technology in Western Canada has led to research being done into the co-storage of H_2S and potentially SO_2 with CO_2 in China in a CCS context (Li, Q. *et al*., 2011). The control of H_2S and SO_2 emissions is an urgent need and the co-storage of these substances with CO_2 can be an effective way to reduce the costs of CCS.

The systems in saline aquifers are similar to coal seam systems in that they are both saturated with brine (IPCC, 2005). However, coal formation water is already bicarbonate-rich (i.e. rich in CO_2) and therefore significant solids precipitation is not expected (Reeves and Schoeling, 2000). It is recommended that the long term reaction processes in coal seam systems are investigated (Reeves and Schoeling, 2000) and insight can be gained from the methods utilised in saline aquifer research.

2.3 Components

The main components in the experiments conducted in this project are the storage medium (coal) and the gaseous components (CO_2, and CO_2-SO_2 mixtures). It is important to have a thorough understanding of all of these components, and thus

their properties, as well as various relevant features, will be discussed in this section.

2.3.1 Coal

Coal is an organic sedimentary rock that contains varying amounts of C, H, N, O, and S as well other trace elements, including mineral matter (Speight, 2005). It is an extremely complex, heterogeneous material that exhibits a wide range of physical properties (Speight, 2005).

Coal is the storage medium, or sorbent in this study, and thus most important property of coal in this regard is its ability to adsorb and absorb CO_2. Coal's affinity for CO_2 is very strong and, depending on the coal rank, between three to thirteen molecules of CO_2 can be preferentially sorbed on the coal for each molecule of CH_4 released (Viljoen *et al*., 2010). Other substances are also accepted by coal to various extents, with H_2S and SO_2 sorbed strongly and N_2 weakly (See previously in Section 2.2.2). For a full discussion on coal's sorption behaviour, refer to Section 2.4.

Coal can be classified according the degree of coalification, which gives an indication of its response to levels of heat and pressure (Schweinfurth, 2009). The categories in this classification system are known as 'ranks'. The rank of a coal is determined according to the fixed carbon, moisture, and volatile matter content of the coal, as well as its calorific value, after the content of mineral matter and sulphur have been subtracted (Schweinfurth, 2009). The coal used in the study is of bituminous rank, which is a dense, usually black coal with a high heating value that is commonly used in power generation applications (Speight, 2005). The material safety data sheet (MSDS) for bituminous coal may be found in Appendix A.1.

Analytical techniques used to characterise coal according to its composition are numerous. A proximate analysis is used to determine the moisture, ash, volatile matter, and fixed carbon composition of a coal (Speight, 2005). Ultimate analysis, determines the coal's elemental composition (C, S, N and O weight percent) (Speight, 2005). Petrography is used to determine the organic maceral (i.e.

vitrinite, inertinite, and liptinite) and inorganic mineral composition of the coal through microscopic evaluations (van Krevelen and Schuyer, 1957). The coal's petrographic composition has been identified to be an important factor for sorption of coal. For example, high-vitrinite coals have a higher adsorption capacity than low-vitrinite coals, whilst coals high in mineral content adsorb less than organic-rich coals (Bhebhe, 2008). The proximate, ultimate and petrographic analyses will all be used to characterise the coal used in the project.

The physical structure of coal, which is linked strongly to the coal's composition, is an important factor in gas storage and recovery. Coal is a porous solid that has a pore structure composed of micropores, mesopores and macropores (Gorbaty *et al*., 1986; Edgar, 1983). In coal seams, two distinctive porosity systems exist: a network of well-defined and distributed natural fractures or cleats; and a highly heterogeneous porous structure within the coal matrix between the cleats (Mandal *et al*., 2004; Shi and Durucan, 2003). The potential adsorption sites are largely within the micropores which are estimated to account for about 95 % of the coal's internal surface (Shi and Durucan, 2003). The structural properties of coal, such as porosity and surface area, may be determined by adsorption analysis of a gas (Edgar, 1983), e.g. Brunauer, Emmett and Teller (BET) analysis using CO_2.

Since the coal of interest in geological storage exists un-mined in coal seams, it is of interest to explore the properties of coal under these conditions. Table 2.3 from Zhang (2008) shows the pressure and temperature expected at various depths in a coal seam. Attention is drawn to depths greater than 800 m at which CO_2 exists in the supercritical phase. At these depths the pressure exceeds 70 bar while the temperature is greater than 42°C. The pressure and temperature specified for the sorption experiments are selected according to relevant conditions underground.

The main focus with regard to coal in this project is to ensure consistency in samples and that the coal is characterised according to proximate, ultimate, petrography, and BET analyses. This sampling and classification is vital to give meaning to the results of the sorption studies. Realistic coal seam storage conditions are selected for the sorption experiments, which are also kept consistent throughout.

Table 2.3: Coal Seam Temperature and Pressure as a Function of Depth (reconstructed from work by Zhang, 2008)

Depth (m)	Coal Reservoir Pressure (bar)	Coal Reservoir Temperature (°C)
100	10	18-21
200	20	21-24
300	30	24-27
400	40	27-30
500	50	30-36
600-700	70	36-42
800-900	90	42-48
1000-1100	110	48-54
1200-1300	130	54-60
1300-1400	150	60-66
1500-1600	170	66-72
1700-1800	190	72

2.3.2 Gases

This section describes the properties of the gaseous components that are used in this study as sorbates (i.e. the substance that sorbs onto the coal sorbent). The components selected are CO_2 and SO_2. SO_2 was selected as it is the impurity that showed the most decisive effects on coal from all the literature surveyed (see the study performed by Sakurovs *et al*. (2011) in Section 2.2.2). It would be highly desirable to perform experiments with other impurities, such as H_2S and NO_2, in addition to SO_2; however, various challenges and time constraints made these experiments unattainable. Pure CO_2 and CO_2 with a variable concentration of SO_2 were used in the experiments and therefore the relevant properties of each of these substances are reviewed. A brief account on liquefied gases is also included as well as a section on relevant equations of state. The former section is important for experimentation purposes, while latter section is important when producing meaningful results.

a) CO_2 (Carbon Dioxide)

CO_2 is a colourless, odourless, non-toxic, slightly acidic substance that exists as a gas at atmospheric conditions, approximately 50 % heavier than air (Asia Industrial Gases Association, 2009; Linde AG, 2002). Its MSDS is provided in Appendix A.2. CO_2 is the principal product of carbonaceous fuel combustion and has the ability to absorb radiant heat (IPCC, 2005). The latter property defines CO_2 as a greenhouse gas (IPCC, 2007).

In this project, CO_2 is used in the gaseous, liquid and supercritical phases, and thus it is important to have a good understanding of its physical properties. The phase change points that are of particular interest in this project are presented in Table 2.4, with the full phase diagram for CO_2 presented thereafter in Figure 2.7. From the below data, it is evident that CO_2 under atmospheric conditions can be compressed isothermally to produce liquid CO_2 at pressures in the region of 60 bar; however, to produce supercritical CO_2, the temperature must be raised above 30.98°C and pressurised to at least 73.77 bar.

The density of CO_2 is also highly relevant in the project. Density varies with pressure and temperature, and a plot of the CO_2 density is provided in Figure 2.8. Reliable density predictions are essential and the reader is referred to the *Equations of State* subsection for further discussion. Other basic physical properties, such as molar mass and solubility in water, are provided in Table 2.5 for completion.

Table 2.4: Important Physical States of CO_2 (NIST, 2011; Span and Wagner, 1994)

Point of Interest	Pressure (bar)	Temperature (°C)
Critical Point	73.77	30.98
Vapour Pressure at 20°C	57.29	20
Triple Point	5.18	-56.56

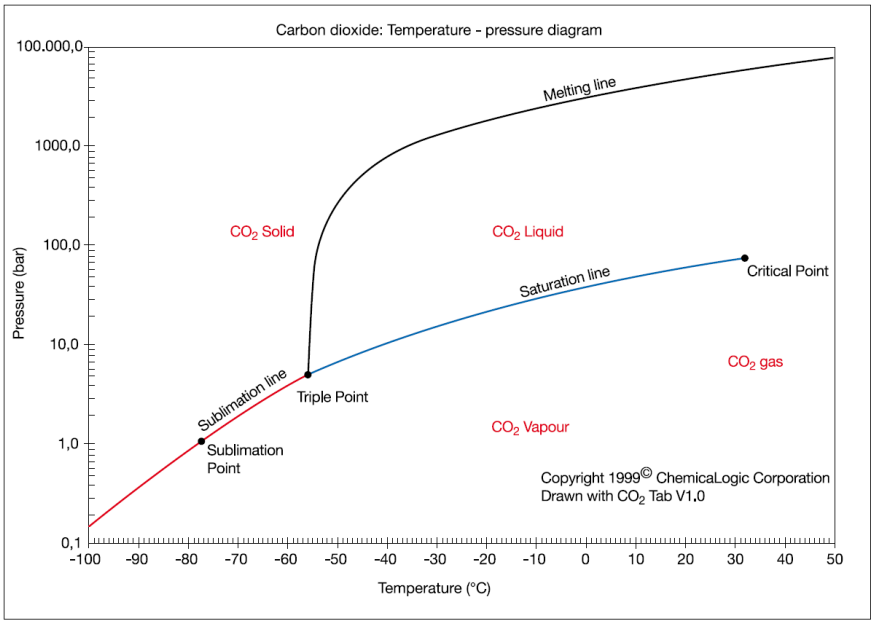


Figure 2.7: Phase diagram of CO_2 (IPCC, 2005)

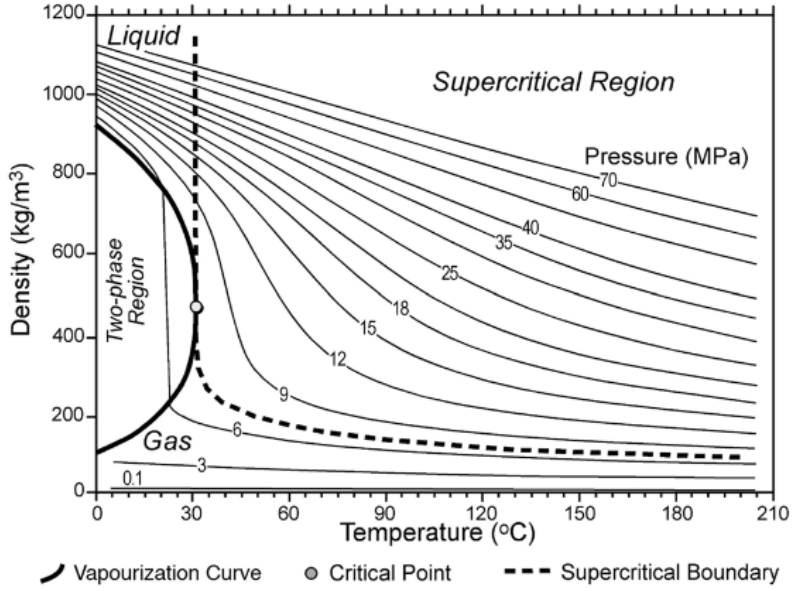


Figure 2.8: CO_2 density as a function of pressure and temperature (IPCC, 2005)

Table 2.5: General Physical Properties of CO_2 (IPCC, 2005)

Property	Value
Molecular weight	44.01
Critical temperature	31.1°C
Critical pressure	73.9 bar
Critical density	467 kg m^{-3}
Triple point temperature	-56.5 °C
Triple point pressure	5.18 bar
Boiling (sublimation) point (1.013 bar)	-78.5 °C
Gas Phase	
Gas density (1.013 bar at boiling point)	2.814 kg m^{-3}
Gas density (@ STP)	1.976 kg m^{-3}
Specific volume (@ STP)	0.506 m^3 kg^{-1}
Cp (@ STP)	0.0364 kJ (mol^{-1} K^{-1})
Cv (@ STP)	0.0278 kJ (mol^{-1} K^{-1})
Cp/Cv (@ STP)	1.308
Viscosity (@ STP)	13.72 µN.s m^{-2} (or µPa.s)
Thermal conductivity (@ STP)	14.65 mW (m K^{-1})
Solubility in water (@ STP)	1.716 vol vol^{-1}
Enthalpy (@ STP)	21.34 kJ mol^{-1}
Entropy (@ STP)	117.2 J mol K^{-1}
Entropy of formation	213.8 J mol K^{-1}
Liquid Phase	
Vapour pressure (at 20 °C)	58.5 bar
Liquid density (at -20 °C and 19.7 bar)	1032 kg m^{-3}
Viscosity (@ STP)	99 µN.s m^{-2} (or µPa.s)
Solid Phase	
Density of carbon dioxide snow at freezing point	1562 kg m^{-3}
Latent heat of vaporisation (1.013 bar at sublimation point)	571.1 kJ kg^{-1}

Where STP stands for Standard Temperature and Pressure, which is 0°C and 1.013 bar.

CO_2 is a compound with chemical properties that make it relevant to a large number of industries and areas of life. The relevant area of interest for this project

is CO_2 interactions with coal under moderate temperatures and elevated pressures applicable to coal seam storage. With regard to reactivity, any chemical reactions causing mineralisation of the CO_2 in coal are expected to take place over geological timeframes (Reeves and Schoeling, 2000). The main interaction mechanism for CO_2 in this study is sorption, including adsorption, absorption and chemisorption, which is discussed in Section 2.4.2

b) SO_2 (Sulphur Dioxide)

SO_2 exists as a colourless gas that is approximately double the density of air at normal temperatures and pressures (Air Liquide Gas Encyclopaedia, 2013). When inhaled, SO_2 has a pungent and irritating odour, and has toxicity rated at 2 ppm (Air Liquide Gas Encyclopaedia, 2013). SO_2 reacts with moisture to form H_2SO_4, which is highly corrosive. Stainless steel is satisfactorily compatible with SO_2, however high quality stainless steel is advised when there is a presence of moisture (Air Liquide Gas Encyclopaedia, 2013). A full MSDS for the substance provided in Appendix A.3. SO_2 can be found in various concentrations in coal combustion flue gas and results due to the presence of sulphur-containing minerals in coal (IEAGHG, 2011).

The critical temperature of SO_2 (157.35°C) is much higher than the moderate temperatures of the experiments conducted and thus only the gas and liquid phases of SO_2 are of relevance in this study (Hasenberg, 2008). The phase diagram and various important phase change points are offered in Figure 2.9 and Table 2.6 respectively. Using this data, it is evident that SO_2 at atmospheric conditions can be liquefied through isothermal compression once the moderate pressure of 3.309 bar is exceeded.

Table 2.6: Important Physical States of SO_2 (NIST, 2011; Hasenberg, 2008; Hogenboom et al., 1996)

Point of Interest	Pressure (bar)	Temperature (°C)
Critical Point	78.8	157.35
Vapour Pressure at 20°C	3.309	20
Triple Point	0.0165	-75.55

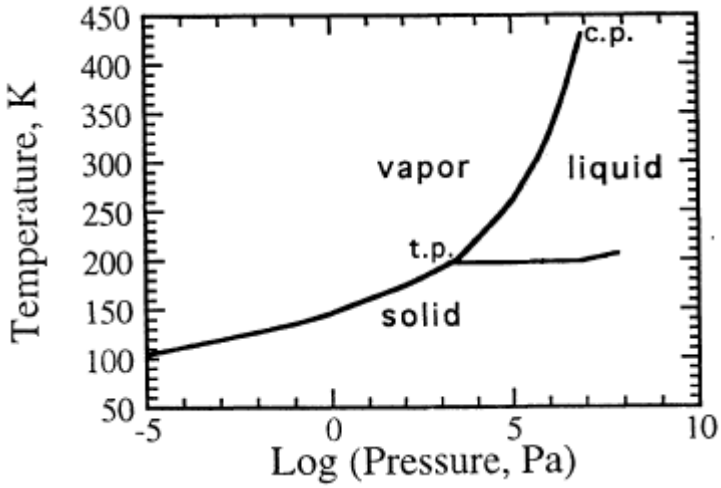


Figure 2.9: Phase diagram of SO_2 (Hogenboom et al., 1996)

c) Vapour-Liquid Equilibrium Systems

A liquefied gas is a substance that exists as a gas at STP, but can be liquefied when its pressure is raised at standard temperature through compression (Linde AG, 2002). Cylinders made with liquefied gases are pressurised so that a vapour-liquid equilibrium (VLE) exists in the cylinder. The liquid, settling at the bottom of the cylinder can be drawn while the cylinder is in the upright position using a dip tube that extends down to the bottom of the cylinder. CO_2 pressurised at its vapour pressure of approximately 57 bar at 20°C in a dip tube fitted cylinder fits this description (Linde AG, 2002). Other condensable gases, such as SO_2, are also easily liquefied at moderate pressures.

When considering a cylinder containing a more than one liquefied gas component, it is important to understand that the components will distribute themselves unequally between the liquid and the gas phase (Cheah, 2000). The VLE compositions will be a function of pressure and temperature and the partitioning of the components will be related to the volatilities of each pure component, i.e. the component that has the higher volatility will feature more prominently in the vapour phase (Cheah, 2000). When applying these principles to a mixture of CO_2 and SO_2, one can expect SO_2 to be more prominent in the liquid phase than in the vapour phase. The same conclusion can be reached by considering SO_2 is much easier to condense than CO_2.

VLE data for CO_2-SO_2 systems is limited even though it is an important impurity for CCS process calculations (Li, H. *et al*., 2011; Li, 2008). According to Li, H. *et al*. (2011), the only VLE data produced for this system was by Caubet (1901) who covered the pressure and temperature ranges of 27-105 bar and 24-143°C respectively. However, the author does question the reliability of Caubet's data due to the fact that it is over 100 years old. If VLE data is available at the relevant pressure and temperature, the liquid composition of the CO_2-SO_2 mixtures made using the mixing system described in Section 3.2 can be estimated.

d) Equations of State

With volumetric adsorption equipment, it is important to convert pressure measurements to density or specific volume, which can then be used to calculate sorption. In order to calculate the fluid density from its pressure, it is necessary to use an equation of state (EOS). A great number of EOS's have been developed, and it is necessary to select one that is appropriate to the components, phase, and temperature and pressure rages of the system. The EOS's suitable for pure CO_2, pure SO_2 and their mixtures at the experimental conditions are discussed in this subsection.

The EOS derived by Span and Wagner (1994) is widely regarded as the most reliable equation for pure CO_2 spanning a wide range of pressure and temperature conditions. This equation is a specialised EOS created empirically for CO_2 and has an estimated uncertainty of 0.05% in the density (Span and Wagner, 1994). The CO_2 density may be conveniently determined as a function and temperature from the NIST data, which uses the Span and Wagner EOS for its calculations. This data may be obtained at http://webbook.nist.gov/chemistry/fluid/ (Lemmon *et al.*, 2011).

Similarly, an empirically determined EOS has been developed for pure SO_2 over a wide range of conditions by Ihmels *et al*. (2003). This equation has reported uncertainty in the density of 0.1% at the conditions relevant to the present study. The SO_2 density can again be conveniently determined from the NIST database which uses Ihmels *et al*.'s (2003) EOS (Lemmon *et al*., 2011).

Obtaining a reliable EOS for high pressure mixtures of SO_2 and CO_2 is a lot more challenging than for its pure components. EOS's that can accurately predict the densities of high pressure mixtures of CO_2 and impurities is an area of interest in in CCS modelling processes (Mantovani *et al*., 2012; Mazzocoli *et al*., 2012; Wilhelmsen *et al*., 2011; Li and Yan, 2009). However, very few papers evaluated the influence of SO_2 with most papers choosing to focus on N_2, H_2, O_2, Ar, and CH_4, while impurities such as H_2O, H_2S and hydrocarbons have been well covered due to their importance in natural gas processing and EOR.

Li and Yan (2009) attempted to find an accurate EOS for CO_2 mixtures with a wide range of species, including SO_2. They evaluated the accuracy of seven different thermodynamic models for predicting the specific volume of different concentrations of CO_2-SO_2 mixtures over a wide range of temperatures, pressures and compositions. The accuracy was evaluated by comparing the model values to experimental values from literature. Li and Yan (2009) also calculated the binary interaction parameter for CO_2-SO_2 mixtures that can be applied to the models for greater accuracy. It is concluded that the Patel-Teja EOS is the most accurate overall for predicting the specific liquid volumes of CO_2-SO_2 mixtures having an absolute average deviation (AAD) from the experimental values of 9.28%. However, this model is seen to become considerably less accurate at concentrations of CO_2 that are higher than 90 mol%, where the AAD is approximately 23%. The performance of the models was not evaluated for mixtures greater than 92.5 mol% CO_2 due to lack of experimental data, as seen in the experimental gaps relayed by Li, H. *et al*. (2011).

It is thus seen that there are concerns around the accuracy of predicting the density of CO_2-SO_2 mixtures relevant to CCS. A simpler, general method used to estimate the density of real gases is through the use of empirical compressibility factors (Felder and Rousseau, 2000). These factors relate the magnitude to which real gases deviate from ideal gas behaviour. The compressibility factor as a function of temperature and pressure can be found for CO_2 in Perry and Green (1999), however that of SO_2 has proved a lot more difficult to find. To overcome this problem, the principle of corresponding states is used, which works on the

principle that all fluids behave similarly relative to their respective critical points (Felder and Rousseau, 2000). It is thus possible to make use of a generalised compressibility factor chart for all components, provided the value is determined at 'reduced' conditions, i.e. the ratio of experimental pressure and temperature to their respective pure component critical points.

Methods used to estimate the compressibility factor of mixtures include Amagat's Law and Kay's Rule. Kay's Rule calculates a 'pseudocritical' point for the mixture based on the molar weighted average of the pure component critical points. This parameter is then used to calculate reduced conditions from which the compressibility factor for the mixture is determined. Amagat's Law, on the other hand, makes use of the assumption that the total volume of the mixture is equal to the sum of the partial volumes of the pure components, at the pressure of the mixture (Felder and Rousseau, 2000). According to this method, the compressibility factor is determined for each pure component at the reduced pressure and temperature of the mixture. The weighted average of the pure component compressibility factors is then used as the compressibility factor of the mixture. It must be noted that that Amagat's Law does not ignore the effect the particle interactions, as does Dalton's Law, but rather assumes that the forces between molecules of different types behave similarly to those between like molecules (Woo and Yeo, 1995). Alternatively, Amagat's Law can also be applied to calculate the density of the mixture directly from the densities of the pure components using the mole fractions of each component in the mixture. This formula is shown below and is the simplest method for calculating the density of a CO_2-SO_2 mixture considering reliable pure component density values are easily obtainable.

$$\rho_{mixture} = 1/\sum {}^{x_i}/_{\rho_i} \tag{2.1}$$

Where $\rho_{mixture}$ and ρ_i are the densities of the mixture and pure component i respectively, and x_i is the mole fraction of component i.

The accuracy of the simple methods has proved to be reasonable in many cases (~10%) (Woo and Yeo, 1995), although it is difficult to deduce this for the

components and conditions in the present study. Since the systems considered contain a high purity of CO_2 (> 95 mol%), the mixture density might not deviate dramatically from that of pure CO_2 and thus estimation methods may be adequate. However, it would be best to compare the mixture density predictions from a complex thermodynamic method, such as the Patel-Teja model, with estimations obtained from simpler methods, e.g. Amagat's Law, and determine the influence this parameter has on overall sorption results.

2.4 CO_2 Storage Capacity and Sorption in Coal

2.4.1 Storage Capacity

Carbon dioxide storage capacity estimates provide an indication of how much CO_2 can be stored in a geological storage medium. These are important parameters for CCS projects as they will help estimate the lifespan for CO_2 storage or if a project is even feasible. Many methods for storage capacity estimation exist and these methods are specific to each type of storage medium (Bachu *et al*., 2007; IPCC, 2005). According to IPCC (2005), the different storage mechanisms and means of trapping suggest, in principle, the following methods:

- Volumetric trapping – the capacity is determined as the product of available volume (pore space or cavity) and CO_2 density at the *in situ* pressure and temperature.
- Solubility trapping – the capacity is the amount of CO_2 that can dissolve in the formation fluid (oil in oil reservoirs, brackish water or brine in saline aquifers).
- Sorption trapping – the capacity is the product of coal volume and its capacity for sorbing CO_2 at the *in situ* conditions.
- Mineral trapping – the capacity is calculated according to the amount of CO_2 that will be used in carbonate precipitation reactions;

Although no universally accepted methods for storage capacity estimation exists, the Carbon Sequestration Leadership Forum recommends techniques that have been established with the aim of producing a standard methodology (Bachu, 2008b). The technique recommended for coal bed storage is presented here in

order to provide a context for the sorption measurements determined in the present study. The theoretical CO_2 storage capacity can be calculated for coal seam storage according to Equation 2.2 below. This capacity represents the base level of storage capacity estimation, from which the more advanced storage capacity estimations can be determined.

$$M_{CO_2} = \rho_{CO_2(std)}.A.h.\widetilde{n_C}.G_C(1 - f_a - f_m) \quad (2.2)$$

Where $M_{CO_2}$is the theoretical CO_2 storage capacity (units of mass of CO_2); $\rho_{CO_2(std)}$ is the CO_2 density at standard (surface) conditions (units of mass per volume); A and h are the area and effective thickness of the coal seam, respectively; $\widetilde{n_C}$ is the bulk coal density; G_C is the coal gas content (dry, ash free) at saturation assuming that the coal will be 100% saturated with CO_2 (in units of volume of gas per unit of coal mass); and f_a and f_m are the ash and moisture mass fractions of the coal, respectively.

The parameter in Equation 2.2 that is most relevant to the project is G_C. This parameter is generally calculated using an adsorption isotherm model, such as the Langmuir isotherm, which can be applied to *in situ* conditions (Bachu, 2008b, 2008). The availability of experimental data specific to the coal in question is important for this parameter to be determined more accurately. The sorption calculated in this study can be converted to a G_C value at specific pressure and temperature conditions relevant to storage.

From the definition of G_C it is evident that it has been assumed that pure CO_2 will be stored independently of impurity gases and thus the effect of impurities on G_C has not been considered. While a factor can be introduced to account for the effect of impurities when they decrease the volume fraction of CO_2 and as well as influence the stream's density (Wang *et al*., 2012), it is more difficult to introduce such a factor for coal storage where experimental data is needed to quantify the effects on sorption. This project will determine whether the neglect of impurities is significant with regard to sorption in coal, and can thus recommend whether it is necessary to extend the definition of G_C to include impurities.

2.4.2 Sorption Theory

Since sorption is the mechanism by which CO_2 and impurity gases are stored in coal, it will be discussed in the literature review by means of this this section. Sorption is a term used to collectively describe interactions that occur between solid and fluid substances. These interactions can be physical (adsorption and absorption) and chemical (chemisorption) (Gertenbach *et al*., 2009; van Bergen *et al*., 2006). Adsorption in coal is the process whereby fluid molecules form a layer/layers on the internal surfaces (micropores) of the coal so that an adsorbed phase exists between the fluid and solid phases (Gertenbach *et al*., 2009). Adsorption and its reverse process, desorption, are often seen to cause volumetric changes to the coal matrix and can cause changes to the coal's porosity and permeability (van Bergen *et al*., 2006). These phenomena are known as coal shrinking and swelling. Reversible adsorption and desorption are expected to attain a state of equilibrium in a coal-CO_2 system relatively rapidly (van Bergen *et al*., 2006). Absorption occurs when the fluid molecules penetrate into the internal structure of the coal, while chemisorption involves the formation of a chemical bond between the fluid and coal surface (Gertenbach *et al*., 2009). It must be noted that adsorption is an exothermic process, as is chemisorption typically, while absorption is usually endothermic (Gertenbach *et al*., 2009). The main differences between the properties of adsorption and chemisorption are shown in Table 2.7.

Table 2.7: Difference between adsorption and chemisorption (Ruthven, 1984)

Adsorption	Chemisorption
Low heat of adsorption (less than 2 or 3 times the latent heat of evaporation)	High heat of adsorption (greater than 2 or 3 times the latent heat of evaporation)
Non specific	Highly specific
Monolayer or multilayer	Monolayer only
No dissociation of adsorbed species	May involve dissociation of adsorbed species
Significant at relatively low temperatures	Possible over a wide temperature range
Rapid, Non-activated, and reversible	Activated, may be slow, and irreversible
No electron transfer, although polarisation of adsorbate may occur	Electron transfer leading to bond formation between fluid and solid

Although adsorption, absorption, and chemisorption are easily distinguishable as concepts, it is often difficult to do so in practice (Ruthven, 1984). The term

'sorption' has been established and, in this project, is used to describe any and all combinations of adsorption, absorption, and chemisorption. Thus, the fluid in a system in which sorption is occurring is referred to as the 'sorbate' (as opposed to 'adsorbate') while the solid (coal) is termed the 'sorbent' (as opposed to 'adsorbent'). The fluid that has been 'sorbed' by the sorbent is said to exist in the 'sorbed' phase. For clarification of the terminology, Figure 2.10 has been produced.

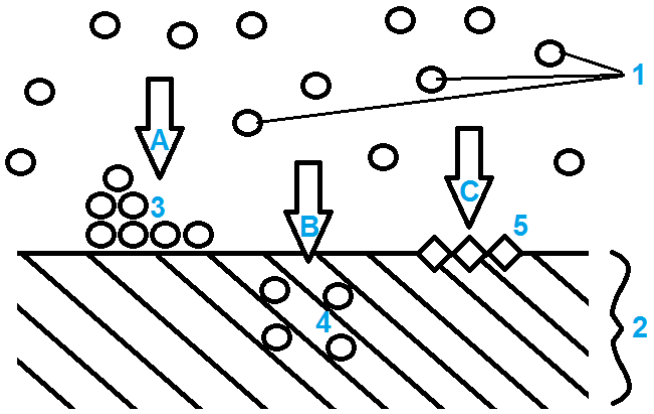


Figure 2.10: Schematic sorption process. A – Adsorption; B – Absorption; C – Chemisorption; (1) – Fluid sorbate molecules; (2) – Solid sorbent; (3), (4) and (5) – Sorbed molecules in sorbed phase

Although absorption and chemisorption are possible in a CO_2-coal system, particularly at supercritical conditions (Day *et al*.,2008), adsorption is expected to be the prevalent process considering that the experimental run time is in the order of days rather than months or years (van Bergen *et al*., 2006). Sulphur dioxide can have clear chemical effects on coal after a three year period in contact with coal, while it is also seen to adsorb very strongly (see Section 2.2.2). Due to the importance of adsorption in the study, some adsorption model theory is described here. Many adsorption models exist and some make different assumptions regarding the nature of the adsorption that occurs. The most common adsorption model is the Langmuir model that defines adsorption according to monolayer theory. This theory works on the basis that molecules are adsorbed at a fixed number of well-defined, localised sites and, once all these sites are filled, the adsorbent is fully saturated and no more adsorption can occur (Ruthven, 1984). Although this model is simple, it has been shown in some cases to successfully model the sorption behaviour of CO_2 and CH_4 in coal indicating that monolayer

adsorption takes place (Gertenbach *et al*., 2009, Chaback *et al*., 1996). Other conventional models include the BET model, where multiple layers of adsorption are accounted for; Freundich's model, which is an empirical model widely applied to heterogeneous surface systems; and Dubinin's micropore-filling model (Foo and Hameed, 2010; Ruthven, 1984; Dubinin, 1966).

Adsorption models can be used to explain and categorise the behaviour of sorption as a function of pressure, or concentration, at constant temperature. The plot of sorption versus pressure, or concentration, is known as a sorption isotherm and is a useful tool in CO_2 storage capacity studies (see Section 2.4.1). A great number of sorption isotherm models of varying complexity exist with a varying level of success observed when they are applied to CO_2-based systems with coal (Pini *et al*., 2010; Wang *et al*., 2009; Ottiger *et al*., 2008; and Chaback *et al*., 1996).

What is also relevant to the study is how to quantify the amount of sorption that occurs from volumetric experimental data. The sorption can be calculated using mass balance principles and an EOS according to the method described in Felder and Rousseau (2000). The initial number of moles of the sorbate is calculated from the volume available for the sorbate (which is possible to be determined by experimental methods) multiplied by the sorbate density at the initial temperature and pressure conditions. This density can be calculated using an EOS as described in Section 2.3.2. The final number of moles of the sorbate can be calculated at the end of the sorption experiment in the same manner. The difference between these two molar quantities is then the number of moles of fluid that have been sorbed. This quantity is known as the 'excess sorption' and is a common means of quantifying sorption (Gertenbach *et al*., 2009).

2.5 Chapter Summary

In the literature review conducted, the broad and specific context of the project was explored. CCS is a technology used to mitigate climate change and has a key role to play in reducing the cost of meeting the desired CO_2 reduction targets. Each stage of CCS was outlined, as they are all linked, and impurities allowed in the storage stage of CCS could influence the impurities desired during production,

separation and transportation stages. Unmineable coal is an unconventional CO_2 storage medium, but is important in a South African context where it is one of the primary onshore options. Sorption studies are of great value when determining the storage capacity in unmineable coal, and are in short supply in South Africa.

Studies on the effect of non-CO_2 gases, particularly strong-sorbing condensable impurities that are common in CCS, on CO_2 sorption in coal are very rare. Only two studies with relevance in this sector have been discovered (Sakurovs *et al*., 2011; Mazumder *et al*., 2006). Of the impurities investigated by Sakurovs *et al*. (2011), SO_2 had the largest effect on sorption capacity of the coal by decreasing it significantly according to the experiments they conducted. Mazumder *et al*. (2006), on the other hand, did not see a significant effect of a small amount of SO_2. Thus, the present study will hope to clarify the effect of SO_2 and make a contribution, whether by way of results and/or methodology, to CCS research as a whole.

CHAPTER 3: Methodology

The methods used to prepare and characterise the coal samples, as well as the detailed experimental procedure used to conduct volumetric sorption experiments with impure CO_2, are outlined in this chapter. Sample preparation and characterisation is included in Section 3.1 while the sorption studies are the subject of Section 3.2. Section 3.3 describes the analysis that was done on coal samples that were run in the sorption experiments.

3.1 Sample Preparation and Characterisation

As discussed in Section 2.3.1, coal is a highly heterogeneous substance and thus care must be taken to prepare representative, characterised samples that can be regarded as being from the same population. In this section, the procedure and methods used to prepare and characterise the coal samples are outlined. The following characterisation analyses were conducted once the samples were prepared, as discussed in Section 3.1.1:

- Proximate Analysis (3.1.2)
- Ultimate Analysis (3.1.3)
- Petrographic Analysis (3.1.4)
- Brunauer, Emmett and Teller (BET) Analysis (3.1.5)
- Sample Volume Determination (3.1.6)

Whilst the composition of the coal is not the focus of the project, and will remain constant throughout, it is still crucial to obtain information regarding the sorbate properties.

3.1.1 Sample Preparation

The aim was to produce thirty representative 3 g coal samples of -250 µm particle size from a large bag (approximately 50 kg) of coal obtained directly from a Witbank coal mine in South Africa. This was achieved through a series of crushing, coning and quartering, sieving, and mechanical splitting steps. Throughout the sample preparation it was assumed that coning and quartering as

well as mechanical splitting ensured that a representative fraction of the original coal sample was obtained.

The bag was initially coned and quartered twice to obtain an eighth of the initial sample. This coal was crushed to -4 mm using crushing facilities at the University of Johannesburg. This particle size was selected so that not too many fine particles were generated during this first crushing stage. The sample was then coned and quartered several more times until approximately 200 g quarters were obtained. One of these quarters was sieved using facilities at Wits so that only the particle size class above 2 mm was retained. This was in accordance with provisional plans to conduct experiments using the equipment at Tshwane University of Technology (TUT) that could not handle fine particles. A quarter of the sieved sample was set aside for runs at TUT while half of the sample was crushed to -250 µm using an in-house mill (Retsch ZM 200) for runs at Wits. The remaining quarter was crushed by the same means to -1 mm, as required for petrography. More coning and quartering as well as use of a mechanical splitter (ERIEZ 15A) was then used to divide the different sample classes evenly into final 3 g samples. The final samples were stored in 25 ml containers that were maintained at constant environment in a refrigerator. 2 g of sample was extracted from these containers for experimentation.

3.1.2 Proximate Analysis

A Perkin-Elmer Thermogravimetric analyser (TGA) situated in the School of Chemical and Metallurgical Engineering at the University of the Witwatersrand (Wits) was used to conduct the proximate analysis. Through a series of temperature ramps, certain components of the coal are combusted and thus the composition of the coal can be identified. An in-house technique was used for this analysis: the temperature was ramped up from ambient temperature until 100°C to determine the moisture content; the heating rate was slowed until 400°C was reached before being increased gradually until 700°C so that the volatile matter were combusted; the temperature was then ramped up very rapidly until 900°C so that the fixed carbon was combusted; the remaining mass indicated the ash

content. The moisture, volatile matter, fixed carbon, and ash content determined through this analysis are reported in Section 4.1.1.

3.1.3 Ultimate and C-S Analyses

The major elemental composition, C, H, and N of the coal samples was determined by ultimate analysis. This analysis was conducted at a commercial laboratory, UIS Analytical Services, to ensure reliable results. Since the S composition was not reported in the UIS findings, the S composition was determined by C-S analysis using a Leco C-S Analyser located at the School of Chemical and Metallurgical Engineering at Wits. Once all of these constituents were determined, the O composition was determined by difference.

3.1.4 Petrographic Analysis

Petrography blocks were prepared with approximately 3 g of -1 mm coal sample to which resin and hardener were applied. The surface of each block was then subjected to multistage polishing using a Struers TegraPol-11 polisher located at Wits' School of Chemical and Metallurgical Engineering, following ISO 7404 part 2.

The petrography blocks were analysed using a petrographic microscope (Leica DM2500P) located at the same venue. This analysis was conducted by Prof. Nicola Wagner and the composition of the maceral groups and mineral matter was determined following ISO 7404 part 4. These results are available in Section 4.1.3.

3.1.5 Brunauer, Emmett and Teller Analysis

The BET analysis was used to determine structural properties of coal that are important for sorption studies and for comparative purposes. These properties include surface area, micropore surface area, and pore volume. They were calculated from low pressure adsorption isotherms produced for the coal. The isotherms were determined up to a relative pressure of approximately 0.03 (experimental pressure/saturation pressure), and CO_2 was used as the adsorbent gas. Approximately 0.2 g of sample was analysed and results were calculated on a

per mass basis. The facilities used for this analysis are located at North West University, Potchefstroom campus.

The coal surface area, calculated by three different methods (BET, Langmuir and Single point), the micropore surface area, calculated by two different methods (Dubinin-Radushkevich and Dubinin-Astakhov), and the pore and micropore volumes are reported in Section 4.1.4.

3.1.6 Sample Volume Determination

It is necessary to determine the volume of the 2 g sample to be used in the sorption experiments for sorption calculation purposes (see Section 4.2 for calculations). A stereopycnometer, Quantachrome Instruments SPY-D160E, located in the School of Chemical and Metallurgical Engineering at Wits, operated with He, was used. This piece of equipment calculates the sample volume based on the principle that the solid coal particles will displace the He, with these small gas molecules able to penetrate into the particles' pores (Quantachrome Instruments, 2009).

The stereopycnometer applies a low pressure of He to cells of known volume, one of which houses the sample. The sample cell is pressurised and, once the pressure reading is recorded, the pressure is then allowed to expand into a larger known volume and the pressure recorded again. The volume of the coal sample can then be calculated using a formula derived from the ideal gas law. See Section 4.1.5 for calculation details and the average sample volume calculated.

3.2 Sorption Experiments

The amount of gas able to be sorbed by the coal samples was determined by volumetric sorption experiments. These experiments contacted gas mixtures and pure CO_2 with the samples at a single pressure and temperature for a suitable period of time. The sorption was then calculated on a volumetric basis.

This section is split into Equipment (Section 3.2.1) and Experimental Procedure (Section 3.2.2) sections. The former section describes the main piece of equipment used in the sorption study so that the reader can have a thorough

understanding of its underlying theory and functionality. The latter section outlines the actions taken to operate the equipment so that a run can be accurately replicated if desired. The results of the sorption experiments are presented in Section 4.2.

3.2.1 Equipment

The main pieces of equipment that are fundamental to this study on the sorption capacity of gas mixtures on coal are:

a) Volumetric Adsorption System (VAS) located at Wits

b) Mixture Producing System at Wits

c) Gas Chromatography (GC) at Wits.

A subsection is dedicated to describing each of these pieces of equipment.

a) Volumetric Adsorption System

A VAS is a system that aims to simulate the conditions of geological storage. This unit brings a sample, or sorbent, into contact with a fluid, or sorbate, under specified conditions of pressure and temperature, and enables the amount of sorption that occurs in a certain time period to be determined using the volumetric, or P-V-T, method. This is one of the most common methods adapted for high pressure sorption measurements (Belmabkhout *et al*., 2003). In this method, the amount of sorption is calculated indirectly using pressure measurements, an equation of state, and a mass balance (see Section 4.2 for more details).

The operating principle of the VAS can be explained through the use of Figure 3.1. Fluid is pumped into the expansion volume through V1 until the desired pressure is measured by the pressure sensor. V2 is opened and the fluid expands into the sample cell so that the sample is exposed to an instantaneous high pressure after a brief equilibration period. The expansion volume cell usually has a greater volume than the sample cell so that the drop in pressure, that occurs when V2 is opened, is not dramatic. The fluid is then in contact with the sample and sorption may occur. All the valves remain closed so that a rigid system is formed. The pressure is then tracked with time. Since the fluid cannot escape the system, a decrease in pressure indicates that fluid molecules are moving out of the

free space, into the sorbed phase of the sample. The difference in the initial pressure, i.e. once the fluid has expanded through V2 and all the valves are closed, and the final pressure, i.e. once the operator decides to end the experiment, can be used to calculate the amount of fluid sorbed by the sample in the experiment's operation time.

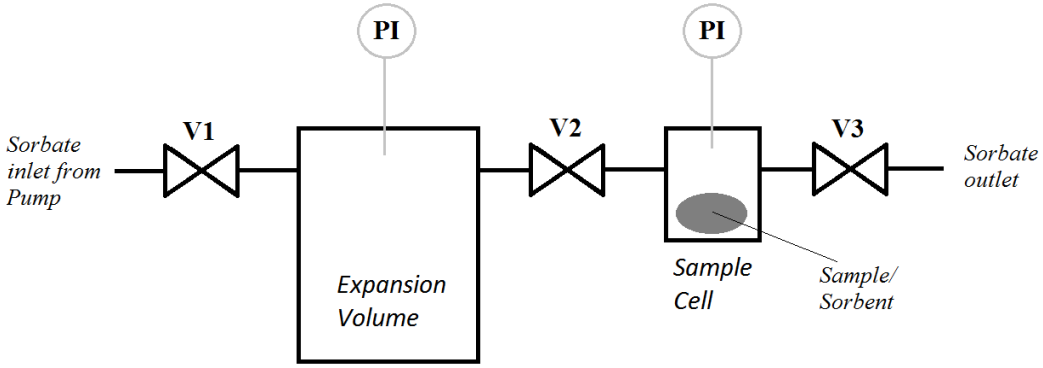


Figure 3.1: Schematic diagram of VAS internals housed in a temperature controlling oven. Valves, pressure indicators, cells, sorbent and sorbate are represented.

The VAS used in this study is located at Wits. The VAS experienced problems with leaks prior to, and for a significant portion of, this project, which frequently affected the reliability of results. Since it is important to have a rigid system for the sorption calculations, inconsistent leaks will render results meaningless. Thus, a number of pressure stability tests were performed in order to locate the leaks so that they could be fixed. Some of these tests are presented in Appendix B.1. Leaks were located at several Swagelok fittings, through several valves, as well as at the sealing surface of the sample cell. It was necessary to replace the leaking fittings with new ones and it was required to take the valves apart to clean the sealing surfaces. The sample cell leaks, however, required an entire new sample cell to be designed with more reliable, disposable seals. While the VAS at Wits was leaking, some runs were attempted using the VAS at TUT. However, these attempts also failed due to leak problems (see Appendix B.2. for a comparison between the VAS at Wits and the one at TUT). Once the VAS at Wits was modified, a pressure stability test was produced indicating that the system was leak-free before the sorption experiments were run (see Appendix B.1).

To perform a run on the VAS, it is necessary to select the desired starting pressure, number and size of incremental pressure steps, as well as the

equilibration time at each pressure. For the project it was decided that the experiments would be run at the constant pressure of approximately 85 bar for a period of 48 hours, as opposed to stepping the pressure up over a range of values to produce sorption isotherms. The selection of these parameters is justified using the following reasoning:

- Experiment runtime – If a sorbent-sorbate system is allowed to stand for a sufficient period of time, a state of equilibrium is reached where desorption occurs at the same rate as adsorption (Section 2.4.2). The experiment runtime for sorption studies varies greatly in literature (4 hours to weeks are reported for adsorption equilibrium attainment in different coals (Day *et al*., 2007; Gertenbach, 2009)), but longer times are deemed preferable where the system is allowed to reach equilibrium. From preliminary experiments for the system at hand, it was seen that it could take up to 20 hours for the pressure to plateau, indicating that equilibrium had been reached. Thus, a safe experiment runtime of 48 hours was selected for the project, which, due to time constraints, allowed for only one pressure to be tested. The presence of impurity gases in the sorbate and their unknown influence in the sorbent also played a role in the decision for a longer experiment runtime.
- Single pressure – The pressure of 85 bar was selected as this corresponds to a depth of 700 – 800 m below the surface, which is relevant to CO_2 storage (see Section 2.3.1). Since the focus of the project is on the effect of the impurity components on sorption capacity, it was deemed sufficient to compare sorption capacities calculated for a single, relevant pressure. Varying the pressure was left as a recommendation pending the project results.
- Experiment temperature – In order to simulate underground storage conditions, the temperature corresponding to the depth of 700 – 800 m was selected. This temperature is approximately 40°C (see Section 2.3.1) and was applied as a set point to the oven.
- Sorbate sampling – If the pressure was stepped up, it would require a sorbate sample to be drawn and sent to the GC at each pressure step. This

sampling procedure is not automated and thus a run could not be left to run over night without requiring the operator to be there at odd hours.

The full procedure for the VAS experiments is explained further in Section 3.2.2.

Overview of Operation. The reader is directed to Figures 3.1 (VAS oven internals) and 3.2 (full VAS system) which supplement the description. A liquid phase CO_2-rich gas is supplied from a cylinder/vessel fitted with a dip tube (either located in an external cylinder storage cage or the mixing setup, see next subsection) to an automatic Teledyne Isco syringe pump. The pump is able to control the pressure to a desired set point in an expansion volume cell, which is connected to the pump via a pneumatic valve (V1) (Figure 3.1). The gas can be sampled from the expansion volume cell through a GC sampling system made up of a manual system of valves so that the composition of the gas before analysis may be determined. Once the pressure in the expansion volume is set to the desired pressure, the fluid is expanded through a second pneumatic valve (V2) into a sample cell in which a storage medium sample (in this instance coal) may be placed. V2 is closed and the fluid sample from the expansion volume is sent to the GC. The system is left pressurised for a desired amount of time. Both the cells and the interconnecting valves are housed in an oven in which the temperature can be held at a set-point. Pressure and temperature sensors measure the respective conditions of both cells, and acquisition hardware collects this data and transfers it to a PC. Once the time has elapsed, the run is stopped and the contents of the cells vented to the atmosphere through V3 (another pneumatic valve that leads out of the sample cell and has remained closed thus far) and an external instrument panel. Before the fluid is vented, a sorbate sample from the sample cell may be extracted through another route of the GC sampling system for analysis. The events described thus far, other than the fluid sampling, may be automated via PC programming.



Figure 3.2: Complete VAS as viewed in the Laboratory at Wits
Labelled Components:
A- Teledyne Isco Syringe pump for raising fluid pressure
B- Oven housing high pressure system (expansion volume and sample cells)
C- Instrument Panel to GC for fluid sampling
D- Instrument Panel to vent and vacuum pump
E- Control panel operating pneumatic valves with pressure display
F- National Instruments CompactRIO hardware for data capture and automation. Out of picture to the left is the fluid supply, and to the right is the PC linked to the CompactRIO

Description of VAS Components. Various important components making up the VAS are isolated and described in more detail here. The components were ordered from a variety sources and custom made by Chemvak cc, based in Centurion, Pretoria. A number of students have completed their MSc and PhD studies using this VAS, including Maphada (2012) and Maphala (2012).

Liquid CO_2 and Mixture Supply – Liquid CO_2 is supplied to the syringe pump from a standard Afrox liquid CO_2 cylinder fitted with a dip tube. The mixtures are supplied after being mixed from pure components supplied by standard cylinders in the laboratory using a mixing system designed and custom-made by Chemvak cc (discussed further in 3.2.1(b)).

Teledyne Isco 260D Syringe Pump – Pressurises the fluid and supplies it to the expansion volume until the desired pressure is reached. The pump is specifically designed for high pressure fluid and contains an automated pressure control system.

Expansion Volume Cell – An off-the-shelf stainless-steel vessel of approximately 30 ml specified to 120 bar. It is pressurised with the fluid sorbate to a specified set-point before the fluid is allowed to enter the sample cell.

Sample Cell – A predominantly stainless-steel 'vessel' of approximately 4 ml manufactured from Swagelok fittings that houses the sample of geological storage medium. These fittings are specified to hold pressures in excess of 300 bar. It is detached from the system and filled with a sample when necessary. Copper seals are used to ensure the cell is pressure tight and require frequent changing. Once the expansion volume has been fully pressurised, the gas is allowed to enter this vessel to contact the sample.

Pneumatic Valves – Swagelok valves run by compressed air supplied from a cylinder at 8 – 10 bar. They can be operated manually, at a control panel, or automatically, via software, to control the flow of fluid into and out of each storage vessel.

Oven – The vessel system is housed in an oven that can be used to create an approximately isothermal environment for the vessels. The temperature can be specified from ambient conditions up to 60°C and controlled to within 0.5°C.

GC Sampling System – A manually operated system of valves that enables the withdrawal of fluid samples from either the expansion volume or sample cell. The sampling system leads directly to a line connected to the GC. A N_2 purge line and line to a vacuum pump also exist to prevent sample contamination.

Brüker 430 GC – This unit is used to analyse the composition of the gas samples from the VAS before and after the sorption experiments are run. It contains a thermal conductivity detector (TCD), auto-sampling valve, and HayeSep N packed column that enables the separation of CO_2 and SO_2. The carrier gas used is N_2. More information on the GC analysis conditions is provided in Section 3.2.1(b).

Instrument Panel to Vent and Vacuum Pump – An instrument panel with manually operated Swagelok valves that control the flow of the fluid once it leaves the sample vessel. The gas may be vented to the atmosphere or the oven system may be vacuumed prior to being pressurised using a vacuum pump. The panel also directs the flow for sample degasification.

Sample Degasifying system – Consists of a clamp-on heater, zeolite volatiles trap, and the same vacuum pump used to vacuum the oven vessels and GC sampling system. Prior to connecting the sample vessel to the system in the oven, the sample must be degasified to purge it of all impurities and open the sample pores. This is achieved by attaching the sample vessel to the clamp-on heater and vacuuming the sample, through the volatiles trap if needed, by selecting the desired flow course on the instrument panel for the desired amount of time.

Control Panel – Allows for the manual operation of the pneumatic valves and contains displays for the pressure and temperature of the vessels that have been measured with appropriate instrumentation setups. A switch enables automated or manual operation to be selected.

National Instruments CompactRIO and PC – The data acquisition, measurement, display and control processes are handled by a National Instruments CompactRIO and Systems Integration hardware supplied by National Instruments coupled to a PC with LabVIEW software programmed by JAD Systems. More specifically, the pneumatic valves and Teledyne Isco pump can be operated automatically via the CompactRIO and LabVIEW programming which also collects the pressure and temperature data over the course of the experiment.

b) Mixing System

The mixing system is a system designed and custom-built by Chemvak cc that makes it possible to produce liquid mixtures of up to five component inputs. This piece of equipment was introduced to the laboratory in 2013 and the present study is the first project to involve it. The substances input to the mixing system are typically pure species, and the liquid phase of the mixture is only ensured if the mixture is predominantly liquid CO_2. The mixture is made up roughly using pressure readings and an equation of state, and then the composition is verified via GC analysis. A rotational setup is required to ensure the components mix thoroughly. The mixing system is portrayed in Figure 3.3.

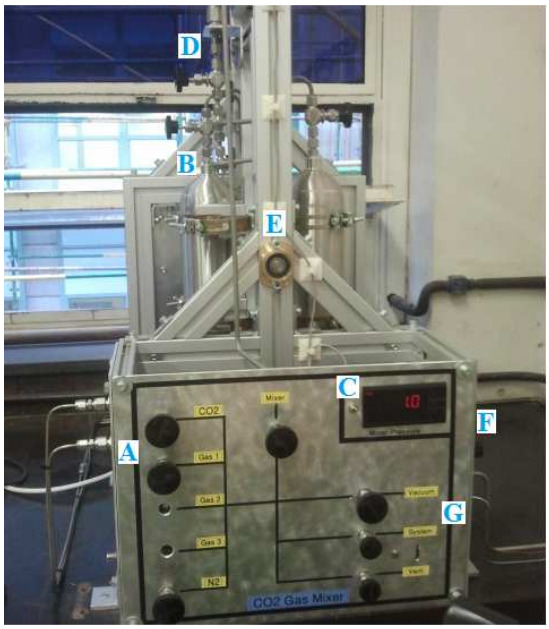


Figure 3.3: Mixing System as viewed in the Laboratory at Wits
Labelled Components:
A- Inlet ports and valves – Control entry of pure components from respective cylinders
B- Mixing Vessels – Stainless steel vessels, fitted with dip tubes and containing ball bearings, that mix and house mixture
C- Pressure display – Relays pressure in the Mixing Vessels
D- Valves leading into Mixing Vessels – Controls entry and exit of fluids into Mixing Vessels
E- Axis around which Mixing Vessels rotate – Allows for thorough mixing of components
F- Rotation controls (out of sight) – Controls speed of Mixing Vessel rotation
G- Outlet ports and valves – Control exit of mixture from Mixing Vessels to VAS and vent, as well as line to vacuum pump

Motivation for Mixing System. In order to appreciate the need for a custom-made mixing system, it is necessary to have an understanding of the operation of the Teledyne Isco syringe pump. This pump supplies the fluid to the VAS vessels and functions similarly to a syringe. It compresses the fluid in a rigid space within the pump until the desired pressure is obtained. Once this is achieved, the fluid is sent to the rest of the system. For the pump to operate effectively with CO_2, a liquid feed is required. If gaseous CO_2 is fed to the pump, and a high pressure output is required, the pump will compress the CO_2 until it liquefies and beyond. Due to the small volume of liquid CO_2 compared to the gaseous CO_2 that was initially present, the pressure supplied to the VAS vessels when the fluid is released to the rest of the system may not be sufficiently high.

The mixtures desired for the project are theoretical imitations of captured CO_2 streams of which the composition is 90% CO_2 or greater. Thus, based on the

requirements of the Teledyne Isco syringe pump, liquid phase mixtures of the desired captured CO_2 stream composition are necessary. Local gas suppliers, Afrox and Air Liquide, were unwilling to supply ready-made cylinders containing liquid mixtures of CO_2 and a condensable impurity. They were only prepared to supply pure liquid CO_2 or gas phase mixtures, neither of which was sufficient for the task at hand. Thus, it was decided to design and construct equipment that would enable the production of liquid mixtures from pure components on lab-scale.

Liquid Mixture Theory. The challenge with liquid mixtures relates to the VLE existing in a liquefied gas cylinder. The reader is referred to the relevant section of Section 2.3.2 for more information on liquefied gases. If a small amount of SO_2 is introduced into a liquefied CO_2 cylinder, the SO_2 will partition itself between the liquid and the vapour phase. A literature study produced by Chemvak cc (2012) determined that, although a VLE will form in the mixture (both components existing in sTable Doncentrations in each phase), this may take, in some cases, an inordinately long time. Thus, in order to promote a homogeneous mixture it is necessary to agitate the mixture (Chemvak cc, 2012). In this project, this is done by rotating vessels with ball bearings within the vessels (see Figure 3.3). Small volumes of mixtures that can be used soon after they are made up have been selected in order to avoid settling out of components. It is difficult to predict the concentration of the liquid mixtures made up accurately; however this problem is overcome by analysing the mixtures by GC analysis prior to introduction into the sample cell of the VAS.

Overview of Operation. Components are loaded one at a time into the mixing vessels, starting with the component that is supplied at the lowest pressure or is required to be at the lowest composition in the mixture. For instance, for a binary mixture of SO_2 and CO_2 to be produced, the low pressure SO_2 is loaded first until the desired pressure reading is achieved in the mixing vessels (e.g. 1 – 2 bar). Liquid CO_2 (~45 bar) is then allowed to enter the mixing vessels slowly until they are topped up. It is important to vent, flush and vacuum the common lines to the mixing vessels when loading different components for precise operation. Now

that both components are present in the mixing vessels, they are rotated mechanically for approximately 15 minutes, so the components can be assumed to be homogenously mixed. The mixture is then ready to be fed to the VAS for GC analysis and sorption experiments.

c) Gas Chromatography Analysis

The GC analysis had two functions: firstly, to accurately quantify the concentration of the mixture sent to the VAS from the Mixing System; and, secondly, to determine the change in concentration of the sorbate from the beginning of the sorption experiment to its completion. Thus, it was possible to deduce whether selective sorption had taken place to the extent that the concentration of the sorbate changed through the course of the experiment.

GC Specifications. A GC is an instrument that operates on the principle that different compounds have different elution rates when passed through a specialised column. The individual components are thus separated in the column and detected once they exit the column by a means that reacts proportionally to the amount of component present (Poole, 2012). The GC used in this study is a Brüker 430-GC, and is connected via a line to the sampling system of the VAS. The Brüker is equipped with a HayeSep N packed column that is capable of separating sulphur gases. The detector used is a TCD, which is a bulk property detector that detects changes in thermal conductivity. A disruption, or 'peak', in the carrier gas baseline indicates that a substance has passed through the detector. N_2 is used as the carrier gas that 'carries' the sample through the column and an auto-sampling valve is equipped.

A relatively short temperature programme for the GC oven that would allow for good peak separation of the components in question (CO_2 and SO_2) was set up through a trial and error method upon sample injections. This temperature programme of the oven is shown graphically in Figure 3.4. The injection temperature and detector temperature in the GC program were set to 140°C and 270°C respectively. The reference flow for the carrier gas was 30 ml/min with a make-up flow of 5 ml/min.

The GC was calibrated for relevant concentrations of SO_2. In order to do this it was necessary to run standard gas samples of SO_2 through the GC and produce a plot of peak area versus concentration to which a calibration curve could be fitted. This calibration curve is presented in Figure 3.5. The calibration gas samples were drawn from certified gas mixture cylinders (1.5% SO_2 and 5% SO_2 in CO_2) purchased from Afrox, which were loaded into Altef™ gas sampling bags. Five injections per sample were run and the average value plotted for each. The fitted calibration curve is linear and is used to calculate the concentration of unknown mixtures using the peak area response obtained when running it through the GC.

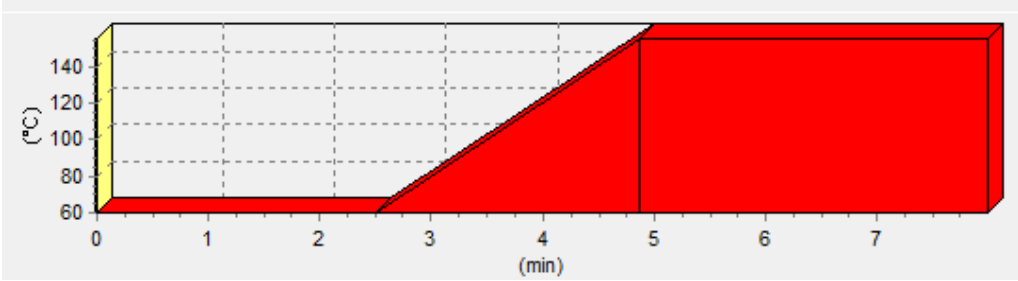


Figure 3.4: Temperature Program for GC method

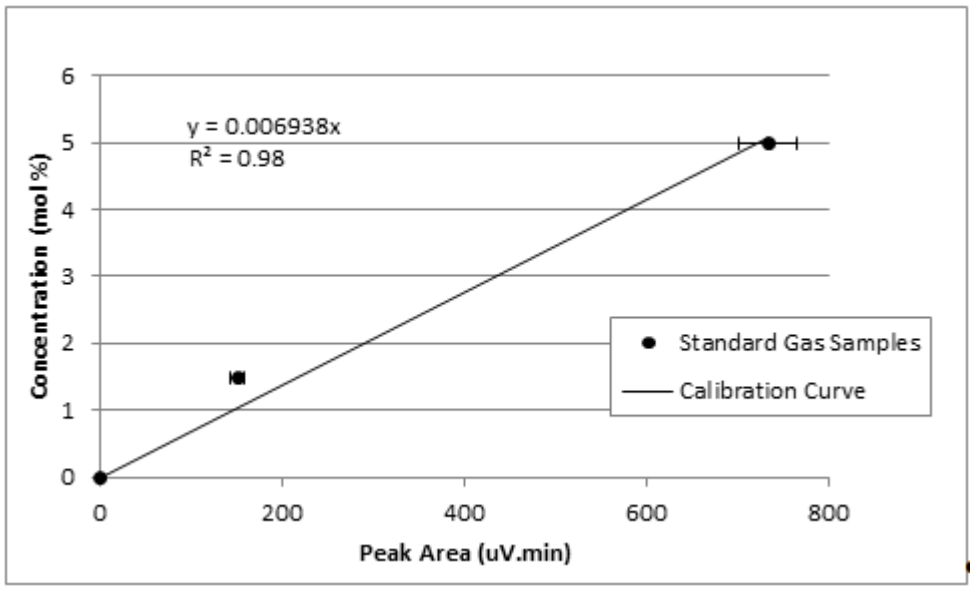


Figure 3.5: Calibration Curve produced for SO_2

Overview of Operation. The GC is first prepared for sample injection according to the procedure described in Section 3.2.2. Once the VAS has been fully loaded with the mixture made in the Mixing System, the fluid is allowed to pass to the sample cell, and all VAS valves closed; a fluid sample is drawn from the reference cell and allowed to pass through the line to the GC. The gas from the

reference cell is analysed a number of times to obtain an average, but precise, value. At the end of the VAS experiment, a sorbate sample that has been in contact with the coal sample for 48 hours is drawn from the sample cell and analysed in the same fashion by the GC. The chromatograms for the sorbate are thus available at the outset and end of the sorption experiments. The GC analysis results for the project are presented in Section 4.2.4.

3.2.2 Procedure

In this section, the sorption experiments are divided into stages, which make up the complete experiment. Full instructions are given in bullet form in Appendix C so that the experiments may be repeated precisely if required.

a) Sample Degassing

It was necessary to heat and vacuum the coal sample to ensure that unwanted volatiles did not escape from the sample during the sorption experiment runs and interfere with results. The vacuum system shown in Figure 3.6 and experimental details are given in Appendix C.1.

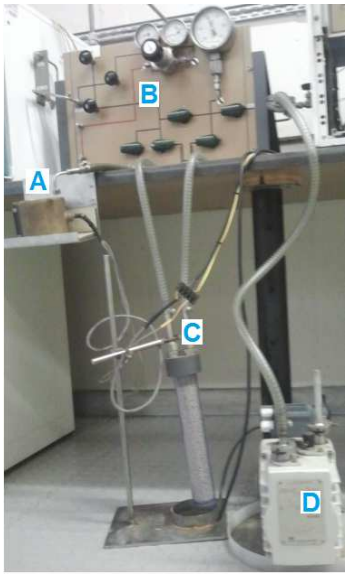


Figure 3.6: Vacuum setup for sample degassing.
Labelled components: A- reactor heating jacket; B-Instrument Panel; C- Cold trap; D- Vacuum pump

b) Free Volume Determination

In order to calculate the amount of sorption occurring in the experiments it was required to know the volume available for the fluid surrounding the sample in the

rigid VAS vessel system. See Figure 3.7 for a depiction of this volume, which is referred to as the 'free volume'.

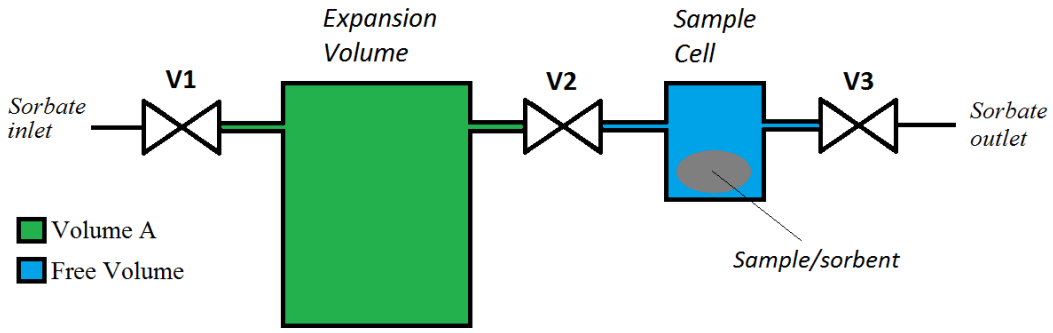


Figure 3.7: Schematic diagram of VAS pressure vessels indicating volumes of interest, i.e. the volume between V1 and V2 (Volume A) and the volume between V2 and V3 (Free Volume)

The VAS volumes were calculated using the ideal gas law in various pressuring and expansion experiments using He gas at low pressures. The detailed procedure for determining the free volume is provided in Appendix C.2.

The results for the free volume of the system calculated are presented in Section 4.2.1.

c) VAS Operating Procedure

The procedure presented in Appendix C.3 describes step by step how to run the VAS as used in the sorption experiments. The VAS is central to the sorption experiments, as described in Section 3.2.1.a. Twelve runs in the VAS were performed – 3 runs for pure CO_2 and 9 runs for mixtures. In each case, the procedure was designed so that the raw data necessary to calculate amount of sorption that took place in a degassed 2 g coal sample was obtained. Sorption took place for 48 hours at constant temperature and pressure (40°C and 85 bar), and the component-wise sorption of each gas in the mixture was also identified. The procedure for drawing gas samples from the VAS is also described in Appendix C.3.

d) Mixing System Operation Procedure

The systematic procedure followed to produce nine different gas mixtures used in the VAS sorption experiments is presented in Appendix C.4. The mixtures consisted of CO_2 and SO_2 where the concentration of SO_2 ranged from

approximately 0.2 mol% to 6.7 mol%. These concentrations were made up through estimation on a pressure basis, as described in Section 3.2.1.b.

e) GC Operating Procedure

Gas samples were analysed from the sorption experiments via GC analysis at the beginning and end of each VAS run, as described in the VAS Operating Procedure (see Appendix C.3). In order to obtain an average concentration measurement for each sorption experiment, three to five gas samples were analysed. The column was conditioned according to suitable GC operating guides prior to the experiments. The procedure used to operate the GC is outlined in Appendix C.5.

3.3 Post-Sorption Analysis

Fourier transform infrared spectroscopy (FTIR) analysis was performed on selected coal samples once the sorption experiments were completed and the sorption quantified. The samples were removed from the sample cell, thereby being restored to atmospheric conditions, after being exposed to the high pressure fluids for 48 hours and sent to the School of Chemistry at Wits where the analysis was conducted. FTIR analysis was not included in the original plans of the project which aimed to determine how sorption was affected by the presence of impurities; but was rather added to supplement sorption results by attempting to explain why certain impurity effects are observed.

FTIR analyses the surface functionalities and the type of functional groups present on the pulverised coal sample by measuring their absorbance of infrared radiation (Thermo Nicolet Corporation, 2001). It is valuable in this project as it can be used to determine whether there have been any changes to the chemical structure of the coal, and can thus identify whether there have been any lasting effects on the coal (e.g. chemisorption) as opposed to only reversible adsorptive processes during the sorption experiments (Goodman *et al*., 2005). The experimental procedure for the analysis included the use of a Brüker Tensor 27 Fourier Transform Infrared spectrometer which recorded the spectra in the range of 550-4000 cm^{-1} with a

resolution of 4 cm^{-1}. The samples were not degassed before analysis and the experiments were performed at ambient conditions.

Three coal samples that had been treated with different concentrations of supercritical CO_2-SO_2 mixtures were analysed, and were compared with a sample that had been treated with pure supercritical CO_2 and a sample that had not been treated. The samples for the CO_2-SO_2 mixtures were selected on the basis that different sorption results had been observed for these samples that could benefit from further analysis (see Section 4.2.6(b)). The FTIR results are presented in Section 4.2.5.

3.4 Chapter Summary

In this section, the methodology derived to achieve the aims and objectives of the study is presented. The means by which the coal samples were prepared was described, along with the methods used to characterise the coal so that its important characteristics are known. The volumetric adsorption experiments (headed 'Sorption Experiments') are described in full. The relevant pieces of equipment, i.e. VAS, Mixing System, and GC, are explained and the operating procedure for each is provided. The Mixing System and GC analysis linked to the VAS are introduced for the first time in this report.

CHAPTER 4: Results and Discussion

This chapter is split into the coal sample characterisation results (Section 4.1) and the sorption experiment results (Section 4.2) that were obtained from conducting the experiments described in the methodology, Section 3. This chapter follows a format in which the results are first presented and then discussed.

4.1 Coal Characterisation

The coal analysed in this study is a bituminous coal extracted from a South African coal mine in a Witbank coalfield. Small samples that are assumed to be homogenous were prepared from this coal as described in Section 3.1.1. These samples were then subjected to proximate, ultimate, petrographic, BET, and volume determination analyses, as described in Sections 3.1.2 to 3.1.6. These analyses are important so that the findings of the main sorption experiments can be deemed applicable to a coal with specific properties. The results of each characterisation analysis are reported in the sub-sections that follow.

4.1.1 Proximate Analysis

Three runs of 15 mg of the coal sample were performed on the TGA in order to determine the average moisture, volatile, fixed carbon and ash content of the coal samples. The results obtained are presented in Table 4.1.

Table 4.1: Composition of Coal as determined from Proximate Analysis

Run	Percentage of Sample (%)			
	Moisture	**Volatile Matter**	**Fixed carbon**	**Ash**
1	4.62	16.70	42.39	36.29
2	3.86	20.50	42.66	32.98
3	3.68	20.01	41.55	34.76
Average (wet basis)	**4.05**	**19.07**	**42.20**	**34.68**
Average (dry basis)	**-**	**19.87**	**43.98**	**36.14**

It is evident that the coal has a high ash content that is typical of South African coal from the Witbank area. Due to the high ash content, the volatile yield and fixed carbon content are in the lower range expected of a bituminous coal (Speight, 2005).

4.1.2 Ultimate and C-S Analyses

The C, H, and N composition in the coal was determined from the ultimate analysis, while the S composition was determined from C-S analysis, as described in Section 3.1.3. Thus, once the O composition is determined by difference, the composition of all major coal constituents is known, and the results are presented in Table 4.2.

Table 4.2: Major Elemental Composition of Coal Sample

Element	Percentage of Sample (%)
C	42.2
H	2.86
N	0.99
S	0.88
O	14.34

Note: *O composition was determined on an ash free, dry basis, based on the Proximate analysis results (Section 4.1.1)*

In order to interpret the results, they are compared to ranges expected for bituminous coal reported in Speight (2005). The elemental C and H composition are lower than typical values (65% to 80% for C and 4.5% to 6% for H). However, this is due to the greater presence of inorganic ash present in the coal which exceeds the typical range of 4% to 15% by a great margin (see Section 4.1.1). The N and S composition fall within the expected range, and the O content is seen to be only slightly higher than the 4.5% to 10% range in reported in literature.

4.1.3 Petrographic Analysis

The maceral and mineral composition of the coal was determined through the petrographic analysis described in Section 3.1.4. The summarised results are displayed in Table 4.3 and the full report, including sub-maceral and mineral groups, is available in Appendix E.2.

Table 4.3: Petrographic Composition of Coal

Maceral Groups	Volume Percent (%)
Vitrinite	33.1
Liptinite	5.1
Inertinite	36.7
Mineral Matter	25.1

From these results, the coal has been described as a typical high ash, inertinite-rich, high volatile bituminous C Witbank coal.

4.1.4 BET Analysis

The surface area, micropore surface area, and pore volume of a 0.2080 g sample of the coal in question were determined. This was achieved through modelling calculations conducted on a low pressure CO_2 isotherm produced experimentally for the coal. The isotherm on which the calculations were based, along with more experimental details, is presented in Appendix E.3.

The surface area available to adsorb CO_2 per mass of sample was calculated according to three different methods, namely: Langmuir, BET and Single Point (at a specified pressure) methods. The results are shown in Table 4.4.

The micropore surface area was calculated by the Dubinin-Radushkevich (DR) and Dubinin-Astakhov (DA) methods. The maximum pore volume was calculated by the Horvath-Kawazoe (HK) method using a single point and the limiting micropore volume was determined according to the DA method. The monolayer capacity was also determined by the DR method. These results are depicted in Table 4.4.

Table 4.4: Summarised BET Results specifying the modelling methods used for calculation

Surface Area (m^2/g)		
Numerical Method:	Langmuir	87.30
	BET	81.71
	Single Point	70.62
Micropore Surface Area (m^2/g)		
Numerical Method:	DR	122.78
	DA	150.91
Maximum Pore Volume (cm^3/g)		
Numerical Method:	HK	0.0293
Limiting Micropore Volume (cm^3/g)		
Numerical Method:	DA	0.0634
Monolayer Capacity (cm^3/g)		
Numerical Method:	DR	26.88

From the results in Table 4.4 it is evident that there is some variation between the specific surface area and micropore surface area values that are calculated by the different methods. Differences in these values are, however, expected and are due to the different assumptions implicit to each calculation method. In this study, these details are provided so that accurate comparisons can be made.

The values in Table 4.4 were compared with those of Maphala (2012), who also conducted surface area and pore analysis on a finely crushed, bituminous South African coal. Maphala (2012) considered Langmuir, BET and single point methods in his analysis, and all compared results were similar; as would be expected due to the similarity in coal type and region, as well as the sample preparation technique.

4.1.5 Sample Volume

In order to determine the average volume of the coal samples, three 2 g samples were run in a stereopycnometer. For the average measurement, two pressure readings per stereopycnometer run were taken, and three runs per sample were performed. Three samples were used in the stereopycnometer in order to obtain sufficient data for a confident volume measurement. To calculate the sample volume, the pressure readings recorded were inserted into Equation D.1 that is presented and described fully in Appendix E.1.

A description of the experimental procedure accompanied by detailed working is offered in Appendix E.1. The summary of the results is reported below in Table 4.5.

Table 4.5: The volume determined for three identically prepared 2 g coal samples

Sample	Volume (cm^3)
1	0.977
2	1.000
3	0.928
Average	**0.968**

Thus, the average volume of 2 g of -250 µm particles of the Witbank coal used is calculated to be 0.968 cm^3.

In order to check this value of the sample volume, the density of the coal is calculated by dividing it by the mass of sample (2 g). The density of the sample is thus 2.07 g/cm^3. This value is a high considering the density of bituminous coal is reported to range from 1.28 g/cm^3 to 1.35 g/cm^3 (Speight, 2005).

The reason for the inaccurate density determined is suspected to be due to several sources of experimental error during the stereopycnometer runs. The pressure in the stereopycnometer cells was seen to fluctuate a great deal at times when it was required to take pressure readings. This made taking experimental readings challenging and could lead to inaccurate measurements. The main reason for the fluctuations encountered arises from the sensitivity of the pressure in the stereopycnometer cells to fluctuations with temperature. Factors contributing to unstable temperature include heat dissipation from the equipment, and the temperature of the sample equilibrating. Volatiles escaping from the sample could also influence the stability of the pressure. The calculations are strongly dependent on pressure measurements and thus minor errors in the readings are magnified.

Nevertheless, relatively small errors in the value of the sample volume will not have a great bearing in calculations used to determine the magnitude of the excess sorption (the sample volume is relatively small compared to the sample cell volume; see Section 4.2.1). The magnitude of the sample volume will also have no consequence when comparing the amount sorption occurring across runs. Thus the sample volume of 0.968 cm^3 was deemed adequate for the project, and this value was used in the free volume calculations (Section 4.2.1).

4.2 Sorption Capacity

This section presents the results of the experiments described in Section 3.2 and provides discussion on the findings. Descriptions of how the data obtained were converted into meaningful results are also provided. This is the most important section of the dissertation with regard to satisfying the project's aims and objectives. In this section, the parameters important to sorption calculations that

were determined experimentally or theoretically occupy Sections 4.2.1 and 4.2.2 while the primary results follow in Section 4.2.3.

4.2.1 Free Volume

The volume in the sample cell system, between V2 and V3, which is free to be occupied by the sorbate, is termed the 'free volume' (see Figure 3.6). This parameter is required in the excess isotherm equation (Equation 4.3 in Section 4.2.6(a)).

The procedure and experimental work required to determine the free volume are outlined in Section 3.2.2, while a comprehensive explanation of the calculations used and experimental results are provided in Appendix D.1. Only the final results are presented in this section.

The empty volume between V2 and V3 ($V_{V2\text{-}V3}$) calculated is presented in Table 4.6. The average volume calculated of 8.17 cm^3 seems reasonable as the Swagelok sample cell is estimated to have a volume of approximately 4 cm^3.

Table 4.6: Sample cell system volume

Run	$V_{V2\text{-}V3}$ (cm^3)
1	8.26
2	8.45
3	7.80
Average	**8.17**
Standard Deviation	**0.34**

The free volume is then calculated by subtracting the volume of the sorbent sample from $V_{V2\text{-}V3}$. The sorbent sample volume was calculated in Section 4.1.5 to be 0.968 cm^3, and thus the free volume is 7.20 cm^3.

4.2.2 Density Calculations

In order to calculate the sorption from the raw results obtained from the experiments described in Section 3.2.2, it is necessary to convert pressure measurements into density. This is typically done using an equation of state, as described in Section 2.3.2.

The density of pure CO_2 and pure SO_2 can be determined reliably using component-specific, empirical equations of state (Section 2.3.2). Density data that

were calculated from these equations of state were obtained from the NIST database (http://webbook.nist.gov/chemistry/fluid/, Lemmon *et al.*, 2011). The data were plotted as a function of pressure in the pressure range of the experiments (82 bar to 87 bar) at the experiment temperature of 40°C. Polynomials that fit the data almost perfectly in the relevant range were applied to the data so that the density could be predicted without having to continually return to the website. The relevant details are provided in Appendix D.2.

It is more difficult to predict the density of high pressure CO_2-SO_2 mixtures accurately. The reader is referred to Section 2.3.2 for a full discussion on this topic. Since the concentration of SO_2 in the experimental mixtures is relatively low, Amagat's law, which is an assumption of additive partial volumes, is introduced to estimate the density of the mixtures. This law will be used to estimate the mixture density based on the densities of the pure components comprising the mixture, which can be reliably determined at the mixture conditions. Equation 2.1 is the equation that will be used to calculate the density of the mixtures and is presented again here for greater convenience.

$$\rho_{mixture} = 1/\sum {}^{x_i}/_{\rho_i} \tag{2.1}$$

Where $\rho_{mixture}$ and ρ_i are the densities of the mixture and pure component i respectively, and x_i is the mole fraction of component i.

The sorbate density according to Equation 2.1 is plotted as a function of the pressures and SO_2 concentrations relevant to the study. These results are presented in Figure 4.1.

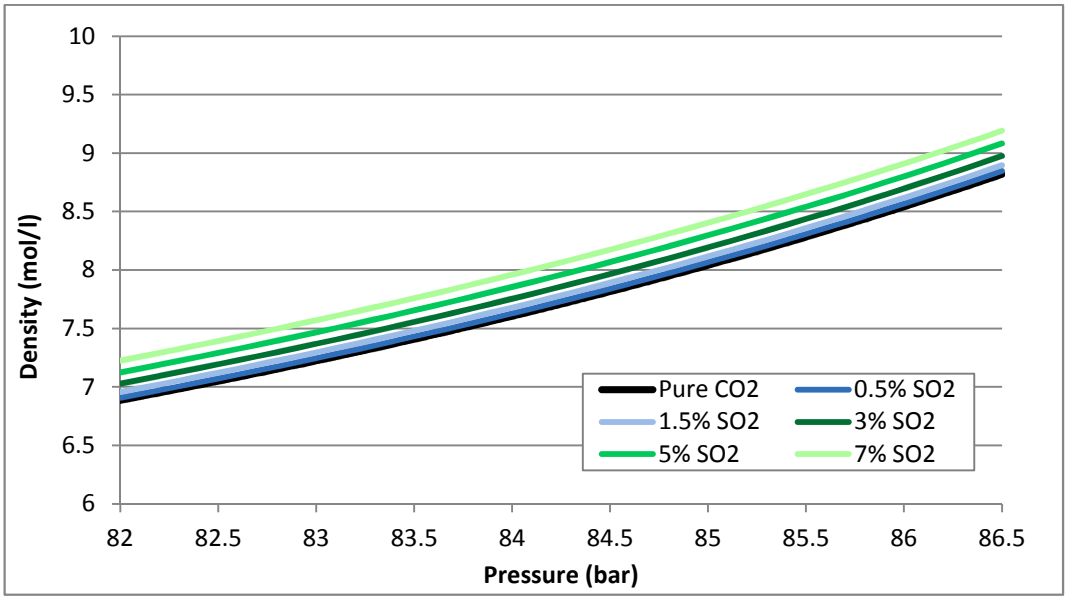


Figure 4.1: Density of relevant CO_2-SO_2 mixtures as a function of pressure at 40°C calculated using Amagat's Law

The density of pure SO_2 (see Appendix D.2) is much higher than that of pure CO_2 and remains relatively constant at these high pressures at a value of approximately 21 mol/l. Thus, it is seen that the presence of SO_2 increases the density of the mixture which is in accordance with literature (Li, 2008). If the concentration of SO_2 is 3 mol %, then the density of the mixture deviates by an average of less than 2% from the density of pure CO_2 over the pressure range of the experiment.

In addition to using Amagat's law, it was attempted to predict the mixture density using the Patel-Teja EOS, which is a more complex, cubic model. This EOS is presented in Equation 4.1 and is described fully in Appendix D.2. In order to solve for the density under the desired conditions, the model was programmed into *Matlab* software (see Appendix D.2 for code).

Patel-Teja EOS: $$P = \frac{RT}{V - b_{mix}} - \frac{a_{mix}(T)}{V(V+b_{mix})+c_{mix}(V-b_{mix})} \quad (4.1)$$

Mixing Rules:

$$a_{mix} = \sum_i \sum_j \xi_{ij}\, x_i x_j \sqrt{a_i a_j}\,;\; b_{mix} = \sum_i x_i b_i\,;\; c_{mix} = \sum_i x_i c_i\,;\; \xi_{ij} = \xi_{ji} \quad (4.2)$$

Where V is the molar volume (inverse of molar density), P is pressure, T is temperature, and R is the universal gas constant. a, b, and c are parameters defined in more detail in Appendix D.2. It is important to note that these parameters were solved for each pure component, i and j, and then mixing laws

(Equation 4.2) were used to determine their mixture values. The binary interaction parameter, ξ_{ij}, is a very important parameter used in the mixing laws as it accounts for the attraction forces between pairs of non-similar molecules (Li and Yan, 2009). This parameter is obtained from literature for mixtures of specific components where it is generally determined from best-fits to experimental VLE data, since it is more sensitive to derivative or partial properties such as fugacity coefficients than to total properties such as mixture molar volumes (Li and Yan, 2009). That said, ξ_{ij} regressed from VLE data is not guaranteed to result in a good accuracy on the density calculations, and it has been shown that significant errors can occur if the if the value of ξ_{ij} is not accurately calibrated (Li and Yan, 2009).

The Patel-Teja EOS was recommended by Li (2008) for predicting the density of CO_2-SO_2 mixtures under a variety of concentrations, pressures, temperatures. The binary interaction parameter for CO_2-SO_2 mixtures was also obtained from Li (2008), where it was calibrated to predict the saturation pressure of mixtures at VLE to within 5%. Since the experimental conditions are supercritical and not VLE, and since ξ_{ij} is merely a 'best fit' parameter at certain conditions, it cannot be taken for granted that the density will be predicted to this level of accuracy at the conditions of the experiments. It must also be noted that ξ_{ij} was not fitted to data where CO_2 concentrations exceeded 92.5% due to lack of VLE experimental data. There could also be reason to doubt the reliability of the VLE experimental data as it was produced from experiments conducted over a hundred years ago (Li, H. *et al*., 2011). Nevertheless, this is one of the few models in literature that was applied to CO_2-SO_2 mixtures under any conditions with some level of success, and thus it is included as a comparison for the Amagat densities.

The density predictions of the Patel-Teja model as a function of pressure and concentration values that are relevant to the study are presented in Figure 4.2.

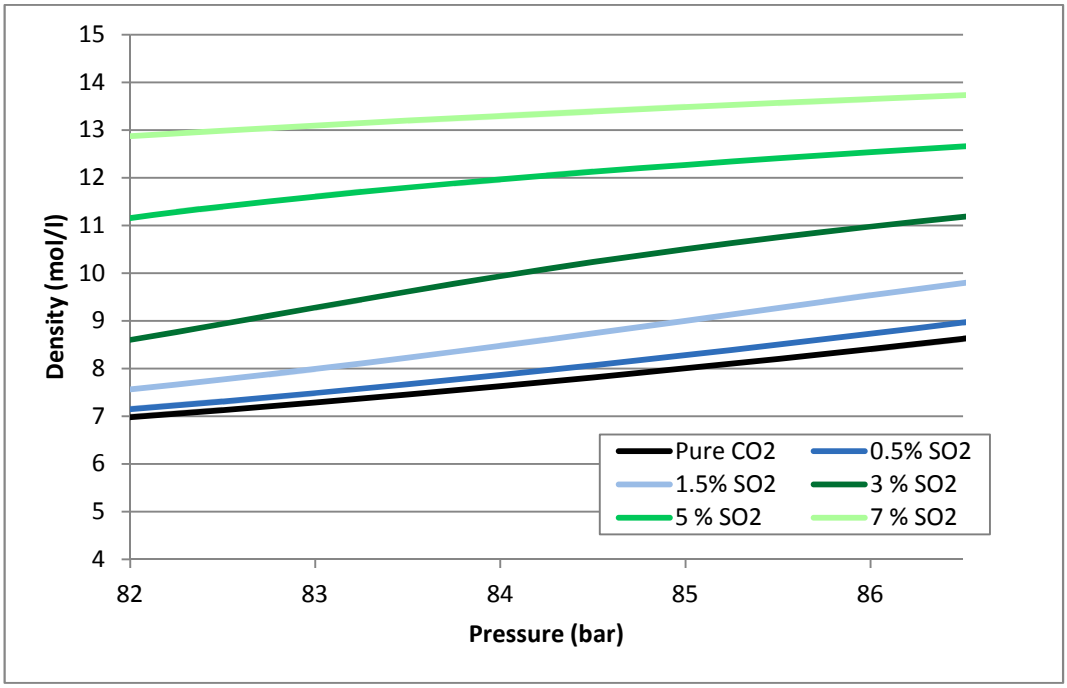


Figure 4.2: Density of different CO_2-SO_2 mixtures as a function of pressure at 40°C as predicted according to the Patel-Teja model

From the results in Figure 4.2, it is clear that the presence of even small amounts of SO_2 has a large influence on the density of the mixture when predicted by the Patel-Teja EOS. This is contrary to the predictions of Amagat's law, where the influence of SO_2 is seen to be small. For instance, the density of 3 mol% SO_2 predicted by the Patel-Teja model is seen to be an average of 28.6% greater than that of pure CO_2 over the experimental pressure range, while Amagat's law only predicts a 2% increase in density.

In order to check for errors in the model predictions, the pure CO_2 and pure SO_2 densities predicted by the model were compared to the respective NIST values. The NIST values were, however observed to be predicted accurately with absolute average deviations of 0.9% and 1.7% being observed for CO_2 and SO_2 over the experimental pressure range respectively. The great influence of SO_2 cannot be in doubt due to incorrect pure densities predicted by the model. The great influence of SO_2 is rather attributed to the mixing laws applied to the model as well as due to the mixture's binary interaction parameter. Both the mixing laws and binary interaction parameter were applied as recommended by Li (2008).

Although the model is mathematically sound, there is no literature indicating that the predictions are accurate outside of VLE conditions. There is also no reason to believe the Amagat predictions are any more reliable, as no literature confirming this is available either. Thus the density predictions from both methods will be used to calculate the sorption and the effect of the different predictions on the final findings noted.

4.2.3 Pressure versus Run Time

Sorption experiments were conducted by contacting a coal sample with a fluid mixture of the desired CO_2-SO_2 composition for a suitable amount of time to allow sorption to take place. This experiment is described in greater detail in Section 3.2. Pressure and temperature measurements are taken throughout the experiment using LabVIEW software. The reduction in pressure from the outset of the experiment can be used to quantify the amount of fluid that has been sorbed by the sample in that period of time. It is important that the temperature remain constant throughout the experiment to avoid any effects of the temperature on the pressure that interfere with sorption calculations.

Selected pressure and temperature data that was obtained from three sorption experiments is presented below, for illustration purposes, while the data for all runs are presented in Appendix D.3. All runs were allowed to continue for 48 hours and the oven was set at 40°C. Figures 4.3 to 4.5 below were obtained for 0.2 mol%, 1 mol%, and 2.5 mol% SO_2 respectfully. It must be noted that the temperature values on the secondary axes differ slightly from the temperature of the oven due to a calibration discrepancy when the software was set up.

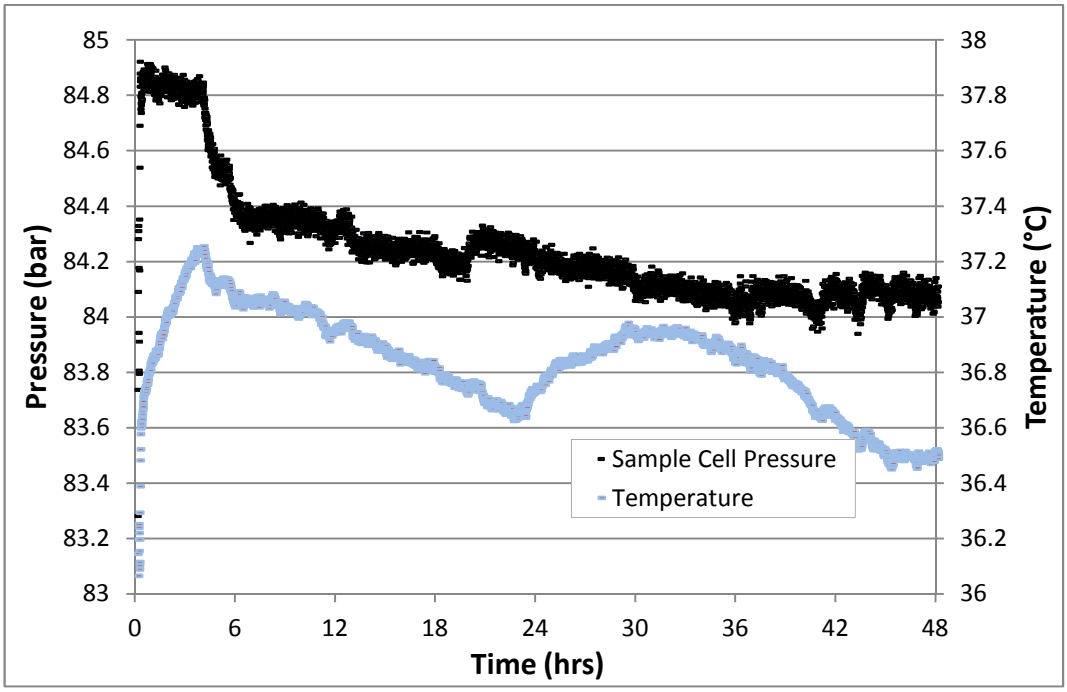


Figure 4.3: Sample cell pressure and temperature throughout a volumetric sorption experiment with a sorbate containing 0.16 mol% SO_2 and 99.84 mol% CO_2.

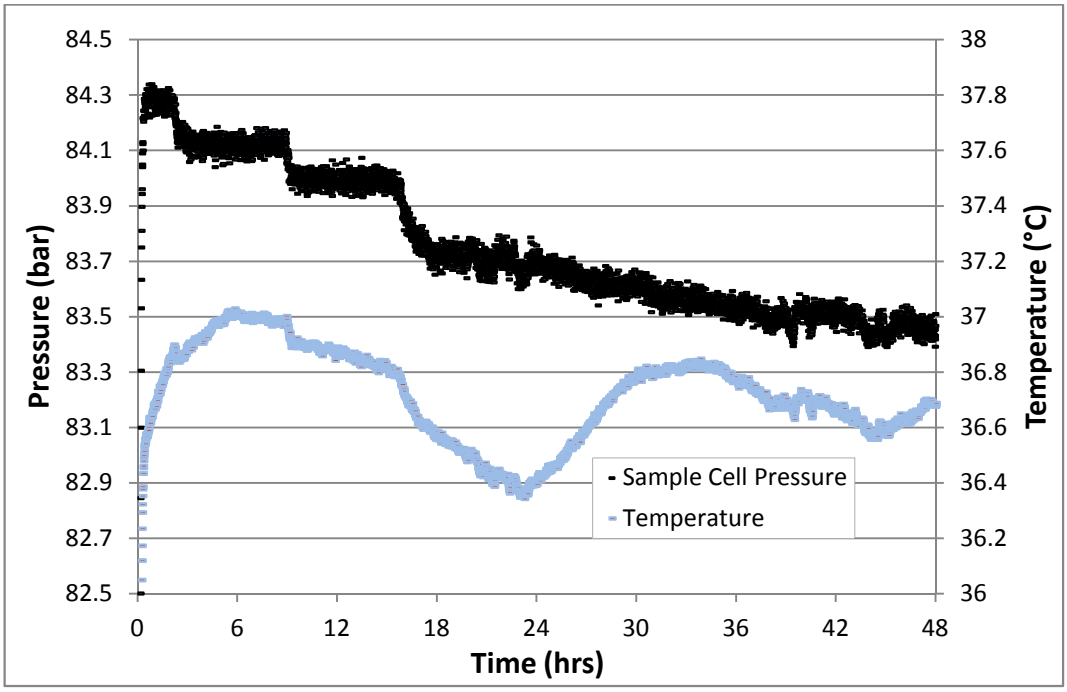


Figure 4.4: Sample cell pressure and temperature throughout a volumetric sorption experiment with a sorbate containing 0.95 mol% SO_2 and 99.05 mol% CO_2.

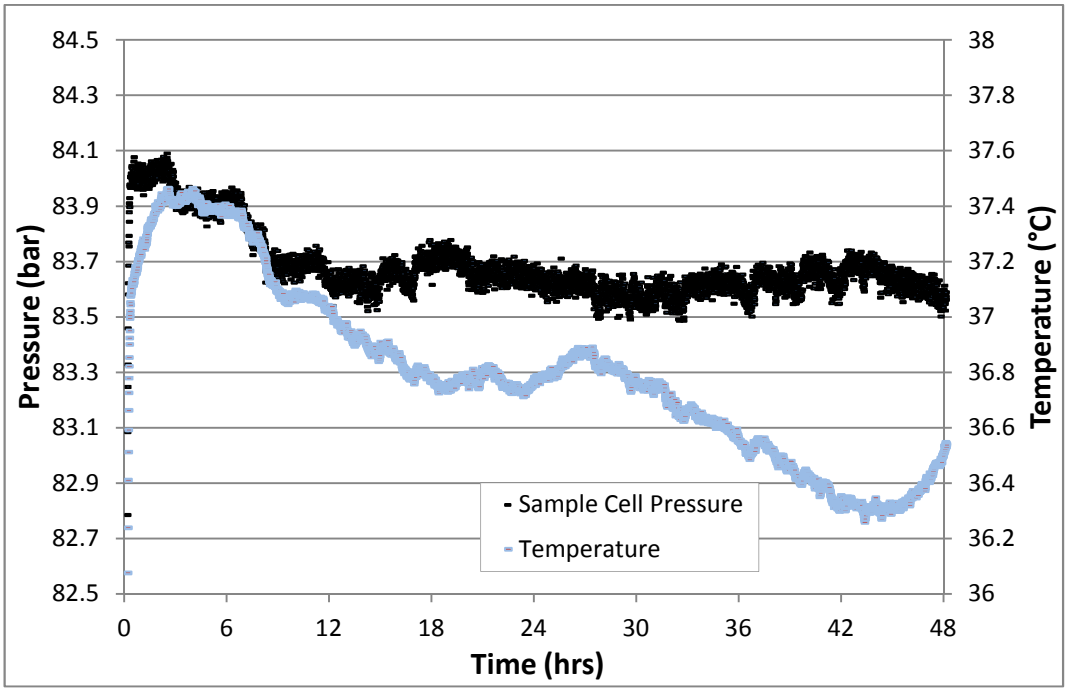


Figure 4.5: Sample cell pressure and temperature throughout a volumetric sorption experiment with a sorbate containing 2.52 mol% SO_2 and 97.48 mol% CO_2.

From the results, it is evident that the pressure drops relatively quickly over the first 6 to 18 hours, at which point it starts to level off to a relatively constant value. This behaviour is in accordance with adsorption theory where it is expected that an equilibrium between the adsorption and desorption processes will eventually occur resulting in a stable pressure being reached. In some cases, the pressure is seen to take almost the full 48 hours to stabilise completely with a very slow decrease in pressure occurring after the initial drop, before levelling off (see Figure 4.4). This justifies the need for a long 48 hour experimental run time.

The temperature is usually seen to cycle to within 1°C as expected according to the control system of the oven, although more temperature variation is noted on some runs than others (e.g. Figure 4.5 as opposed to Figures 4.4 and 4.6). This greater variation was noted to occur when the external temperature was markedly colder than for the runs when the temperature was more stable. However, no consistent influence of these minor temperature changes on the pressure is seen, although a constant temperature environment in the laboratory is recommended.

Another parameter that deserves some attention is the initial pressure in the sample cell. This pressure is achieved after the expansion volume has been

pumped to the pressure of 119 bar with the fluid (whether pure CO_2 or mixture) and is then allowed to expand to the sample cell for 60 seconds where it is trapped. The initial pressure is calculated as the average pressure over the second hour of the run as the pressure is seen to take up the first hour to equilibrate while the temperature rises steadily. The final pressure is calculated as the average pressure over the final hour of the experiment. These pressure values are important for use in Equation 4.3 (Section 4.2.6(a)).

It was expected that the initial pressure would remain constant from run to run as the expansion volume was set to pressurise to the same set point; however, this was seen not to be the case. The initial pressure reached in the sample cell for the pure CO_2 runs was approximately 86 bar, while that of the impure CO_2 runs was lower, between 83 and 85 bar. This difference in initial pressures may be explained by the liquid CO_2 cylinder supplying the Teledyne Isco pump directly, in the case of pure CO_2; but indirectly (via the Mixing System) in the case of the mixtures, where the fluid was brought to a lower pressure. The higher pressure pure CO_2 was hence delivered to the expansion volume at a higher flowrate than the mixtures were, which caused the pressure set points for the CO_2 runs to be overshot slightly. Thus slightly elevated initial pressures for the pure CO_2 runs resulted.

A plot of the initial pressure versus SO_2 concentration is provided in Figure 4.6 in order to investigate whether a trend between these two parameters exists. From this plot no clear evidence that a trend between the two variables exists, even though the higher starting pressures of the three pure CO_2 runs are apparent.

This subsection is of great importance as the pressure data forms the basis of the sorption capacity calculations. This data should be referred to if there is indication of an error or outlying points.

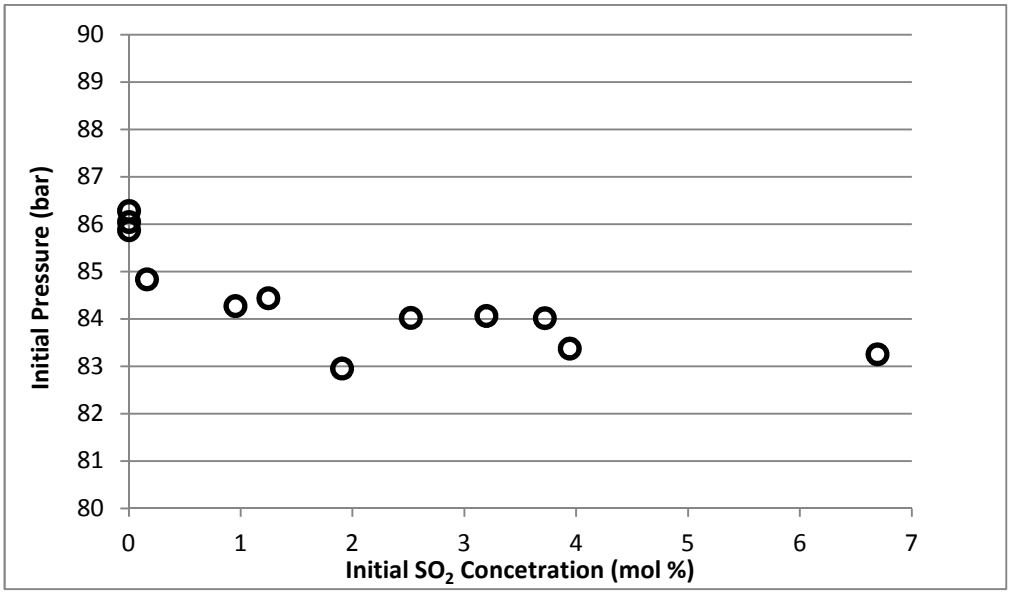


Figure 4.6: Initial pressure of sample cell versus initial SO_2 concentration of mixture

4.2.4 Gas Composition Analysis

The SO_2 content of the sorbate was determined before and after 48 hours of sorption had taken place. This was done using GC analysis according to the method described in Section 3.2.1. Chromatograms were produced for each sorbate sample drawn from the VAS, and the concentration determined from the average peak area for SO_2 and a calibration curve (see Figure 3.5 in Section 3.2.1). The initial and final SO_2 peak area, peak area standard deviation and SO_2 concentration for each VAS run are presented in Table 4.7. The SO_2 concentrations determined are represented again in Figure 4.7, for greater clarity.

The peak areas determined for each mixture in general were acceptable, with an average percentage deviation for all runs at 11.6%. However, the peak areas determined for mixtures 4, 6, 7, 8 and 9 have relatively high standard deviations, as is best observed from the error bars in Figure 4.7. Mixture 6, which was determined to have an initial concentration of 3.20% SO_2, was seen to have high standard deviations for both the initial and final concentrations measured. This could have bearing on the excess sorption and density results, which use these mixture compositions in calculations. The experimental data for the GC analysis is presented in Appendix D.4.

Table 4.7: SO_2 experimental peak areas and calculated concentrations

Mixture	Average Peak Area (uV.min)		Peak Area Standard Deviation (uV.min)		SO_2 Concentration (mol%)	
	Initial	Final	Initial	Final	Initial	Final
1	23.16	0	3.9	0	0.16	0
2	137.2	32.44	5.7	10.5	0.95	0.23
3	179.54	57.08	22.4	2.3	1.25	0.40
4	274.62	69.44	61.2	1.7	1.91	0.48
5	363.26	197.2	29.7	19.8	2.52	1.37
6	460.62	202.04	91.9	33.9	3.20	1.40
7	535.9	211.1	6.7	46.9	3.72	1.46
8	568.02	387.64	57.5	15.2	3.94	2.69
9	964.68	434.68	98.3	47.0	6.69	3.02

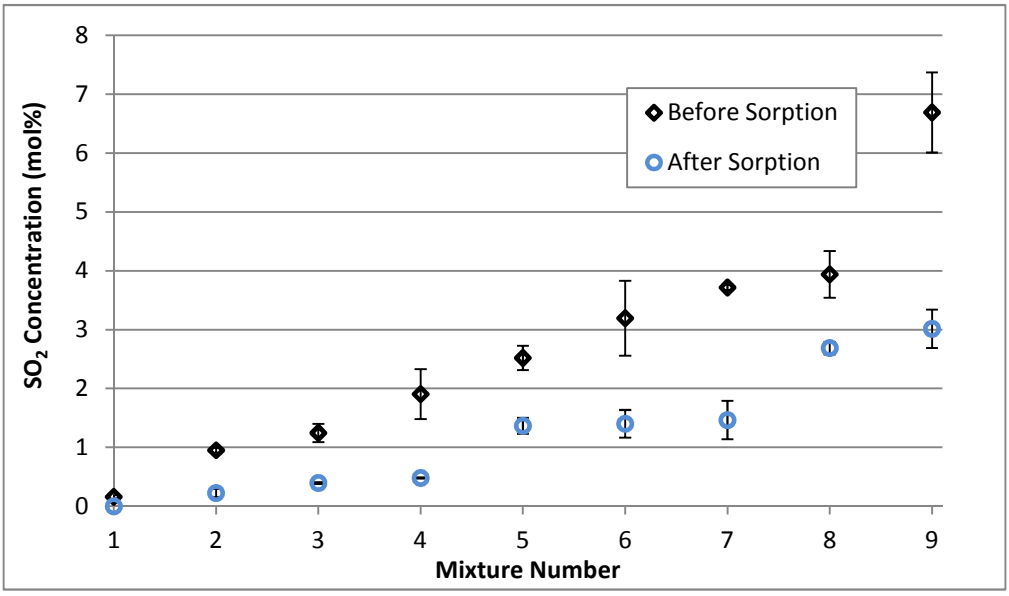


Figure 4.7: Comparison of the SO_2 concentration of each mixture determined before and after the sorption experiments. Error bars indicate the level of experimental deviation obtained from repeat concentration measurements on the GC.

When comparing the initial and final sorbate concentrations, it is evident that a significant decrease in the SO_2 level in the sorbate occurs. This is attributed to the occurrence of sorption, as SO_2 is expected to have strong sorbing properties on coal (see Section 2.2.2). The molar concentration of the mixture is an important

factor in sorption calculations as it is used to calculate the mixture density as well as determine the percentage of each component sorbed.

4.2.5 Fourier Transform Infrared Spectroscopy

FTIR analysis was performed on a coal samples that had undergone no treatment other than degassing (described in Section 3.2.2) as well as on samples that had been treated with the following mixtures under supercritical conditions of 85 bar and 40°C for 48 hours:

- 100% CO_2
- 0.16% SO_2, 99.84% CO_2
- 3.20% SO_2, 96.80% CO_2
- 6.69% SO_2, 93.31% CO_2

The results produced from FTIR analysis are spectra, which are plots of wavenumber (cm^{-1}) versus percentage transmittance. These plots describe the amount of infrared radiation that was absorbed by the bonds of the sample. The 'peaks' observed at each radiation wavenumber thus identify the presence of a certain functional group and the size of the peak is an indication of the amount of material present (Thermo Nicolet, 2001).

The spectra produced for each sample analysed are presented in Figures 4.8 to 4.12. The results are compared with each other and the conclusive findings highlighted in the in the discussion to follow.

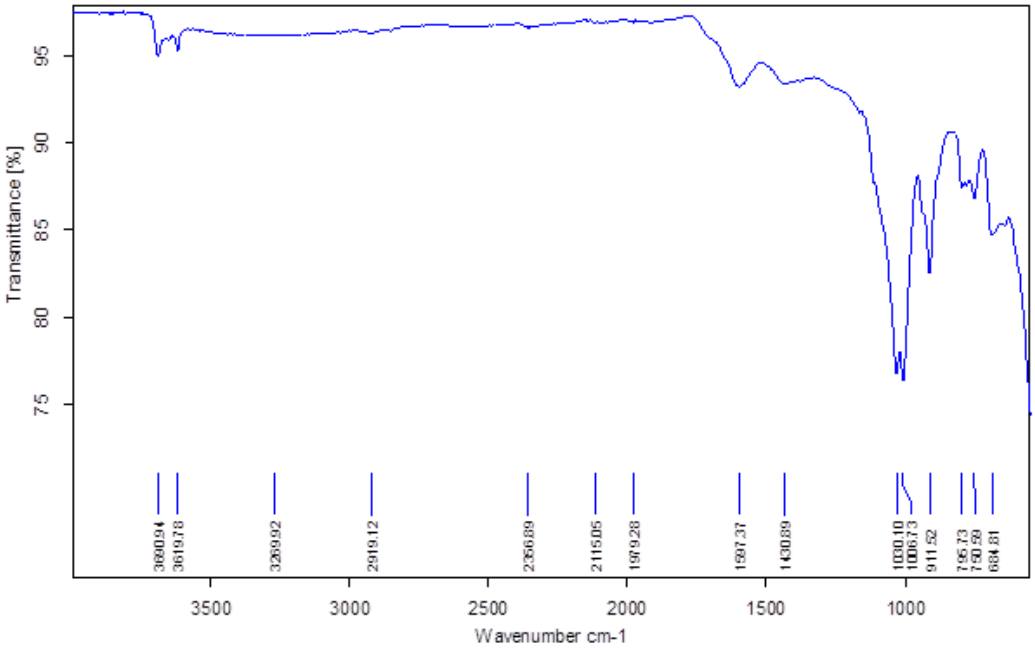


Figure 4.8: FTIR Spectrum produced for coal sample without sorption treatment

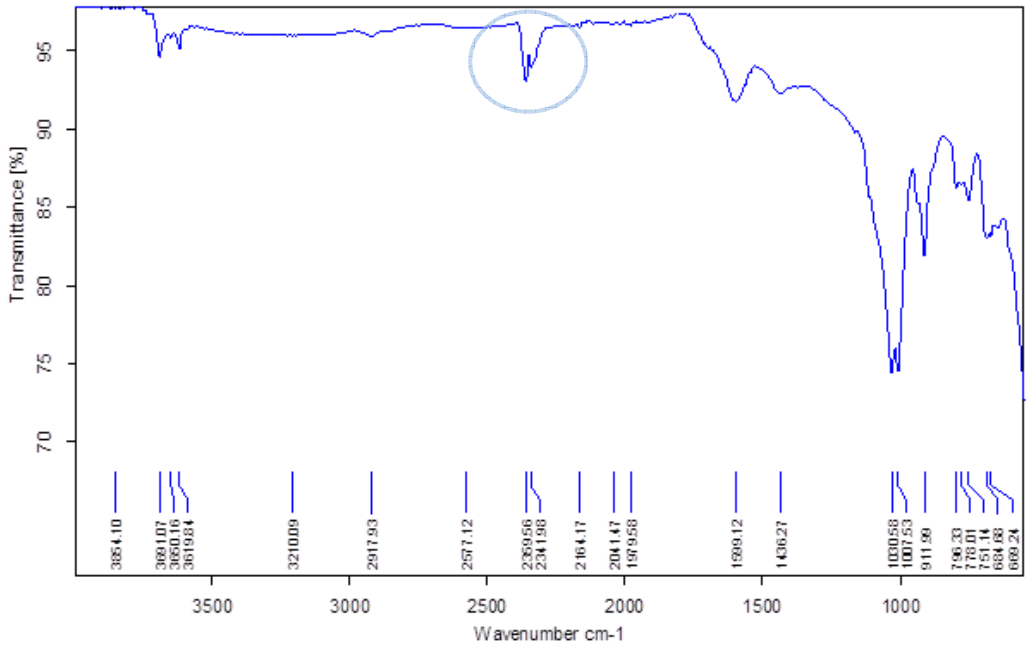


Figure 4.9: FTIR Spectrum produced for coal sample treated with pure CO_2 at 85 bar and 40 ℃ for 48 hours. The peak indicating the CO_2 retained by the coal is circled.

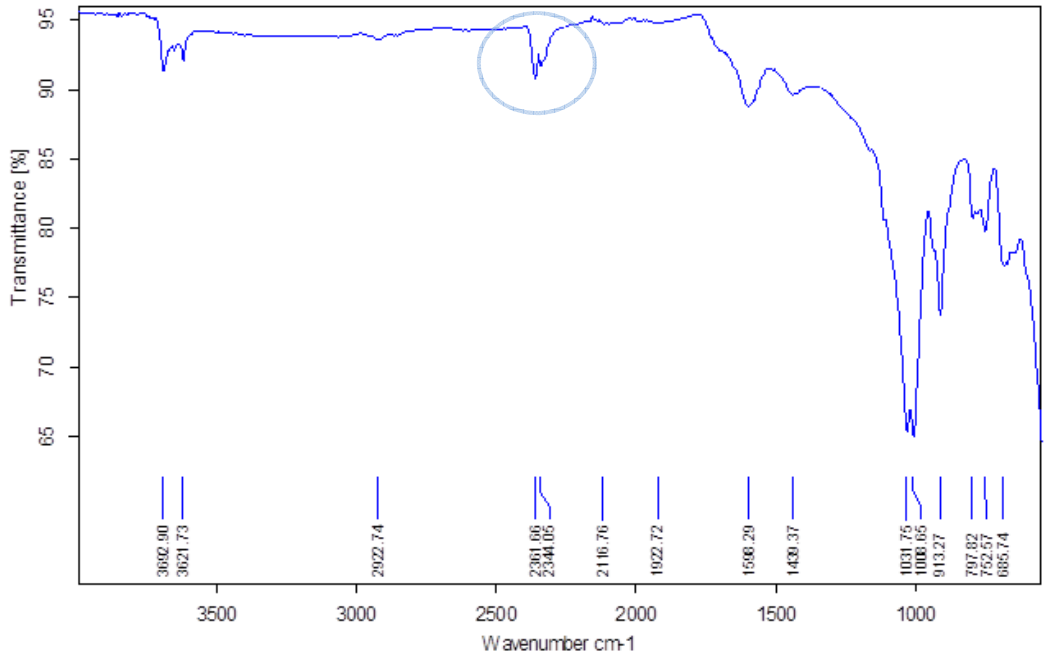


Figure 4.10: FTIR Spectrum produced for coal sample treated with 0.16% SO_2 (balance CO_2) at 85 bar and 40℃ for 48 hours. The peak indicating the CO_2 retained by the coal is circled.

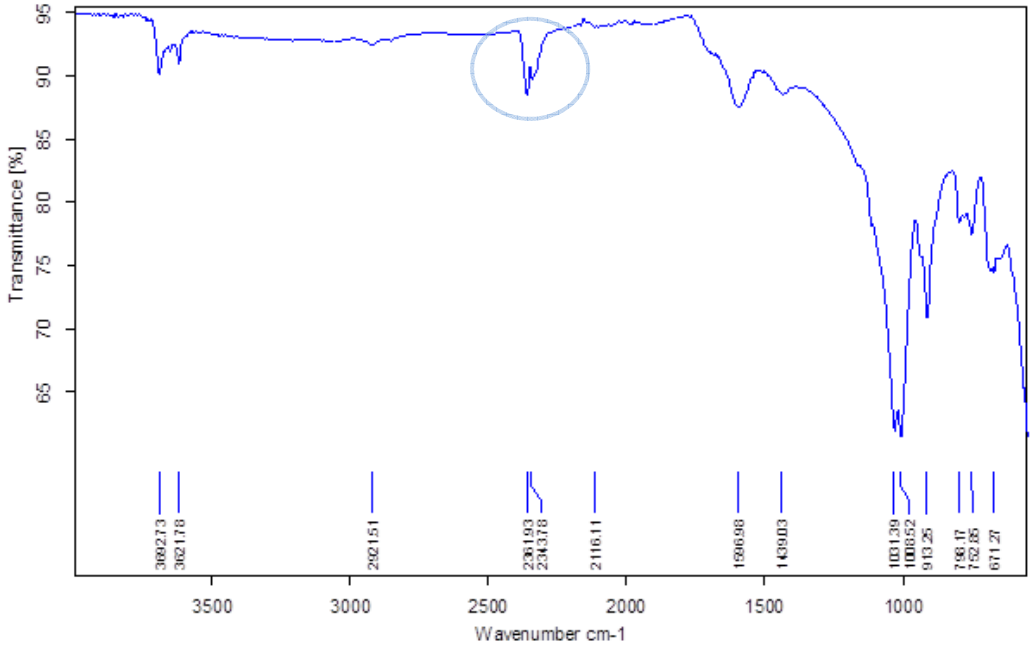


Figure 4.11: FTIR Spectrum produced for coal sample treated with 3.20% SO_2 (balance CO_2) at 85 bar and 40℃ for 48 hours. The peak indicating the CO_2 retained by the coal is circled.

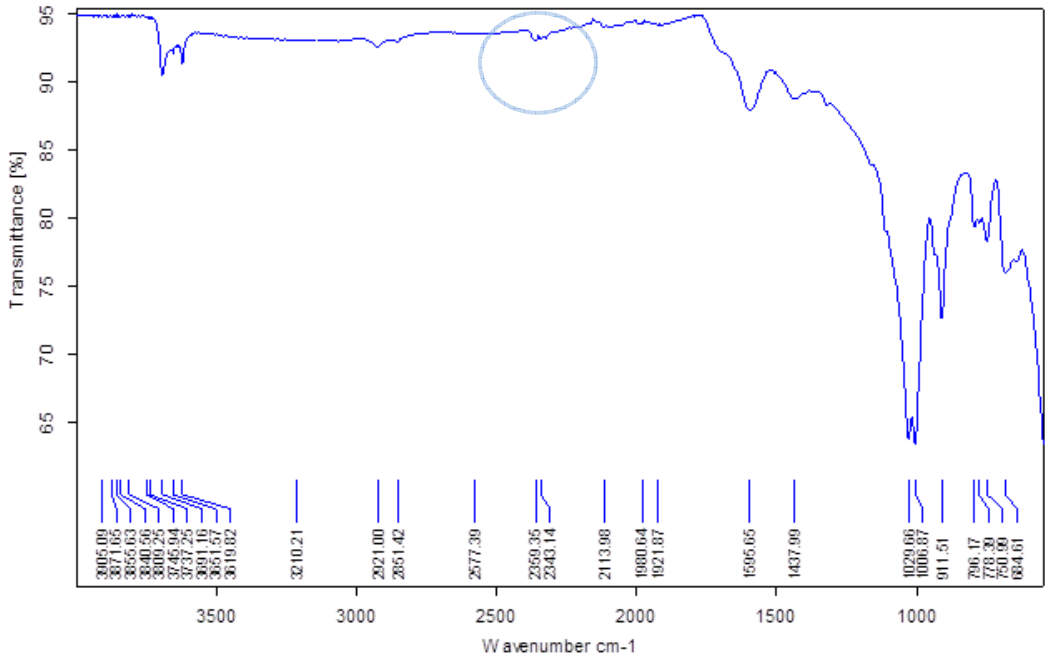


Figure 4.12: FTIR Spectrum produced for coal sample treated with 6.69% SO_2 (balance CO_2) at 85 bar and 40 ℃ for 48 hours. The peak indicating the CO_2 retained by the coal is circled.

By comparing the peaks observed in Figures 4.8 through to 4.12, the most obvious peak of interest lies between 2340 cm^{-1} and 2360 cm^{-1} (as highlighted by the circles introduced to the spectra plots). The position of this peak corresponds very closely to the position of the peak observed for physisorbed CO_2 on coal by Goodman *et al*. (2005) at 2332 cm^{-1}. Faust (1992) identifies this peak to be due to the asymmetrical stretch of the CO_2 molecule. Since the position of this peak is seen to vary slightly from coal to coal (Goodman *et al*., 2005), the peak in the present study is deduced to identify physisorbed CO_2. The presence of these peaks after the samples were allowed to return to ambient pressure indicates that some CO_2 remains either absorbed or adsorbed to the coal. Similar observations to this were made by Maphala (2012).

The physisorbed CO_2 peak does not appear in the coal sample that was not treated, as expected (Figure 4.8), and is prominent in the samples treated with pure CO_2, 0.16% SO_2, and 3.20% SO_2 (Figure 4.9 to 4.11). This peak, although still present, decreases substantially in magnitude when the sample was treated with the highest SO_2 concentration of 6.69% (Figure 4.12). This decrease in the physisorbed CO_2 peak magnitude could indicate that there is higher competition for pore occupancy at this high level of SO_2; bearing in mind that SO_2 has a high

affinity for coal than CO_2. However, the physisorbed CO_2 peak is slightly larger in the case of 3.2% SO_2 (Figure 4.11) than that of 0.16% SO_2 (Figure 4.11), and thus further analysis may be required to explain this observation suitably.

The position of SO_2 on the spectrum corresponds to 1360 cm^{-1} (asymmetrical stretch), 1150 cm^{-1} (symmetrical stretch), and 540 cm^{-1} (bending) (Faust, 1992). However, no peaks were identified at these wavenumbers, and thus it can be deduced that all SO_2 that had physisorbed to the coal, desorbed once the sample was depressurised. Other functional groups of interest to the study are all groups that include S, which are located at a variety of wavenumbers that are defined in Table 4.8, as well as the hydroxyl group, which is located between 3200 cm^{-1} and 3600 cm^{-1}. The functional groups containing S are of relevance as they would appear if SO_2 chemisorbed to the coal; while the hydroxyl group is of importance to sorption studies as a high hydroxyl group on the surface would induce a higher CO_2 adsorption (Maphala, 2012). However, no conclusive findings were evident at these wavenumbers when the spectra of the different sorption-treated samples were compared with each other.

Table 4.8: Characteristic infrared absorption frequencies of S-containing functional groups (Table of IR Absorption Frequencies, unknown)

Bond	Compound Type	Frequency range (cm^{-1})
	Organic Sulphur Compounds	
S–H stretching	Aliphatic mercaptans, thiophenols	2550–2600 (w)
	Thioketos	2415 (b)
C–S stretching	Sulfides	600–700 (w)
S–S stretching	Disulfides	400–500 (w)
C=S stretching	Thiocarbonyls	1020–1250
	Thiobenzophenones	1207–1224
	Compounds Containing Sulphur–Oxygen Bonds	
S=O stretching	Organic sulfoxides	1030–1070 (s)
	Sulfones	1120–1160 (s) & 1300–1350 (s)
	Sulfonyl chlorides	1177–1204 (s) & 1380–1410 (s)
	Sulfonamides	1155–1170 (s) & 1335–1370 (s)
	Covalent sulfonates	1168–1195 (s) & 1335–1372 (d, s)
	Organic sulfates	1185–1200 (s) & 1380–1415 (s)
	Sulfonic acids	1150–1165 (s) & 1342–1350 (s)
	Sulfonate salts	1055 (s) & 1175 (s)
N–H stretching	Sulfonamides	
	1E	3247-3300 (s) & 3330–3390 (s)
	2E	3265 (s)

Abbreviations: s = strong, w = weak, d = doublet, b = broad

Another observation made was that there are a great number of small peaks between 3905 and 3737 cm^{-1} for the 6.69% SO_2-treated coal (Figure 4.12) that were not identified for the other samples. However, these peaks are very small as they are not easily observable with the human eye. Although the occurrence of chemisorption of SO_2 or CO_2 looks unlikely from the FTIR findings, Raman spectroscopy, with more visible organic peaks, or XRD analysis, with focus on mineral behaviour, may provide greater insight on this subject. These two analyses were not undertaken in the study but will form part of the recommendations.

4.2.6 The Effect of Impurities on Sorption

The amount of fluid the coal samples sorbed during the 48 hour VAS experiments was calculated for different SO_2 mixtures. The sorption quantification procedure is described in Part (a) of this section and the sorption results, as calculated using different density predictions, are presented in Part (b). Part (b) comprises of the sorption results produced when (i) Amagat's law and the (ii) Patel-Teja EOS are

used to predict the density, and the results obtained from these two methods are compared with each other in a final subsection (iii).

a) Excess Sorption

The amount of sorption of the coal samples is quantified using the excess sorption equation presented as Equation 4.3 below. This Equation Dalculates the number of moles of substance sorbed per gram of sample (N_{sorbed}, in mmol/g) from the difference in initial and final number of moles in the sorbate, through the course of the experiment, according to mass balance principles (Felder and Rousseau, 2000). The parameters needed are: the molar densities of the total sorbate, whether it is a pure component or a mixture, at the outset and completion of the experiment ($\rho_{initial}$ and ρ_{final} respectively, in mmol/*l*); the free volume in the sample cell (V_{free}, in *l*); and the mass of sample (m, in g). The density is a function of pressure (P) and the molar composition of the sorbate (x).

$$N_{sorbed} = V_{free}\left(\rho_{initial}|_{(P_{initial};\, x_{initial})} - \rho_{final}|_{(P_{final};\, x_{final})}\right)/m \qquad (4.3)$$

The free volume was determined in Section 4.2.1 and the sample mass is consistently 2 g. The initial and final pressures and molar concentrations were recorded experimentally (see Sections 4.2.3 and 4.2.4). These experimental values were used to calculate the relevant sorbate densities according to methods described in Section 4.2.2. In the case of mixtures, the component-wise sorption, as opposed to the total sorption, can be calculated by modifying Equation 4.3 so that Equation 4.4 is achieved.

$$\boldsymbol{N_{(i)sorbed}} = \boldsymbol{V_{free}\left(x_{(i)initial}\cdot\rho_{initial}|_{(P_{initial};\, x_{initial})} - x_{(i)final}\cdot\rho_{final}|_{(P_{final};\, x_{final})}\right)/m} \qquad (4.4)$$

Where $x_{(i)initial}$ and $x_{(i)final}$ are the initial and final mole fractions of component i in the sorbate.

The sorption of pure CO_2 on three coal samples was calculated in order to determine the variation of the excess sorption from run to run. Pure CO_2 was selected for this purpose as it was more easily reproducible than for a mixture

where the exact concentration would have to be reproduced. These results are presented in Table 4.9.

Table 4.9: Excess sorption calculated for three samples runs with pure CO_2

Run	Sorption Capacity (mmol/g)
1	2.409
2	1.653
3	2.047
Average	**2.036**
Standard Deviation	**0.378**

Note: Since the sorbate is pure CO_2, the density was calculated using NIST data

The percentage deviation from the average sorption value is relatively high at 18.6%. Reasons for the deviation between runs could be due to differences in temperature fluctuations, differences in initial pressure, and errors in sample handling. However, an isolated cause of the significant differences between these runs is not clear. The raw data for these runs is presented in Appendix D.3. Nevertheless, it is assumed that the sorption capacity values calculated for each sorbate mixture will fall within a ±18.6% error range.

The results comparing the sorption for the mixtures with the average sorption for pure CO_2, as presented in Table 4.9, is presented in Part (b) that follows. The detailed excess sorption calculations for all runs are presented in Appendix D.3.

b) Sorption as a function of SO_2 content

The total excess sorption is calculated for a variety of binary CO_2-SO_2 concentrations, ranging from pure CO_2 to approximately 7 mol% SO_2. The initial pressure of each run ranged from 83 bar to 86 bar while the oven temperature was at 40°C. Equations 4.3 and 4.4 are used to quantify the sorption for each mixture run which is based on the experimental data provided in Appendix D.3. A worked example of how the sorption is quantified is also presented in Appendix D.3.

In Section 4.2.2 it was determined that an important variable in the excess isotherm equation is the sorbate density. It is possible to calculate this variable, when both SO_2 and CO_2 are present in the sorbate, in a great number of ways with some level of uncertainty surrounding the application of all prediction models. It was therefore decided to determine the effect of SO_2 content on sorption using

two different methods to predict the sorbate density so that the bearing of the density prediction methods on final results/trends can be observed. The results produced for the different density predictions are presented in two parts separated by different subheadings. The results in each part are thoroughly discussed before being compared with each other at the end of the section.

i. Mixture density estimation based on Amagat's Law

The density of the mixture can be estimated using a technique based on the assumption of Amagat's law. This method calculates the density of a mixture by combining the pure component densities, assuming additive volumes (see Section 2.3.2). A reason for the selection of this approach is that it is easy to apply if the NIST database is used to compute the complex EOS's that describe the densities of CO_2 and SO_2 accurately. When this approach is used to estimate the density and the excess sorption is calculated, Figure 4.13 is produced. This figure describes the sorption capacity of coal samples, from the same batch of coal, for nine different CO_2 mixtures of varying SO_2 concentration. The amount of each component sorbed, as calculated according to Equation 4.4, is also expressed.

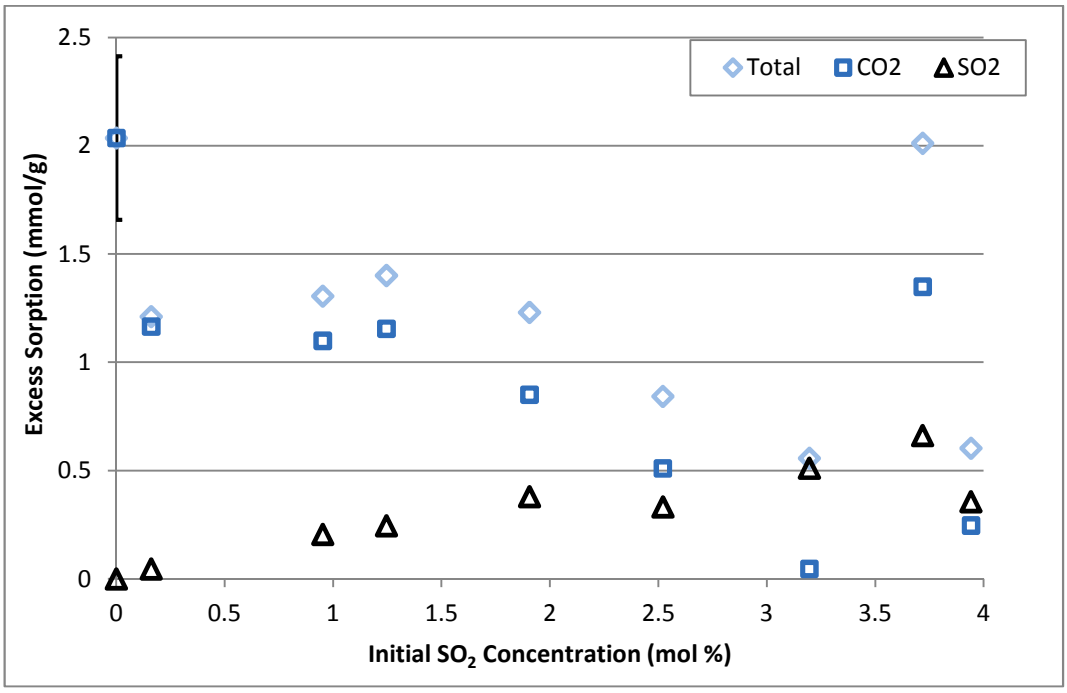


Figure 4.13: Excess sorption in a typical South African coal when exposed to CO_2 mixtures with differing initial sorbate concentrations of SO_2. The temperature is 40 ℃ and the initial pressure is approximately 85 bar. The mixture density was calculated using Amagat's Law and the standard deviation at 0% SO_2 is shown via error bars.

The excess sorption is seen to range from 0.6 mmol/g to 2.4 mmol/g, which is in the same order of magnitude as CO_2 and CH_4 sorption in various coals (Gertenbach *et al*., 2009) although being on the lower side. This is understandable as the coal's vitrinite content (the main sorbing component) is relatively low at 33.1% (see Section 4.1.3). The large range of excess sorption values indicates that the presence of SO_2 has a significant influence.

An important observation from Figure 4.13 is that the total sorption generally decreases as the concentration of SO_2 increases. This trend is also evident for component-wise sorption of CO_2, while the sorption of SO_2 clearly increases with an increase in its concentration. When comparing the sorption of the pure CO_2 stream with that of the 0.16% SO_2 mixture, the total sorption is seen to drop dramatically, by about 60%, even though only a small amount of SO_2 is present in the sorbate. However, the experimental deviation should be considered (indicated by the error bar for the 0% SO_2) which could influence the magnitude of this drop.

Another experimental error for the dramatic initial decrease in sorption from pure CO_2 to 0.16% SO_2 could be due to the slightly higher initial pressure obtained for the pure CO_2 runs (approximately 86 bar, as opposed to 85 bar for the 0.16% SO_2 run) – see Figure 4.6. That is, the higher starting pressure of the pure CO_2 runs would create a greater driving force for sorption than the slightly lower pressure of the 0.16% SO_2 run; which would result in the results not being directly comparable as the effect of SO_2 is not isolated as the only changing variable. The reason for the different initial pressures observed may be due to the set point pressure in the expansion volume being overshot slightly as the Teledyne Isco pump was fed by pure liquid CO_2, which is at a slightly higher pressure than was achieved in the mixing system (see Section 4.2.3). Even though some experimental error is likely here, no data are removed as it is likely that only the magnitude of the drop in sorption between 0% and 0.16% SO_2 will be influenced, as opposed to the trend observed being contradicted.

If Figure 4.13 is analysed in greater depth, several additional observations can be made. The CO_2 sorption remains relatively constant for SO_2 concentrations above 0.16% and below 1.25%, but since the SO_2 sorption still rises over this range, a

slight increase in the total sorption occurs. At SO_2 concentrations greater than 1.25%, the total, and pure CO_2 sorption start declining again until an outlying point occurs at 3.72% SO_2. The pressure versus run time plot of this point was reviewed in order to investigate the reason for it deviating from the trend, and it was evident that this plot was significantly different to the plots produced for the other mixtures (see Figure 4.14). The pressure during this run is seen to decrease relatively linearly with run time and did not level off to a constant pressure value, as was observed for the other runs (see Appendix D.3). This may be attributed to a very small leak which caused the pressure to escape the apparatus rather than sorb. For this reason, this point is discarded for all discussion from here on in.

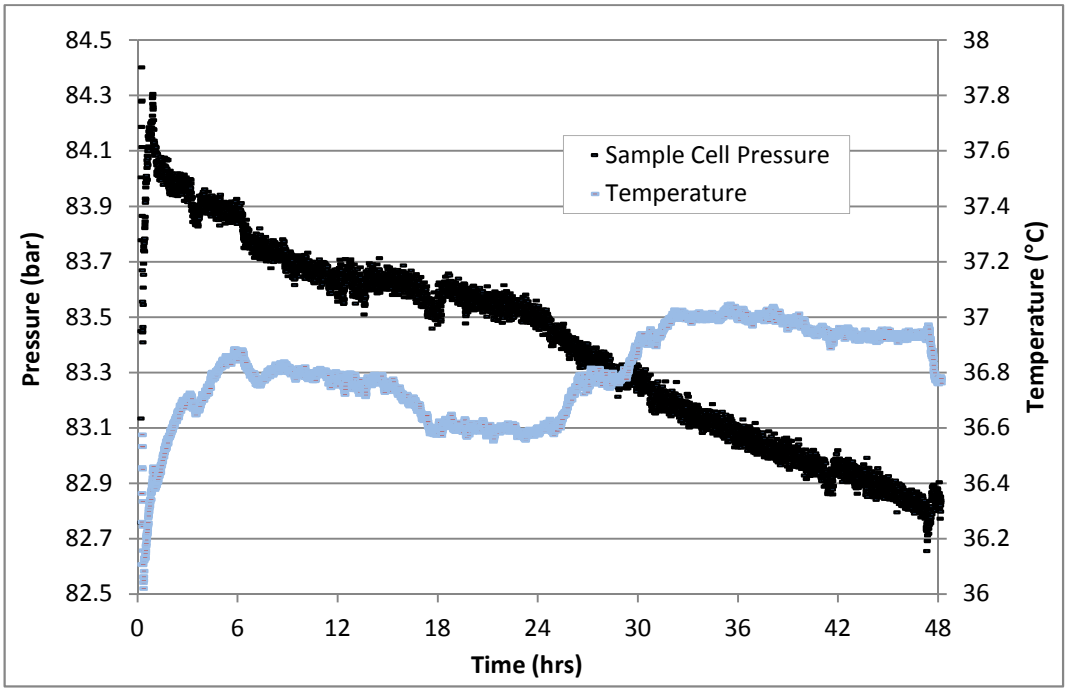


Figure 4.14: Sample cell pressure and temperature throughout a volumetric sorption experiment with a sorbate containing 3.72 mol% SO_2 and 96.28 mol% CO_2.

The CO_2 sorption is seen to increase from an almost negligible value at an SO_2 concentration of 3.20%, where SO_2 sorption accounts for almost the total amount of sorption, to a slightly higher value of 0.25 mmol/g at 3.94% SO_2. This raises questions as to what will happen to the sorption at SO_2 concentrations higher than 4%. Thus, a sorption experiment was run at a much higher concentration of 6.96% SO_2. It must be noted that the SO_2 content is never likely to exceed 2% in a captured CO_2 stream; although SO_2 could potentially accumulate underground

due to its strong sorbing qualities, which are apparent in this study, causing regions of higher SO_2 content to be formed (Sakurovs *et al.*, 2011). The updated plot including the excess sorption at 6.69% SO_2 is presented in Figure 4.15.

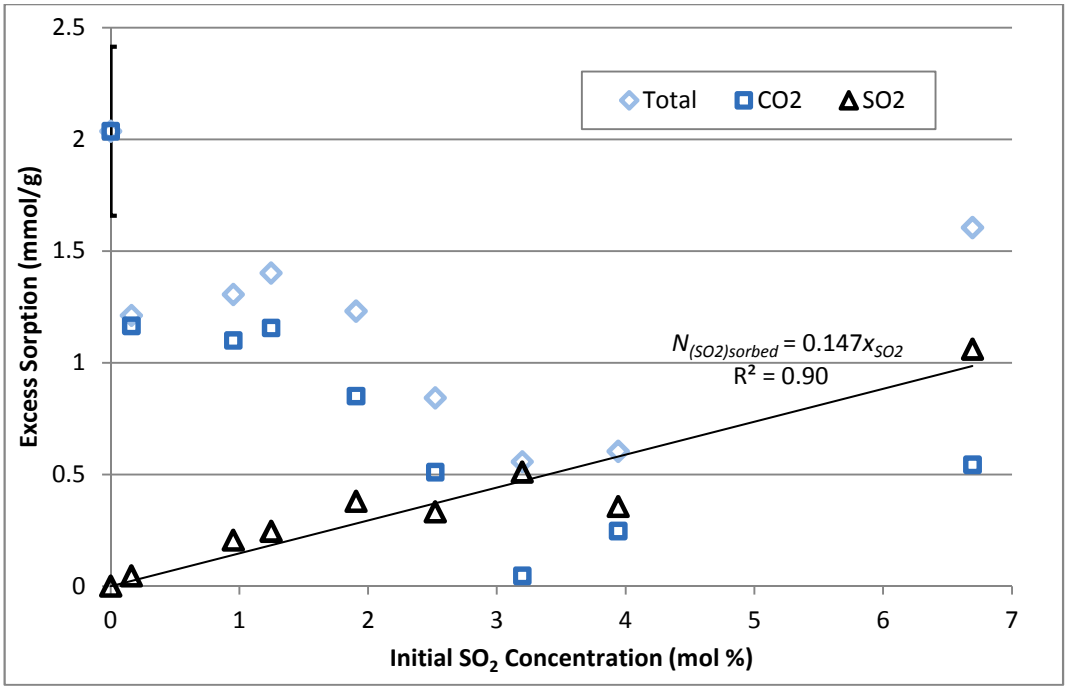


Figure 4.15: Excess sorption as a function of initial sorbate SO_2 concentration, at approximately 85 bar and 40 ℃, observed up until 6.69 mol% SO_2. The Henry's law adsorption model is fitted to the SO_2 sorption. The mixture density used in excess sorption calculations was calculated using Amagat's Law.

From Figure 4.15, it is apparent that at the much higher SO_2 concentration of 6.69% the amount of CO_2 sorbed has increased by 0.3 mmol/g when compared with the amount of CO_2 sorbed at 3.94% SO_2. The sorption of SO_2, on the other hand, has continued with the same increasing trend as was observed for concentrations below 4% SO_2. These results lead to a much higher total sorption taking place at 6.69% SO_2, which approaches the amount of total sorption that occurred for pure CO_2. However, the amount of CO_2 sorbed is still very low at about 25% of the sorption occurring when the CO_2 is pure.

When considering the trends of the excess sorption of SO_2 and CO_2 as a function of their respective concentrations, theoretical sorption isotherm models can be used to describe the data (Chaback *et al.*, 1996). It is observed from Figure 4.15 that SO_2 as it follows a linear trend relatively accurately (R^2 = 0.90). This behaviour is in accordance with Henry's law adsorption, which is a model that

typically describes adsorption at low sorbate concentrations (Silva da Rocha *et al*., 1998). This behaviour is shown to hold true at low concentrations for many adsorption theories, e.g. Langmuir model (Silva da Rocha *et al*., 1998). The Henry's constant for the fitted model was determined to be 0.147.

The CO_2 sorption data, when plotted against its concentration, exhibits a trend that is not typical of CO_2 sorption in coal (Gertenbach *et al*., 2009) (see Appendix D.5). The reader is referred to Appendix D.5, where the CO_2 sorption was modelled by typical adsorption models (Langmuir, Freundlich and DR), and was shown to have a poor fit in each case. It is therefore likely that SO_2 has a complex effect on the CO_2 sorption. Varying the CO_2 concentration by the addition of SO_2 is seen not to be equivalent to varying its concentration through the addition of N_2 or CH_4, as was done by Chaback *et al*. (1996), which did not cause the CO_2 sorption to stray from Langmuir adsorption behaviour. A related observation is the great amount by which the CO_2 sorption is seen to vary (almost 100%) over the small concentration range considered (93% to 100% CO_2). This indicates that it is likely that the concentration of CO_2 is not the main driving force for its sorption, and leads to the same conclusion that the CO_2 adsorption cannot be successfully modelled independently of interactive SO_2 effects.

The SO_2 sorption following Henry's law indicates that the sorption of this component occurs independently of the presence of CO_2 and only relies on its concentration in the sorbate. According to adsorption site theory, as the SO_2 concentration increases, it preferentially occupies the sorption sites, which in turn decreases the amount of sorption of CO_2 that can take place. However, if the same number of adsorption sites are available for each coal sample, then the total amount of sorption would remain the same regardless of the SO_2 concentration. The fact that the total moles sorbed per gram coal drops for the increased levels of SO_2, indicates that SO_2 is having additional effects on the CO_2 sorption other than displacing CO_2 from a proportional amount of adsorption sites.

To explain the drop in total sorption and the deviation of CO_2 sorption from typical adsorption behaviour, it is postulated that SO_2 not only preferentially occupies the adsorption sites, but also has an interactive effect with CO_2 that

inhibits the CO_2's sorption. It is possible that the adsorbed SO_2 decreases the total amount of space available for adsorption due to its larger molecular size. i.e. better coverage of the micropore surface area of the coal would be possible if only smaller CO_2 molecules were adsorbed. The presence of SO_2 on the surface of the coal could also decrease the amount of absorption of CO_2 into the coal matrix, which has been proposed to occur under supercritical conditions (Day *et al*., 2007). This theory is partially backed up by the FTIR results in Section 4.2.5, which reveal a decrease in the size of the 'physisorbed CO_2' peak at the greatest concentration of SO_2. However, the size of the physisorbed CO_2 peak does not decrease for lower SO_2 concentrations (3.20% SO_2), where the total sorption is the least, which therefore strays from the trend. Even though much speculation is possible as to the mechanisms by which the CO_2 sorption is inhibited, a key observation from these results that corresponds to the aim of the study is that SO_2 has a clear interactive influence on CO_2 sorption.

The rise in CO_2 sorption at 6.69% SO_2 seen in Figure 4.15 (even though CO_2 physisorption is clearly low for this sample according to the FTIR results in Section 4.2.5) could be due to chemical effects the higher concentration of SO_2 could have that enhance the coal's sorption characteristics. This is, however, in contrast to findings of Sakurovs *et al*. (2011) who found that coal exposed to pure SO_2 for a three year period chemically reduced the sorptive abilities of the coal. Sakurovs *et al*.'s (2011) experiment was fundamentally different to the present study though, and different chemical effects could have occurred over their much longer experimental run time. Since there is only a single data point at these very high levels of SO_2, it may also be necessary to produce more data in this region to validate the trend. Nevertheless, no conclusive evidence of chemical effects was observed through the FTIR results (Section 4.2.5), and thus other post sorption analyses would be necessary to shed light onto this speculation. It is concluded that other post sorption analyses, such as Raman spectroscopy, XRD or BET, could be valuable for a greater level of understanding of the results as a whole by helping to distinguish between the mechanisms of adsorption, absorption and chemisorption.

If the attention is shifted away from Figure 4.15 and towards the composition of the sorbed phase, additional discussion points reveal themselves. Literature states that in the presence of multiple gases, the amount of each gas in the adsorbed state would be approximately in proportion to the respective affinities of each to the coal (Bachu, 2008a). Since SO_2's affinity for coal is far greater than that of CO_2, one would expect it to exist in a high proportion in the adsorbed state. This behaviour is evident from the results produced, as SO_2 is sometimes observed to comprise the majority of the sorbed phase even though it exists in a minor amount in the sorbate. The reader is referred to Figure 4.16 which plots the percentage of SO_2 and CO_2 in the sorbed phase versus the initial concentration of the sorbate.

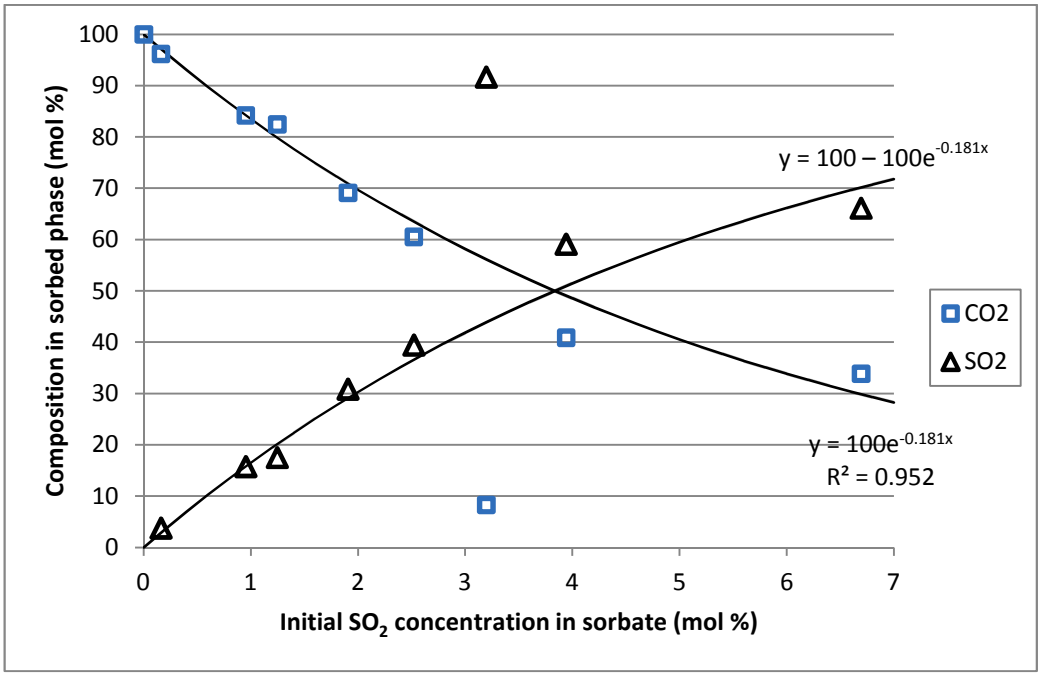


Figure 4.16: Percentage of SO_2 and CO_2 in the sorbed phase as a function of its initial concentration of the sorbate. Note: the outlying points at 3.20% SO_2 are excluded from the trendline functions.

From Figure 4.16, it is evident that the percentage of CO_2 in the sorbed phase decreases as the initial level of SO_2 present increases. This relationship is seen to follow an exponential trend, in this concentration range. This trend is consistent if the outlying points at 3.20% SO_2 are omitted – a large standard deviation exists on the GC measurements for 3.20% SO_2, which can explain the great deviation from this trend without affecting the excess sorption calculated as significantly; see Section 4.2.4. The bearing the modelling of the sorbed phase composition has is

that, if the initial concentration of SO_2 is known, then it may be possible to predict the number of moles of each component (SO_2 and CO_2) sorbed at the end of a future sorption experiment without GC analysis conducted at the end of each run. i.e. the functions fit to the experimental data in Figure 4.16 could be used to instead of drawing a sorbate sample from the sample cell and analysing its concentration (if all experimental parameters, such as pressure, temperature, and coal, were identical). The production of a verified function of this kind may thus reduce the need for elaborate experimental setups for experiments of this nature.

The main findings in this section reveal that the presence of SO_2 decreases the sorption of CO_2 at supercritical conditions of approximately 85 bar and 40°C. This is in accordance with literature, which states that it is likely that SO_2 will be preferentially adsorbed by coal due to coal's strong affinity for it, thus reducing the storage capacity for CO_2 (IPCC, 2005). Although, there is evidence in Figure 4.15 to suggest that the effects of SO_2 are not limited purely to simple preferential adsorption at the high pressure conditions of the study. It can, nevertheless, be concluded that SO_2 is unfavourable when it is desired to store CO_2 in coal through the process of sorption at any concentration between 0% and 6.69% SO_2. SO_2, even at low concentrations relevant to CCS (< 2%), can reduce the total and CO_2 sorption significantly, and should therefore be accounted for in storage capacity estimations if it is present in the CO_2 stream.

ii. Patel-Teja Equation of State Density Prediction

The Patel-Teja EOS is a cubic model that has been used to predict the VLE properties of CO_2-SO_2 mixtures relatively accurately (see Section 4.2.2 for a full discussion). This method has been used to predict the mixture densities relevant to the experiment, which are then used to calculate the respective sorption values. Figure 4.17 has thus been produced, which is analogous to Figure 4.15 which used Amagat's law for its mixture density predictions. Figure 4.17 is presented and the outlying point at 3.72% SO_2 that was discarded due to experimental error described previously has been omitted on the same grounds (see discussion in Part (i)).

The total excess sorption values calculated ranged from 1.3 mmol/l to 6.6 mmol/l when the SO_2 concentration in the feed was less than 4%, and 14.4 mmol/l when the SO_2 concentration is higher at 6.69%. These sorption values far exceed those seen in literature for pure CO_2 and CH_4 streams (0.6 mmol/g – 2.5 mmol/g; Gertenbach *et al*. (2009)) and thus point to a very significant influence of SO_2.

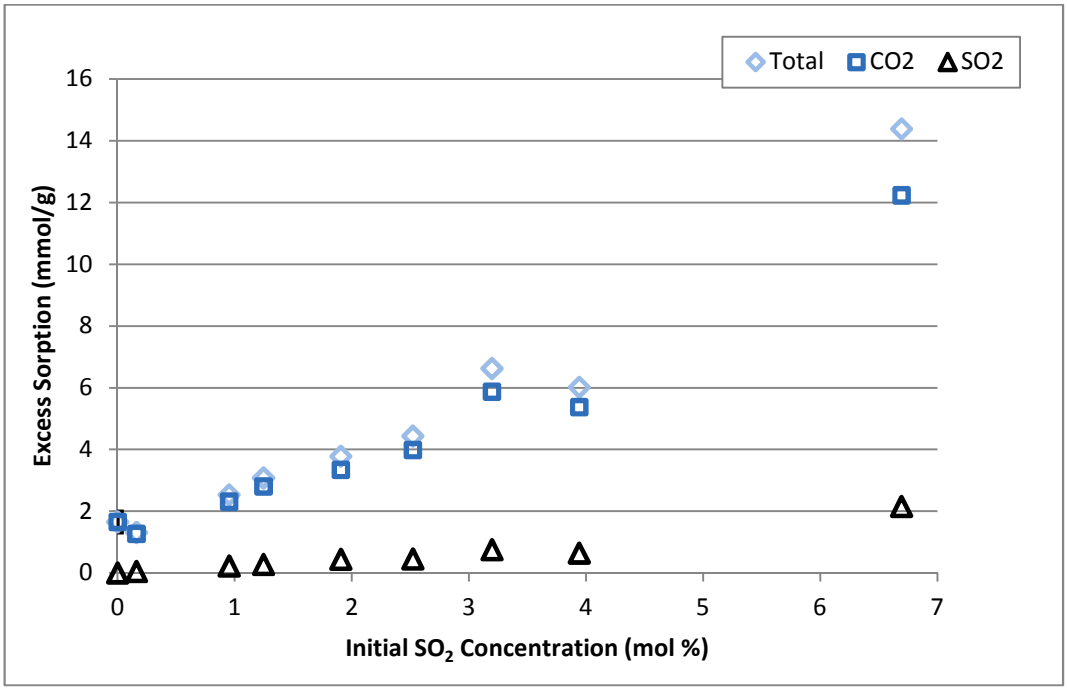


Figure 4.17: Excess sorption in a typical South African coal when exposed to CO_2 mixtures with differing initial sorbate concentrations of SO_2. The temperature is 40 ℃ and the initial pressure is approximately 85 bar. The mixture density was calculated using the Patel-Teja EOS.

From Figure 4.17 it is evident that the total sorption, as well as that of SO_2 and CO_2 individually, increases with increasing SO_2 concentration. The increase of the SO_2 sorption can again be described relatively well by Henry's law adsorption (R^2 = 0.89). However, the sorption of CO_2 clearly cannot be described by a conventional adsorption model due to its sorption increasing greatly as its concentration in the mixture decreases. It is apparent that SO_2 not only sorbs strongly itself to coal, but its presence also greatly improves the sorption of CO_2. For instance, the addition of 1.91% SO_2 doubles the amount of CO_2 sorbed when compared with the case of pure CO_2, while the addition of 6.69% SO_2 improves CO_2 sorption more than 7 fold. It is reinforced that these results were produced at the same pressure and temperature conditions (approximately 85 bar and 40°C) and the coal samples were from the same population.

Before considering how SO_2 was able to modify the sorption properties of the coal, it is worth considering how the presence of SO_2 could enhance the properties of the sorbate. It is seen in Section 4.2.2 that, according to the Patel-Teja EOS, the density of the mixture is very strongly dependent on the concentration of SO_2 in the mixture, where the more SO_2 there is present, the greater the density of the sorbate will be. This means that if the sample cell is filled with sorbate to a set pressure for each run, by performing runs with increasing levels of SO_2, the starting density of the mixture will increase from run to run. In turn the starting number of moles of all components will be greater for higher concentrations of SO_2 than for lower concentrations. In general, the greater the number of moles of sorbate present at the beginning of the experiment, the greater the driving force for sorption to take place, which could explain the increasing sorption trends observed in Figure 4.17. In order to avoid comparing the amount of sorption that occurs when the starting number of moles of sorbate differ, sorption isotherms are sometimes plotted as a function of density rather than pressure. Figure 4.18 is thus produced which plots the mixture density as a function of initial SO_2 concentration in order to see whether the starting density for each mixture varied significantly, which would render the results incomparable.

It must be noted that the problem of not maintaining a consistent density for each experimental run could have been overcome if sorption isotherms where produced as opposed to considering only a single pressure step. However, this problem was not foreseen and only manifested itself when the mixture density is a strong function of the concentration (even at low impurity levels). The preferable use of sorption isotherms will thus be one of the recommendations listed in Section 5.2. However, additional experimental time should be accounted for in the future project if it is desired to maintain the hold-times of 48 hours at each pressure.

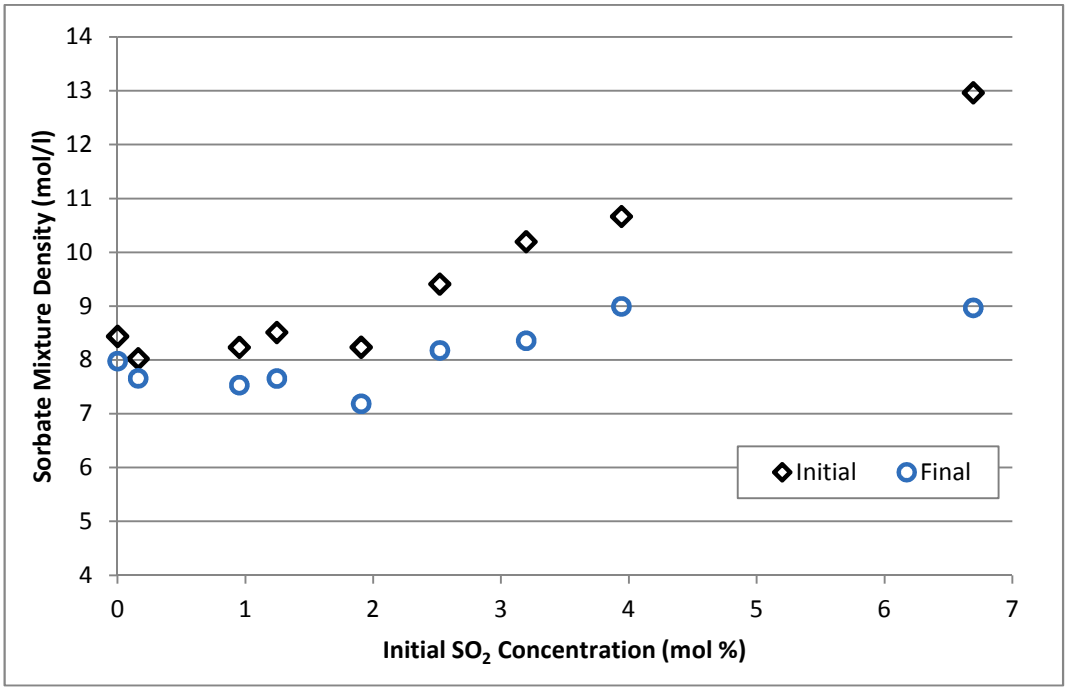


Figure 4.18: The initial and final sorbate densities determined by the Patel-Teja EOS corresponding to each sorption experiment run for different initial concentrations of SO_2

From Figure 4.18 it is clear that the densities for the mixtures that are greater than 2% SO_2 are significantly higher than those for mixtures less than 2% SO_2. For this reason, the sorption capacities calculated for the mixtures greater than 2% SO_2 cannot be compared with pure CO_2 or the other mixtures. Due to the initial sorbate density for the mixtures less than 2% SO_2 being relatively constant (due to slight variations in initial pressure in addition to the composition changes), it is still possible to compare the sorption capacities of the mixtures below this concentration. The CO_2 sorption still increases by a significant amount with increasing SO_2 levels in this range (40% and 100% increases at 0.95% SO_2 and 1.91% SO_2 respectively). This could be due to the CO_2 sorption characteristics of the coal being enhanced due to a reactive effect of the coal with SO_2. Another possibility is that these sorption results are erroneous due to incorrect mixture density predictions. The possibility of erroneous density predictions are discussed further in Part (iii).

When the Patel-Teja EOS is used to predict the mixture densities, it can be concluded that SO_2 is strongly sorbed by the coal and has a clear interactive effect on the sorption of CO_2, whereby the sorption of CO_2 significantly improved. This behaviour could only be observed when the SO_2 concentration was less than 2%,

due to experimental error at higher concentrations. The positive effects of SO_2 on the sorption capacity are in contrast with effects observed by Sakurovs *et al*. (2011) and trends expected by IPCC (2005). The mechanism by which the amount of CO_2 sorption is increased due to the presence of SO_2 remains unclear; even after considering FTIR analysis results (see Section 4.2.5). However, further analysis of the treated coal, which is beyond the scope of the present study, may be able to shed light on these mechanisms.

iii. Comparison of Sorption Results obtained from different Density Prediction Methods

By comparing the results and discussions in Parts (i) and (ii), it is clear that the density predictions can have a strong impact on the sorption results and trends observed. The density predicted by Amagat's law, in Part (i), is not a very strong function of the SO_2 concentration, while the density predicted by the Patel-Teja EOS, in Part (ii), is strongly influenced by even small amounts of SO_2 (see Section 4.2.2). This difference leads to contradictory trends being observed in the effect of sorption as a function of SO_2. The sorption of CO_2 is seen to decrease when SO_2 is present in Part (i) leading to the conclusion that SO_2 is unfavourable for CO_2 storage; while in Part (ii) the opposite effect is observed where SO_2 is seen to increase the sorption of CO_2 resulting in SO_2 being viewed as favourable for CO_2 storage. These observations are highlighted through the use of Figure 4.19.

The discrepancy between the sorption results that have been produced by each density prediction method is purely mathematical. It is difficult to define which method is more correct as there is little literature available where the density of SO_2-CO_2 mixtures has been predicted at the specific pressure, temperature and concentration conditions of the experiment. The Patel-Teja EOS has proved relatively accurate at certain VLE conditions, while Amagat's law is a density *estimation* technique and its accuracy cannot be confirmed unless experimental data is available.

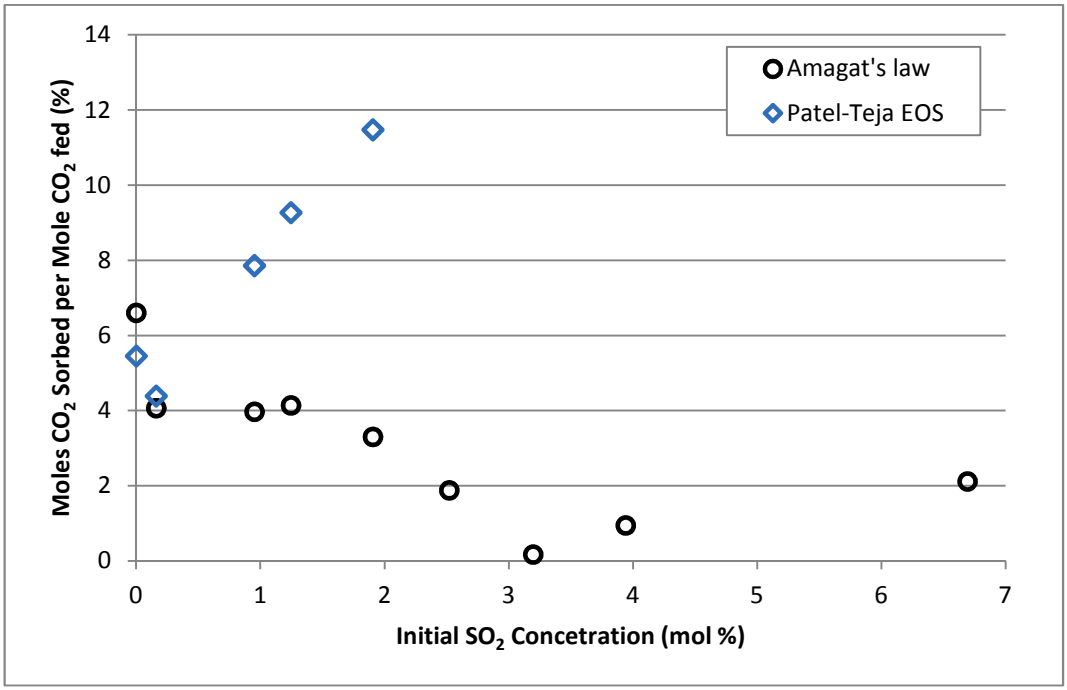


Figure 4.19: Percentage CO_2 sorbed, calculated as* 100 x *(Moles CO_2 sorbed)/(Moles CO_2 fed), as a function of the initial SO_2 concentration in the mixture. This is compared for scenarios where the mixture density was determined using Amagat's law and the Patel-Teja EOS.

Based on the results of the excess sorption capacities calculated, there is some reason to doubt the accuracy of the Patel-Teja model density predictions, since very high CO_2 sorption capacities, e.g. 12 mmol/g for a 6.69% SO_2 mixture, were observed (see Figure 4.17). This level of CO_2 sorption is deemed unlikely as the adsorption in some zeolites, which are synthesised specifically to adsorb CO_2, is less than 12 mmol/g at optimum high pressure conditions (Youn *et al.*, 2010). Errors in measuring the concentration of the mixtures will also have a large impact on the density predictions when the Patel-Teja method is used. The standard deviation on the peak areas generated in the chromatograms was seen to be as high as 32% (see Section 4.2.4) which would also have an influence on the accuracy of the sorption capacities calculated. A simple error analysis showed that if the peak areas were lowered by 10%, the excess sorption of pure CO_2 predicted decreased by an average of 7.2%.

Another possible source of error is the value of the binary interaction parameter applied to the Patel-Teja EOS. As was mentioned in Section 4.2.2, there is sufficient reason to doubt the value used that was obtained from literature (see discussion in Section 4.2.2 for more details). A simple error analysis revealed that

if the binary interaction parameter is decreased from the value reported in literature of 0.953 to 0.94, the excess sorption of CO_2 decreases by 5.7% on average over the SO_2 concentration range. It is known that this parameter is taken to be unity if no literature data is available, but may also be significantly above or below unity. The great influence of small changes to this parameter, and its empirical nature, makes it possible that it contributed most to the amount of sorption being over-predicted.

The excess sorption capacities produced through the Amagat's law approach, on the other hand, were all reasonable, and thus the accuracy of these density predictions cannot be doubted on this basis. It may therefore be possible that the mixture densities estimated under these conditions by Amagat's law are closer to the real density values even though it is the more basic of the density prediction techniques considered. It is proposed that the Patel-Teja EOS, which is relatively sophisticated, may be prone to greater errors if an accurately calibrated value of the binary interaction parameter under the experimental conditions is not available and experimental error exists in the concentration determination. However, this speculation cannot be verified and must thus be treated with caution.

4.3 Summary of Key Findings

This chapter presented all relevant results from the study and discussed them with more detail being provided in areas that relate directly to satisfying the aims and objectives of the study.

The coal used in the study has been characterised according to its elemental, proximate, and petrographic composition; its surface and structural properties according to BET analysis, as well as its density (sample volume). These results lead to the confirmation of the coal as a typical bituminous South African coal with high ash content and high inertinite composition. The properties analysed provide suitable grounds to judge whether the sorption capacity results of other studies are comparable with those of this study.

The bulk of the chapter was dedicated to the sorption capacity results and their analysis. The important parameters, both experimentally determined and

calculated, that are used to quantify the sorption in the coal were presented and discussed along with the errors associated with the determination of these parameters. The free volume, sorbate density, pressure data, and gas composition are all key parameters for excess sorption determination. Of these parameters, it is necessary to highlight that the accurate prediction of the density of SO_2-CO_2 mixtures at supercritical conditions is very challenging due to a lack of literature on this topic as a comparative basis. Thus, the mixture density was calculated using two techniques for comparison: (i) a density estimation technique based on Amagat's law; and (ii) a cubic model, the Patel-Teja EOS. Post-sorption sample analysis results, produced via FTIR spectroscopy, were also interpreted. Finally, the sorption is quantified and discussed in depth with regard to the influence of SO_2 concentration in the CO_2 stream on its magnitude.

Key findings are that the sorption of SO_2 is very strong in the coal and that its sorption increases with increasing concentration initially present in the CO_2 stream contacted with the coal. The concentration of SO_2 present in the sorbed phase at the end of the experiment far exceeds its concentration in the sorbate at the beginning of the experiment. These observations agree well with literature (Bachu, 2008a; IPCC, 2005). A finding of the FTIR analysis was that physisorbed CO_2 was clearly observed in the depressurised coal samples that had been treated in the sorption experiments. In addition, the amount of physisorbed CO_2 observed was considerably lower for the sample that was exposed to the highest concentration of SO_2 (6.69%), indicating a significant influence of SO_2.

The influence of SO_2 on the sorption of pure CO_2, as observed from the excess sorption plots (Figures 4.15 and 4.17), is more complex and different trends are observed depending on how the SO_2-CO_2 mixture density is determined from the parameters of pressure and concentration. When the density estimation approach based on Amagat's law was employed:

- The CO_2 sorption of the coal generally decreased as a function of the sorbate SO_2 concentration when SO_2 levels ranged from pure CO_2 to 3.94% in CO_2.

- The SO_2 appeared to adsorb preferentially on the adsorption sites of the coal, which decreased the adsorption of CO_2. This agrees well with speculation in literature.
- This leads to the conclusion that SO_2 is unfavourable for coal seam CO_2 storage.

Alternatively, when the Patel-Teja EOS was used to predict the mixture density:

- An increased presence of SO_2 in the sorbate greatly enhanced the sorption of CO_2 in the coal.
- This observation alludes to a more complex influence of SO_2 on sorption, and further insight explaining these results was not possible from FTIR analysis.
- The conclusion that SO_2 has favourable influences coal seam CO_2 storage follows from the results.
- However, these results did produce suspiciously high sorption values (~14 mmol/g for 6.69% SO_2) and thus are expected to contain errors.

Hence, it is seen that accurate density predictions are vital when performing sorption analyses on mixtures as inaccurate modelling can lead to meaningless results. The accurate prediction of the density of SO_2-CO_2 mixtures at supercritical conditions should be investigated further. Thus, the conclusions that can be drawn on the effect of SO_2 on the coal sorption of CO_2 are limited to the accuracy of the density prediction method employed. Even though the results and trends observed when the Amagat's law approach is used seem more reliable than those observed when the complex EOS is utilised, there is no evidence that can support either of these density predictions as experimental density data is scarce. Thus, no high level of certainty can be offered with regard to the sorption trends observed.

CHAPTER 5: Conclusions and Recommendations

A project with the aim of exploring the effects of impurity gases on the sorption capacity of coal was conceived. After a literature survey was conducted, it was observed that the biggest research gaps existed with respect to minor component impurities that are present in variable amounts in captured CO_2 streams. Of these components, SO_2 was selected as the focus as it was seen from literature to have interesting sorption properties and effects on coal. The project was thus refined by defining specific aims and objectives that are described in Section 1.3.

A methodology was produced, which centred around volumetric adsorption studies. The amount of sorption was determined when coal samples were in contact with pure CO_2 as well as CO_2-SO_2 mixtures of different concentration at supercritical conditions (85 bar and 40°C) for 48 hours. The main set of results was a plot of the excess sorption of the coal as a function of SO_2 concentration. These results were analysed with respect to satisfying the aims and objectives of the study. This final chapter will describe the conclusions that can be drawn from the findings of the project in bullet form under various subheadings pertaining to the aims and objectives of the study in Section 5.1. Recommendations for future projects are provided separately in Section 5.2.

5.1 Conclusions

Equipment Modifications

- In order to introduce impure CO_2 streams to the volumetric adsorption setup at Wits and analyse the results meaningfully, certain equipment modifications were necessary.
- A mixing system was built and commissioned (by Chemvak cc.) that enabled impurity gases to be mixed with liquid CO_2 so that mixtures representative of different captured CO_2 streams could be produced and supplied successfully to the VAS. In the case of the project, CO_2 was spiked with small amounts of SO_2 so that different SO_2-CO_2 mixtures were produced.

- A means of sampling the mixtures prior to as well as after the sorption experiments was necessary so that the initial concentration of the mixture could be determined along with the proportion of each component sorbed by the coal. A sampling system was thus installed which enabled fluid samples to be drawn from the expansion volume and sample cell of the VAS and sent for GC analysis.
- The experiment modifications were successful and enabled the production of SO_2-CO_2 mixtures for the project ranging from 0.16% to 6.69% SO_2. It was easy to determine the amount of each component sorbed from concentration measurements taken both prior to and after sorption.

Sorption Behaviour of SO_2

- SO_2 was seen to sorb very strongly to coal when it exists in a binary mixture with CO_2. After being in contact with the coal for 48 hours at supercritical conditions, the final concentration of the SO_2 in the sorbate was significantly lower than present at the beginning of the experiment, which indicates that it is sorbed preferentially to CO_2 in the coal (if CO_2 and SO_2 were sorbed at the same rate, the sorbate concentration would remain constant).
- The amount of SO_2 sorbed increased with increasing concentration of SO_2 originally present in the sorbate. The percentage of SO_2 in the sorbed phase at all concentrations of SO_2 is far greater than its concentration in the fluid phase.
- These findings agree well with literature which reveals that SO_2 adsorbs more strongly to coal than CO_2 and will thus be present in a high concentration in the adsorbed phase (IPCC, 2005). This behaviour can now be confirmed to hold true under supercritical conditions for a 48 hour sorption period.

Sorption Calculations for SO_2-CO_2 mixtures

- An important parameter when calculating the amount of sorption occurring in a volumetric sorption experiment is the sorbate density at the outset and end of the experiment run time. The sorbate density can be

determined with a high level of accuracy when the sorbate is pure CO_2 or most other pure components due to well-developed equations of state, that are often semi-empirical, being readily available.

- However, it is more difficult to make accurate density predictions when the sorbate is a mixture. The density predictions for SO_2-CO_2 mixtures are identified to be very challenging when compared with predictions for other SO_2-impurity mixtures relevant to CCS (Li and Yan, 2009).
- Two methods were thus used to predict the densities of the mixtures: (i) an approach based on Amagat's law that is simple to apply when NIST database resources are used; and (ii) a cubic model, the Patel-Teja EOS, which has been applied to SO_2-CO_2 mixtures in previous work (Li and Yan, 2009). The Amagat's law approach is generally used as an 'estimation' technique and would not be expected to give highly accurate results; while the more complex model is very dependent on a binary interaction parameter that is typically required to be empirically determined over narrow pressure-temperature-concentration ranges to ensure accurate results. Thus, there is uncertainty for both approaches considered.
- The sorption calculated using each of these methods revealed contradictory trends for the effect of SO_2 on the CO_2 sorption. It can thus be concluded that a great amount of emphasis and care should be placed on the density prediction model used in sorption studies involving mixtures.

Effect of SO_2 on the sorption of CO_2 in coal

- The influence of SO_2 on the sorption of CO_2 was determined primarily by plotting the excess sorption, calculated from the data obtained from the volumetric adsorption experiments, as a function of the SO_2 concentration. With the hopes of supplementing the sorption findings, FTIR analysis was performed on the post-sorbed samples. The most conclusive findings of the FTIR analysis were that: (i) physisorbed CO_2 was clearly observed in the coal samples treated in the sorption experiments, and (ii) the amount of

physisorbed CO_2 observed was considerably low for the sample exposed to the highest concentration of SO_2 considered.

- When the Amagat's law density estimation approach is employed, the sorption of CO_2 decreases as the SO_2 concentration of the mixture increases. From adsorption theory it is possible to deduce that SO_2 competes with CO_2 for the coal's adsorption sites and, since it is more strongly adsorbed, reduces the adsorption of CO_2 significantly over the SO_2 concentration range of 0.16% to 6.69%. The excess sorption of CO_2 is seen to drop by 43% when introducing 1.25% SO_2 to the sorbate, which is a realistic amount of SO_2 in an oxyfuel captured stream. The influence of SO_2 is, however, not limited to simple adsorption interactions as there are indications of more complex sorption behaviour being influenced; however, these influences could not be clearly understood without further analytical procedures. Due to the effects observed, SO_2 is judged to be undesirable in coal seam storage where a high sorption capacity is important.
- When the Patel-Teja EOS is used to predict the mixture density, the CO_2 sorption increases significantly as a function of SO_2 concentration, while the SO_2 sorption also increases as a function of SO_2 concentration. This is difficult to explain using adsorption theory, while the chemical effects observed from FTIR analysis performed on the sorption-treated samples could not support these findings either. Either further analysis on the samples is necessary in order to explain these findings or there is an experimental error inducing erroneous results. The excess sorption calculated at certain SO_2 concentrations was suspiciously high (up to 14.4 mmol/g) which alludes to the latter explanation. A likely source of error is the use binary interaction parameter in the model which, although obtained from literature to be calibrated for the components in the mixture, was not calibrated for specific conditions of the experiment.
- From both methods it is observed that the amount of CO_2 sorbed by the coal is influenced significantly by the concentration of SO_2. Thus, there is enough evidence to suggest that SO_2 effects should be taken into account

when calculating the storage capacity of coal seams if SO_2 is present in a the CO_2 stream to be stored. This holds true even for low levels of SO_2.

- There is no evidence that can support the accuracy of the mixture density predictions for when either method is considered, as experimental density measurements, under the desired conditions, to which the predictions can be compared are scarce. Thus, no degree of certainty can be offered with regard to the sorption results produced, due to the high dependence of the calculated sorption on density predictions.

5.2 Recommendations

At the completion of the project, it has become clear as to how many aspects of the project could be improved to provide more reliable, consistent, and/or insightful results. Recommendations for future work in order to advance research into coal sorption-impurity interactions are listed here.

- This study chose to analyse the sorption at a single set of pressure-temperature conditions in order to accommodate for longer experimental run times and analyse a greater number of SO_2 concentrations. Several short-comings, due to this, were however encountered where several pressures were overshot and/or the presence of SO_2 influenced the starting density. The variation of these variables, in addition to the SO_2 concentration, caused experimental error when comparing sorption capacities. Thus it is recommended that more than one pressure be considered for each SO_2 concentration in order to overcome this problem and ideally sorption isotherms for each mixture should be compared. Interest should be extended to sub-critical conditions as several sources quote these as preferable coal seam storage conditions due to permeability considerations.
- It is recommended that He be used as the carrier gas in the GC analysis as opposed to N_2 used in this study. Helium is expected to give sharper signals for low concentrations of SO_2, and would thus help reduce experimental errors observed.

- It has been highlighted in this study that there is significant uncertainty surrounding density prediction methods for SO_2-CO_2 mixtures. In order to predict the sorption capacity accurately using the volumetric method, the density of the mixture must be predicted as accurately as possible. If there are several different density prediction methods recommended for a mixture, each should be considered in order to determine the effect of this parameter on the sorption capacity. In this study, the results from two different density models for SO_2-CO_2 mixtures are compared. It is possible for more density models to be applied to the experimental data for a greater comparison of the effect of density prediction on sorption. Some additional EOS's that can be included for further analysis are the SRK and PR EOS's and their modifications.

  When binary interaction parameters are used in EOS models, these parameters should be determined as accurately as possible under the most relevant conditions as possible. From the literature survey, it was established that the experimental data which can be used to determine accurate SO_2-CO_2 binary interaction parameters is very scarce. It is thus proposed that further data for regression of binary interaction parameters are produced experimentally for a variety of CCS conditions. Alternatively, prediction methods that do not rely on binary interaction parameters, may also be applied. Such methods include the Lee-Kessler type equations.

  In order to know which model predicts the density accurately, it is necessary to know the true density at conditions similar to those which are being modelled. Hence, it is essential to have reliable experimental density data in order to validate any model. Since this data is not freely available for SO_2-CO_2 mixtures under high pressure conditions, it is recommended that experiments are conducted to produce this data. An experimental setup that combines flue gas density measurement with sorption determination would be ideal for the purposes of the study (see experimental setup of Mazumder *et al*. (2006)).

Since sorption capacity determination for SO_2-CO_2 mixtures using the volumetric method is very dependent on density modelling, it could be advantageous to bypass this dependence by using gravimetric sorption apparatus. Thus, if the certainty of the SO_2-CO_2 mixture density predictions cannot be improved, a gravimetric experimental method could potentially be used, as alternative to the volumetric method, to determine the sorption accurately.

- One of the ideas considered when the project was conceived was that the impact of several different impurities would be included in the study. However, this idea was abandoned in order to focus in greater depth on a single component. Although the influences of SO_2 are still not completely understood, it is recommended that future projects consider the impacts of common gaseous impurities, such as NO_2, H_2S, O_2, Ar, etc., in coal sorption studies.
- From the sorption results there is evidence to suggest that mechanisms other than just adsorption occurred in the 48 hour sorption period, and a greater understanding of the specific sorption processes occurring would help with the interpreting of the effect of the impurity. Thus, FTIR analysis was introduced, and, while it shed light on some areas, was not wholly conclusive. There is, therefore, a need for robust, post-sorption analysis on the samples that have been treated with the high pressure fluids. Some analyses that may provide insight into the samples that have been exposed to the sorption experiments include Raman spectroscopy, XRD, and BET analyses.
- The sorption experiments in this study were run for a relatively short time of 48 hours with the focus on reaching adsorption equilibrium. If long term experiments were run (for periods in the order of months or years) simultaneously with the short term experiments, greater chemical effects could be observed. These results would also be more representative of underground storage, where long term effects are important.
- Other variables that could be modified to make the study more representative of underground conditions include: the introduction of

moisture to the coal (the presence of H_2O would certainly influence the impurity effects), and the consideration of large coal particles instead of pulverised coal.

REFERENCES

Aydin, G., Karakurt, I. and Aydiner, K. 2010, "Evaluation of geologic storage options of CO_2: Applicability, cost, storage capacity and safety", *Energy Policy*, vol. 38, no. 9, pp. 5072-5080.

Air Liquide Gas Encyclopaedia. 2013, [Online] Available at: <http://encyclopedia .airliquide.com/encyclopedia.asp> [Accessed 13 August 2014]

Asia Industrial Gases Association. 2009, *Carbon Dioxide*, AIGA 068/10, 7th Edition [Online] Available at: <http://www.asiaiga.org/docs/AIGA%20068_ 10%20Carbon%20Dioxide_reformated%20Jan%2012.pdf> [Accessed 28 March 2013]

Bachu, S. 2008a, "CO_2 storage in geological media: Role, means, status and barriers to deployment", *Progress in Energy and Combustion Science*, vol. 34, no. 2, pp. 254-273.

Bachu, S. 2008b, *Comparison between Methodologies recommended for Estimation of CO_2 Storage Capacity in Geological Media, Phase III Report*. The Carbon Sequestration Leadership Forum (CSLF) Task Force on CO_2 Storage Capacity Estimation, Canada.

Bachu, S., Bonijoly, D., Bradshaw, J., Burruss, R., Holloway, S., Christensen, N.P. and Mathiassen, O.M. 2007, "CO_2 storage capacity estimation: Methodology and gaps", *International Journal of Greenhouse Gas Control*, vol. 1, no. 4, pp. 430-443.

Bachu, S. and Gunter, W.D. 2005, "Overview of acid-gas injection operations in Western Canada" in *Greenhouse Gas Control Technologies 7*, eds. Elsevier Science Ltd, Oxford, pp. 443-448.

Bhebhe, S. 2008, *The Effect of Coal Composition on Carbon Dioxide Adsorption*. MSc. University of the Witwatersrand.

Belmabkhout, Y., Frère, M. and De Weireld, G. 2004, "High-pressure adsorption measurements. A comparative study of the volumetric and gravimetric methods", *Measurement Science and Technology*, vol. 15, no. 5, pp. 848.

Beck, B. 2012, *CCS: Globally and in South Africa*. Guest presentation in CHMT 7068 course, 1 October 2012, University of the Witwatersrand and the Norwegian University of Technology, in association with the Fossil Fuel Foundation of Southern Africa, unpublished.

Beck, B., Surridge, T., Liebenberg, J. and Gilder, A. 2011, "The current status of CCS development in South Africa", *Energy Procedia*, vol. 4, no. 0, pp. 6157-6162.

Bolland, O. 2012, *CO_2 Capture in Power Plants*. CHMT 7068. University of the Witwatersrand and the Norwegian University of Technology, in association with the Fossil Fuel Foundation of Southern Africa, unpublished.

British Geological Survey. 2012, *CO_2 Storage — Sleipner field beneath the North Sea*. [Online] Natural Environment Research Council. Available at: <http://www.bgs.ac.uk/science/CO2/home.html> [Accessed 8 October 2012]

Chaback, J.J., Morgan, W.D. and Yee, D. 1996, "Sorption of nitrogen, methane, carbon dioxide and their mixtures on bituminous coals at in-situ conditions", *Fluid Phase Equilibria*, vol. 117, no. 1–2, pp. 289-296.

Cheah, S.M. 2000, *Vapour-Liquid Equilibria*. [Online] Available at: <http://www.separationprocesses.com/Distillation/MainSet1.htm> [Accessed 15 June 2013]

Chemvak cc. 2012, *Proposed CO_2 Gas Mixing System: System Description and Budget Quote*. pp. 1-5.

Courtright, H. and Howard, M. 2009, *Creating a Secure Low-Carbon Future*. [PDF Presentation] Electric Power Research Institute. Available at: <http:// www.rff.org/Documents/Events/Seminars/First_Wed_Seminars/090915_EPRI_Howard.pdf> [Accessed 01 August 2013]

Crandell, L.E., Ellis, B.R. and Peters, C.A. 2010, "Dissolution Potential of SO_2 Co-Injected with CO_2 in Geologic Sequestration", *Environmental science & technology*, vol. 44, no. 1, pp. 349-355.

Day, S., Duffy, G., Sakurovs, R. and Weir, S. 2008, "Effect of coal properties on CO_2 sorption capacity under supercritical conditions", *International Journal of Greenhouse Gas Control*, vol. 2, no. 3, pp. 342-352.

De Silva, P.N.K. and Ranjith, P.G. 2012, "A study of methodologies for CO_2 storage capacity estimation of saline aquifers", *Fuel*, vol. 93, no. 0, pp. 13-27.

de Visser, E., Hendriks, C., Barrio, M., Mølnvik, M.J., de Koeijer, G., Liljemark, S. and Le Gallo, Y. 2008, "Dynamis CO_2 quality recommendations", *International Journal of Greenhouse Gas Control*, vol. 2, no. 4, pp. 478-484.

Directive 2009/31/EC of the European Parliament and of the Council on the geological storage of carbon dioxide. 2009, (c.4) Official Journal of the European Union.

Dubinin, M.M. 1967, "Adsorption in micropores", *Journal of colloid and interface science*, vol. 23, no. 4, pp. 487-499.

Edgar, T.F. 1983, *Coal Processing and Pollution Control Handbook*. Houston, Texas: Gulf Publishing Co.

Faust, C.B. 1992, *Modern Chemical Techniques*. Royal Society of Chemistry. Education Department.

Felder, R.M. and Rousseau, R.W. (eds.), 2000, *Elementary Principles of Chemical Processes*. Third edition. New York: John Wiley & Sons, Inc.

Foo, K.Y. and Hameed, B.H. 2010, "Insights into the modeling of adsorption isotherm systems", Chemical Engineering Journal, vol. 156, no. 1, pp. 2-10.

Gertenbach, R.M. 2009, *Methane and carbon dioxide sorption studies on South African coals*. MSc. University of Stellenbosch.

Goodman, A.L., Campus, L.M. and Schroeder, K.T. 2005, "Direct Evidence of Carbon Dioxide Sorption on Argonne Premium Coals using Attenuated Total Reflectance Fourier Transform Infrared Spectroscopy", *Energy Fuels,* vol. 19, no. 2, pp. 471-476.

Gorbaty, M.L., Mraw, S.C., Gethner, J.S. and Brenner, D. 1986, "Coal physical structure: porous rock and macromolecular network", *Fuel Processing Technology,* vol. 12, no. 0, pp. 31-49.

Göttlicher, G. and Pruschek, R. 1997, "Comparison of CO_2 removal systems for fossil-fuelled power plant processes", *Energy Conversion and Management,* vol. 38, Supplement, no. 0, pp. S173-S178.

Hasenberg, L. 2008. *Sulfur Dioxide*. In: Kreysa, G. and Schutze, M. (eds.), 2008, *Corrosion Handbook: Corrosive Agents and Their Interaction with Materials: vol. 10: Sulfur Dioxide, Sodium Sulfate*. Weinheim: Wiley-VCH Pub. pp. 1-21.

Heeschen, K., Risse, A., Ostertag-Henning, C. and Stadler, S. 2011, "Importance of co-captured gases in the underground storage of CO_2 : Quantification of mineral alterations in chemical experiments", *Energy Procedia,* vol. 4, no. 0, pp. 4480-4486.

Hogenboom, D. L., Kargel, J. S. and Reiter, M. L. 1996, “Pressure-Volume-Temperature and Phase Relationships of Sulfur Dioxide”. *Lunar and Planetary Science,* vol. 27, pp. 553-554.

IEA. 2010, *Energy Technology Perspectives 2010: Scenarios & Strategies to 2050*, Organisation for Economic Co-operation and Development Publishing.

IEAGHG. 2011, *Effects of Impurities on Geological Storage of CO_2*. 2011/04.

Ihmels, E.C., Lemmon, E.W. and Gmehling, J. 2003, "An equation of state and compressed liquid and supercritical densities for sulfur dioxide", *Fluid Phase Equilibria,* vol. 207, no. 1–2, pp. 111-130.

IPCC. 2005, *IPCC Special Report on Carbon Dioxide Capture and Storage*. Prepared by Working Group III of the Intergovernmental Panel on Climate Change [Metz, B., Davidson, O., de Coninck, H. C., Loos, M. and Meyer, L. A. (eds.)]. Cambridge University Press, Cambridge, United Kingdom and New York, USA, 442 pp.

IPCC. 2007, *Climate Change 2007: The Physical Science Basis*. Contribution of Working Group I to the Fourth Assessment. Report of the Intergovernmental Panel on Climate Change [Solomon, S., Qin, D., Manning, M., Chen, Z., Marquis, M., Averyt, K.B., Tignor M. and Miller H.L. (eds.)]. Cambridge University Press, Cambridge, United Kingdom and New York, USA, 996 pp.

Last, G.V. and Schmick M.T., 2011. *Identification and Selection of Major Carbon Dioxide Stream Compositions*, prepared for United States Department of Energy, 2011/06. Pacific Northwest National Laboratory, Richland, Washington.

Lemmon, E.W., McLinden, M.O., and Friend, D.G. 2011, "Thermophysical Properties of Fluid Systems" in NIST Chemistry WebBook [Online], NIST Standard Reference Database Number 69**,** [Linstrom, P.J. and Mallard, W.G. (eds.)], National Institute of Standards and Technology, Gaithersburg MD, 20899, Available at: <http://webbook.nist.gov> [Accessed 2 April 2012]

Li, H. 2008, *Thermodynamic Properties of CO_2 Mixtures and Their Applications in Advanced Power Cycles with CO_2 Capture Processes*. Ph. D. KTH, Royal Institute of Technology, School of Chemical Science and Engineering.

Li, H. and Yan, J. 2009, "Impacts of equations of state (EOS) and impurities on the volume calculation of CO_2 mixtures in the applications of CO_2 capture and storage (CCS) processes", *Applied Energy*, vol. 86, no. 12, pp. 2760-2770.

Li, H., Jakobsen, J.P., Wilhelmsen, Ø. and Yan, J. 2011, "PVTxy properties of CO_2 mixtures relevant for CO_2 capture, transport and storage: Review of available experimental data and theoretical models", *Applied Energy*, vol. 88, no. 11, pp. 3567-3579.

Li, Q., Li, X., Wei, N. and Fang, Z. 2011, "Possibilities and potentials of geological co-storage CO_2 and SO_2 in China", *Energy Procedia*, vol. 4, no. 0, pp. 6015-6020.

Li, Z., Dong, M., Li, S. and Huang, S. 2006, "CO_2 sequestration in depleted oil and gas reservoirs—caprock characterization and storage capacity", *Energy Conversion and Management*, vol. 47, no. 11–12, pp. 1372-1382.

Lilliestrale, A. 2013, *The impact of the quality of CO_2 on transport and storage behaviour - IMPACTS*, presentation at the 7th Trondheim Conference on CO_2 Capture, Transport and Storage, Norwegian University of Technology, 4-6 June 2013.

Linde AG. 2002, *Safety Instructions: Working with Carbon Dioxide*. [Online] Available at: <http://www.lindegas.hu/internet.lg.lg.hun/en/images/1270_15655.pdf> [Accessed 28 March 2013]

Mandal, D., Tewari, D.C. and Rautela, M.S. 2004, "Analysis of Micro-fractures in Coal for Coal Bed Methane Exploitation in Jharia Coal Field", In: 5th Conference and Exposition on Petroleum Geophysics, Hyderabad, India, pp. 904-909, 15 – 17 January.

Mantovani, M., Chiesa, P., Valenti, G., Gatti, M. and Consonni, S. 2012, "Supercritical pressure–density–temperature measurements on CO_2–N_2, CO_2–O_2 and CO_2–Ar binary mixtures", *The Journal of Supercritical Fluids*, vol. 61, no. 0, pp. 34-43.

Maphada, M. 2013, *Verification of a CO_2 volumetric adsorption system*. MSc. University of the Witwatersrand.

Maphala, T. 2012, *Effects of carbon dioxide storage in coal on the physical and chemical properties of coal*. Ph.D. University of the Witwatersrand.

Mazumder, S., van Hemert, P., Busch, A., Wolf, K.A.A. and Tejera-Cuesta, P. 2006, "Flue gas and pure CO_2 sorption properties of coal: A comparative study", *International Journal of Coal Geology*, vol. 67, no. 4, pp. 267-279.

Mazzoccoli, M., Bosio, B. and Arato, E. 2012, "Analysis and Comparison of Equations-of-State with p-ρ-T Experimental Data for CO_2 and CO_2-Mixture Pipeline Transport", *Energy Procedia*, vol. 23, no. 0, pp. 274-283.

Michael, K., Arnot, M., Cook, P., Ennis-King, J., Funnell, R., Kaldi, J., Kirste, D. and Paterson, L. 2009, "CO_2 storage in saline aquifers I—Current state of scientific knowledge", *Energy Procedia*, vol. 1, no. 1, pp. 3197-3204.

Mikunda, T. and de Coninck, H.C. 2011, *Possible impacts of captured CO_2 stream impurities on transport infrastructure and geological storage formations: Current understanding and implications for EU legislation*. Deliverable 4.1.4 of the CO_2 Remove project 2011/05. ECN (Energy Research Centre of the Netherlands) project no. 77762.

Mondal, M.K., Balsora, H.K. and Varshney, P. 2012, "Progress and trends in CO_2 capture/separation technologies: A review", *Energy*, vol. 46, no. 1, pp. 431-441.

Monea, M. 2013, *Boundary Dam – Progress and Status*, presentation at the 7th Trondheim Conference on CO_2 Capture, Transport and Storage, Norwegian University of Technology, 4-6 June 2013.

National Grid UK. 2013, *National Grid delivers on major milestone for Carbon Capture and Storage.* [Press release] 7 August 2013, Available at: <http://www.nationalgrid.com/corporate/Media+Centre/Press+Releases/Glob

al+Press+Releases/National+Grid+delivers+on+major+milestone+for+Carbon+Capture+and+Storage+06.08.13.htm> [Accessed 9 August 2013]

NORAD (The Norwegian Agency for Development Cooperation). 2011, *EnPe-NORAD´s Master Programme within the energy and petroleum sector: Application form 2011-2014*. 4th Call. Partners: University of the Witwatersrand, South Africa, and Norwegian University of Science and Technology (NTNU), Norway.

Ottiger, S., Pini, R., Storti, G. and Mazzotti, M. 2008, "Measuring and Modeling the Competitive Adsorption of CO_2, CH_4, and N_2 on a Dry Coal", *Langmuir*, vol. 24, no. 17, pp. 9531-9540.

Patel, N.C. and Teja, A.S. 1982, "A new cubic equation of state for fluids and fluid mixtures", *Chemical Engineering Science*, vol. 37, no. 3, pp. 463-473.

Perry, R.H. and Green, D.W. (eds.), 1998, *Perry's Chemical Engineers' Handbook*. Seventh edition. New York: McGraw-Hill Professional Publishing.

Pini, R., Ottiger, S., Burlini, L., Storti, G. and Mazzotti, M. 2010, "Sorption of carbon dioxide, methane and nitrogen in dry coals at high pressure and moderate temperature", *International Journal of Greenhouse Gas Control*, vol. 4, no. 1, pp. 90-101.

Pires, J.C.M., Martins, F.G., Alvim-Ferraz, M.C.M. and Simões, M. 2011, "Recent developments on carbon capture and storage: An overview", *Chemical Engineering Research and Design*, vol. 89, no. 9, pp. 1446-1460.

Poole, C. (ed). 2012, *Gas Chromatography*. Amsterdam: Elsevier.

Quantachrome Instruments. 2009, *Stereopycnometer Operation Manual: Part number 05006 Rev D SPY-D160-E*. pp. 1-14.

Reeves, S.R. 2001, "Geologic Sequestration of CO_2 in Deep, Unmineable Coalbeds: An Integrated Research and Commercial-Scale Field Demonstration Project". Paper No. SPE 71749. In: *Society of Petroleum Engineeers Annual Technical Conference and Exhibition*, New Orleans, 30 September – 3 October.

Reeves, S.R. and Koperna, G.J. 2008, "Geologic Sequestration of CO_2 in Deep, Unmineable Coalbeds: An Integrated Research and Commercial-Scale Field Demonstration Project". prepared for United States Department of Energy, 2008/10. Advanced Resources International, Inc., Houston, Texas.

Reeves, S.R. and Schoeling, L. 2000, "Geological Sequestration of CO_2 in Coalseams; Reservoir Mechanisms, Field Performance and Economics", In: *International Conference on Greenhouse Gas Control Technologies* (GHGT-5), Cairns, 13-16 August.

Ringrose, P. 2012. *Large-scale CO_2 storage: What does it take?*. [PDF Presentation] Statoil and Norwegian University of Technology. Available at: <http://www.sintef.no/project/NORDICCS/Presentations%20Technoport/Philip%20Ringrose%20Large-scale_CO2_storage_Technoport.pdf> [Accessed 10 September 2012]

Ruetters, H. 2013, *A matter of purity: Requirements for the CO_2 stream purity along the entire CCS chain*, presentation at the 7th Trondheim Conference on CO_2 Capture, Transport and Storage, Norwegian University of Technology, 4-6 June 2013.

Rutherford, A. 2012, *What is CCS?*. Available at: <http://www.co2storage.org.uk/what-is-ccs/> [Accessed 10 August 2012]

Ruthven, D.M. 1984, *Principles of Adsorption and Adsorption Processes*. New York: John Wiley and Sons, Inc.

Sakurovs, R., Weir, S., French, D. and Day, S. 2011, "Effect of impurity gases in carbon dioxide on sorption behavior and mineral matter in an Australian bituminous coal", *International Journal of Coal Geology*, vol. 86, no. 4, pp. 367-371.

Schweinfurth, S.P. 2009, *An introduction to coal quality*, in Pierce, B.S., and Dennen, K.O. (eds.), *The National Coal Resource Assessment Overview*: U.S. Geological Survey Professional Paper 1625–F, Chapter C, pp. 16

Shi, J.Q. and Durucan, S. 2003, "A bidisperse pore diffusion model for methane displacement desorption in coal by CO_2 injection", *Fuel*, vol. 82, no. 10, pp. 1219-1229.

Silva da Rocha, M., Iha, K., Faleiros, A.C., Corat, E.J. and Suárez-Iha, M.E.V. 1998, "Henry's Law as a Limit for an Isotherm Model Based on a Statistical Mechanics Approach", *Journal of colloid and interface science*, vol. 208, no. 1, pp. 211-215.

Span, R. and Wagner, W. 1996, "A New Equation of State for Carbon Dioxide Covering the Fluid Region from the Triple-Point Temperature to 1100 K at Pressures up to 800 MPa". *Journal of Physical and Chemical Reference Data*, vol. 25, no. 6, pp. 1509–1596.

Speight, J.G. 2005, *Handbook of Coal Analysis*. Volume 166. Hoboken, New Jersey: John Wiley and Sons, Inc.

Table of IR Absorption Frequencies. Unknown, Compiled from: Silverstein, R.M. and Webster F. X. 1998, *Spectrometric Identification of Organic Compounds*, 6th edition, New York: Wiley, and Solomons, T.W.G. and Fryhle C. 2001, *Organic Chemistry*, 7th edition upgrade, New York: Wiley. Available at: <www.files.chem.vt.edu/RVGS/ACT/lab/Experiments/IR_frequencies.doc> [Accessed 10 September 2012]

Tans, P. and Keeling, R. 2013, *Trends in Atmospheric Carbon Dioxide* [Online] U.S. Department of Commerce, National Oceanic and Atmospheric Administration, Earth System Research Laboratory, Global Monitoring Division. Available at: <http://www.esrl.noaa.gov/gmd/ccgg/trends/> [Accessed 22 August 2013]

Thermo Nicolet Corporation. 2001, *Introduction to Fourier Transform Infrared Spectrometry*. [Online] Available at: <http://mmrc.caltech.edu/FTIR/FTIRintro.pdf> [Accessed 10 September 2013]

Total. 2007, *Lacq CO_2 Capture and Geological Storage Pilot Project. Project information Dossier*. [Online] Available at: <http://www.pnnl.gov/main/publications/external/technical_reports/PNNL-20493.pdf> [Accessed 11 October 2012]

Valdelievre, M. 2012, *Coal: A Clean and Sustainable Fuel for Power Generation Today and Tomorrow?* International advanced course - The International Perspective for developing nations. University of the Witwatersrand, and the Professional Development Division of the Fossil Fuel Foundation of South Africa, unpublished.

van Bergen, F., Hol, S., Spiers, C. and Peach, C. 2006, *Chemical interaction between CO_2 and coal under high pressure*. [Online] CO_2 Capture, Transport and Storage in the Netherlands Publication. Available at: <http://www.co2-cato.org/cato-download/516/20090917_123325_TUD_symposium_paper_ Frank_van_Bergen.pdf.> [Accessed 15 August 2013]

van Krevelen D. W. and Schuyer J. 1957, *Coal Science: Aspects of Coal Constitution*. Elsevier: Amsterdam.

Viljoen, J.H.A., Stapelberg, F.D.J. and Cloete, M. 2010, *Technical Report on the Geological Storage of Carbon Dioxide in South Africa*. Council for Geoscience.

Wang, J., Ryan, D., Anthony, E.J., Wigston, A., Basava-Reddi, L. and Wildgust, N. 2012, "The effect of impurities in oxyfuel flue gas on CO_2 storage capacity", *International Journal of Greenhouse Gas Control*, vol. 11, no. 0, pp. 158-162.

Wang, Z., Fu, Z., Zhang, B., Wang, G., Rudolph, V. and Huo, L. 2009, "Adsorption and desorption on coals for CO_2 sequestration", *Mining Science and Technology (China)*, vol. 19, no. 1, pp. 8-13.

Woo, K.W. and Yeo, S.I. 1995, *Dalton's Law vs Amagat's Law for the Mixture of Real Gases.* [Online] Available at: <http://s-space.snu.ac.kr/bitstream/10371/72458/1/04.pdf> [Accessed 05 August 2013]

Wilhelmsen, Ø., Skaugen, G., Jørstad, O. and Li, H. 2012, "Evaluation of SPUNG* and Other Equations of State for Use in Carbon Capture and Storage Modelling", *Energy Procedia*, vol. 23, no. 0, pp. 236-245.

Youn, H., Kim, J., Chandrasekar, G., Jin, H. and Ahn, W. 2011, "High pressure carbon dioxide adsorption on nanoporous carbons prepared by Zeolite Y templating", *Materials Letters*, vol. 65, no. 12, pp. 1772-1774.

Zhang, Q. 2008, "Adsorption mechanism of different coal ranks under variable temperature and pressure conditions", *Journal of China University of Mining and Technology*, vol. 18, no. 3, pp. 395-400.

APPENDICES

Appendix A: Material Safety Data Sheets (MSDS)

The MSDS's for all the main components in the study are presented in this appendix. The MSDS's for each component has been obtained from the websites listed below.

- Bituminous Coal: Appendix A.1
  http://avogadro.chem.iastate.edu/MSDS/BituminousCoal.pdf
- SO_2: Appendix A.2
  http://www.afrox.co.za/internet.global.corp.zaf/en/images/Sulphur_Dioxide266_27766.pdf
- CO_2: Appendix A.3
  http://www.afrox.co.za/internet.global.corp.zaf/en/images/Carbon_Dioxide266_27627.pdf

A.1 Bituminous Coal

Sprague

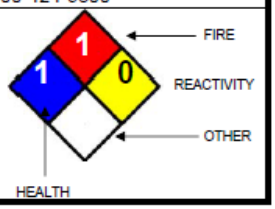
PUT OUR ENERGY TO WORK FOR YOU.

Two International Drive, Suite 200, Portsmouth, NH 03801
Tel (603) 431-1000 FAX (603) 430-7290
An Axel Johnson, Inc. Company

MATERIAL SAFETY DATA SHEET

BITUMINOUS COAL

Content Last Revised 1/94; 10/12/00; 07/26/02; 06/05
4 pages.

SECTION 1 - MATERIAL IDENTIFICATION		24 HOUR EMERGENCY INFORMATION	
PRODUCT / CHEMICAL NAME:	BITUMINOUS COAL	Sprague:	603-431-1000
PRODUCT / CHEMICAL SYNONYMS:	WASHED COAL, CLEAN COAL, SOFT COAL	Chemtrec:	800-424-9300
CHEMICAL FAMILY / FORMULA:	ALIPHATIC AND AROMATIC HYDROCARBONS / VARIABLE	HMIS / NFPA HAZARD RATING	
MATERIAL USE OR OCCURRENCE:	-	4=EXTREME 3=SERIOUS 2=MODERATE 1=SLIGHT 0=MINIMAL	

SECTION 2 – INGREDIENTS & RECOMMENDED OCCUPATIONAL EXPOSURE LIMITS			
COMPOSITION	% WEIGHT AS RECEIVED	OSHA PEL	ACGIH TLV
	(Typical)	None established.	None established.
MOISTURE	1.0 – 10.0		
ASH	4.0-20.0	15 mg/M³ as nuisance dust less than 1% quartz	10 mg/M³ as nuisance dust less than 1% quartz
TOTAL SULFUR	0.5-2.2	5.0 ppm as SO_2	2.00 ppm as SO_2
FIXED CARBON	50.0-72.0	None established	None established
VOLATILE MATTER* INCLUDING ELEMENTAL AND COMPOUNDS OF:	17.0-37.0		
HYDROGEN	4.8-5.3	None established	None established
NITROGEN	1.2-1.6	None established	None established
CHLORINE	.08-.19	1.0 ppm	1.0 ppm
COAL DUST		2.4 mg/ M³ respirable fraction, < 5% SiO_2 10 mg/ M³ > 5% SiO_2 % SiO_{2+2}	2 mg/M³ respirable fraction, < 5% SiO_2 10 mg/ M³ > 5% SiO_2 % SiO_{2+2}

SECTION 3 - PHYSICAL DATA			
IGNITION TEMPERATURE:	260°-365°F	% VOLATILITY BY VOLUME:	Negligible
MELTING POINT:	750° F	VAPOR DENSITY (AIR = 1):	N/A
AVERAGE SPECIFIC GRAVITY (H2O = 1):	1.43	SOLUBILITY IN WATER:	Non-soluble
HETEROGENOUS - CARBONACEOUS			
APPEARANCE & ODOR: Irregular, rectangular-shaped chunks or particles, dense, grayish-black to black color with slight, minimal dank odor.			

Sprague

MATERIAL SAFETY DATA SHEET

BITUMINOUS COAL

Content Last Revised 1/94: 10/12/00: 07/26/02; 06/05 4 pages

SECTION 4 - FIRE AND EXPLOSION HAZARD DATA

FLASH POINT: When exposed to flame of temperatures in excess of 260° F.

EXTINGUISHING MEDIUM: Foam, carbon dioxide, dry chemical, halon, and water fog.

SPECIAL FIRE FIGHTING PROCEDURES: Use washdown and spread out method.

UNUSUAL FIRE AND EXPLOSION HAZARDS: Susceptible to spontaneous combustion. Highly combustible and/or explosive when in dust or powder form.

SECTION 5 - HEALTH DATA

TOXICOLOGICAL TEST DATA: Coal may liberate various polycyclic aromatic hydrocarbons (PAH's) upon thermal decomposition. There is no clear evidence that coal is carcinogenic to man or experimental animals because of their polycyclic aromatic hydrocarbon content. However, there is evidence that these PAH's may play an active role in the generation of lung cancer seen in cigarette smokers or tar-roofing workers.

Coal may release small quantities of methane gas over a period of time. Progression of tuberculosis is greatly increased in pneumoconiosis but susceptibility is apparently not increased.

	ACUTE HEALTH EFFECTS	CHRONIC HEALTH EFFECTS
INHALATION	The principal health hazard associated with coal occurs during its mining and transport. Coal workers' pneumoconiosis (CWP) can occur in miners after as little as 15 years of excessive inhalation of respirable coalmine dust. Respirable quartz particles and free silica may be co-implicated. Coal dust is deposited in the lungs where its site of action is the lung parenchyma, lymph nodes and hila. The severity of the disease is directly related to the amount of coal dust in the lungs. In the simple stages, the disease is detectable by x-ray as round, irregular "macules"of 1-5 mm. This stage typically does not change lung function or shorten life.	The chronic stage of CWP, however, involves massive pulmonary fibrosis that does impair pulmonary function and shorten life. Chronic Bronchitis (lung inflammation, coughing attacks, difficult breathing, etc.) and emphysema can result from excessive coal dust inhalation. Rheumatoid arthritis can be exacerbated by pneumonias leading to rapidly developing lung damage (Caplan's Syndrome).
INGESTION	May cause irritation.	No data available
SKIN CONTACT	May cause irritation.	No data available.
EYE CONTACT	Irritation of the eye.	No data available

FIRST AID  **PROCEDURES**

First aid procedures generally don't apply to this product. Maintain exposure to coal dust according to applicable regulatory standards.

Sprague

MATERIAL SAFETY DATA SHEET

BITUMINOUS COAL

Content Last Revised 1/94: 10/12/00: 07/26/02; 06/05 4 pages

SECTION 6 - REACTIVITY DATA	
STABILITY:	Stable if properly stored to inhibit oxidation.
HAZARDOUS POLYMERIZATION:	Hazardous polymerization has not been known to occur under normal temperatures and pressures. However, coal dust may react slowly with oxygen at room temperature. Heat accelerates the process, which could lead to spontaneous ignition in piles of coal dust.
CONDITIONS TO AVOID:	1. Allowing coal to stand in water. 2. Storing coal on loose or porous ground. 3. Piling coal around upright steel or wooden posts, crane supports, underground drains, steam or hot water lines or areas where there is refuse such as wood, straw, growing vegetation or other organic material. 4. Storage in closed hampers, bins, receptacles, etc. without positive ventilation.
INCOMPATIBLES:	
TYPICAL DECOMPOSITION PRODUCTS:	May liberate hydrogen, methane, carbon monoxide, oxides of sulfur and hydrogen, coal tar pitch volatiles upon thermal decomposition.

SECTION 7 - SPECIAL PROTECTION		
RESPIRATORY PROTECTION:		Use with adequate ventilation.
VENTILATION	**LOCAL EXHAUST:**	MSHA/NIOSH approved dust respirator. Appropriate respirator depends upon type and magnitude of exposure.
	MECHANICAL (General):	Recommended for use in enclosed or semi-enclosed work areas.
EYE PROTECTION:		Splash goggles or shields with safety glasses
PROTECTIVE GLOVES:		Neoprene, PVC
OTHER PROTECTIVE CLOTHING OR EQUIPMENT:		Employee must wear appropriate impervious clothing and equipment to prevent repeated or prolonged skin contact with this substance.

SECTION 8 - SPECIAL PRECAUTIONS	
PRECAUTIONS FOR SAFE HANDLING & STORAGE:	Do not permit accumulation of dust or spillage. See also conditions to avoid, above.
SPILL AND LEAK PROCEDURES:	Cleanup by excavation, vacuum collection or washdown.
WASTE DISPOSAL METHOD:	1. Incinerate in combustion device or system. 2. Dispose in approved, regulated landfill.

SECTION 9 - DOT HAZARDOUS MATERIAL INFORMATION		
PROPER SHIPPING NAME: BITUMINOUS COAL		**REQUIRED PLACARDING:** NONE
HAZARD CLASS: Non-Hazardous	**PACKING GROUP (P.G.):** III	**N.A/U.N. NUMBER:** NONE

A.2 CO_2

AFROX

MATERIAL SAFETY DATA SHEET (MSDS)
CARBON DIOXIDE

DATE: November 2010 Version 2 Page 1 of 2

Ref. No.: MS028

1 PRODUCT AND COMPANY IDENTIFICATION

Product Name Carbon Dioxide

Chemical Formula CO_2

Company Identification African Oxygen Limited
23 Webber Street
Johannesburg, 2001
Tel. No: (011) 490-0400
Fax No: (011) 490-0506

EMERGENCY NUMBER **0860 020202 or (011) 873 4382 (24 hours)**

2 COMPOSITION/INFORMATION ON INGREDIENTS

Chemical Name	Carbon Dioxide
Chemical Family	Carbon Anhydride
Synonyms	Carbonic Acid Gas
CAS No.	124-38-9
UN No.	1013
ERG No.	120
Hazchem Warning	2 C Non flammable gas

3 HAZARDS IDENTIFICATION

Main Hazards. Carbon dioxide does not support life. It can act as a simple asphyxiant by diluting the concentration of oxygen in air below the levels necessary to support life. As it is heavier than air it will tend to concentrate at lower levels. All cylinders are portable gas containers, and must be regarded as pressure vessels at all times.

Adverse Health effects.
Carbon dioxide acts as a stimulant and depressant on the central nervous system. Increases in heart rate and blood pressure have been noted at a concentration of 7.6 percent, and dyspnea (laboured breathing), headache, dizziness and sweating occur if exposure at that level is prolonged.

Chemical Hazards.
Carbon dioxide is relatively non-reactive and non-toxic. In the presence of moisture it can aggressively bring about corrosion in a variety of steel materials.

Biological Hazards.
The greatest physiological effect of carbon dioxide is to stimulate the respiratory centre, thereby controlling the volume and rate of respiration. It is able to cause dilation and constriction of blood vessels and is a vital constituent of the acid-base mechanism that controls the pH of the blood.

Vapour Inhalation.
At concentrations of 10% and above, unconsciousness can result in one minute or less. Impairment in performance has been noted during prolonged exposure to concentrations of 3% carbon dioxide even when the oxygen concentration was 21%.

4 FIRST AID MEASURES

Eye/Skin Contact: No known effect.
Ingestion: (See Section 3 above).
Inhalation: Prompt medical attention is mandatory in all cases of overexposure to carbon dioxide. Rescue personnel should be equipped with self-contained breathing apparatus. Gaseous carbon dioxide is an asphyxiant. Concentrations of 10% or more can produce unconsciousness or death. Lower concentrations may cause headache, sweating, rapid breathing, increased heartbeat, shortness of breath, dizziness, mental depression, visual disturbances and shaking. Conscious persons should be assisted to an uncontaminated area and inhale fresh air. Quick removal from the contaminated area is most important. Unconscious persons should be removed to an uncontaminated area, and given mouth-to-mouth resuscitation and supplemental oxygen

5 FIRE FIGHTING MEASURES

Extinguishing media. Carbon dioxide is an extinguishing medium.

Specific Hazards. Carbon dioxide does not support life. It can act as a simple asphyxiant by diluting the concentration of oxygen in the air below the levels to support life.

Emergency Actions. If possible, shut off the source of excess carbon dioxide. Evacuate area. All cylinders should be removed from the vicinity of the fire. Cylinders that cannot be removed should be cooled with water from a safe distance. Cylinders that have been exposed to excessive heat should be clearly identified and returned to the supplier. CONTACT THE NEAREST AFROX BRANCH.

Protective Clothing and Self-contained breathing apparatus. Safety gloves and shoes, or boots, should be worn when handling cylinders.

Environmental precautions. Carbon dioxide is heavier than air and could accumulate in low-lying areas. Care should be taken when entering a potentially oxygen-deficient environment. If possible, ventilate the affected area.

6. ACCIDENTAL RELEASE MEASURES

Personal Precautions.
Do not enter any area where carbon dioxide has been spilled unless tests have shown that it is safe to do so.

Environmental precautions.
As carbon dioxide is classified as a "greenhouse" gas, any spillage should be avoided at all times.

Small spills.
Shut off the source of escaping carbon dioxide. Ventilate the area.

Large spills.
Evacuate the area. Shut off the source of the spill if this can be done without risk. Restrict access to the area until completion of the clean-up procedure. Ventilate the area using forced-draught if necessary.

7 HANDLING AND STORAGE

Do not allow cylinders to slide or come into contact with sharp edges. Carbon dioxide cylinders should be stacked vertically at all times, and should be firmly secured in order to prevent them from being knocked over. Use a "first-in first-out" inventory system to prevent full cylinders from being stored for excessive periods of time. Keep out of reach of children.

8 EXPOSURE CONTROLS/PERSONAL PROTECTION

Occupational Exposure Hazards.
As carbon dioxide is a simple asphyxiant, avoid any areas where spillage has taken place. Only enter once testing has proved the atmosphere to be safe, and remember that the gas is heavier than air.
Engineering control measures.
Engineering control measures are preferred to reduce exposure to oxygen-depleted atmospheres. General methods include forced-draught ventilation, separate from other exhaust ventilation systems. Ensure that sufficient fresh air enters at, or near, floor level.

Personal protection.
Self-contained breathing apparatus should always be worn when entering area where oxygen depletion may have occurred. Safety goggles, gloves and shoes, or boots, should be worn when handling cylinders.
Skin. No known effect.

9 PHYSICAL AND CHEMICAL PROPERTIES

The Stripe Symbol and the word "AFROX" are AFROX Group Trademarks.

MATERIAL SAFETY DATA SHEET (MSDS)
CARBON DIOXIDE

Ref. No.: MS028

PHYSICAL DATA

Chemical Symbol	CO_2
Molecular Weight	44.01
Specific volume @ 20°C & 101,325 kPa	547 ml/g
Density gas @ 101,325 kPa & 20°C	1.839 kg/m^3
Relative density (Air=1) @ 101,325 kPa	1,522
Colour	None
Taste	Acidic
Odour	None

10 STABILITY AND REACTIVITY

Conditions to avoid.
The dilution of oxygen in the atmosphere to levels which cannot support life. Never use cylinders as rollers or supports, or for any other purpose than the storing of carbon dioxide. Never expose the cylinders to excessive heat, as this may cause sufficient build-up of pressure to rupture the cylinders.

Incompatible materials.
As dry carbon dioxide is inert it may be contained in systems constructed of any of the common metals that have been designed to safely withstand the pressures involved.

Hazardous decomposition products. None

11 TOXICOLOGICAL INFORMATION

Acute Toxicity	TLV 5000 VPM
Skin & eye contact	No known effect
Chronic Toxicity	No known effect
Carcinogenicity	No known effect
Mutagenicity	No known effect
Reproductive Hazards	No known effect

(For further information see Section 3. Adverse Health effects.)

12 ECOLOGICAL INFORMATION

When discharged in large quantities may contribute to the greenhouse effect.
Global Warming Factor 1

13 DISPOSAL CONSIDERATIONS

General
Do not discharge into any place where its accumulation could be dangerous. Discharge to atmosphere in large quantities should be avoided. Contact Afrox if guidance is required.

14 TRANSPORT INFORMATION

ROAD TRANSPORTATION

UN No.	1013
ERG No	120
Hazchem warning	2C Non-flammable gas
SEA TRANSPORTATION	
IMDG	1013
Class	
Packaging group	
Label	Non-flammable gas

AIR TRANSPORTATION

ICAO/IATA Code	1013
Class	2.2
Packaging group	
Packaging instructions	
-Cargo	200
-Passenger	200
Maximum quantity allowed	
-Cargo	150 kg
-Passenger	75 kg

15 REGULATORY INFORMATION

EEC Hazard class Non-flammable

Risk Phrase	Description	Safety Phrase	Description
R44	Risk of explosion if heated under confinement	S2	Keep out of reach of Children
R58	May cause long-term adverse effects in the environment	S3	Keep in a cool place
		S9	Keep container in a well-Ventilated place
		S36	Wear suitable protective clothing
		S38	In case of insufficient ventilation, wear suitable respiratory equipment

Refer to SANS 10265 for explanation of the above.

16 OTHER INFORMATION

Bibliography
Compressed Gas Association, Arlington, Virginia
Handbook of Compressed Gases - 3rd Edition
Matheson. Matheson Gas Data Book - 6th Edition
SANS 10265 - Labelling of Dangerous Substances

EXCLUSION OF LIABILITY
Information contained in this publication is accurate at the date of publication. The company does not accept liability arising from the use of this information, or the use, application, adaptation or process of any products described herein.

A.3 SO_2

AFROX
A Member of The Linde Group

MATERIAL SAFETY DATA SHEET (MSDS)
SULPHUR DIOXIDE

DATE: May 2010 Version 2

Ref. No.: MS 026

1 PRODUCT AND COMPANY IDENTIFICATION

Product Names	SULPHUR DIOXIDE
Synonym	Sulfurous Acid Anhydride
Chemical Formula	SO_2
Trade Name	Sulphur Dioxide
Colour coding	Brunswick green (H.O7) body with a Golden yellow (B49) shoulder Valve CGA 240 – Steel 3/8 inch 18 NGT right hand female
Company Identification	African Oxygen Limited 23 Webber Street Johannesburg, 2001 Tel. No: (011) 490-0400 Fax No: (011) 490-0506
Emergency Number	**086 011 1185 or** **(011) 873 4382 [24 hours]**

2 COMPOSITION/INFORMATION ON INGREDIENTS

Chemical Name	Sulphur Dioxide
Chemical Family	Inorganic, acidic gas
CAS No.	7446-09-5
UN No.	1079
ERG No.	125
Hazchem Warning	Toxic and corrosive gas

3 HAZARDS IDENTIFICATION

Main Hazards
All cylinders are portable gas containers, and must be regarded as pressure vessels at all times. Sulphur dioxide is a highly irritating gas; it readily elicits respiratory reflexes. It is intensely irritating to the eyes, throat, and respiratory tract.

Adverse Health effects
Inhalation of this gas in concentrations of 8-12ppm in air causes throat irritation, coughing, constriction of the chest, lachrimation, and smarting of the eyes. A concentration of 150 ppm can be endured only a few minutes, because of eye irritation and the effect on the membranes of the nose, throat and lungs. Exposure to a concentration of 500 ppm by volume in air for a few minutes is very dangerous.

Chemical hazards
Sulphur dioxide dissolves in water forming sulphurous acid, which is unstable toward heat. In many of its reactions, sulphur dioxide behaves as a reducing agent.

Biological Hazards
Liquid Sulphur dioxide may cause skin and eye burns upon contact with these tissues, which results from the freezing effect of the liquid on the skin or eyes. Low (1%) concentrations of the vapour are irritating to moist skin within a period of 3 minutes.

Vapour Inhalation
Acute exposure through inhalation may result in dryness and irritation of the nose and throat, choking, sneezing, coughing, and bronchospasm. Severe overexposure may cause death through systemic acidosis, from pulmonary oedema, or from respiratory arrest.

Eye Contact
Corneal burns, opacification of the cornea, and blindness may result if liquid Sulphur dioxide is splashed in the eyes. Sulphur dioxide can penetrate the intact cornea and cause iritis.

Skin Contact
Liquid sulphur dioxide can cause frostbite and skin burns, and it converts to sulphurous acid in moist environments, which may cause skin irritation.

Ingestion
Severe burns to the mouth, throat, and gastrointestinal system may occur.

4 FIRST AID MEASURES
Move victims of sulphur dioxide inhalation to fresh air. If breathing has ceased, begin artificial respiration immediately. Administer oxygen if exposure has been severe and breathing is difficult. Skin exposure first aid treatment includes flushing the contaminated skin with copious amounts of water, and continuing as required in order to control burning sensation. Medical attention should be sought if irritation persists, or if skin is broken or blistered. In the event of eye contact, flush eyes immediately with copious amounts of water for at least 15 minutes. Eyelids should be held apart to ensure complete irrigation. Seek medical attention immediately.

5 FIRE FIGHTING MEASURES

Extinguishing Media
As sulphur dioxide is non-flammable, the correct extinguishing media should be used for the surrounding fire.

Specific Hazards
Water should never be sprayed at or into a tank or system which is leaking sulphur dioxide. The presence of water causes sulphur dioxide to be very corrosive, and water directed into a tank would also increase the venting rate.

Emergency Actions
A sulphur dioxide container exposed to a fire should be removed. If for any reason it cannot be removed, the container should be kept cool with a water spray until well after the fire is out. Fire fighting personnel should be equipped with protective clothing and respiratory equipment. CONTACT THE NEAREST AFROX BRANCH.

Protective Clothing
Exposed fire fighters should wear approved self- contained breathing apparatus with full face mask.

Environmental Precautions
When sulphur dioxide is released to the environment, the appropriate regulatory agency should be notified. In the event of a release however, provincial, municipal, and/or local reporting regulations must be complied with. It is most important that the response groups in the area affected be notified as quickly as possible.

6 ACCIDENTAL RELEASE MEASURES

Personal Precautions
It is essential that every facility handling sulphur dioxide has an emergency plan outlining the actions that employees should take in case of specific emergencies. These actions should include alerting fellow employees and area emergency control groups of the nature and extent of the emergency. The plan should also include co-ordination procedures with area emergency control groups in the event of a major release. If, despite all precautions, persons should become trapped in a sulphur dioxide atmosphere, they should breathe as little as possible and open their eyes only when necessary. Partial protection may be gained by holding a wet cloth over the nose and mouth.

Environmental Precautions
Only personnel trained for and designated to handle emergencies should attempt to stop a leak. Respiratory equipment of a type suitable for sulphur dioxide must be worn. All persons not so equipped must leave the affected area until the leak has been stopped.

AFROX is a member of The Linde Group
The Stripe Symbol and the word "AFROX" are AFROX Group Trademarks.

Small spills
If sulphur dioxide is released, the irritating effect of the vapour will force personnel to leave the area long before they have been exposed to dangerous concentrations. Sulphur dioxide is fairly soluble in cool water and therefore the vapour concentration can be reduced by the use of spray or fog nozzles. If disposal of sulphur dioxide becomes necessary, such as from a leaking container or vessel, it can be vented into a lime or caustic soda solution. The resulting salt solution should be taken to a plant treating unit for neutralisation and disposal.

Large spills
See "Personal Precautions" above.

6 HANDLING AND STORAGE

Sulphur dioxide should be handled only in a well-ventilated area, preferably a hood with forced ventilation. Personnel handling sulphur dioxide should wear chemical safety goggles and/or plastic face shields, approved safety shoes, and rubber gloves. Additional gas masks, air-line gas masks, and self-contained breathing apparatus should be conveniently located for use in emergencies. Instant-acting safety showers should be available in convenient locations. Cylinders should always be transported in the upright position, with the valve uppermost, and be firmly secured. Use the "first in - first out" inventory system to prevent full cylinders from being stored for excessive periods of time. Compliance with all relevant legislation is essential. Keep away from children.

8 EXPOSURE CONTROLS/PERSONAL PROTECTION

Occupational exposure hazards
Prolonged or repeated exposure may cause impaired lung function, bronchitis, hacking cough, nasal irritation and discharge, increased fatigue, alteration in the sense of taste and smell, and longer duration of common colds.

TLV	2 ppm
STEL	(15 minutes) 5 ppm
IDLH	100 ppm

Engineering control measures
Engineering control measures are preferred to reduce exposures. General methods include mechanical ventilation, process or personal enclosure, and control of process conditions. Administrative controls and personal protective equipment may also be required

.

Personal protection
Use an approved gas mask or self contained breathing apparatus when entering a sulphur dioxide contaminated area.

Eyes
Wear a chemical safety goggle or full face shield when handling cylinders.

Hands
Wear suitable protective gloves when handling cylinders.

Feet
Wear protective foot wear when working with cylinders.

Skin
Wear suitable protective clothing to prevent the gas from coming into direct contact with skin.

9 PHYSICAL AND CHEMICAL PROPERTIES

PHYSICAL DATA

Chemical Symbol	SO_2
Molecular Weight	64,063
Specific volume	@ 20°C & 101,325 kPa 366.9 ml/g
Relative density of gas	@ 101,325 kPa (Air = 1) 2,263
Boiling point	@ 101,325 kPa - 10°C
Colour	None
Taste	Acidic
	Odour Pungent, Sulphurous

10 STABILITY AND REACTIVITY

Conditions to avoid
Overheating of cylinders. Never use cylinders as rollers or supports; or for any other purpose than the storage of sulphur dioxide.

Incompatible Material
Moist sulphur dioxide is corrosive to carbon steel; therefore, other materials of construction have to be considered in this case.

Hazardous Decomposition Products
Sulphur dioxide is not flammable, or explosive, in either the gaseous or liquid state. It is a relatively stable chemical. Temperatures above 2000°C are required to bring about detectable decomposition of sulphur dioxide.

11 TOXICOLOGICAL INFORMATION

Acute Toxicity
In extreme cases, dental cavities, loss of fillings, gum disorders, and the rapid and painless destruction of teeth may result from repeated overexposure. See section 3.

Skin & eye contact
See Section 3

Chronic Toxicity
See Section 3

Carcinogenicity
No known effect

Mutagenicity
No known effect

Reproductive Hazards
No known effect

12 ECOLOGICAL INFORMATION

Environment
Poses a severe hazard to the ecology in the form of "acid rain".

13 DISPOSAL CONSIDERATIONS

Disposal Methods
Due to the complexity and scope of sulphur dioxide disposal procedures, care must be taken to ensure that all existing regulations are complied with. For more detailed information or guidance. CONTACT THE NEAREST AFROX BRANCH.

14 TRANSPORT INFORMATION

ROAD TRANSPORTATION

UN No.	1079
Class	2.3
Subsidiary risk	Toxic and corrosive gas
ERG No	125
Hazchem warning	Toxic and corrosive gas

SEA TRANSPORTATION
IMDG 1079
Class 2.3
Label Toxic gas

AIR TRANSPORTATION

ICAO/IATA Code	1079
Class	2.3
Subsidiary risk	Toxic and corrosive gas

Packaging instructions
- Cargo 200
- Passenger Forbidden

Maximum quantity allowed
- Cargo 25 kg
- Passengers forbidden

15 REGULATORY INFORMATION

EEC Hazard class Toxic, Corrosive gas.

Risk phrases	R23	Toxic By Inhalation
	R34	Causes burns
Safety phrases	S(1/2)	Keep locked up and out of reach of children
	S9	Keep container in a well-ventilated place
	S26	In case of contact with eyes, rinse immediately with plenty of water and seek medical advice
	S29	Do not empty in drains
	S(36/37/39)	Wear suitable protective clothing, gloves and eye/face protection
	S45	In case of accident or if you feel unwell, seek medical advice immediately and show label were possible
	S51	Use only in well ventilated areas
	S57	Use appropriate containment to avoid environmental contamination

National legislation None
Refer to SANS 10265 for explanation of the above.

16 OTHER INFORMATION

Ensure all national/local regulations are observed. Ensure operators understand the toxicity hazard. Users of breathing apparatus must be trained. Ensure operators understand the toxicity hazard. Before using this product in any new process or experiment, a through material compatibility and safety study should be carried out.

Bibliography

Bibliography
Compressed Gas Association, Arlington, Virginia
Handbook of Compressed Gases - 3rd Edition
Matheson Gas Data Book - 6th Edition
SANS 11014 - Safety data sheet for chemical products: Content and order of sections
SANS 10265 – Classification and Labelling of Dangerous Substances

17 EXCLUSION OF LIABILITY

Information contained in this publication is accurate at the date of publication. Whilst AFROX made best endeavour to ensure that the information contained in this publication is accurate at the date of publication, AFROX does not accept liability for an inaccuracy or liability arising from the use of this information, or the use, application, adaptation or process of any products described here

Sprague

MATERIAL SAFETY DATA SHEET

BITUMINOUS COAL

Content Last Revised 1/94: 10/12/00: 07/26/02; 06/05 4 pages

SECTION 10 - EPA SARA TITLE III INFORMATION			
SECTION 311/312 HAZARD CLASSIFICATION: Non-Hazardous	ACUTE: N/A		CHRONIC: N/A
	FIRE: N/A	PRESSURE: N/A	REACTIVE: N/A

SECTION 11 – REMARKS

This material contains fused polycyclic hydrocarbons. The OSHA interpretation of coal tar pitch volatiles (Section 1910, 1002) is as follows: "Coal tar pitch volatiles include the fused polycyclic hydrocarbons which volatize from the distillation residues of coal, petroleum, wood, and other organic matter." The OSHA PEL and ACGIH TLV for coal tar pitch volatiles is 0.2 mg/M³ (basis one soluble fraction).

SECTION 12 - ADDITIONAL REGULATORY DATA

REPORTABLE COMPONENTS: FEDERAL EPA	%	SARA RQ	CERCLA RQ	RCRA NO.
BITUMINOUS COAL	100	-----	-----	-----

NOTE: OSHA Regulations 29 CFR 1910.1200 (Hazard Communication) do not consider coal as a "hazardous material" and a Material Safety Data Sheet (MSDS) is not required. The information contained herein is based on data available at this time and is believed to be accurate. However, no warranty is expressed or implied regarding the accuracy of these data or the results to be obtained from the use thereof. Since information contained herein may be applied under conditions beyond our control and with which we may be unfamiliar, no responsibility is assumed for the results of its use. The person receiving this information shall make his own determination of the suitability of the material for his particular purpose.

Appendix B: Equipment

B.1 Leak Tests

When the project commenced, the VAS was observed to have large and yet slow leaks in the sample cell system, which was comprised of a custom built stainless steel reactor, Swagelok fittings and pneumatic valves. These leaks could not be detected using soap solution due to the very low leak rate, and the occurrence of these leaks could only be identified when pressure stability tests were run for a long period of time. The pressure decreasing in the sample cell with time even though the reactor is sample free indicates a leak (no pressure drop should ensue as no sorption would be taking place). If a sample was loaded in a leaking reactor, the sorption measured would be greatly exaggerated. It was also impractical to compensate for leaks in calculations as the leaks were seen not to be consistent every time.

In an attempt to stop the leaks, all fittings which were frequently loosened and tightened were replaced along with a new seal placed in the reactor. A pressure stability test was then performed and results can be seen in Figure B.1 below.

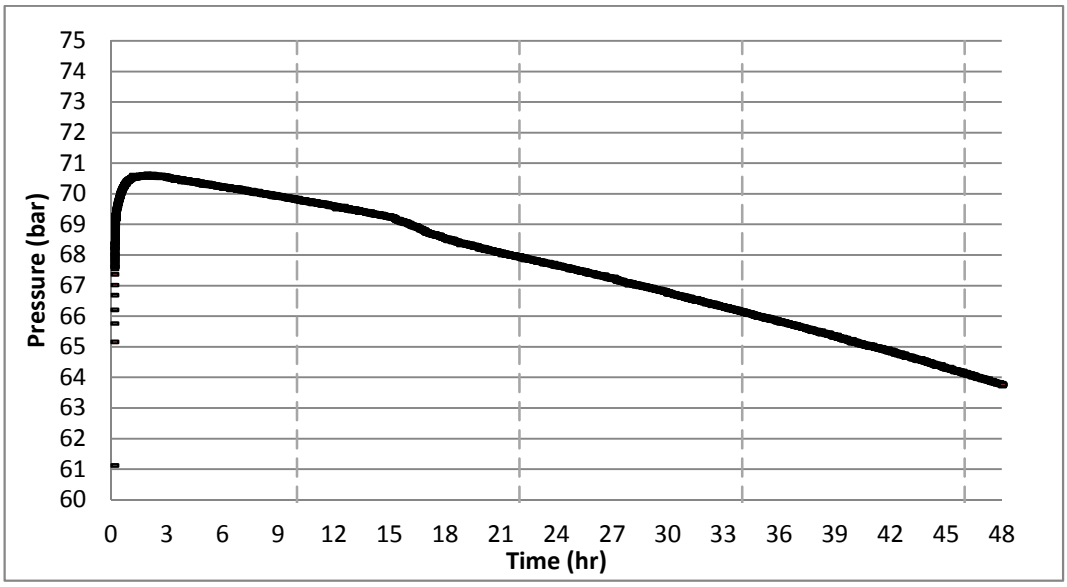


Figure B.1: Pressure stability test with empty reactor after fittings and reactor seal were replaced

As can be seen in Figure B1, leaks were still present in the sample cell system. It was suspected that there may be an inline leak through the pneumatic valves. A

tube was attached to the port leaving the sample cell system and placed in an upturned water-filled flask. After a pressure stability test was run, it was clear that CO_2 was leaking through the closed valve and displacing the water in the flask. In order to stop these inline leaks, the valves were tightened with modified spanners. The results from the leak test that was run after the valves were tightened is shown below in Figure B.2.

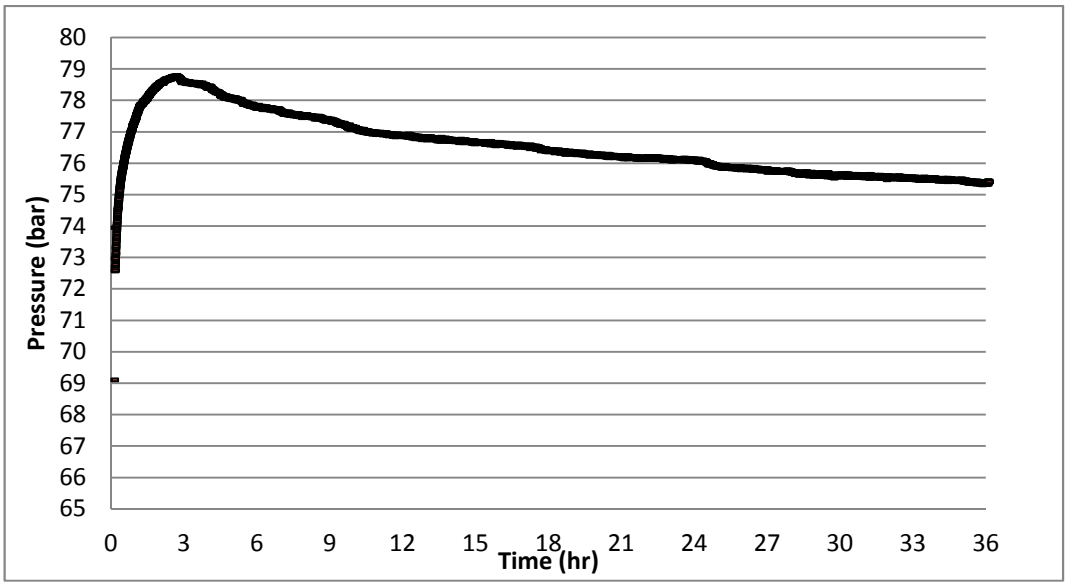


Figure B.2: Pressure stability test with empty sample cell after pneumatic valves were tightened

Although the inline leaks were successfully stopped, the system still leaked 4 bar after 36 hours. The VAS was sent in to the supplier to be tested leak tested with high pressure He and relevant He detectors. It was necessary for the suppliers to make several more modifications to the valves to prevent leaks in this area. It was also evident that the reactor seal was not sealing tight. It was expected that the sealing surface was damaged even though discrepancies could not be seen with the naked eye. The sealing surfaces were thus mechanically polished in order to attempt to solve these problems. The manufacturer of the expensive seals also had to be replaced at the time with a new supplier due to financial considerations. The new seal design was thicker than the previous design and thus it was expected that a greater amount of tightening of the reactor bolts was required. Pressure stability tests were performed on the new seals in the polished reactor surface with various degrees of reactor bolt tightening, and the results are presented in Figure B.3.

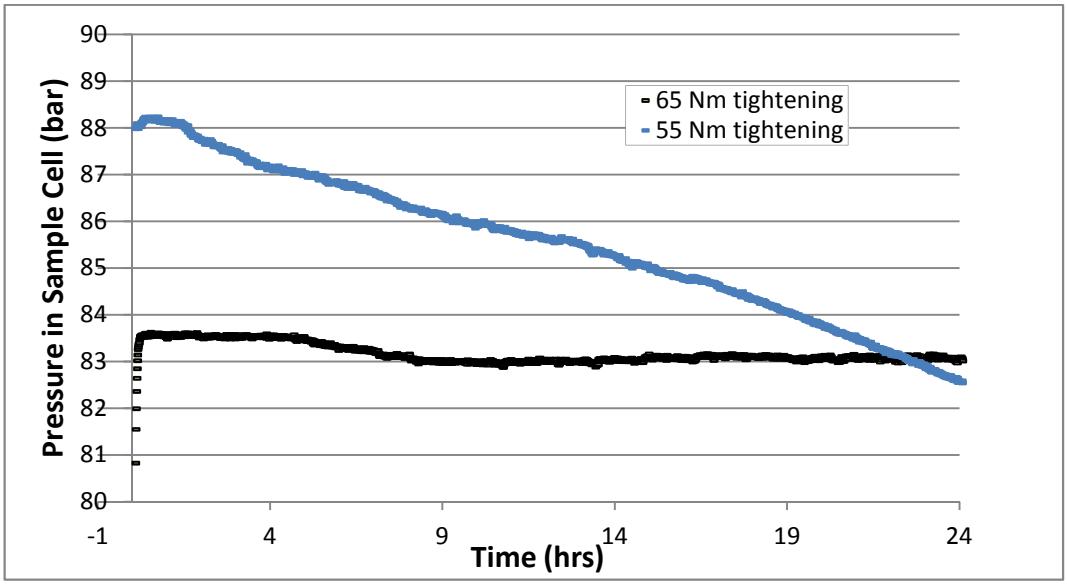


Figure B.3: Pressure stability test with empty sample cell with new seal design, polished reactor sealing surface under different levels of reactor bolt tightening

From Figure B.3 it is evident that the system was leak-free if the reactor bolts were tightened to a certain torque. However, after further experimentation it was discovered that the sealing was not consistently tight and the new seal design was unreliable. It was thus desired to replace the custom-built reactor with a new, simplified reactor that was assembled from off-the-shelf Swagelok parts. This simplified reactor required inexpensive copper seals that could be easily replaced after every run if necessary. This reactor proved reliably leak-free and is the sample cell used in the sorption experiments. Figure B.4 shows the results of a pressure stability test of the new reactor that was performed shortly before the sorption experiments

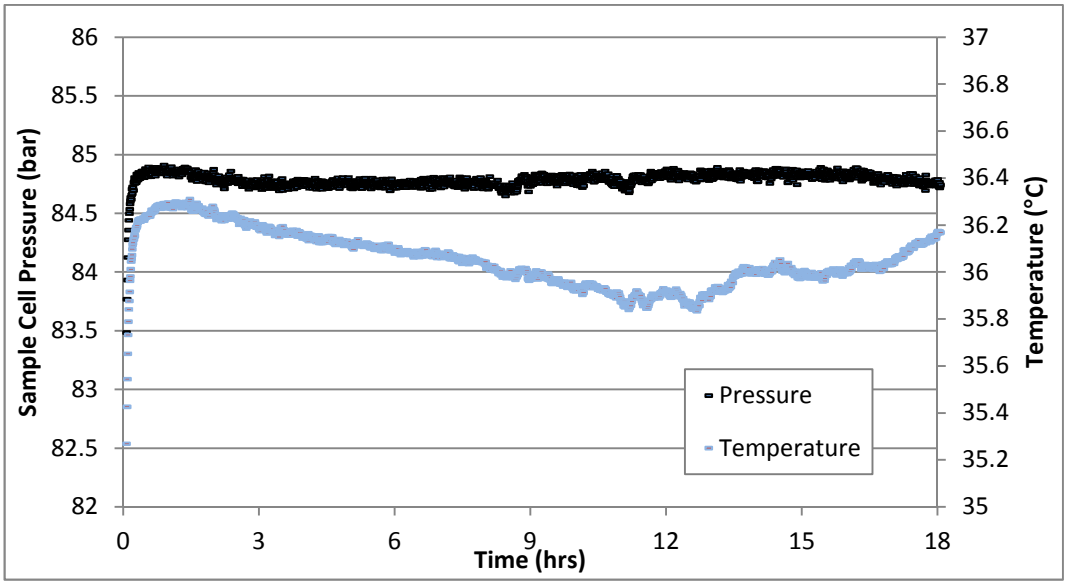


Figure B.4: Pressure stability test for sample cell assembled from Swagelok parts using a copper seal

B.2 Volumetric Adsorption System at TUT

The VAS at TUT was used for several sorption experiments while the VAS at Wits was leaking. This VAS was used to perform extended runs over weekends. The results produced using the equipment at TUT are not presented in this project as the experimentation had to be cut short at an early stage due to persistent leakage problems. Nevertheless, the VAS equipment setup at TUT and how it compares to the equipment at Wits is described in this Appendix.

The fundamentals of the VAS at TUT are identical to that of the unit at Wits and therefore the reader is referred to the main body of the report in Section 3.2.1 for a description of the unit. However, an annotated picture of this VAS is provided for completion below in Figure B.1. The main mechanical differences between the units belonging to the two universities are listed in Table B.1 below.

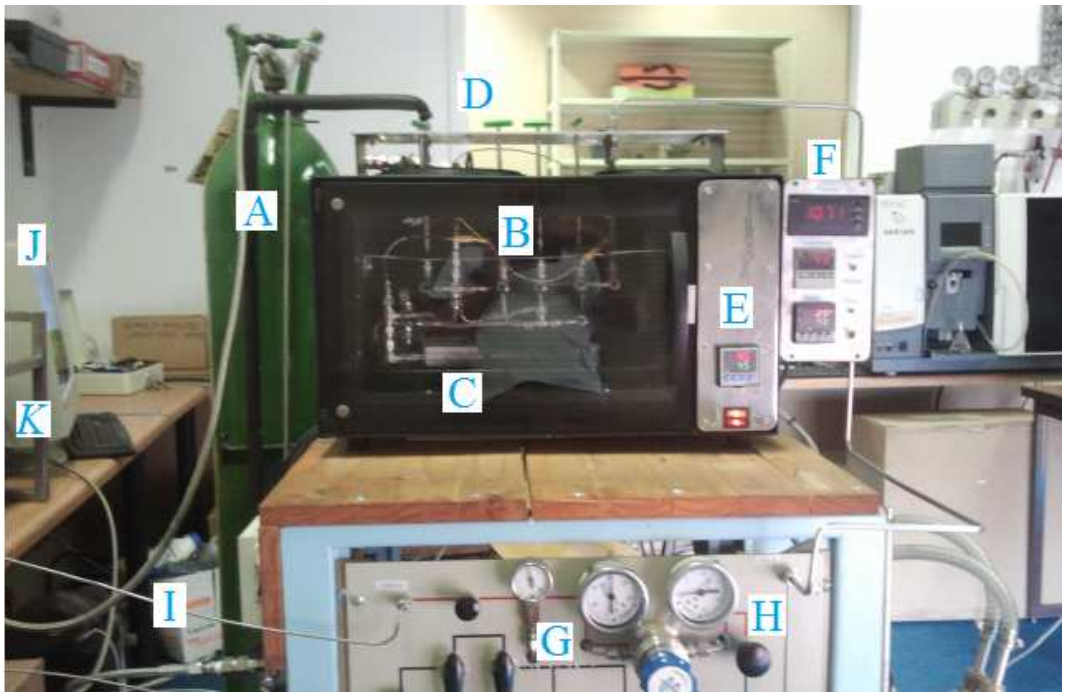


Figure B.5: VAS located at TUT. Labelled components:
A – Liquefied CO_2 cylinder. Supplies fluid to system. May be replaced by gas mixture cylinder.
B – Oven housing high pressure vessels.
C – Sample Cell seen within oven. Houses sample.
D – Manual valves. Control fluid flow in oven vessel system.
E – Temperature control of oven. Imitates isothermal conditions.
F – Pressure Display. Displays pressure in oven vessels.
G – Instrument Panel. Directs flow of fluid leaving the oven.
H – Valve leading to vacuum pump.
I – Line to GC <out of picture> For gas composition analysis.
J – PC. Collects pressure and temperature data from vessels.
K – Gas and Liquid Pumps <out of picture>. Liquid pump raises pressure of liquefied CO_2 in vessels; Gas pump performs the same task for gas mixtures.

Table B.1: Main differences between the VAS units at Wits and TUT

Wits	**TUT**
Fully automated. Has data collector	Has data collector but is operated manually.
Pneumatic valves operate between vessels	Manual valves operate between vessels
Small volume in expansion volume cell and sample cell (~20 ml)	Relatively large volume in expansion volume cell and sample cell (~500 ml)
Powdered samples can be used	Larger samples must be used (no less than 2 mm in particle size)
Pressure sensors on both expansion and sample cells	Pressure sensor only on expansion volume cell. The valve between the expansion volume and sample cell must be left open during runs
Has pump for liquefied fluids with a control system	Has two pumps without control systems. One for liquefied fluids and one for gases

Appendix C: Experimental Procedures

This appendix presents the detailed experimental procedures followed to perform the sorption experiments described in Section 3.2. The experimental procedures are broken into sections representing each stage of the experiment (sections C1 to C5)

C.1 Sample Degassing

Figure 3.6 (replicated below) should be used to supplement the sample degassing procedure.

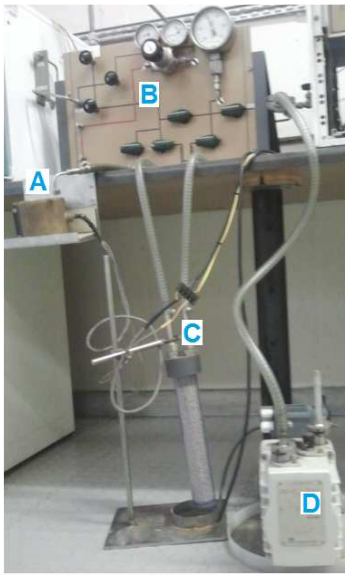


Figure 3.6: Vacuum setup for sample degassing.
Labelled components: A- reactor heating jacket; B-Instrument Panel; C- Cold trap; D- Vacuum pump

- The desired mass of sample prepared according to Section 3.1.1 is weighed out on an electronic scale using adequate sample containers. About 0.5 g over the required 2 g of sample required is weighed out to compensate for the change in mass that occurs during degassing.
- The sample is secured in a custom sized reactor that fits into a heating jacket that is part of the VAS.
- The reactor, placed securely in the heating jacket, is connected to a line that leads to the vacuum pump of the VAS.
- The correct valves in the VAS instrument panel are positioned to allow an open pathway from the reactor to the vacuum pump.

- The heating jacket and vacuum pump are turned on and left to run and degas the sample for an hour. The heating jacket is set to a temperature of 80°C.
- Once the run is completed, the heating jacket and vacuum pump are turned off and the reactor disconnected.
- 2 g of the degassed sample is weighed out using the same scale and is placed in the sample cell that is used in the VAS oven. Each sample must be degassed once before it is used in the pressurised tests.

C.2 Free Volume Determination

Figure 3.7 is presented below to accompany the procedure to determine the VAS free volume.

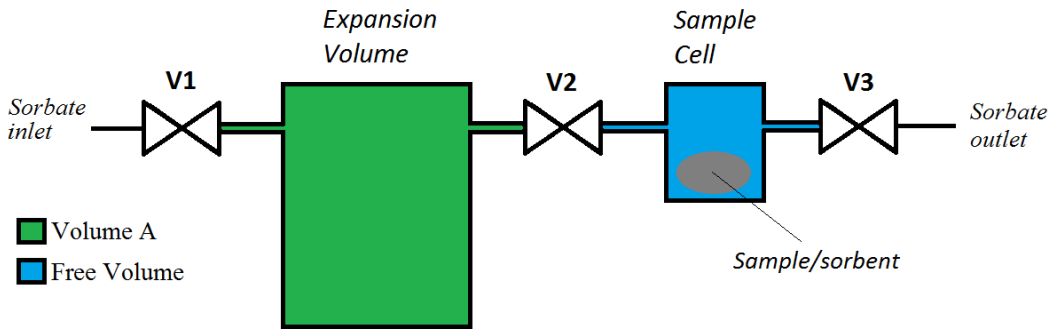


Figure 3.8: Schematic diagram of VAS pressure vessels indicating volumes of interest, i.e. the volume between V1 and V2 (Volume A) and the volume between V2 and V3 (Free Volume)

(i) Sample Cell is not loaded with a sample

- Close all valves housed in the VAS oven and set the oven to 40°C
- Evacuate the VAS using the vacuum pump and ensure LabVIEW is recording all pressure and temperature data.
- Open the He line and set the outlet of the regulator to approximately 6 bar
- Open the valves leading from the He source to the VAS, including V1, and allow the expansion volume to be pressurised to approximately 5 bar.
- Close V1 and allow the system pressure a moment to stabilise
- Open V2 and allow the He to expand to the sample cell
- Allow the system a few moments to stabilise, the vent contents
- Use the pressure data obtained from the experiment in the relevant calculations presented in Appendix D.1.
- Repeat this experiment three to five times.

(ii) Sample Cell is loaded with a sample

- Load a sample of known volume into the sample cell (the sample volume may be determined using the stereopycnometer according to the descriptions provided in Section 3.1.6 and Appendix E.1)
- Follow the procedure described in the bullets in Step (i)
- All the information is now obtained to calculate the free volume – Refer to Appendix D.1 for calculation procedure and formulae derivations

C.3 VAS

The procedure differs slightly when running mixtures produced in the Mixing System, and running pure CO_2 straight from the cylinder. The VAS procedure provided here assumes a mixture is used, as this is the most complex case. The procedure is described 'per coal sample' and was repeated for 12 sample runs. Refer to Figures 3.1 and 3.2 (presented again below) for notation used in the description that follows.

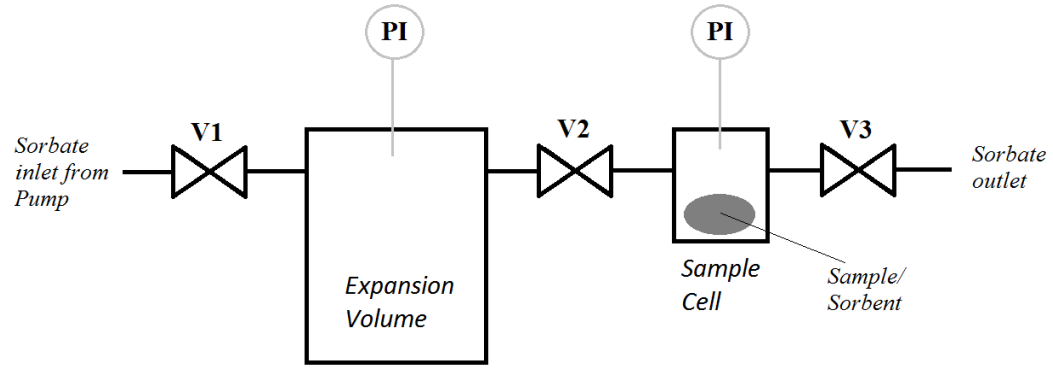


Figure 3.1: Schematic diagram of VAS internals housed in a temperature controlling oven. Valves, pressure indicators, cells, sorbent and sorbate are represented.



Figure 3.2: Complete VAS as viewed in the Laboratory at Wits
Labelled Components:

A- Teledyne Isco Syringe pump for raising fluid pressure
B- Oven housing high pressure system (expansion volume and sample cells)
C- Instrument Panel to GC for fluid sampling
D- Instrument Panel to vent and vacuum pump
E- Control panel operating pneumatic valves with pressure display
F- National Instruments CompactRIO hardware for data capture and automation. Out of picture to the left is the fluid supply, and to the right is the PC linked to the CompactRIO

(i) VAS Preparation

- Turn on extractor fan and open windows as a precaution for SO_2 being released into the lab. Ensure SO_2 sensor, situated directly above the SO_2 source, sensor is operational.
- Turn on plug at wall so that the pumps, oven and compactRio have power.
- Open compressed air line and set regulator outlet to 9 bar so that the pneumatic valves can operate.
- Empty Teledyne Isco Syringe pump (hereby referred to as the 'Teledyne pump'). If the Teledyne pump is not empty and it is desired for the experiment to run a new mixture, open V1 and run the Teledyne pump. When empty, stop running immediately before it can refill.
- Vent VAS. Open only: the vent valve, the valves on the Instrument Panel leading to the oven, V3, V2, V1, and the valves leading to the Sampling System, in that order, so that the content of the VAS may be released to the external environment. Close all valves.
- Vacuum VAS. Open only: the valves leading to the Sampling System, V1, V2, V3, and the valves on the Instrument Panel leading to the vacuum pump. Turn on vacuum pump and monitor pressure displays on Control Panel. When stable, close all valves and turn off vacuum pump. It can be assumed that the VAS is now SO_2-free.

(ii) Sample Loading

- Detach Sample Cell from VAS oven system using appropriate spanners.
- If a sample was present, empty Sample Cell completely into a sample container which must be labelled and stored. The sample cell must be thoroughly cleaned with acetone to ensure all remnants of the previous coal sample are removed. The sample cell must then be rinsed with water and dried thoroughly.

- Load 2 g of the degassed sample into Sample Cell. Secure Sample Cell and use funnel to ensure no coal is spilled.
- Weigh approximately 0.03 g of glass wool using electric scale and place it carefully in the Sample Cell over coal. Ensure no glass wool fibres are sticking out as this could cause leaks. The glass wool is used to prevent the sample from being blown out when the VAS is pressurised, vacuumed or vented.
- Replace Cu seal with a new one.
- Secure Sample Cell where appropriate in oven so that its finger tight. Fasten it tightly using spanners to ensure a leak-free seal.
- Vacuum VAS as described in in the 'Prepare VAS' section (Step (i))

(iii) Commence Run

- Set oven to 40°C
- Ensure all valves are closed other than vent valve.
- Flip switch on Control Panel from 'manual' to 'LabVIEW'
- Open LabVIEW software in PC and connect to CompactRio. Input experimental parameters as tabulated below. These parameters will allow a pressure of approximately 85 bar to be held in the sample cell for 48 hours.

Table C.1: VAS run parameters

Experimental Parameter	Value
Start Pressure	119 bar
End Pressure	119 bar
Pressure Steps	0
Hold-time	48 hours (2880 mins)

*Additional inputs made to the software include: record data every 30 seconds; hold V2 open for 60 seconds when transferring sorbate from expansion volume to sample cell; prevent content from venting once the experiment has completed.

- 'Initialise script' to commence run. The Teledyne pump will raise the fluid pressure and run will continue automatically.

- The pressure will be set, all valves closed, and the VAS will run for 48 hours.
- Monitor pressure in the sample cell for several minutes to be sure there are no leaks.

(iv) Sample Gas for GC Analysis – Only done when mixtures are used

At beginning of 48 hour VAS runtime

- Flush GC line. Open valve at GC end and valve to GC line only. Open valve from N_2 source slowly and ensure 2 bar is not exceeded in the Sampling System (SS) pressure gauge. When line is thoroughly flushed, close all SS valves
- Vacuum SS. Open SS valve to vacuum pump and valve to GC line only. Turn on vacuum pump and vacuum system thoroughly. Close SS valves and turn off vacuum pump.
- Flush line with expansion volume gas. Open SS valve leading from expansion volume. Open valve at GC end. Open valve to GC line slowly ensuring 2 bar is not exceeded. Flush line thoroughly and close all SS valves apart from the valve leading from the expansion volume.
- Analyse initial concentration of sorbate. Open valve to GC line until 2 bar is reached and close valve. Ensure GC is ready to run a sample (see GC Operating Procedure), open valve at GC end, and press button to activate GC auto-sampling valve. Repeat this bullet three to five times until consistent chromatograms are produced.
- Close SS valve to expansion volume.
- Turn off extractor fan and close windows to prevent drastic temperature changes in the laboratory.

Once 48 hour VAS runtime is complete

- Turn on extractor fan and open windows.
- Vent SS contents. Open SS vent valve; open valve to GC line; close SS vent valve.
- Flush GC line with N_2 as described previously.

- Flush line with sample cell gas. Open SS valve leading from sample cell. Open valve at GC end. Open valve to GC line slowly ensuring 2 bar is not exceeded. Flush line thoroughly and close all SS valves apart from the valve leading from the sample cell.
- Analyse final concentration of sorbate. Follow procedure analogously to how the initial concentration was analysed.

(v) VAS Shutdown

- Turn off oven.
- Extract results from LabVIEW using *Filezilla*
- Empty Teledyne pump as described previously.
- Vent VAS as described previously.
- Flush VAS with N_2. Open SS N_2 valve, open valve leading from SS to expansion volume, open V2. Close SS N_2 valve. Vent VAS.
- Vacuum VAS as described previously.
- Remove sample cell and empty its contents if desired
- Turn off extractor fan and close windows.
- Close compressed air line.
- Turn off power supply to VAS.

C.4 Mixing System

Figure 3.3, which is presented again below, should be used to supplement the procedure.

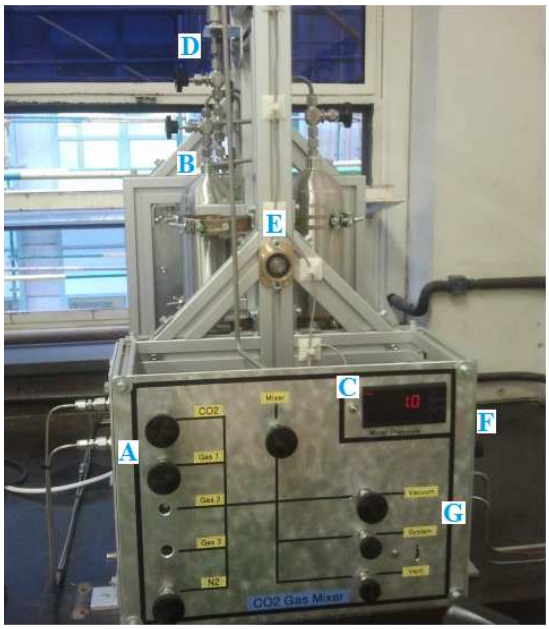


Figure 3.3: Mixing System as viewed in the Laboratory at Wits
Labelled Components:
A- Inlet ports and valves – Control entry of pure components from respective cylinders
B- Mixing Vessels – Stainless steel vessels, fitted with dip tubes and containing ball bearings, that mix and house mixture
C- Pressure display – Relays pressure in the Mixing Vessels
D- Valves leading into Mixing Vessels – Controls entry and exit of fluids into Mixing Vessels
E- Axis around which Mixing Vessels rotate – Allows for thorough mixing of components
F- Rotation controls (out of sight) – Controls speed of Mixing Vessel rotation
G- Outlet ports and valves – Control exit of mixture from Mixing Vessels to VAS and vent, as well as line to vacuum pump

(i) Pre-experimental

- Ensure correct gas sensor is installed and functioning correctly
- Open nearby windows
- Turn on extractor
- Close all Mixing System (MS) valves
- Ensure Teledyne pump is empty. If not, run it until empty through the VAS according to VAS Operating Procedure
- Close VAS Instrument Panel valves that lead to the: vent line; and vacuum pump
- Ensure the line at the top of the Mixing Vessels is coupled at the connector port
- Ensure the MS pressure display LED Wire on top of the Mixing Vessels is coupled

- Switch on MS pressure display LED and note system pressure

(ii) Vent MS

- Close all MS valves
- Excluding MS vent valve, systematically open all valves leading from MS vent valve to Mixing Vessels
- Open System Valve (outlet valve to the VAS)
- Open MS Vent Valve
- Ensure contents has been completely vented (Note Pressure Display LED)
- Close all MS valves

(iii) Flush MS with CO_2

- Close all MS valves
- Excluding CO_2 inlet valve, systematically open all valves leading from the CO_2 inlet to Mixing Vessels
- Open outlet valve to the VAS (Labelled “System”)
- Open CO_2 inlet valve and thoroughly flush the system
- Close CO_2 inlet valve
- Vent MS according to Vent MS Procedure
- Close all MS valves

(vi) Vacuum MS

- Close all MS valves
- Ensure MS has been vented and flushed according to the respective procedures
- Open MS vacuum valve
- Systematically open all valves leading to mixing vessels
- Open System valve
- Turn on VAS vacuum pump
- Allow MS to be thoroughly vacuumed (Note Pressure Display LED)
- Turn off VAS vacuum pump
- Close all MS valves

(vii) Load MS

Note: Fluids must be loaded one at a time in increasing magnitude of pressure as supplied to the MS (e.g. SO_2 at ~ 3 bar must be loaded first, followed by CO_2 at ~ 40 bar).

- Close all MS valves
- Ensure MS has been vented, flushed and vacuumed according to the respective procedures.
- Ensure selected fluid is able to flow freely from its source to MS
- Open: Valves leading directly into both of the Mixing Vessels; the valve second in line to the Mixing Vessels
- Open fluid inlet valve and allow fluid to enter fully
- Slowly open valve labelled “Mixer” on Instrument Panel that leads up towards Mixing Vessels; carefully monitor the pressure on the MS pressure display LED
- When desired pressure is reached in Mixing Vessels, close mixer valve
- Close: fluid inlet valve; and the valve second in line to the Mixing Vessels
- Open mixer valve
- Partial Vent: Open MS vent valve - releases unwanted fluid and decreases pressure. Close MS vent valve
- Partial Flush: When the fluid loaded is SO_2, open CO_2 inlet valve and flush thoroughly. Close CO_2 inlet valve. Open MS vent valve and allow content to escape. Close MS vent valve.
- Close source of fluid external to MS.
- Partial Vacuum: Open MS vacuum valve. Turn on VAS vacuum pump. Allow adequate time for vacuuming. Turn off VAS vacuum pump. Close MS vacuum valve.
- To load CO_2, return to third bullet of Load MS procedure and repeat.
- When done loading CO_2 – Move on to Step (vi).

(viii) Mix MS

- Ensure valves leading directly into Mixing Vessel containing the mixture are open

- Ensure valve second in line to the Mixing Vessels is closed
- Double check that the area before the valve that is second in line to the Mixing Vessels has been vented and flushed. See Partial Vent and Partial Flush procedures
- Ensure all valves on the instrument panel are closed
- Decouple line leading to Mixing Vessels at the horizontal Al platform using appropriate spanners
- Remove Cu seal from inside connection and stow for re-use
- Stow disconnected line out of the way on movable Al platform
- Disconnect MS pressure display LED Wire at Al platform (pull it up at connection and stow out of the way)
- Commence rotating of Mixing Vessels – Activate motor by toggling 'Mix' switch.
- Adjust speed of rotation, by turning 'Speed' knob.
- Allow Mixing Vessels to rotate at set speed for 10 minutes.
- Slow rotations using 'Speed' knob until Mixing Vessels are perfectly vertical and the line and connecting port are aligned. Toggle 'Mix' switch to "Off" position. Use jog option if necessary.
- Replace Cu seal and re-couple connection using appropriate spanners.
- Replace Pressure Display LED Wire.

(ix) Run

- Vacuum the portion of the MS not exposed to the mixture – Open MS vacuum and mixer valves and use VAS vacuum pump until vacuumed sufficiently.
- Close MS vacuum valve
- Open valve to allow fluid to flow out of the Mixing Vessels
- Test for leaks at the coupled connection with soap solution. Other leak indications are a steadily decreasing pressure on the LED and activating the gas sensor. If no leaks, proceed to next bullet. If leaking and not triggering sensor, tighten nut further with spanners and re-test. If still leaking and components are dangerous, vent system and evacuate.

- Open mixer valve; and system valve
- Refill the empty Teledyne pump of the VAS and press “Stop” when full.
- VAS experimentation can now commence.
- Leave valves in these positions for duration of VAS experimentation

(x) MS Shutdown

- Vent, flush and vacuum MS as described previously
- Run Teledyne pump until empty according to VAS Operating Procedure
- Turn off extractor
- Switch off MS pressure display LED
- Close all MS valves

C.5 GC

- Open the N_2 line and set the outlet regulator between 4 and 6 bar for adequate carrier gas flow.
- Turn the GC and connecting PC on. Open *Compass* software
- Load the GC’s ‘HayeSep Turn on’ method and run it once the set points have been reached in order to prepare the column for sample injection.
- Load the method designed for mixtures of CO_2 and SO_2, ‘HayeSep CO2-SO2 Mixtures’. Wait for the method’s set points to be achieved.
- When the gas sample is ready to flow through the column, run the loaded method and inject the sample using the button for the auto-sampling valve.
- When the run is complete and the chromatogram produced, integrate the peaks in the chromatogram manually using the software to obtain a measurement of the peak area.
- Calculate the mixture concentrations from the calibration curve produced (Section 3.2.1)
- Repeat the steps in the above three bullets for each sample required to be run.
- When all samples have been run, load the ‘Brüker Shutdown’ method. Turn off the GC once the set points are attained and close the N_2 line.

Appendix D: Sorption Experiment Calculations and Results

D.1 Free Volume Determination

In this Appendix, the equations used to calculate the free volume, that is required to calculate sorption capacity, are derived. The relevant experimental results are also presented.

Derivation

Figure D.1 below has been copied from Section 3.2.2 and presented below for convenient reference.

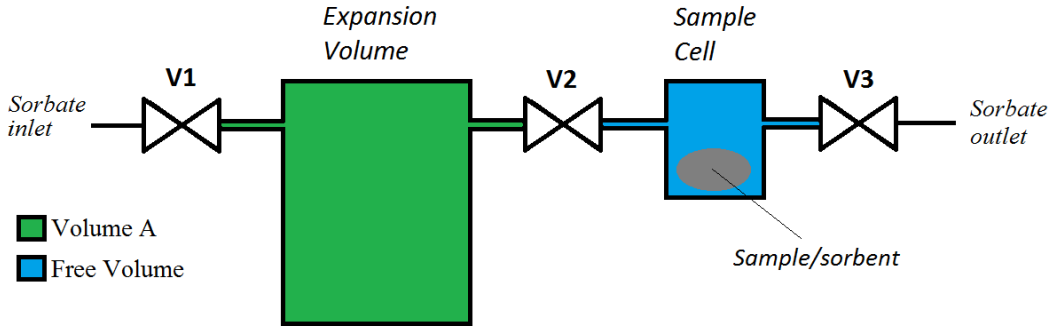


Figure D.1: Schematic diagram of VAS pressure vessels indicating volumes of interest, i.e. the volume between V1 and V2 (Volume A) and the volume between V2 and V3 when a sample is loaded into the sample cell (Free Volume)

The calculations require two experimental steps:

- Step 1 – Volume A (v_A), the total volume between valve 1 (V1) and valve 2 (V2), is pressurised with He to a known pressure, P_1. P_1 is typically low, 5 bar to 10 bar.
- Step 2 – The He is allowed to expand through V2 so that the total volume between V1 and valve 3 (V3), v_{TOT}, is occupied. This system will be at a new pressure of P_2.

These steps are repeated for two scenarios:

- Scenario (i) – The sample cell is empty
- Scenario (ii) – The sample cell contains a sample of known volume, v_P.

Additional parameters of interest are:

- Volume B (v_B) – The volume between V2 and V3 with the sample cell under Scenario (i)
- Free Volume (v_{free}) - The volume between V2 and V3 with the sample cell under Scenario (ii)

Important assumptions made are:

- The He gas behaves according to the Ideal Gas Law under the experimental conditions. i.e. $Pv = nRT$

  Where P is pressure, v is volume, n is the number of moles of He, R is the universal gas constant, T is temperature
- The temperature of the system remains constant at the temperature of the oven throughout the experiments

The derivations are offered in a logical sequence below.

Ideal Gas Law for steps 1 and 2:

$$P_{1(i)}v_{A(i)} = nRT \quad \text{and} \quad P_{2(i)}v_{TOT(i)} = nRT \qquad \text{(D1) \& (D2)}$$

Sum volume components of $V_{TOT(i)}$:

$$v_{TOT(i)} = v_{A(i)} + v_{B(i)} \qquad \text{(D3)}$$

Combine and rearrange Equations D1, D2 and D3 to solve for the ratio of $v_{B(i)}\ to\ v_{A(i)}$:

$$\frac{v_{B(i)}}{v_{A(i)}} = \frac{P_{1(i)}}{P_{2(i)}} - 1 \qquad \text{(D4)}$$

Consider Ideal Gas Law equivalent to Equations D1 and D2 for Scenario (ii). Combine and rearrange them to form Equation D5 below.

$$\frac{P_{1(ii)}}{P_{2(ii)}} = \frac{v_{TOT(ii)}}{v_{A(ii)}} \qquad \text{(D5)}$$

Sum volume components of $v_{TOT(ii)}$.

Note that $v_{A(i)} = v_{A(ii)}$ and $v_{B(ii)} = v_{B(i)} - v_P$

$$v_{TOT(ii)} = v_{A(i)} + v_{B(i)} - v_p \qquad \text{(D6)}$$

Substitute D6 into D5 and solve for $v_{A(i)}$.

$$v_{A(i)} = \frac{v_P}{1 + \frac{v_{B(i)}}{v_{A(i)}} - \frac{P_{1(ii)}}{P_{2(ii)}}} \qquad \text{(D7)}$$

The entire right hand side of Equation D7 can be determined experimentally and/or solved for. $v_{A(i)}$ can thus be calculated and used to determine $v_{B(i)}$ according to Equation D8 below.

$$v_{B(i)} = v_{A(i)} \times \frac{v_{B(i)}}{v_{A(i)}} \quad \text{(D8)}$$

Once $v_{B(i)}$ is known, v_{free} can be calculated by subtracting the known volume of sorbent used in the sorption experiments from $v_{B(i)}$.

Experimental Results

The results for one run of the experiments described in Steps 1 and 2 above are displayed in Figures D2 and D3. The latter figure is for a run when there is a solid sample loaded into the sample cell, while the former figure was obtained for when the sample cell was empty. The sample volume was measured using a stereopycnometer to be 1.92 cm^3 with a standard deviation of 0.004 cm^3.

Instantaneous pressures before and after V2 was opened, once the temperature had equilibrated, were used for the calculations. It is seen that the assumption of constant temperature is fair, as the drop in temperature from one state of equilibrium to the next is not sufficiently large. The vacuum pressure and atmospheric pressure are added to the gauge pressure readings to obtain true pressure values. Three runs were performed for each scenario in order to obtain an average value of the free volume.

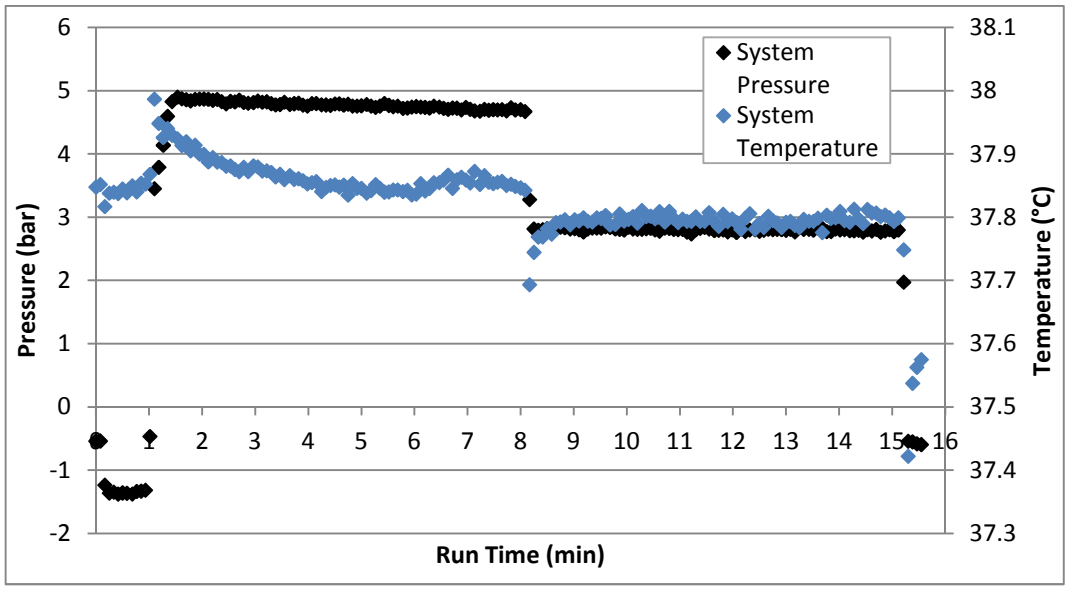


Figure D.2: Behaviour of pressure and temperature in VAS cells during volume determination experiment when sample cell is empty

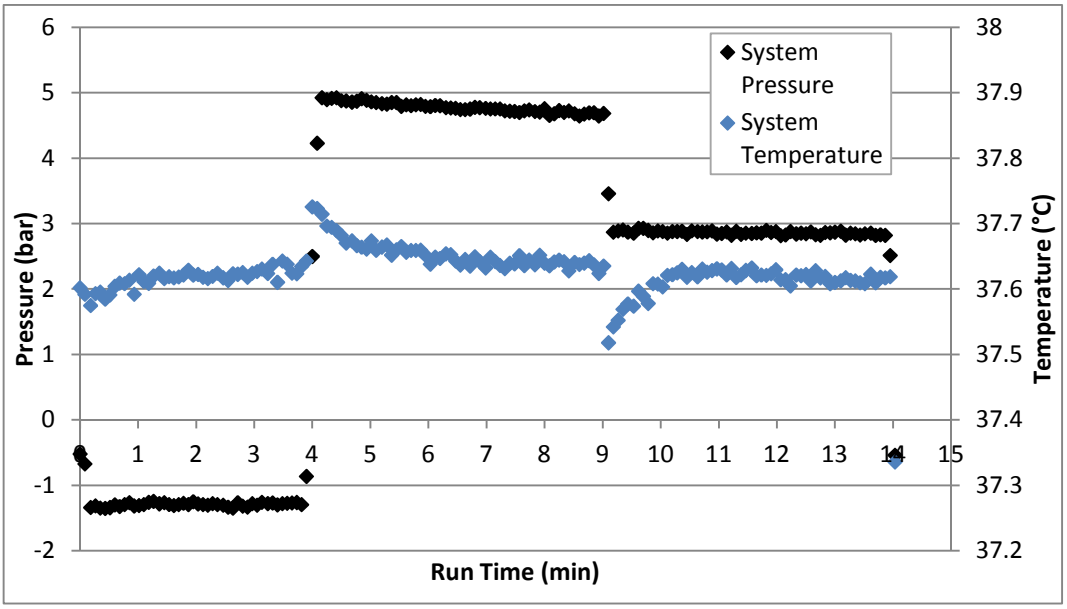


Figure D.3: Behaviour of pressure and temperature in VAS cells during volume determination experiment when sample cell contains a sample

The tabulated calculations for $v_{B(i)}$ and $v_{A(i)}$ are presented in Table D.1.

Table D.1: Experimental and calculated values for system volume determination

	System is empty			
	Initial Pressure (P_1) (bar)	Pressure in entire System (P_2) (bar)	P_1/P_2	$v_B/v_A = P_1/P_2 - 1$
Run 1	6.063	4.173	1.453	0.453
Run 2	6.024	4.134	1.457	0.457
Run 3	6.131	4.237	1.447	0.447
AVERAGE				0.452
STD DEV				0.00511

	Sample of known volume in Sample Cell					
	Initial pressure (P_1) (bar)	Pressure in entire system (P_2)	P_1/P_2	Sample Volume (V_p) (cm^3)	$v_A = v_p/(1+v_B/v_A - P_1/P_2)$ (cm^3)	$v_B = v_B/v_A * v_A$ (cm^3)
Run 1	7.004	5.199	1.347	1.917	18.267	8.263
Run 2	6.952	5.151	1.350	1.916	18.682	8.450
Run 3	6.954	5.186	1.341	1.924	17.240	7.798
AVERAGE				1.919	18.063	**8.170**
STD DEV				0.004	0.743	0.336

The empty sample cell volume was thus calculated to be 8.17 cm^3 with a standard deviation of 0.336 cm^3. The free volume is thus 7.202 cm^3 when the volume of the

2 g coal sample (0.968 cm^3, see Appendix E.1 for calculations) is subtracted from it.

D.2 Density

The methods used to calculate the pure component and mixture densities are outlined in this Appendix. It has been split into sections for NIST data, Amagat's law and Patel-Teja EOS.

NIST Data

The density of pure CO_2 and pure SO_2 can be determined reliably from data obtained from the NIST database at http://webbook.nist.gov/chemistry/fluid/ (Lemmon *et al.*, 2003). Data was retrieved in tabulated form for the desired experimental conditions (40°C and 82 bar to 86.5 bar). This data was plotted and fit with a suitable polynomial using *MS Excel* so that the density at specific conditions could be easily calculated. These plots for CO_2 and SO_2 are presented below in Figures D.4 and D.5 respectively.

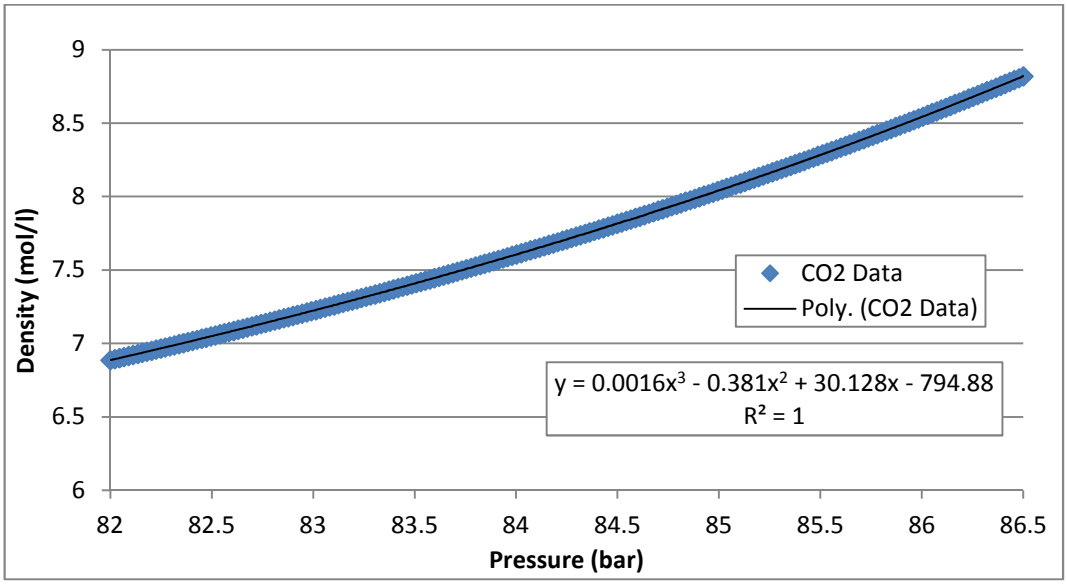


Figure D.4: Density of CO_2 as a function of pressure at 40℃. Data points were determined by the Span Wagner EOS obtained from the NIST database while an almost perfect fit polynomial was applied in this pressure range using MS Excel.

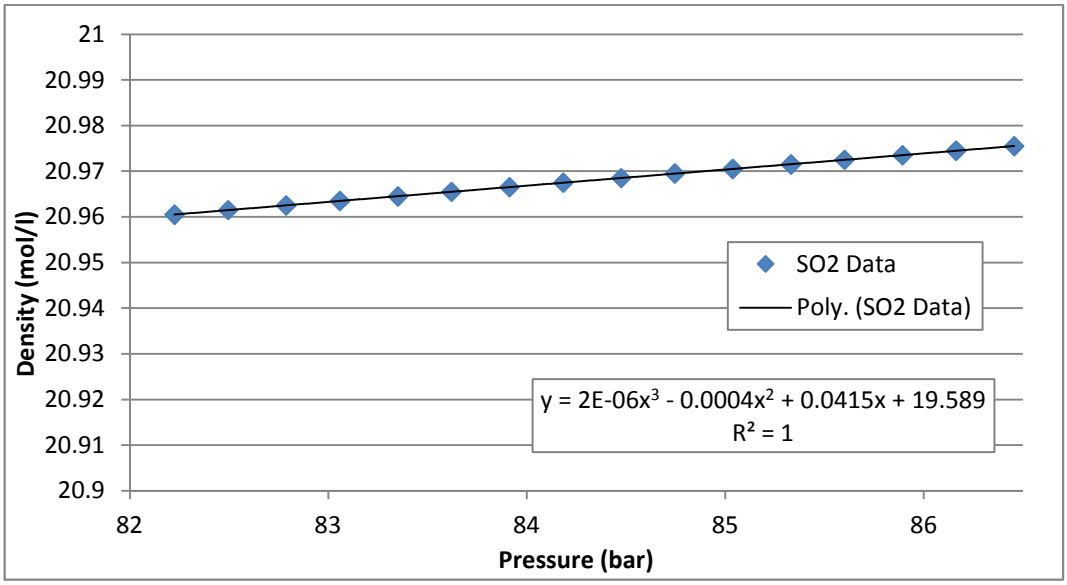


Figure D.5: Density of SO_2 as a function of pressure at 40 ℃. Data points were obtained from the NIST database and an almost perfect fit polynomial was applied in this pressure range using MS Excel.

Amagat's Law

Amagat's law is an assumption that enables the density of mixtures simply from the densities of its pure components. The density of relevant CO_2-SO_2 mixtures at relevant conditions and compositions was calculated from the pure component densities presented in Figures D.4 and D.5 according to Equation D.13 which is derived below.

Assumption: The sum of the theoretical pure component partial volumes is equal to the total volume of the mixture (Felder and Rousseau 2000) (Equation D.9 below).

This assumption is generally superior to the equivalent assumption using the sum of the partial pressures (Dalton's law) (Woo and Yeo, 1995). The following derivation applies Amagat's law to the case where the mixture comprises of a binary mixture of CO_2 and SO_2.

$$v_{mix} = v_{CO_2} + v_{SO_2} \tag{D.9}$$

Dividing through by n_{tot} and inverting both sides

$$\rho_{mix} = {}^{n_{tot}}/_{(v_{CO_2} + v_{SO_2})} \tag{D.10}$$

$$\rho_{mix} = {n_{tot}}\Big/\left(\frac{n_{CO_2}}{\rho_{CO_2}} + \frac{n_{SO_2}}{\rho_{SO_2}}\right) \tag{D.11}$$

Rearranging right hand side and substituting expressions for $x_i = \frac{n_i}{n_{tot}}$

$$\rho_{mix} = {1}\Big/\left(\frac{x_{CO_2}}{\rho_{CO_2}} + \frac{x_{SO_2}}{\rho_{SO_2}}\right) \tag{D.12}$$

Applying Equation D.12 to a general case:

$$\rho_{mix} = 1/\sum {x_i}/{\rho_i} \tag{D.13}$$

Notation: v_{mix} is the total volume of the mixture and v_i is the partial volume of component i; ρ_{mix} is the molar density of the mixture and ρ_i is the molar density of component i; n_{tot} and n_i are the total number of moles and number of moles of component i respectively; and x_i is the mole fraction of component i.

The results obtained when Equation D.13 is used to determine the mixture density for relevant concentrations of SO_2 and CO_2 is presented in Figure D.6.

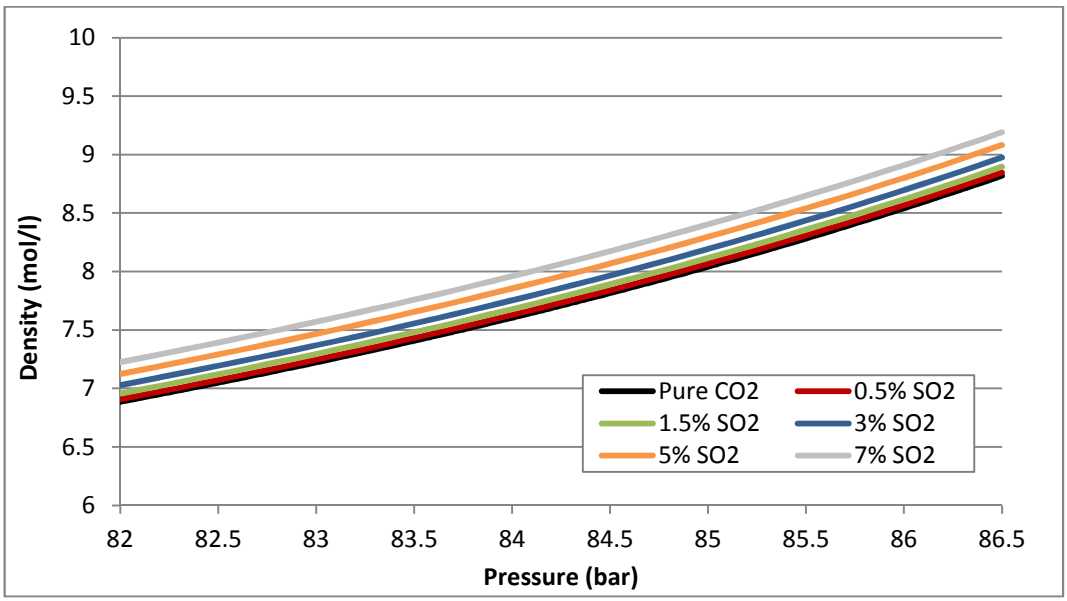


Figure D.6: Density of relevant CO_2-SO_2 mixtures as a function of pressure at 40°C calculated using Amagat's Law

Patel-Teja Equation of State

The Patel-Teja EOS is a cubic EOS that is a modification on the ideal gas law so it can describe the behaviour of certain real fluids accurately (Patel and Teja, 1981). Mixing laws are applied to the EOS so that it can be extended to predicting the behaviour of real fluid mixtures. This EOS is presented in Equation D.14 below. The equations used to fully describe the parameters in the Patel-Teja EOS are presented thereafter.

$$P = \frac{RT}{V - b_{mix}} - \frac{a_{mix}[T]}{V(V+b_{mix})+c_{mix}(V-b_{mix})} \quad \text{(D.14)}$$

Where V is the molar volume (inverse of molar density), P is pressure, T is temperature, and R is the universal gas constant. a_{mix}, b_{mix}, and c_{mix} are parameters that can be calculated from corresponding pure component constants according to van der Waals mixing rules.

$$a_{mix} = \sum_i \sum_j \xi_{ij}\, x_i x_j \sqrt{a_i a_j}\ ;\ b_{mix} = \sum_i x_i b_i\ ;\ c_{mix} = \sum_i x_i c_i\ ;\ \xi_{ij} = \xi_{ji} \quad \text{(D.15)}$$

Where x is the mole fraction, and i and j are different components. ξ_{ij} is the binary interaction parameter and was calculated by Li (2008) from VLE data for CO_2-SO_2 mixtures to be 0.953.

$$\text{For each component: } a = \Omega_a\left(\frac{R^2 T_c^2}{P_c^2}\right)\alpha[T_r]\ ; = \Omega_b\left(\frac{RT_c}{P_c}\right)\ ;\ c = \Omega_c\left(\frac{RT_c}{P_c}\right) \quad \text{(D.16)}$$

Where T_c and P_c and the critical temperature and critical pressure of the component respectively and T_r is the reduced temperature defined by $T_r = T/T_c$.

The critical temperature and pressure for according to Patel and Teja (1981) are presented in Table D.2 below.

Table D.2: Critical properties of CO_2 and SO_2

Component	T_c (K)	P_c (bar)
CO_2	304.13	73.773
SO_2	430.64	78.84

$$\Omega_a = 3\zeta_c^2 + 3(1 - 2\zeta_c)\Omega_b + \Omega_b^2 + 1 - 3\zeta_c \quad \text{(D.17)}$$

$$0 = \Omega_b^3 + (2 - 3\zeta_c)\Omega_b^2 + 3\zeta_c^2\Omega_b + 1 - \zeta_c^2 \quad \text{(D.18)}$$

$$\Omega_c = 1 - 3\zeta_c \tag{D.19}$$

$$\alpha = (1 + F\left(1 - \sqrt{T_r}\right))^2 \tag{D.20}$$

Where ζ_c is an empirical factor that is component specific and is obtained from Patel and Teja (1981) to be 0.309 and 0.307 for CO_2 and SO_2 respectfully. Similarly F is a component specific empirical factor that is 0.707727 and 0.754966 for CO_2 and SO_2 respectfully (Patel and Teja, 1981). Ω_c is determined first and then Ω_b is calculated to be the smallest root of Equation D.18, and then Ω_a can be calculated.

Once Equations D.17 to C.20 are solved, the parameters in Equation D.16 can be solved and then used to solve the parameters in Equations D.15. The molar volume in Equation D.14 can then be calculated using a suitable solver and inverted to finally determine the mixture density predicted by the Patel-Teja EOS.

The algorithm described by Equations D.14 to C.20 was coded into *Matlab* in order to conveniently solve for the mixture density at different conditions. The code produced is presented below.

```
function rho = PT(P,T,x_SO2)
%This function may be called on by a suiTable Eriver to output the
%mixture density of an SO2-CO2 mixture at a specified pressure,
%temperature and mole fraction
%Input P in bar, T in C, and x_SO2 in mol frac
R = 0.0831451; %L.bar/mol.K
T = T + 273.15; %K

%CO2
Tc_CO2 = 30.9782 + 273.15; %K
Pc_CO2 = 73.773; %bar
PARAMETERS
zc_CO2 = 0.309;
TR_CO2 = T/Tc_CO2; %reduced temperature
F_CO2 = 0.707727; %empirical factor

OmegaC_CO2 = 1 - 3*zc_CO2;
OmegaB_CO2 = fzero(@(x)x^3 + (2-3*zc_CO2)*x^2 + 3*zc_CO2^2*x -
zc_CO2^3,0);
OmegaA_CO2 = 3*zc_CO2^2 + 3*(1-2*zc_CO2)*OmegaB_CO2 + OmegaB_CO2^2
+ 1 - 3*zc_CO2;
alpha_CO2 = (1 + F_CO2*(1-TR_CO2^0.5))^2;

a_CO2 = OmegaA_CO2*(R^2*Tc_CO2^2/Pc_CO2)*alpha_CO2;
b_CO2 = OmegaB_CO2*(R*Tc_CO2/Pc_CO2);
```

```
c_CO2 = OmegaC_CO2*(R*Tc_CO2/Pc_CO2);

%SO2
Tc_SO2 = 157.49 + 273.15; %K
Pc_SO2 = 78.84; %bar
PARAMETERS
zc_SO2 = 0.307;
TR_SO2 = T/Tc_SO2; %reduced temperature
F_SO2 = 0.754966; %empirical factor

OmegaC_SO2 = 1 - 3*zc_SO2;
OmegaB_SO2 = fzero(@(x)x^3 + (2-3*zc_SO2)*x^2 + 3*zc_SO2^2*x -
zc_SO2^3,0);
OmegaA_SO2 = 3*zc_SO2^2 + 3*(1-2*zc_SO2)*OmegaB_SO2 + OmegaB_SO2^2
+ 1 - 3*zc_SO2;
alpha_SO2 = (1 + F_SO2*(1-TR_SO2^0.5))^2;

a_SO2 = OmegaA_SO2*(R^2*Tc_SO2^2/Pc_SO2)*alpha_SO2;
b_SO2 = OmegaB_SO2*(R*Tc_SO2/Pc_SO2);
c_SO2 = OmegaC_SO2*(R*Tc_SO2/Pc_SO2);

%MIXING RULES
%Binary interaction parameter
ksi_ij = 0.953;
x_CO2 = 1 - x_SO2;
a_mix = x_CO2^2*a_CO2 + 2*ksi_ij*x_CO2*x_SO2*(a_CO2*a_SO2)^0.5 +
x_SO2^2*a_SO2;
b_mix = x_CO2*b_CO2 + x_SO2*b_SO2;
c_mix = x_CO2*c_CO2 + x_SO2*c_SO2;



%PT EQUATION
%Provide accurate guess for fzero function using previously
%determined Amagat's law function at 40deg C or the Ideal gas Law
%at other temperatures
if T == 40 + 273.15;
    rho_CO2_40C = 0.00161974*P^3 - 0.3809948*P^2 + 30.1281322*P -
794.88245; %rho @ 40degC known
    rho_SO2_40C = 0.00000172992*P^3 - 0.00044373092*P^2 +
0.04147088*P + 19.5889124;
    rho_mix_40C = x_SO2*rho_SO2_40C + x_CO2*rho_CO2_40C; %Amagat's
Law
    guess_v_mix = 1/rho_mix_40C;
else guess_v_mix = R*T/P; %Ideal Gas Law
end

v = fzero(@(v) R*T/(v-b_mix) - a_mix/(v*(v+b_mix)+c_mix*(v-b_mix))
- P,guess_v_mix);
rho = 1/v;
```

The results obtained when the *Matlab* code was run to determine the mixture density for relevant concentrations of SO_2 and CO_2 is presented in Figure D.7 below. The code was seen to predict the NIST density data for pure CO_2 and SO_2 under the experimental conditions relatively well as can be seen in Figure D.8.

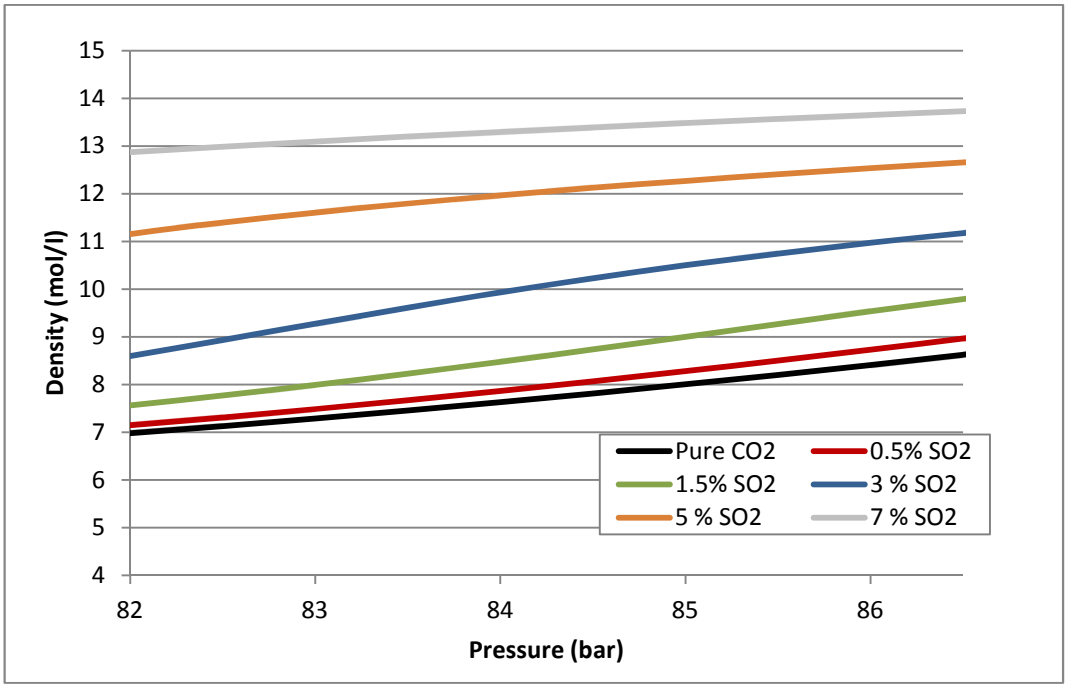


Figure D.7: Density of different CO_2-SO_2 mixtures as a function of pressure at 40°C as predicted according to the Patel-Teja model

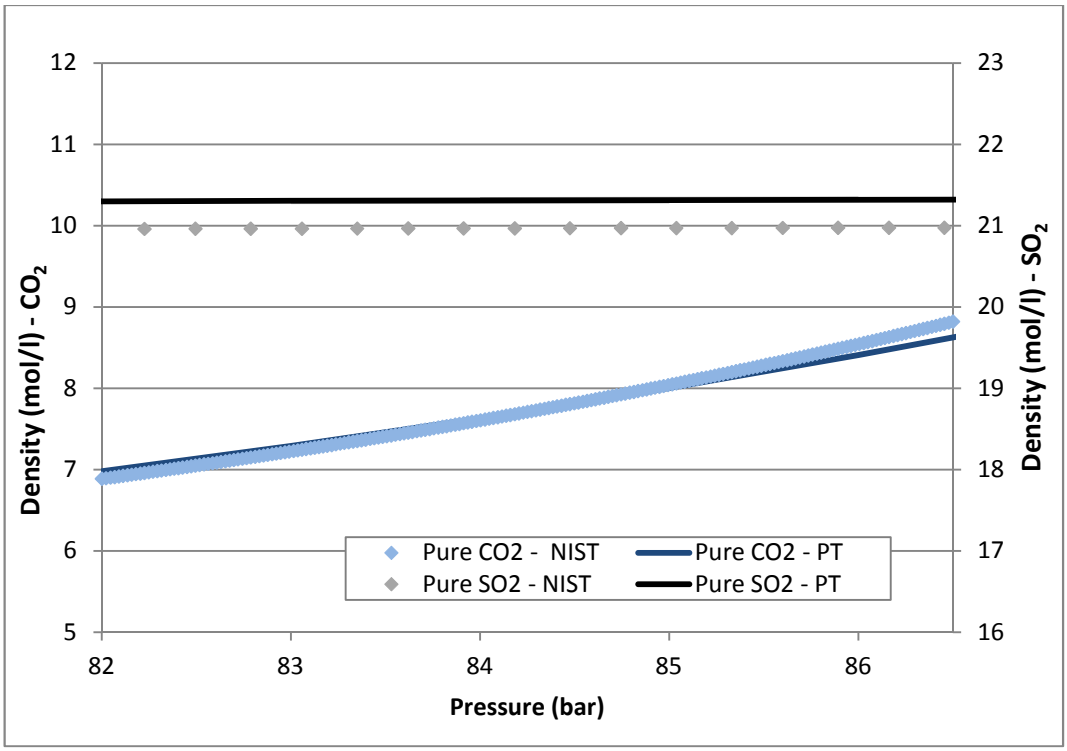


Figure D.8: Patel-Teja EOS pure component densities of SO_2 and CO_2 compared with respective densities obtained from the NIST database

D.3 VAS Results

All raw and manipulated results obtained from the VAS experiments are presented in this Appendix. The raw pressure and temperature versus time plots

for each run are presented in the first subsection; a worked example describing how the excess sorption is derived from this data is presented in the next subsection; and the spreadsheet used to calculate the excess sorption for all runs is presented in the final subsection.

Raw Results

The sample cell of which the pressure and temperature were recorded was 8.17 ml in volume and the mass of the coal sorbent was 2 g. The composition of the sorbate varied from run to run; however, a pure CO_2 sorbate was analysed three times. The other sorbates were mixtures of CO_2 and SO_2 and their concentration varied from 0.16% to 6.7% SO_2. The pressure was set in the expansion volume to 119 bar for each run and the sorbate was allowed to equilibrate into the sample cell for 60 seconds before the sample cell was isolated and the pressure and temperature readings recorded. The oven was set to 40°C, but the temperature readings recorded are lower due to a calibration error. The plots produced for the measured variables as a function of time throughout each 48 hour run are presented in Figures D.9 to D.20.

Total Sorption (mmol/g)	SO_2 Concentration (mol%)
2.41	0

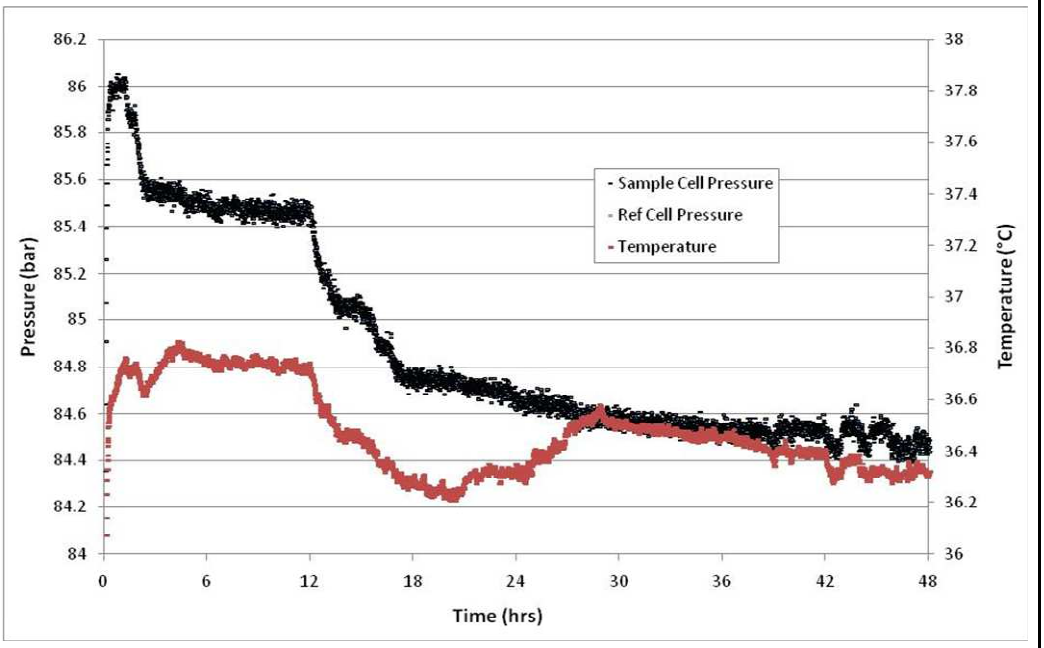


Figure D.9: Sample cell pressure (black) and temperature (red) recorded during VAS experiment. Mixture concentration and sorption calculated are shown. Pure CO_2 – 1.

Total Sorption (mmol/g)	SO_2 Concentration (mol%)
1.65	0

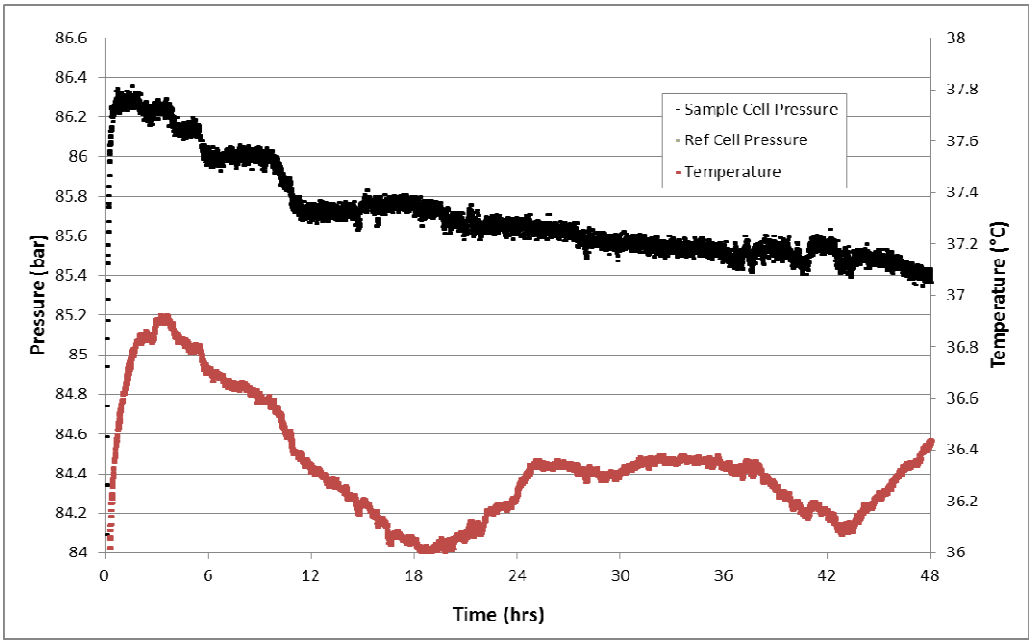


Figure D.10: Sample cell pressure (black) and temperature (red) recorded during VAS experiment. Mixture concentration and sorption calculated are shown. Pure CO_2 – 2.

Total Sorption (mmol/g)	SO_2 Concentration (mol%)
2.05	0

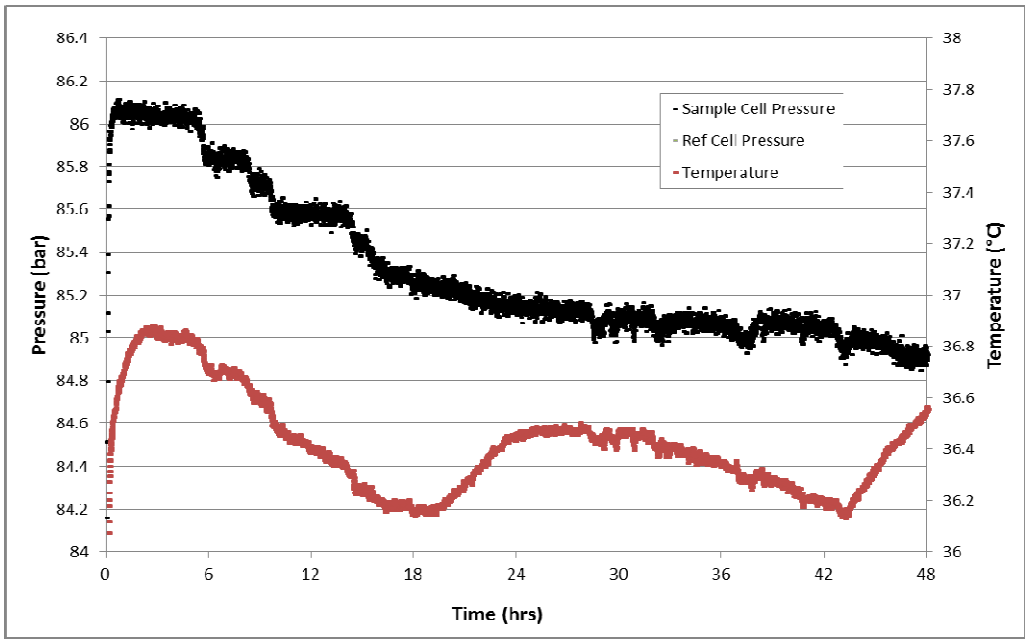


Figure D.11: Sample cell pressure (black) and temperature (red) recorded during VAS experiment. Mixture concentration and sorption calculated are shown. Pure CO_2 – 3.

Total Sorption (mmol/g)	SO_2 Concentration (mol%)
1.28	0.16

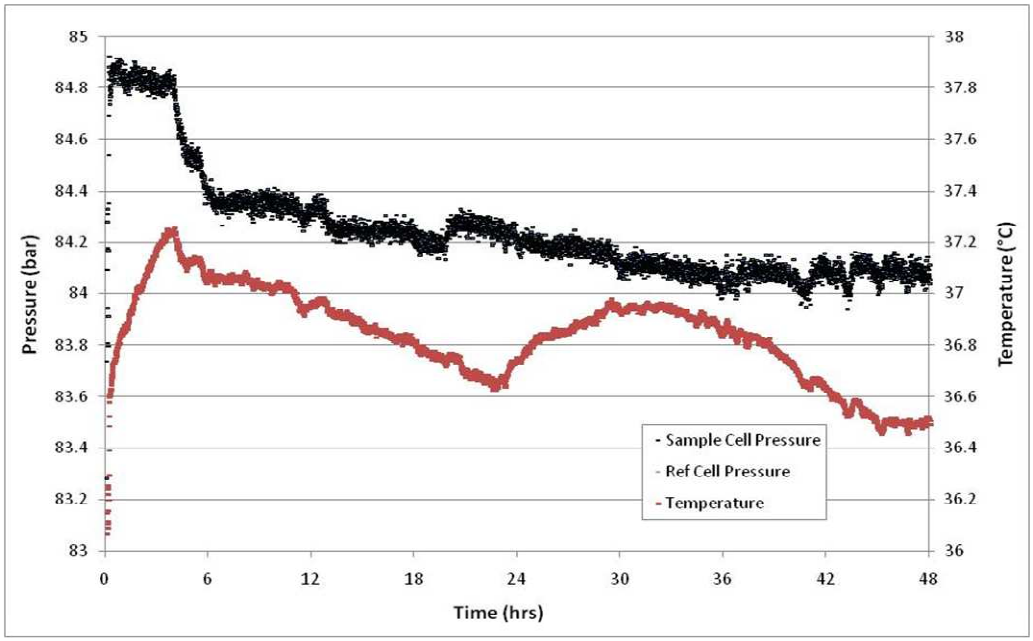


Figure D.12: Sample cell pressure (black) and temperature (red) recorded during VAS experiment. Mixture concentration and sorption calculated are shown. Low SO_2 – 1.

Total Sorption (mmol/g)	SO_2 Concentration (mol%)
1.31	0.95

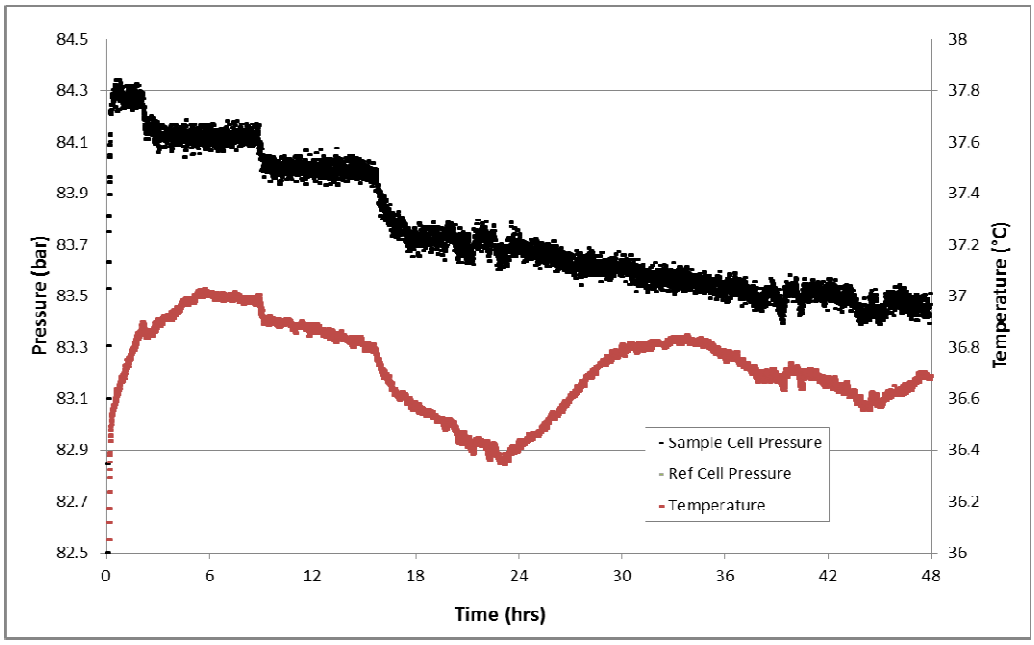


Figure D.13: Sample cell pressure (black) and temperature (red) recorded during VAS experiment. Mixture concentration and sorption calculated are shown. Low SO_2 – 2.

Total Sorption (mmol/g)	SO_2 Concentration (mol%)
1.41	1.25

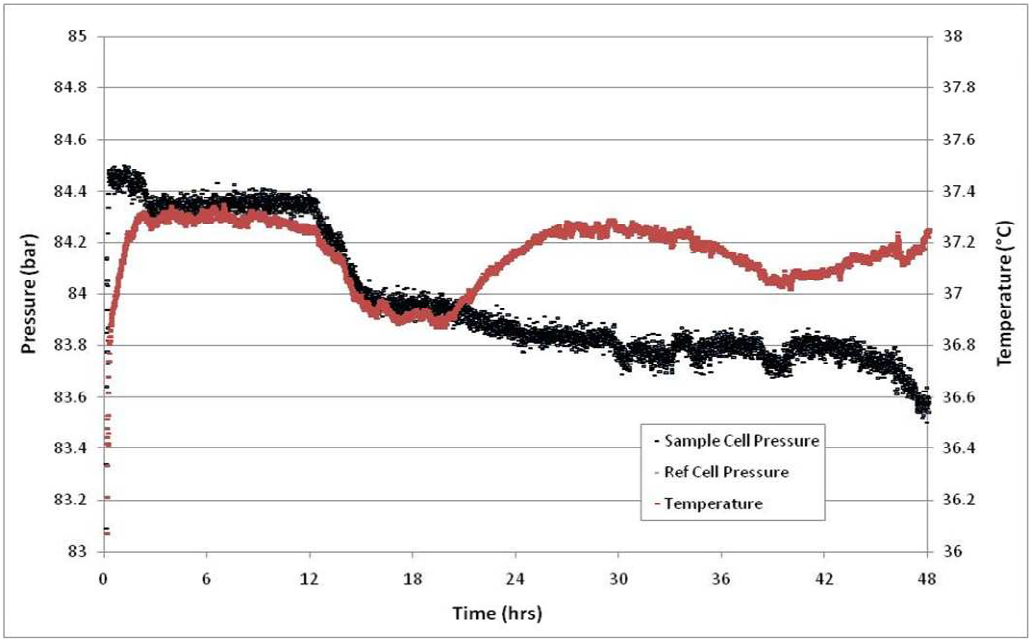


Figure D.14: Sample cell pressure (black) and temperature (red) recorded during VAS experiment. Mixture concentration and sorption calculated are shown. Medium SO_2 – 1.

Total Sorption (mmol/g)	SO_2 Concentration (mol%)
1.20	1.91

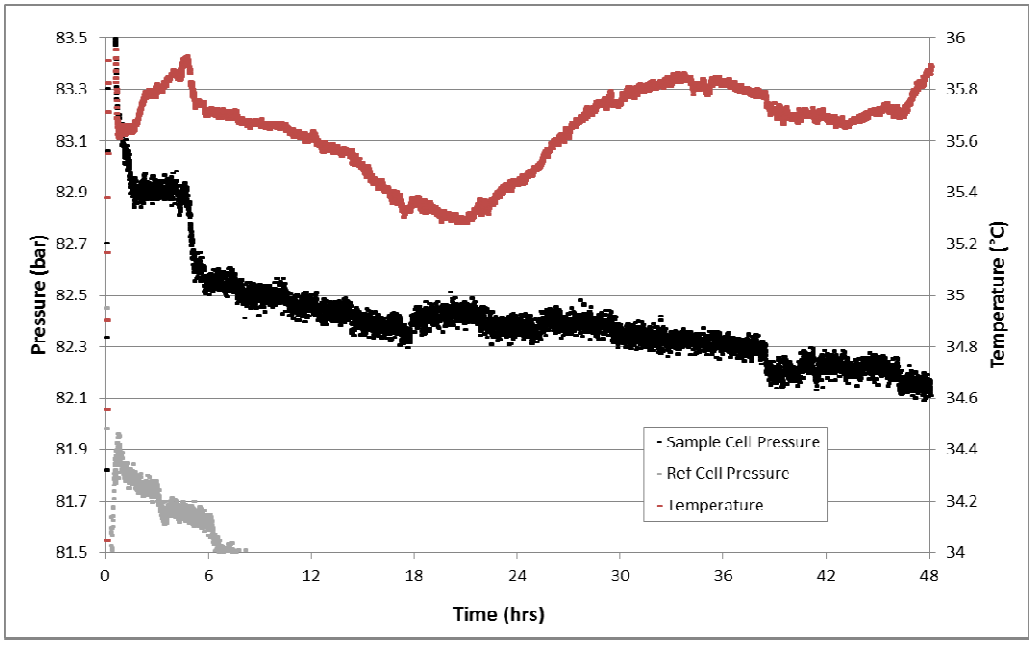


Figure D.15: Sample cell pressure (black) and temperature (red) recorded during VAS experiment. Mixture concentration and sorption calculated are shown. Medium SO_2 – 2.

Total Sorption (mmol/g)	SO_2 Concentration (mol%)
0.84	2.52

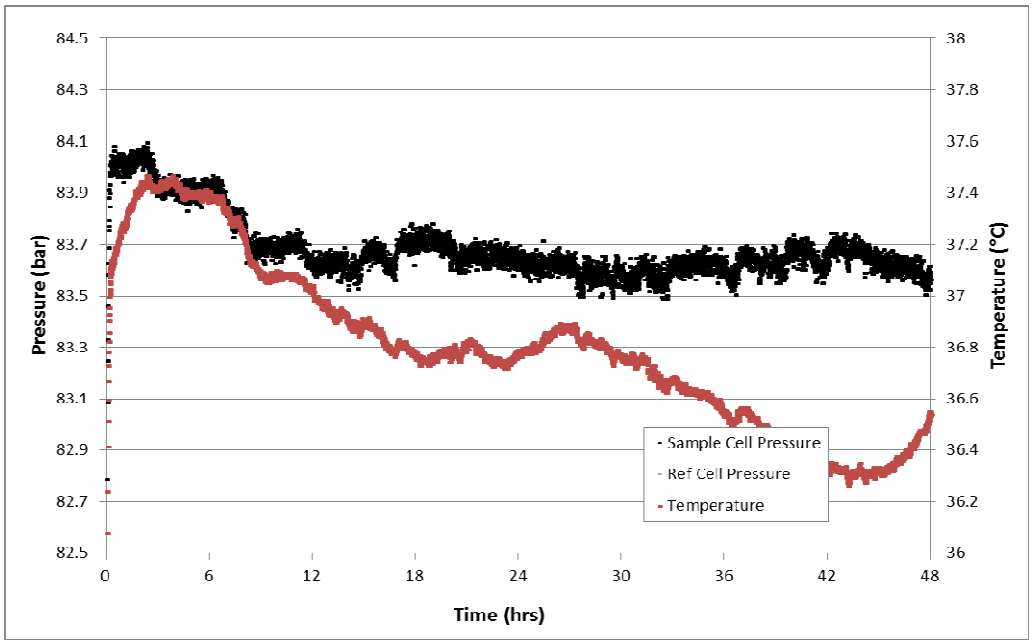


Figure D.16: Sample cell pressure (black) and temperature (red) recorded during VAS experiment. Mixture concentration and sorption calculated are shown. Medium SO_2 – 3.

Total Sorption (mmol/g)	SO_2 Concentration (mol%)
0.55	3.20

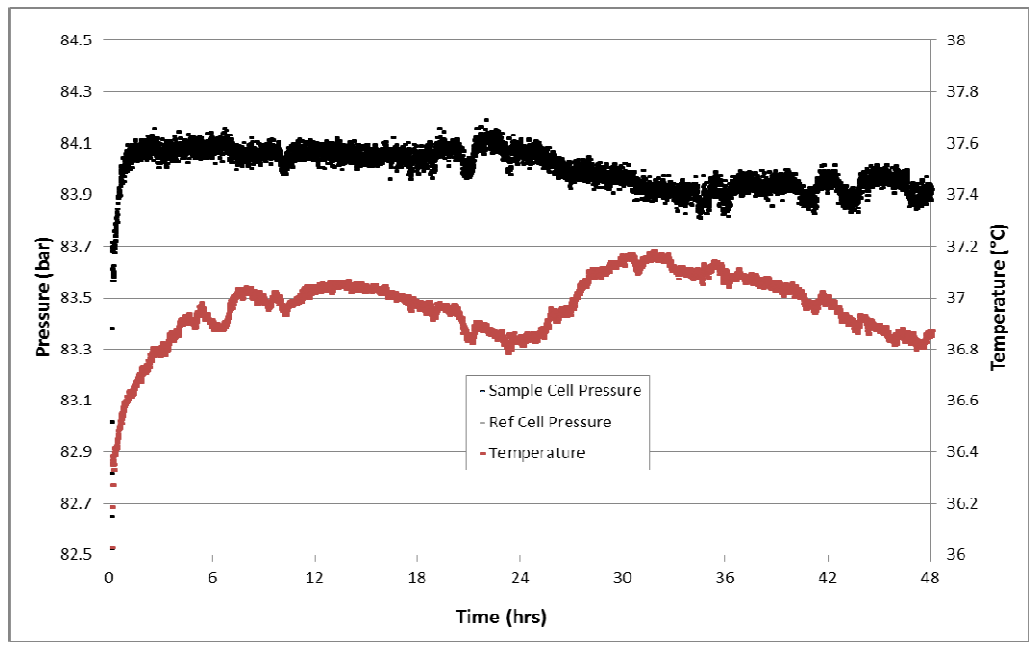


Figure D.17: Sample cell pressure (black) and temperature (red) recorded during VAS experiment. Mixture concentration and sorption calculated are shown. High SO_2 – 1.

Total Sorption (mmol/g)	SO_2 Concentration (mol%)
2.00	3.72

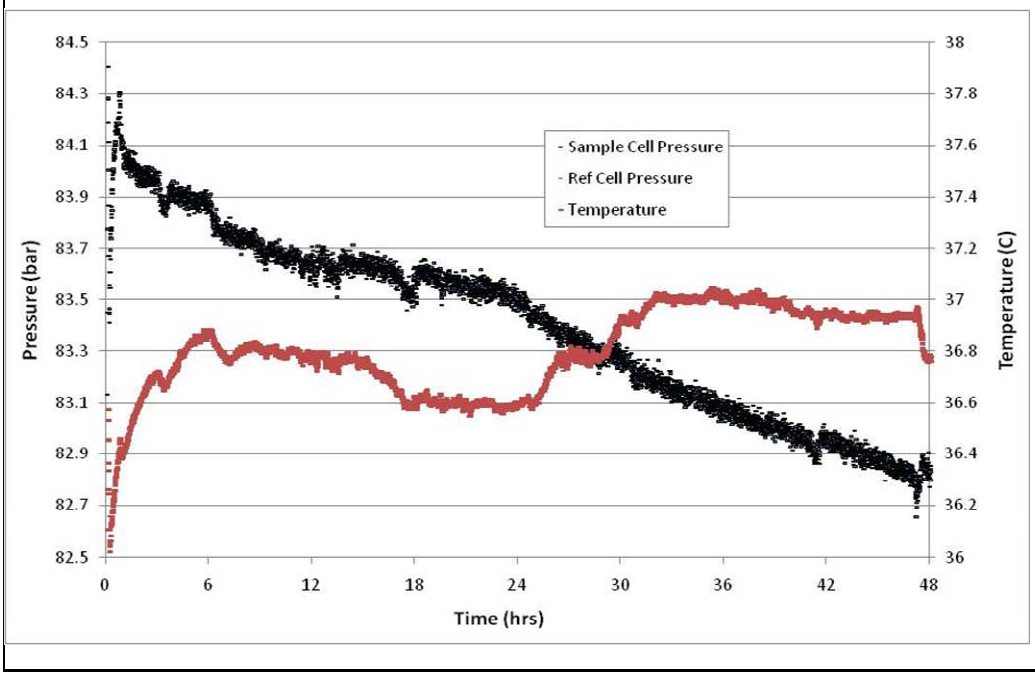


Figure D.18: Sample cell pressure (black) and temperature (red) recorded during VAS experiment. Mixture concentration and sorption calculated are shown. High SO_2 – 2.

Total Sorption (mmol/g)	SO_2 Concentration (mol%)
0.60	3.94

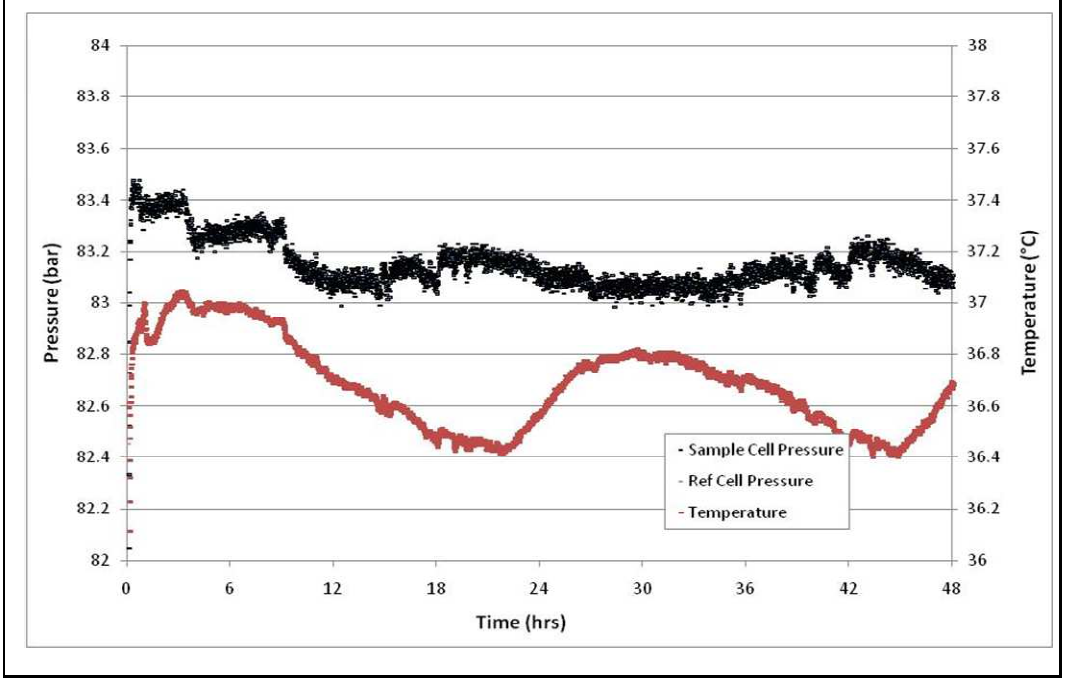


Figure D.19: Sample cell pressure (black) and temperature (red) recorded during VAS experiment. Mixture concentration and sorption calculated are shown. High SO_2 – 3.

Total Sorption (mmol/g)	SO_2 Concentration (mol%)
1.58	6.69

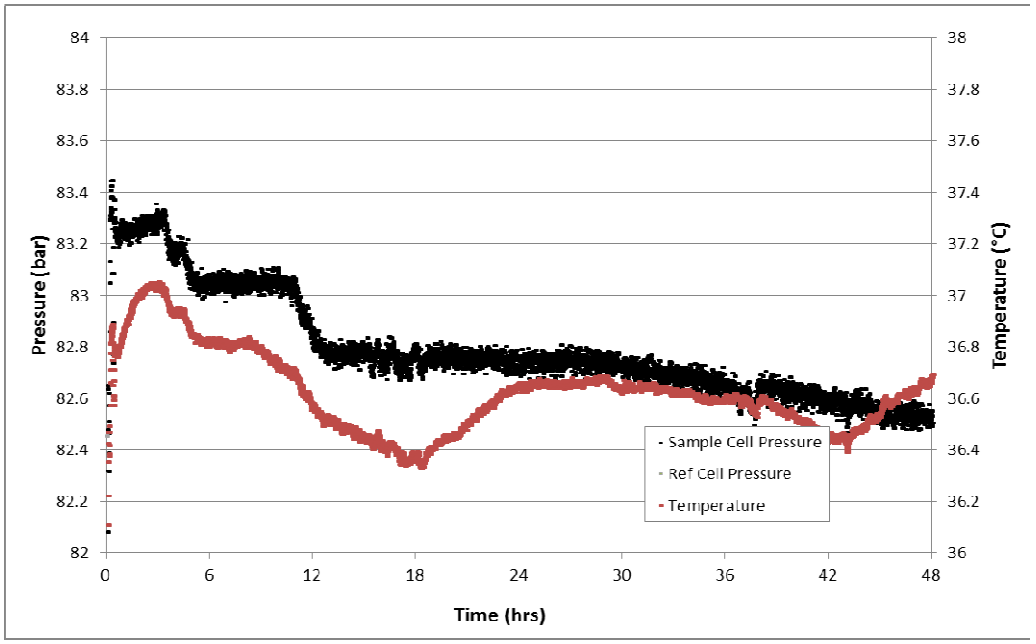


Figure D.20: Sample cell pressure (black) and temperature (red) recorded during VAS experiment. Mixture concentration and sorption calculated are shown. High SO_2 – 4.

Worked Excess Sorption Calculation Example

In this section, the excess sorption will be calculated step-be-step for a CO_2-SO_2 mixture that was measured to be 1.25 mol% SO_2 at the outset of the experiment from GC analysis. Figure D.14 shows the pressure drop over the course of the 48 hour experiment (presented again on the following page) and the final concentration was measured to be 0.40 mol% SO_2. For greater details on how the concentrations were calculated, refer to Appendix D.4.

The sorption is calculated using mass balance principles where the moles sorbed equals the moles of sorbate at the completion of the experiment subtracted from the moles of sorbate at the outset of the experiment. In order to calculate the moles of sorbate, the free volume available for the sorbate is multiplied by the molar density calculated at the pressure, temperature, and concentration of the mixture.

Total Sorption (mmol/g)	SO_2 Concentration (mol%)
1.41	1.25

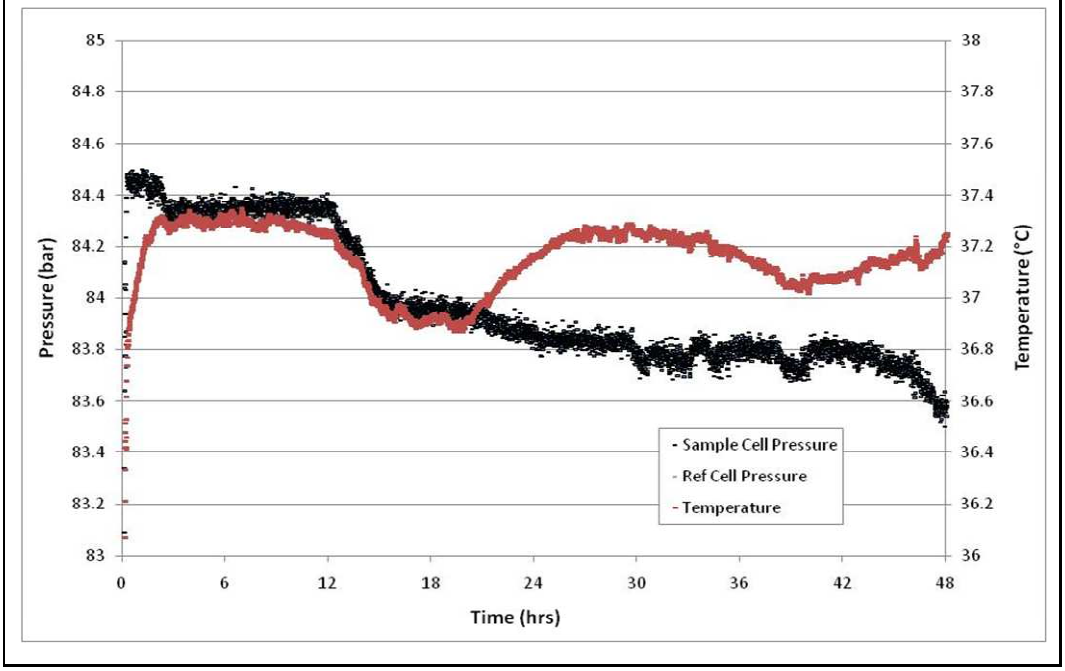


Figure D.14: Sample cell pressure (black) and temperature (red) recorded during VAS experiment. Mixture concentration and sorption calculated are shown. Medium SO_2 – 1.

The free volume available for the sorbate was calculated to be 7.20 cm^3 by subtracting the volume of the coal sample (0.968 cm^3) from the volume of the empty sample cell (8.17 cm^3) (see Appendix D.1), and the temperature of the sorbate throughout the experiment was assumed to be the same as the temperature of the oven at 40°C. This assumption was made as the oven did not fluctuate from the set point by more than 1°C.

It is required to determine the initial and final pressures from Figure D.14. The first hour of the experiment was truncated as the pressure rises as the temperature reaches its set point, and the initial pressure is then calculated to be 84.437 bar which is the average pressure over the second hour of the experiment. Similarly, the final pressure is calculated to be 83.589 bar, which is the average pressure over the last hour of the experiment.

The pressure, temperature and concentration at the initial and final state of the sorption experiment have thus been determined and it is possible to calculate the mixture density at each state. The initial and final molar densities calculated using

Amagat's law are 7.85 mol/l and 7.46 mol/l and the corresponding values calculated using the Patel-Teja EOS are 8.51 mol/l and 7.66 mol/l (see Appendix D.2 for details on the density determination methods).

The total initial and final number of moles can be determined by respective densities by the free volume for the sorbate. The number of moles of each component (SO_2 and CO_2) can be calculated at each state by multiplying the mole fraction of the component at the relevant state by the total number of moles at the relevant state. The total and component-wise sorption can be calculated by subtracting the final number of moles from the initial number of moles present. Finally, the sorption is expressed as an intensive quantity by dividing it by the initial mass of the coal sample (2 g). This sorption calculated is termed the 'excess sorption' and is defined by the definition of the free volume used. The molar and sorption values described are presented in Table D.3 below for each density method case.

Table D.3: Initial and final number of moles present in the sorption experiment with 2 g of coal when the initial SO_2 concentration is 1.25%. The excess sorption is calculated from these values according to mass balance principles. Two alternative density prediction methods are used in calculating these values.

Component	Amagat's Law Density			Patel-Teja EOS Density		
	Initial Moles (mmol)	Final Moles (mmol)	Excess Sorption (mmol/g)	Initial Moles (mmol)	Final Moles (mmol)	Excess Sorption (mmol/g)
Total	56.54	53.74	1.40	61.30	55.14	3.078
CO_2	55.84	53.52	1.16	60.53	54.92	2.805
SO_2	0.704	0.213	0.246	0.764	0.218	0.273

Combined Results Spreadsheet

The tables that follow were extracted from *MS Excel* and present the working data that was used to produce the results in Section 4.2.5.

FINAL RESULTS

	Initial SO_2 Concentration (mol%)	Amagat's Law			Patel-Teja EOS		
		Moles Sorbed (mmol/g)			Moles Sorbed (mmol/g)		
		Total	CO_2	SO_2	Total	CO_2	SO_2
	0	2.409	2.409	0	1.991	1.991	0
	0	1.653	1.653	0	1.310	1.310	0
	0	2.047	2.047	0	1.662	1.662	0
Average	0	2.036	2.036	0	1.654	1.654	0
	0.161	1.212	1.165	0.046	1.312	1.265	0.046
	0.952	1.306	1.100	0.206	2.529	2.308	0.221
	1.246	1.401	1.156	0.246	3.078	2.805	0.273
	1.905	1.231	0.851	0.380	3.778	3.338	0.440
	2.520	0.843	0.510	0.333	4.433	3.982	0.451
	3.196	0.557	0.046	0.511	6.623	5.872	0.752
	3.718	2.012	1.350	0.662	10.292	9.268	1.024
	3.941	0.604	0.247	0.357	6.013	5.371	0.642
	6.693	1.605	0.544	1.061	14.384	12.233	2.150

EXPERIMENTAL PARAMETERS

Peak Area (uV.min)				SO_2 Concentration (mol%)		Concentration Difference (mol%)	Pressure (bar)		Δ P (bar)
Initial	Std Dev	Final	Std Dev	Initial	Final		Initial	Final	
0	0	0	0	0	0	0	85.872	84.475	1.397
0	0	0	0	0	0	0	86.280	85.405	0.875
0	0	0	0	0	0	0	86.046	84.907	1.139
23.16	3.913	0	0	0.161	0	0.161	84.835	84.078	0.758
137.20	5.656	32.44	10.517	0.952	0.225	0.727	84.271	83.456	0.816
179.54	22.441	57.08	2.337	1.246	0.396	0.850	84.437	83.589	0.849
274.62	61.245	69.44	1.736	1.905	0.482	1.424	82.953	82.148	0.805
363.26	29.713	197.20	19.835	2.520	1.368	1.152	84.021	83.577	0.444
460.62	91.947	202.04	33.908	3.196	1.402	1.794	84.063	83.903	0.159
535.90	6.704	211.10	46.944	3.718	1.465	2.253	84.016	82.845	1.172
568.02	57.459	387.64	15.164	3.941	2.689	1.251	83.374	83.091	0.283
964.68	98.253	434.68	46.996	6.693	3.016	3.677	83.254	82.528	0.726

DENSITY

Initial Mole Fraction SO_2	Final Mole Fraction SO_2	Amagat's Law						Patel-Teja EOS	
		Initial Density (mol/l)			Final Density (mol/l)			Density (mol/l)	
		CO_2	SO_2	Mixture	CO_2	SO_2	Mixture	Initial	Final
0	0	8.474	20.969	8.474	7.805	20.969	7.805	8.357	7.804
0	0	8.695	20.972	8.695	8.236	20.972	8.236	8.529	8.165
0	0	8.567	20.970	8.567	7.999	20.970	7.999	8.430	7.968
0.0016	0	7.966	20.967	7.974	7.637	20.967	7.637	8.022	7.658
0.0095	0.0023	7.718	20.965	7.765	7.391	20.965	7.402	8.235	7.533
0.0125	0.0040	7.789	20.965	7.850	7.442	20.965	7.461	8.511	7.656
0.0191	0.0048	7.207	20.960	7.298	6.934	20.960	6.956	8.236	7.187
0.0252	0.0137	7.614	20.965	7.738	7.438	20.965	7.504	9.409	8.178
0.0320	0.0140	7.631	20.966	7.789	7.566	20.966	7.635	10.197	8.358
0.0372	0.0146	7.612	20.963	7.797	7.168	20.963	7.238	10.759	7.901
0.0394	0.0269	7.361	20.964	7.554	7.256	20.964	7.386	10.666	8.996
0.0669	0.0302	7.316	20.962	7.649	7.059	20.962	7.203	12.963	8.969

FREE VOLUME

Chamber Volume (l)	Sample Volume (l)	Free Volume (l)	Sample Mass (g)
0.00817	0.000968	0.00720	2

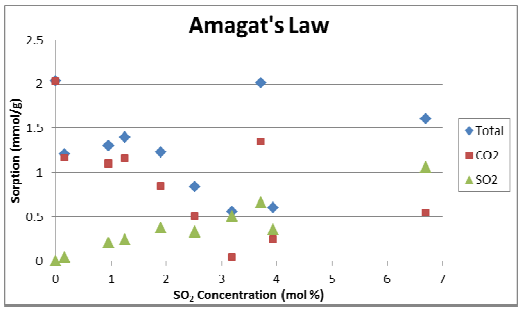
SORPTION CALCULATIONS

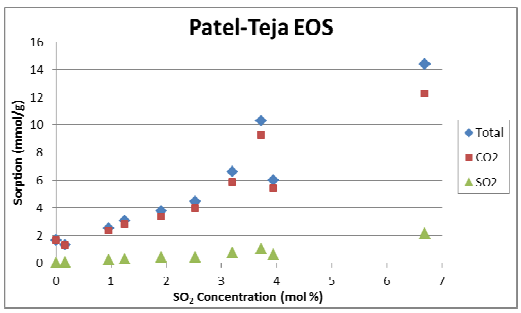
Amagat's Law

Initial Mole Fraction SO2	Final Mole Fraction SO2	Initial Moles (mmol)			Final Moles (mmol)			Percent Component Sorbed (%)		
		Tot	CO_2	SO_2	Tot	CO_2	SO_2	Tot	CO_2	SO_2
0	0	61.033	61.033	0	56.215	56.215	0	7.894	7.894	0
0	0	62.625	62.625	0	59.319	59.319	0	5.280	5.280	0
0	0	61.702	61.702	0	57.608	57.608	0	6.635	6.635	0
0.0016	0	57.428	57.335	0.092	55.004	55.004	0	4.219	4.065	100
0.0095	0.0023	55.923	55.391	0.532	53.311	53.191	0.120	4.670	3.971	77.460
0.0125	0.0040	56.540	55.836	0.704	53.738	53.525	0.213	4.957	4.139	69.784
0.0191	0.0048	52.561	51.559	1.001	50.098	49.857	0.241	4.684	3.301	75.899
0.0252	0.0137	55.732	54.327	1.405	54.046	53.306	0.739	3.025	1.879	47.356
0.0320	0.0140	56.101	54.308	1.793	54.986	54.215	0.771	1.987	0.170	57.009
0.0372	0.0146	56.153	54.065	2.088	52.130	51.366	0.764	7.166	4.993	63.431
0.0394	0.0269	54.403	52.259	2.144	53.196	51.765	1.431	2.219	0.945	33.270
0.0669	0.0302	55.089	51.402	3.687	51.879	50.315	1.565	5.827	2.115	57.566

Patel-Teja EOS

Initial Mole Fraction SO2	Final Mole Fraction SO2	Initial Moles (mmol)			Final Moles (mmol)			Percent Component Sorbed (%)		
		Tot	CO2	SO2	Tot	CO2	SO2	Tot	CO2	SO2
0	0	60.187	60.187	0	56.205	56.205	0	6.616	6.616	0
0	0	61.427	61.427	0	58.807	58.807	0	4.265	4.265	0
0	0	60.713	60.713	0	57.389	57.389	0	5.474	5.474	0
0	0	60.775	60.775	0	57.467	57.467	0	5.452	5.452	0
0.0016	0	57.779	57.686	0.093	55.155	55.155	0	4.540	4.386	100
0.0095	0.0023	59.310	58.745	0.565	54.251	54.129	0.122	8.529	7.858	78.372
0.0125	0.0040	61.296	60.533	0.764	55.141	54.922	0.218	10.042	9.268	71.400
0.0191	0.0048	59.316	58.186	1.130	51.759	51.510	0.249	12.740	11.474	77.936
0.0252	0.0137	67.769	66.061	1.708	58.902	58.096	0.806	13.084	12.057	52.817
0.0320	0.0140	73.442	71.095	2.347	60.196	59.352	0.844	18.036	16.517	64.049
0.0372	0.0146	77.490	74.609	2.881	56.905	56.072	0.833	26.564	24.845	71.072
0.0394	0.0269	76.815	73.788	3.027	64.789	63.046	1.742	15.656	14.557	42.440
0.0669	0.0302	93.366	87.117	6.249	64.598	62.650	1.948	30.812	28.085	68.824





D.4 Gas Analysis

In order to determine the concentration of the CO_2-SO_2 mixtures, gas chromatography was used. The chromatograms were produced by running them through a Brüker 430-GC equipped with a HayeSep N packed column, TCD and auto-sampling valve. N_2 was used as the carrier gas, and the temperature program selected ran the oven at a constant 40°C for the first 2.5 minutes before raising the temperature at 40°C/min until the 150°C was reached and held for approximately 3 minutes. The injection temperature and detector temperature in the GC program were set to 140°C and 270°C respectively. The reference flow for the carrier gas was 30 ml/min with a make-up flow of 5 ml/min. CO_2 and SO_2 peaks are detected at approximately 1.5 minutes and 6.4 minutes respectively and were integrated manually in order to obtain values of the peak areas.

The CO_2-SO_2 mixtures were analysed both before and after the sorption experiments had taken place. The sampled were run 4 to 5 times through the GC so that an average value of the SO_2 peak area could be obtained. This peak area was used to determine the concentration of SO_2 in the mixture using a calibration curve that was produced by running standard CO_2-SO_2 samples through the GC. The calibration curve produced is presented below, while the combined chromatograms for each CO_2-SO_2 sample are presented thereafter. The SO_2 peak is zoomed into for a clearer view of the deviation between runs, and thereafter, the chromatograms produced before and after sorption are plotted on the same set of axes for comparison.

Calibration Curve

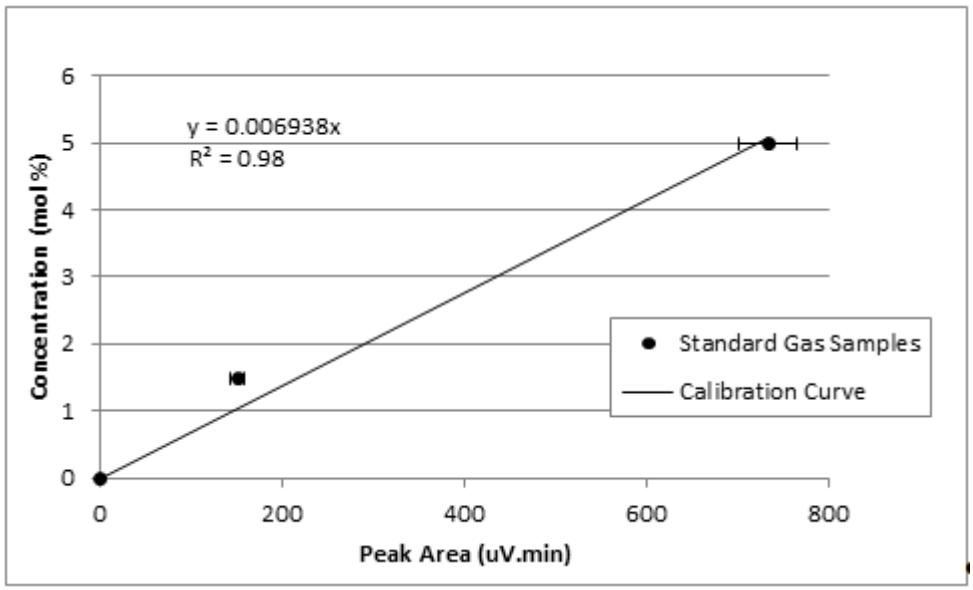


Figure D.21: Calibration Curve produced for SO_2. SO_2 Concentration = 0.006938 x SO_2 Peak Area

High SO_2: Mixture 4

Before Sorption

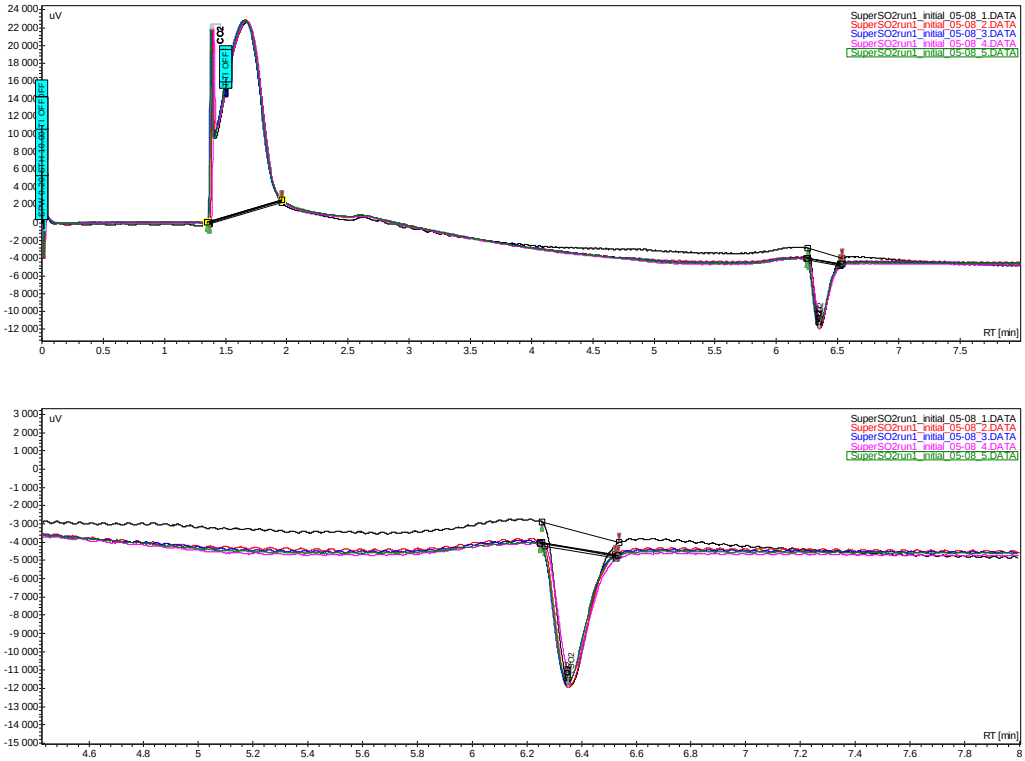


Figure D.22: Chromatograms of 5 gas sample runs of a CO_2-SO_2 mixture with a high level of SO_2 (High SO_2 - Mixture 4) before sorption. The entire chromatogram (top) and SO_2 peak close-up (bottom) are shown.

Table D.4: Summarised average results table for initial concentration of High SO_2 - Mixture 4

	Name	Time [Min]	Quantity [% Area]	Area [uV.Min]	Area % [%]	Concentration Calculated (mol %)
AVERAGE	CO_2	1.39	88.93	7737.78	88.93	93.307
	SO_2	6.35	11.07	964.68	11.07	6.693
STD DEV	CO_2	0.01	0.95	53.06	0.96	
	SO_2	0.00	0.95	98.25	0.96	

After Sorption

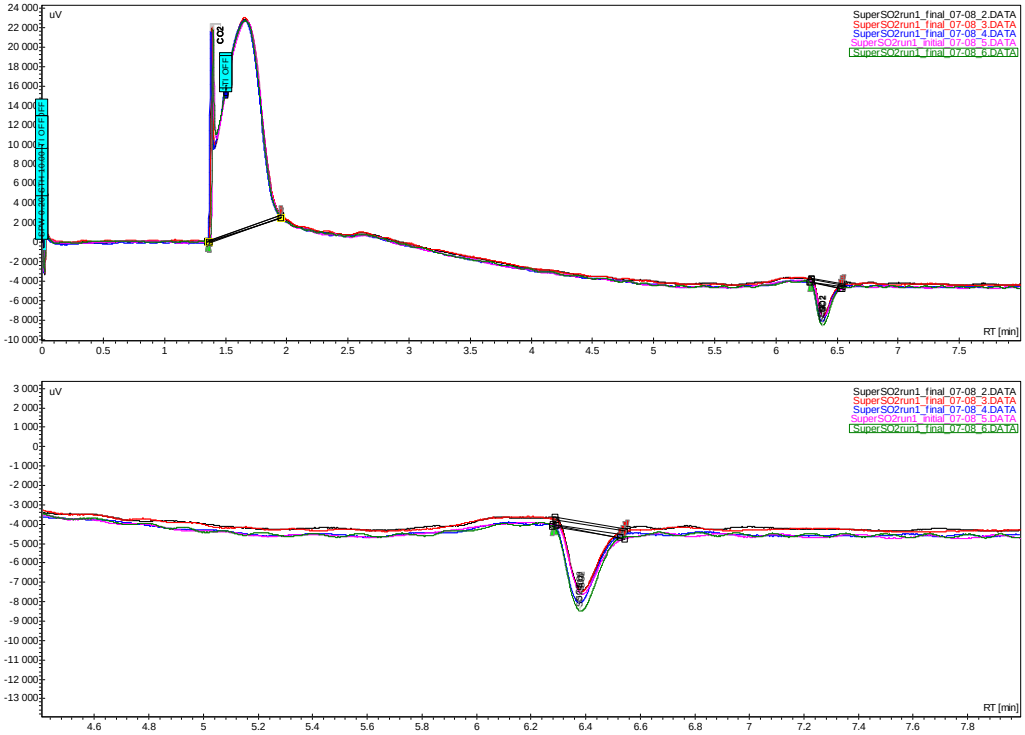


Figure D.23: Chromatograms of five gas sample runs of High SO_2 - Mixture 4 after sorption. The entire chromatogram (top) and SO_2 peak close-up (bottom) are shown.

Table D.5: Summarised average results table for final concentration of High SO_2 - Mixture 4

	Name	Time [Min]	Quantity [% Area]	Area [uV.Min]	Area % [%]	Concentration Calculated (mol %)
AVERAGE	CO_2	1.39	94.65	7684.68	94.65	96.984
	SO_2	6.38	5.35	434.68	5.35	3.016
STD DEV	CO_2	0.01	0.55	33.06	0.55	
	SO_2	0.00	0.55	47.00	0.55	

Comparison

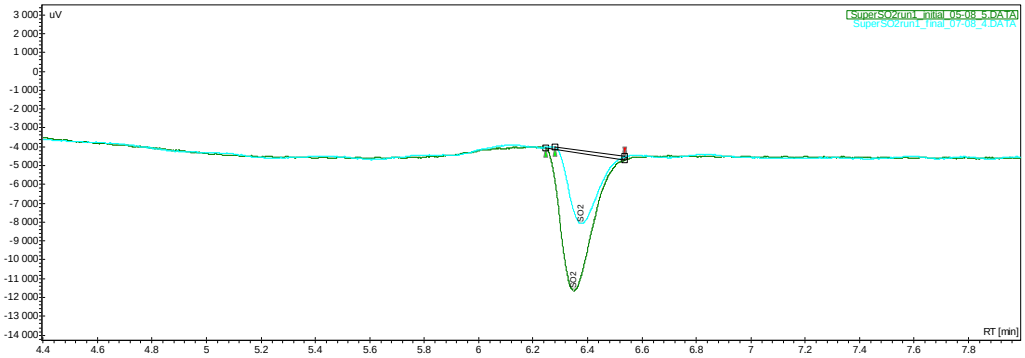


Figure D.24: Comparison of representative SO_2 peaks before and after sorption. High SO_2 - Mixture 4.

High SO_2: Mixture 3

Before Sorption

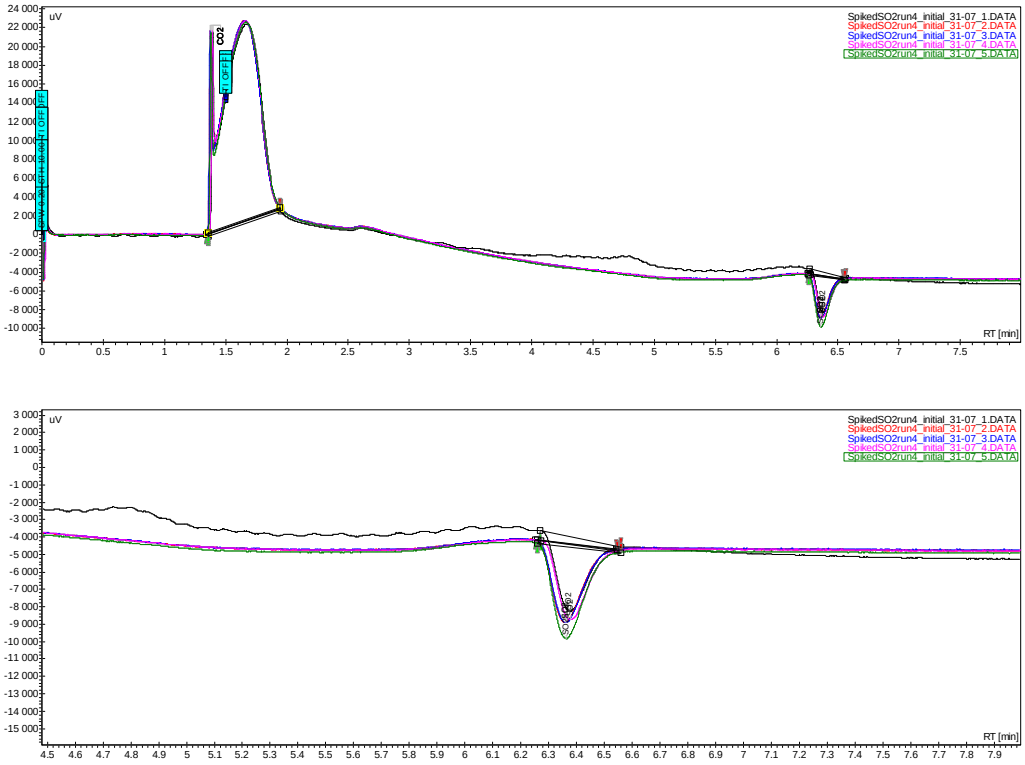


Figure D. 25: Chromatograms of 5 gas sample runs of a CO_2-SO_2 mixture (High SO_2 - Mixture 3) with a high level of SO_2 before sorption. The entire chromatogram (top) and SO_2 peak close-up (bottom) are shown.

Table D. 6: Summarised average results table for initial concentration of High SO_2 - Mixture 3

	Name	Time [Min]	Quantity [% Area]	Area [uV.Min]	Area % [%]	Concentration Calculated (mol%)
AVERAGE	CO_2	1.38	93.07	7628.94	93.07	96.059
	SO_2	6.37	6.93	568.02	6.93	3.941
STD DEV	CO_2	0.01	0.70	88.67	0.70	
	SO_2	0.01	0.70	57.46	0.70	

After Sorption

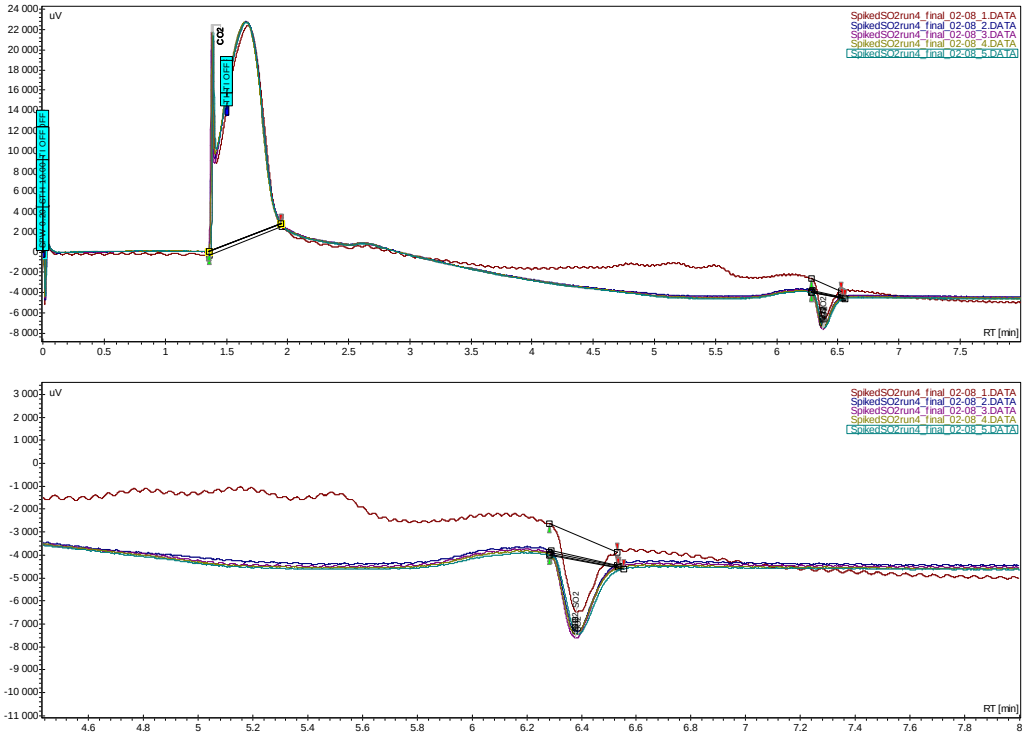


Figure D.26: Chromatograms of five gas sample runs of a CO_2-SO_2 mixture (High SO_2 - Mixture 3) after sorption. The entire chromatogram (top) and SO_2 peak close-up (bottom) are shown.

Table D.7: Summarised average results table for final concentration of High SO_2 - Mixture 3

	Name	Time [Min]	Quantity [% Area]	Area [uV.Min]	Area % [%]	Concentration Calculated (mol%)
AVERAGE	CO_2	1.38	95.16	7623.02	95.16	97.311
	SO_2	6.38	4.84	387.64	4.84	2.689
STD DEV	CO_2	0.01	0.16	56.56	0.16	
	SO_2	0.00	0.16	15.16	0.16	

Comparison

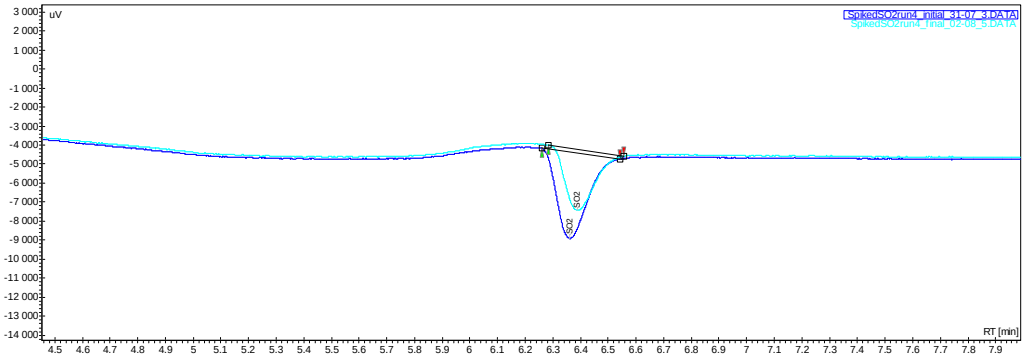


Figure D.27: Comparison of representative SO_2 peaks before and after sorption. High SO_2 - Mixture 3

High SO_2: Mixture 2

Before Sorption

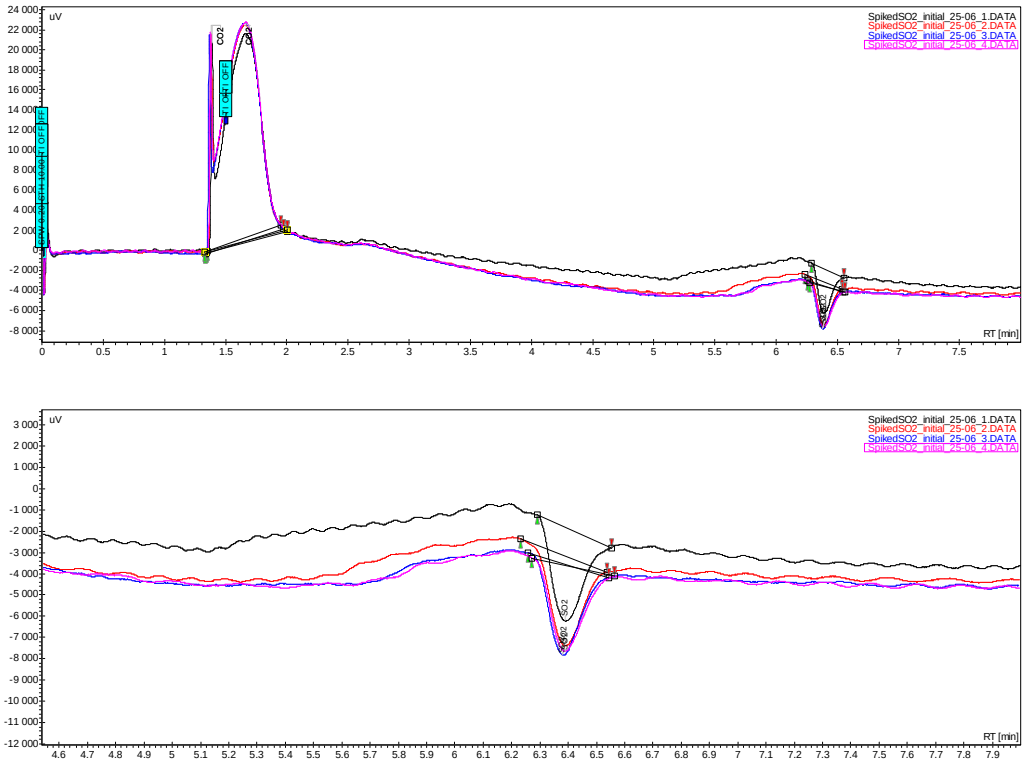


Figure D. 28: Chromatograms of four gas sample runs of a CO_2-SO_2 mixture with a high level of SO_2 (High SO_2 - Mixture 2) before sorption. The entire chromatogram (top) and SO_2 peak close-up (bottom) are shown.

Table D.8: Summarised average results table for initial concentration of High SO_2 - Mixture 2

	Name	Time [Min]	Quantity [% Area]	Area [uV.Min]	Area % [%]	Concentration Calculated (mol%)
AVERAGE	CO_2	1.52	93.46	7686.53	93.46	96.282
	SO_2	6.39	6.54	535.90	6.54	3.718
STD DEV	CO_2	0.16	0.45	458.77	0.45	
	SO_2	0.00	0.45	6.70	0.45	

After Sorption

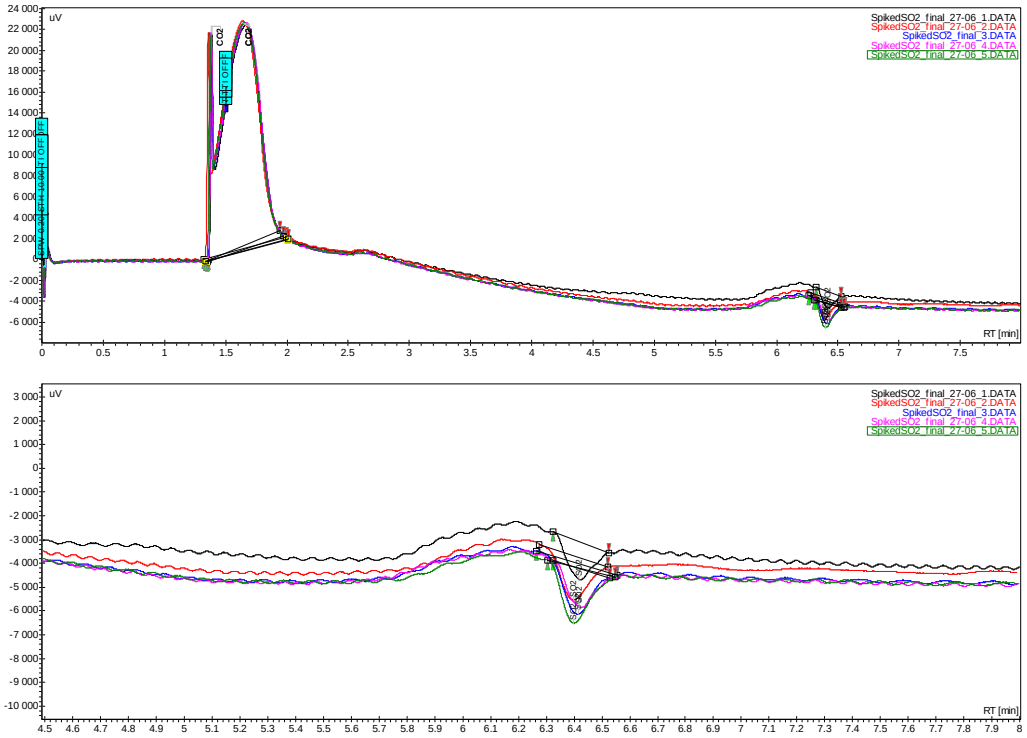


Figure D.29: Chromatograms of five gas sample runs of a CO_2-SO_2 mixture (High SO_2 - Mixture 2) after sorption. The entire chromatogram (top) and SO_2 peak close-up (bottom) are shown.

Table D.9: Summarised average results table for final concentration of High SO_2 - Mixture 2

	Name	Time [Min]	Quantity [% Area]	Area [uV.Min]	Area % [%]	Concentration Calculated (mol%)
AVERAGE	CO_2	1.54	97.38	7815.58	97.38	98.535
	SO_2	6.41	2.62	211.10	2.62	1.465
STD DEV	CO_2	0.14	0.51	255.33	0.51	
	SO_2	0.01	0.51	46.94	0.51	

Comparison

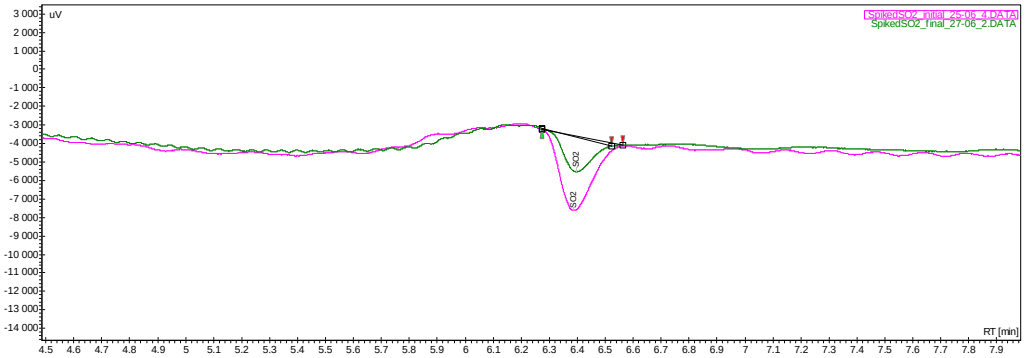


Figure D.30: Comparison of representative SO_2 peaks before and after sorption. High SO_2 - Mixture 2.

High SO_2: Mixture 1

Before Sorption

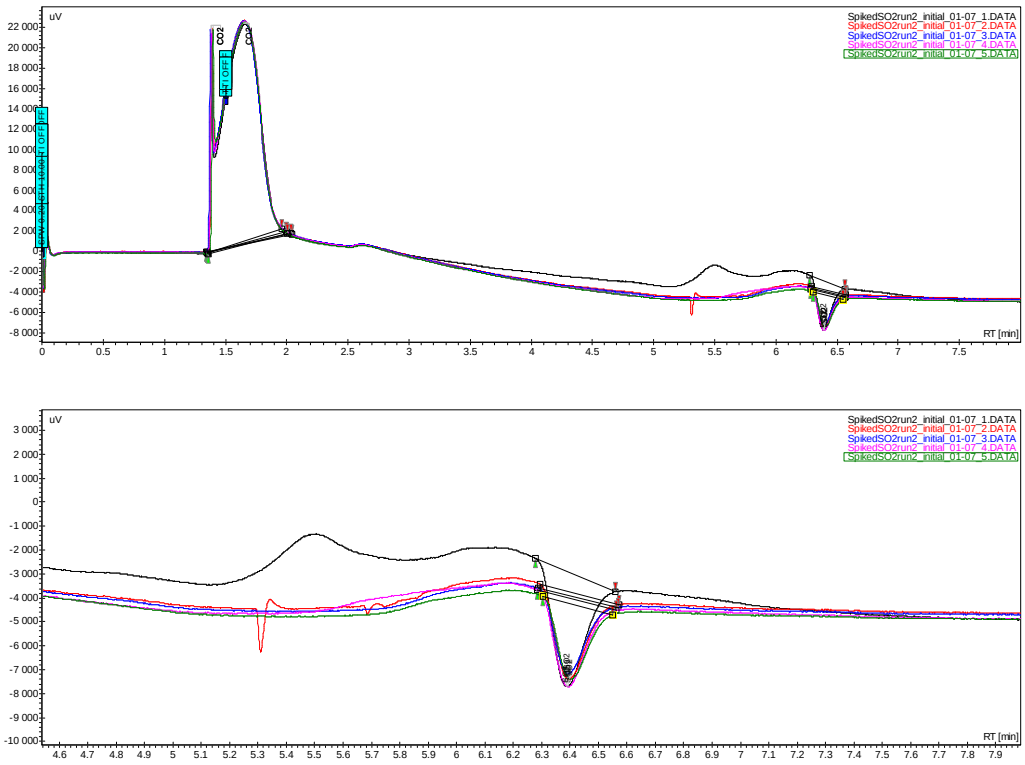


Figure D.31: Chromatograms of four gas sample runs of a CO_2-SO_2 mixture with a high level of SO_2 (High SO_2 - Mixture 1) before sorption. The entire chromatogram (top) and SO_2 peak close-up (bottom) are shown.

Table D.10: Summarised average results table for initial concentration of High SO_2 - Mixture 1

	Name	Time [Min]	Quantity [% Area]	Area [uV.Min]	Area % [%]	Concentration Calculated (mol%)
AVERAGE	CO_2	1.50	94.47	7871.56	94.47	96.80417
	SO_2	6.39	5.53	460.62	5.53	3.195828
STD DEV	CO_2	0.14	1.14	162.20	1.14	
	SO_2	0.00	1.14	91.95	1.14	

After Sorption

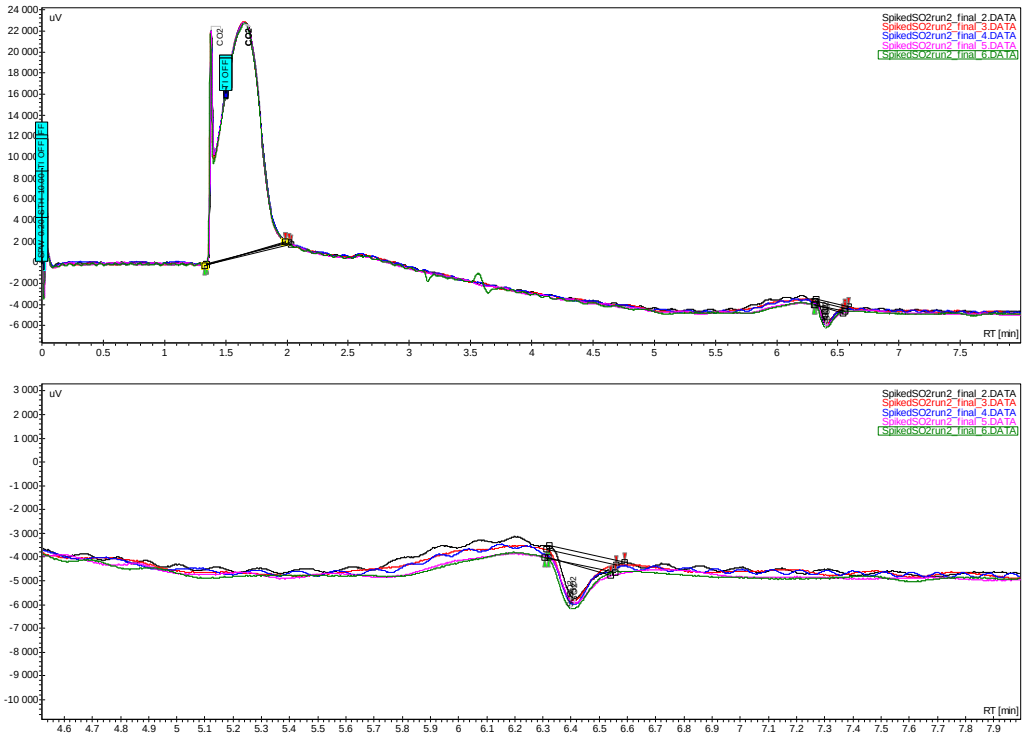


Figure D.32: Chromatograms of five gas sample runs of a CO_2-SO_2 mixture (High SO_2 - Mixture 1) after sorption. The entire chromatogram (top) and SO_2 peak close-up (bottom) are shown.

Table D.11: Summarised average results table for final concentration of High SO_2 - Mixture 1

	Name	Time [Min]	Quantity [% Area]	Area [uV.Min]	Area % [%]	Concentration Calculated (mol%)
AVERAGE	CO_2	1.60	97.55	8060.52	97.55	98.598
	SO_2	6.41	2.45	202.04	2.45	1.402
STD DEV	CO_2	0.12	0.41	75.82	0.41	
	SO_2	0.01	0.41	33.91	0.41	

Comparison

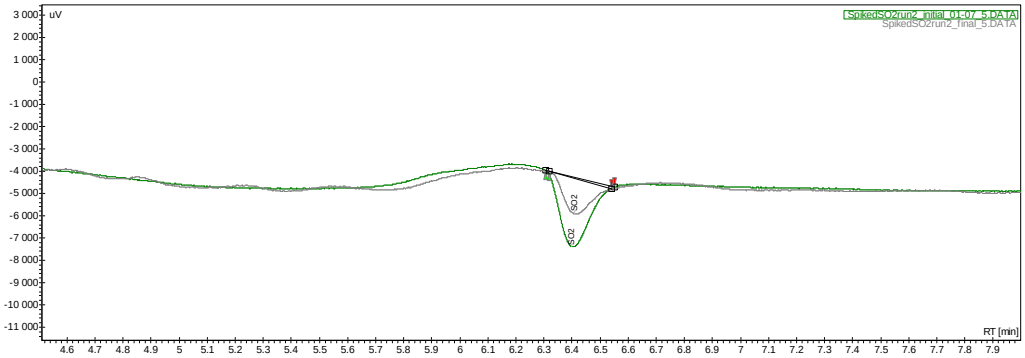


Figure D.33: Comparison of representative SO_2 peaks before and after sorption. High SO_2 - Mixture 1.

Medium SO_2: Mixture 3

Before Sorption

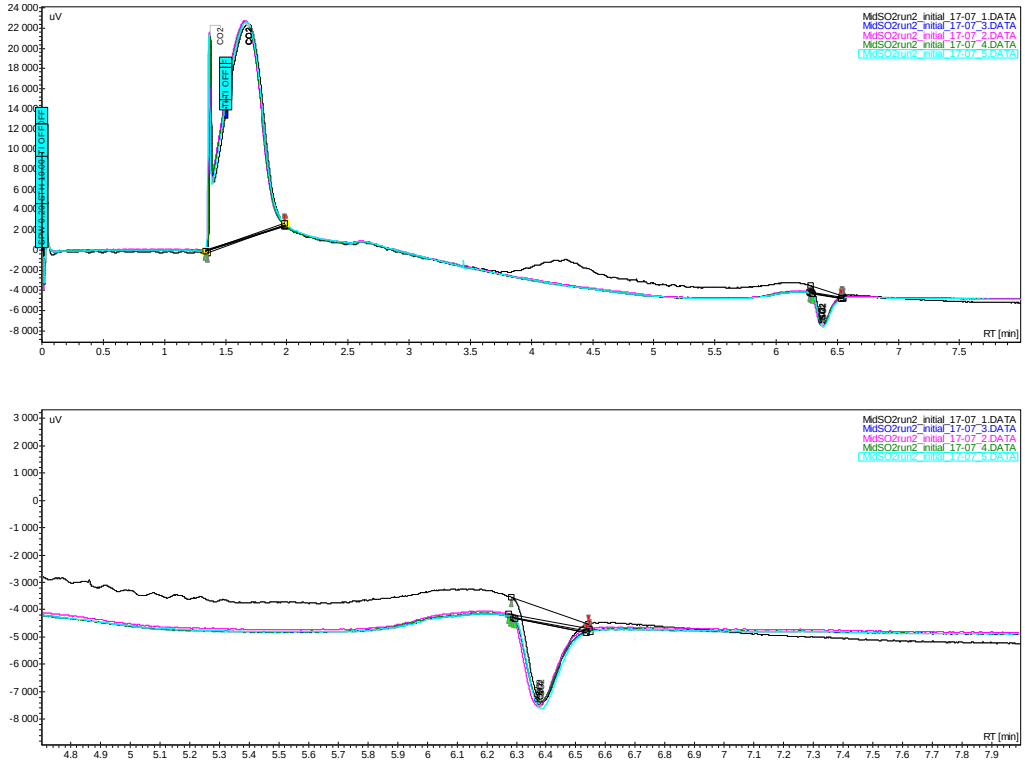


Figure D.34: Chromatograms of five gas sample runs of a CO_2-SO_2 mixture with a mid level of SO_2 (Medium SO_2 - Mixture 3) before sorption. The entire chromatogram (top) and SO_2 peak close-up (bottom) are shown.

Table D.12: Summarised average results table for initial concentration of Medium SO_2 - Mixture 3.

	Name	Time [Min]	Quantity [% Area]	Area [uV.Min]	Area % [%]	Concentration Calculated (mol%)
AVERAGE	CO_2	1.60	95.56	7815.34	95.56	97.480
	SO_2	6.38	4.44	363.26	4.44	2.520
STD DEV	CO_2	0.12	0.36	59.15	0.36	
	SO_2	0.01	0.36	29.71	0.36	

After Sorption

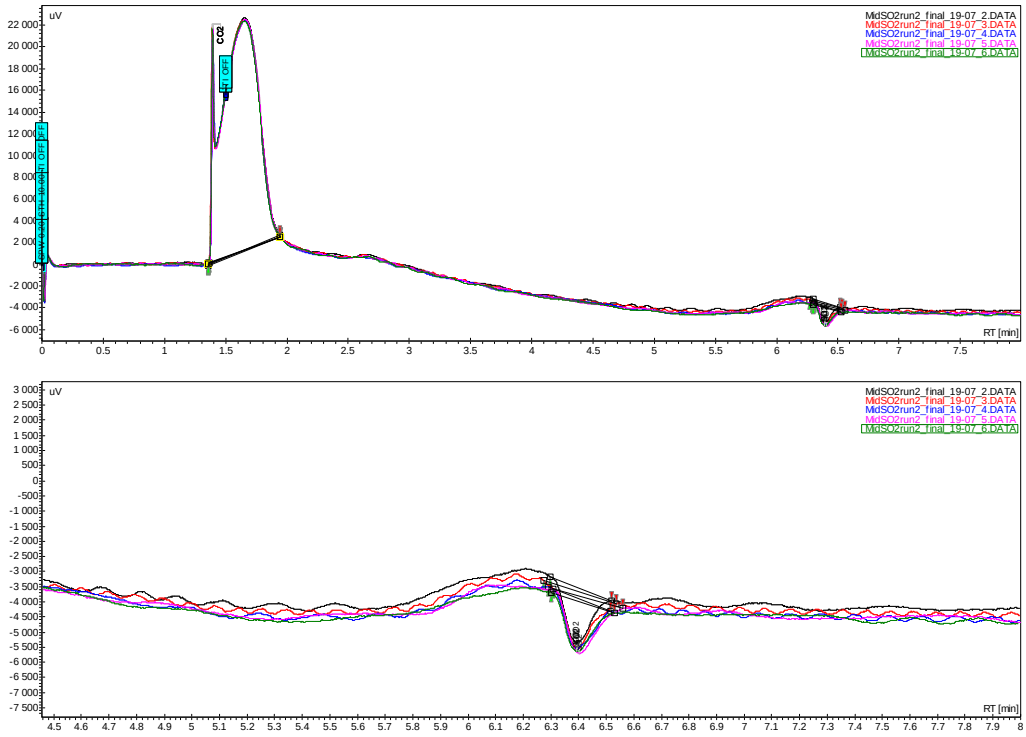


Figure D.35: Chromatograms of five gas sample runs of a CO_2-SO_2 mixture (Medium SO_2 - Mixture 3) after sorption. The entire chromatogram (top) and SO_2 peak close-up (bottom) are shown.

Table D.13: Summarised average results table for final concentration of Medium SO_2 - Mixture 3

	Name	Time [Min]	Quantity [% Area]	Area [uV.Min]	Area % [%]	Concentration Calculated (mol%)
AVERAGE	CO_2	1.39	97.45	7530.70	97.45	98.632
	SO_2	6.39	2.55	197.20	2.55	1.368
STD DEV	CO_2	0.00	0.25	40.76	0.25	
	SO_2	0.00	0.25	19.84	0.25	

Comparison

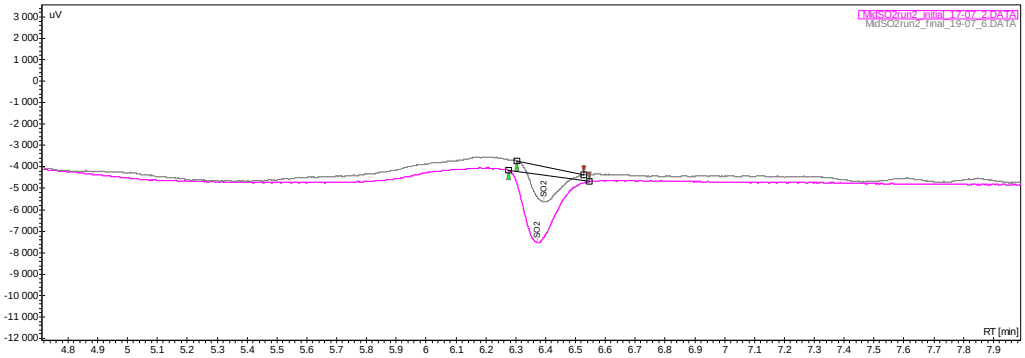


Figure D.36: Comparison of representative SO_2 peaks before and after sorption. Medium SO_2 - Mixture 3.

Medium SO_2: Mixture 2

Before Sorption

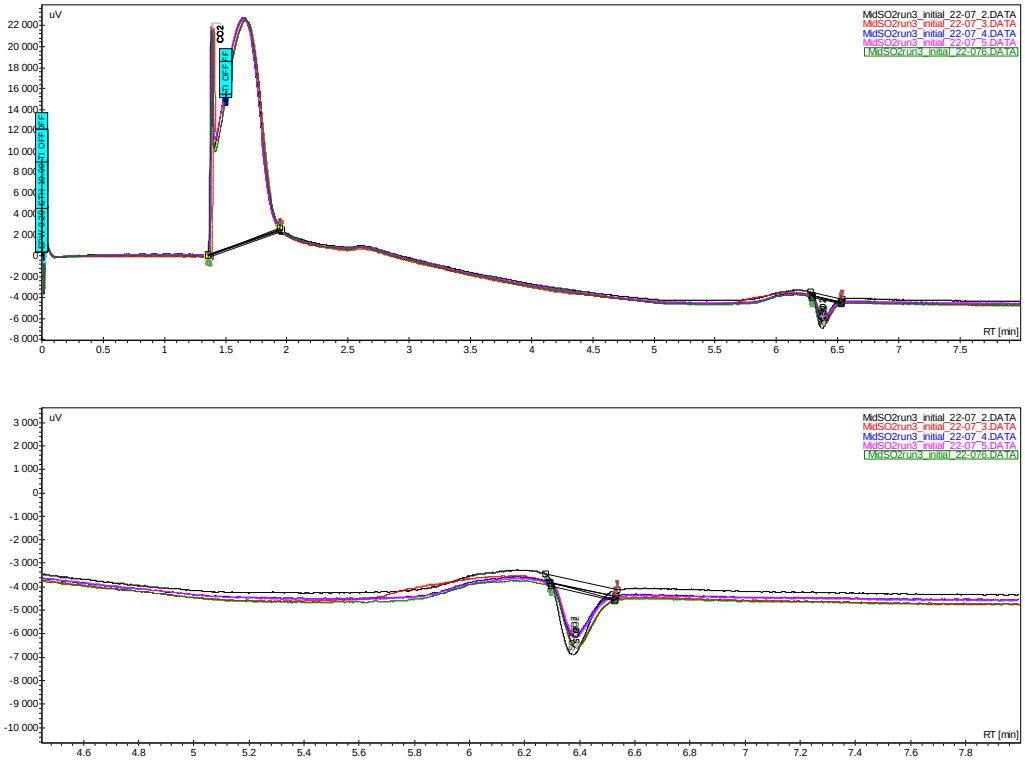


Figure D. 37: Chromatograms of five gas sample runs of a CO_2-SO_2 mixture with a mid level of SO_2 (Medium SO_2 - Mixture 2) before sorption. The entire chromatogram (top) and SO_2 peak close-up (bottom) are shown.

Table D. 14: Summarised average results table for initial concentration of Medium SO_2 - Mixture 2

	Name	Time [Min]	Quantity [% Area]	Area [uV.Min]	Area % [%]	Concentration Calculated (mol%)
AVERAGE	CO_2	1.39	96.53	7623.58	96.53	98.095
	SO_2	6.38	3.47	274.62	3.47	1.905
STD DEV	CO_2	0.01	0.72	73.39	0.72	
	SO_2	0.01	0.72	61.25	0.72	

After Sorption

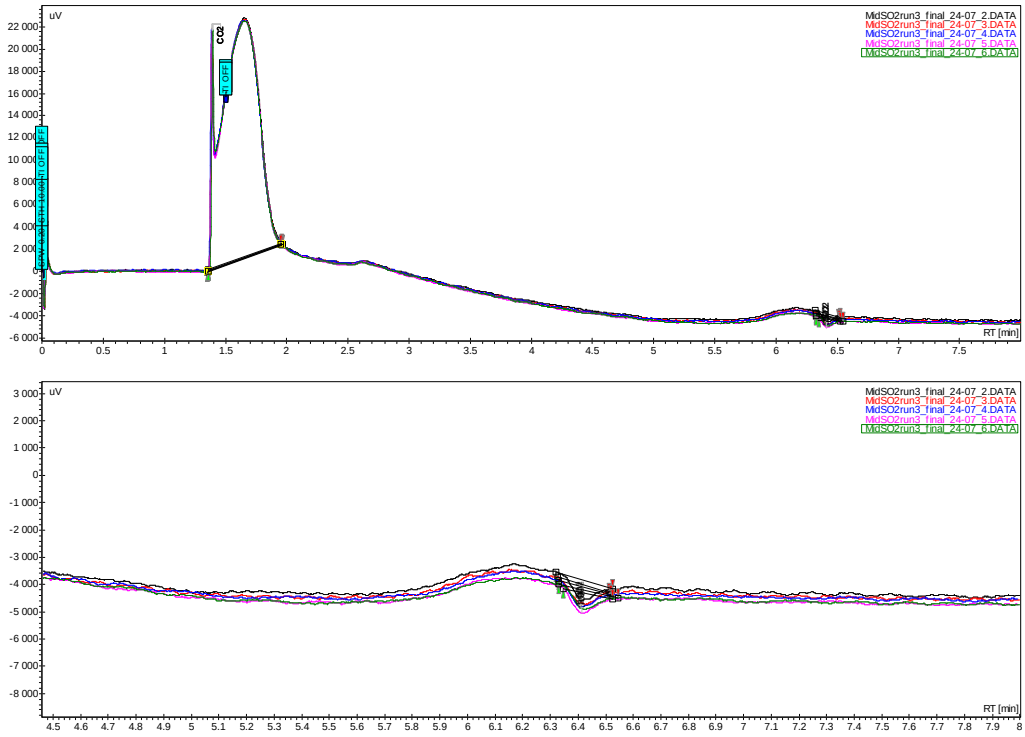


Figure D.38: Chromatograms of five gas sample runs of a CO_2-SO_2 mixture (Medium SO_2 - Mixture 2) after sorption. The entire chromatogram (top) and SO_2 peak close-up (bottom) are shown.

Table D.15: Summarised average results table for final concentration of Medium SO_2 - Mixture 2

	Name	Time [Min]	Quantity [% Area]	Area [uV.Min]	Area % [%]	Concentration Calculated (mol%)
AVERAGE	CO_2	1.39	99.10	7657.06	99.10	99.518
	SO_2	6.41	0.90	69.44	0.90	0.482
STD DEV	CO_2	0.00	0.03	60.35	0.03	
	SO_2	0.00	0.03	1.74	0.03	

Comparison

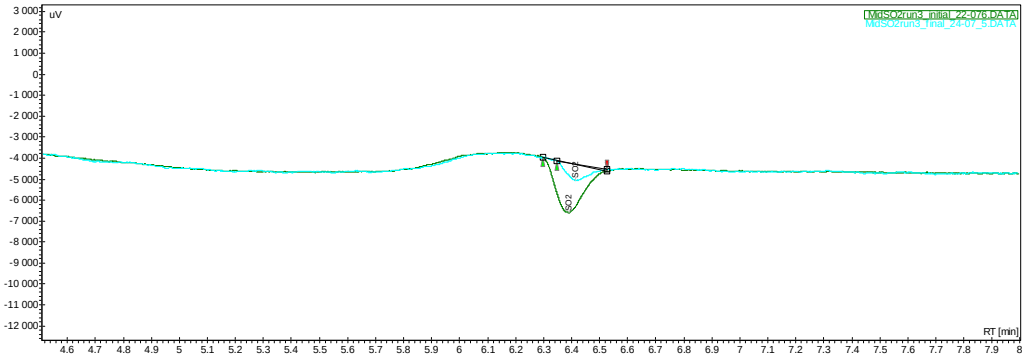


Figure D.39: Comparison of representative SO_2 peaks before and after sorption. Medium SO_2 - Mixture 2.

Medium SO_2: Mixture 1

Before Sorption

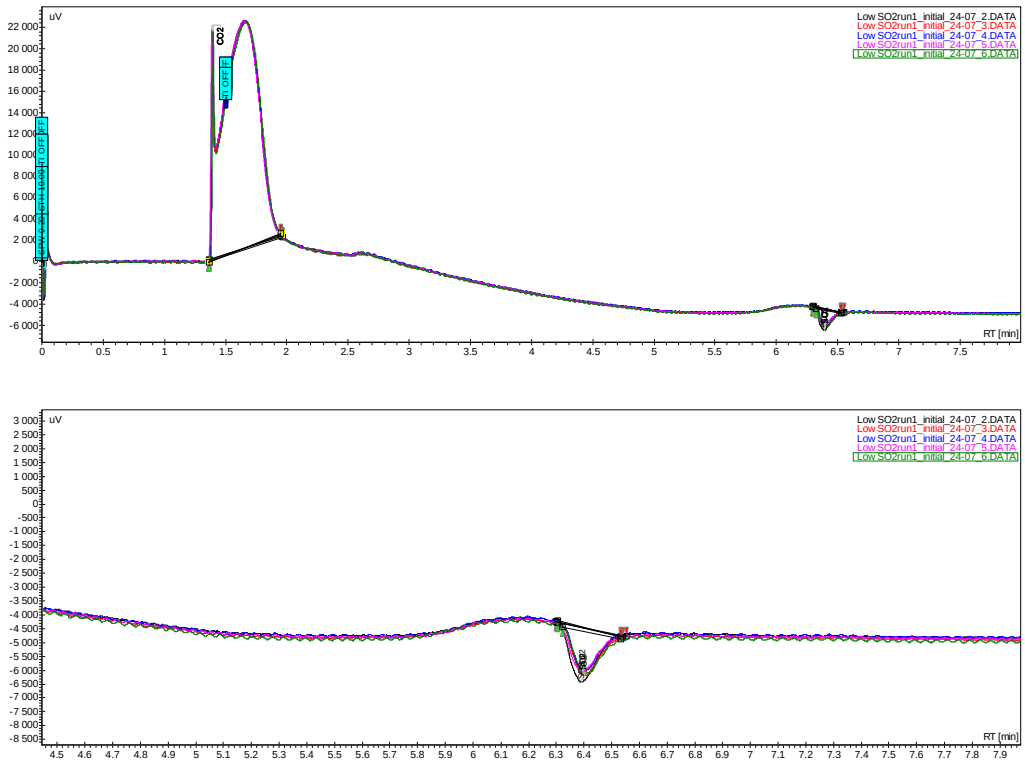


Figure D. 40: Chromatograms of five gas sample runs of a CO_2-SO_2 mixture with a mid level of SO_2 (Medium SO_2 - Mixture 1) before sorption. The entire chromatogram (top) and SO_2 peak close-up (bottom) are shown.

Table D. 16: Summarised average results table for initial concentration of Medium SO_2 - Mixture 1

	Name	Time [Min]	Quantity [% Area]	Area [uV.Min]	Area % [%]	Concentration Calculated (mol%)
AVERAGE	CO_2	1.39	97.70	7607.58	97.70	98.754
	SO_2	6.40	2.30	179.54	2.30	1.246
STD DEV	CO_2	0.00	0.27	48.25	0.27	
	SO_2	0.01	0.27	22.44	0.27	

After Sorption

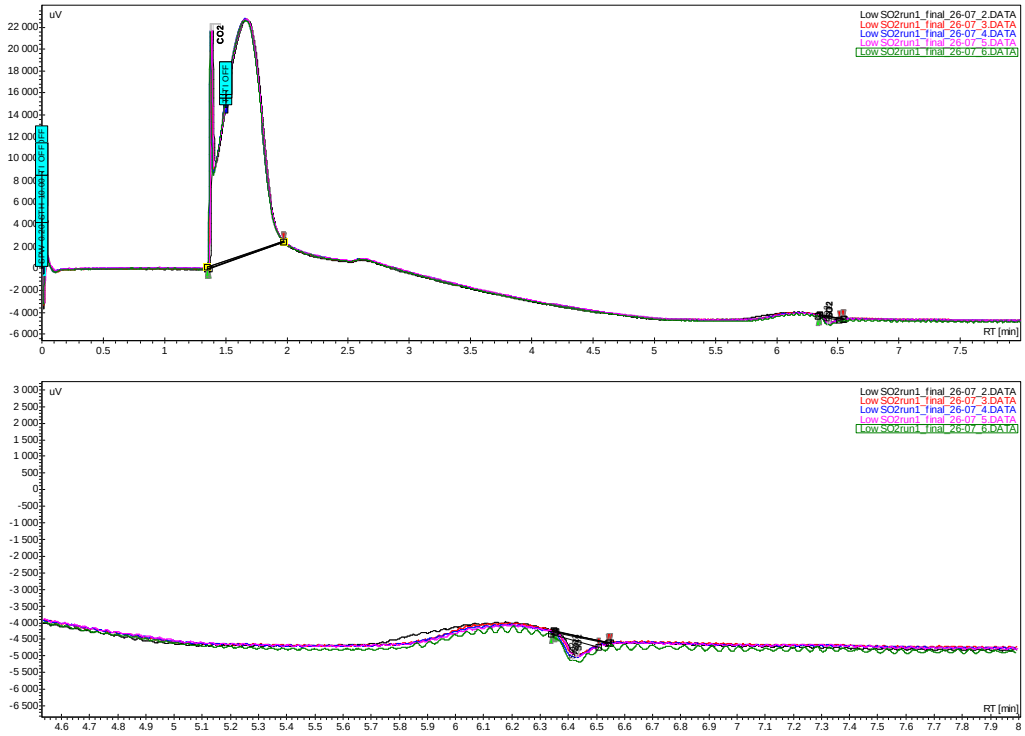


Figure D.41: Chromatograms of five gas sample runs of a CO_2-SO_2 (Medium SO_2 - Mixture 1) mixture after sorption. The entire chromatogram (top) and SO_2 peak close-up (bottom) are shown.

Table D.17: Summarised average results table for final concentration of Medium SO_2 - Mixture 1

	Name	Time [Min]	Quantity [% Area]	Area [uV.Min]	Area % [%]	Concentration Calculated (mol%)
AVERAGE	CO_2	1.38	99.27	7804.56	99.27	99.604
	SO_2	6.43	0.73	57.08	0.73	0.396
STD DEV	CO_2	0.01	0.03	36.90	0.03	
	SO_2	0.01	0.03	2.34	0.03	

Comparison

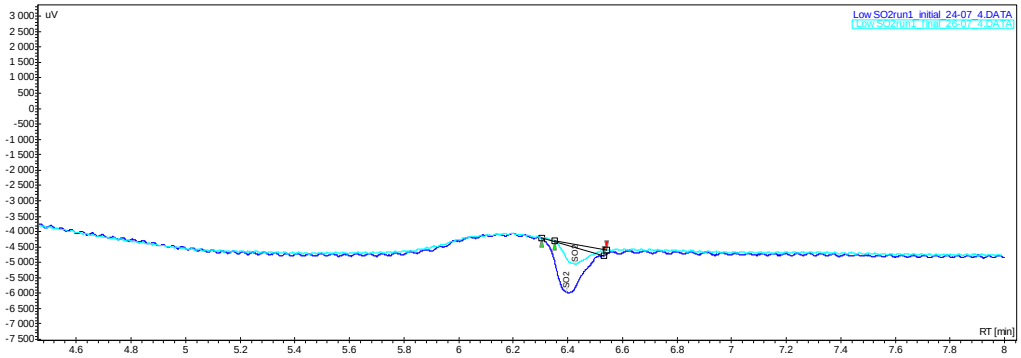


Figure D.42: Comparison of representative SO_2 peaks before and after sorption. Medium SO_2 - Mixture 1.

Low SO_2: Mixture 2

Before Sorption

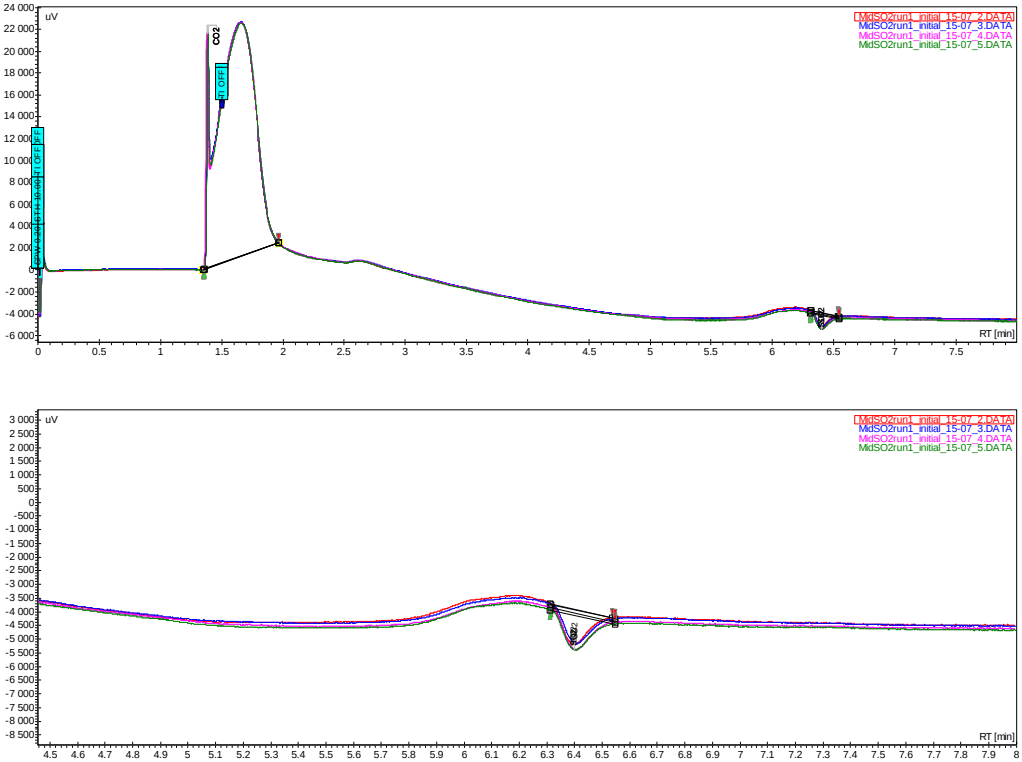


Figure D.43: Chromatograms of four gas sample runs of a CO_2-SO_2 mixture with a low level of SO_2 (Low SO_2 - Mixture 2) before sorption. The entire chromatogram (top) and SO_2 peak close-up (bottom) are shown.

Table D.18: Summarised average results table for initial concentration of Low SO_2 - Mixture 2

	Name	Time [Min]	Quantity [% Area]	Area [uV.Min]	Area % [%]	Concentration Calculated (mol%)
AVERAGE	CO_2	1.39	98.25	7698.95	98.25	99.048
	SO_2	6.40	1.75	137.20	1.75	0.952
STD DEV	CO_2	0.01	0.07	31.91	0.07	
	SO_2	0.00	0.07	5.66	0.07	

After Sorption

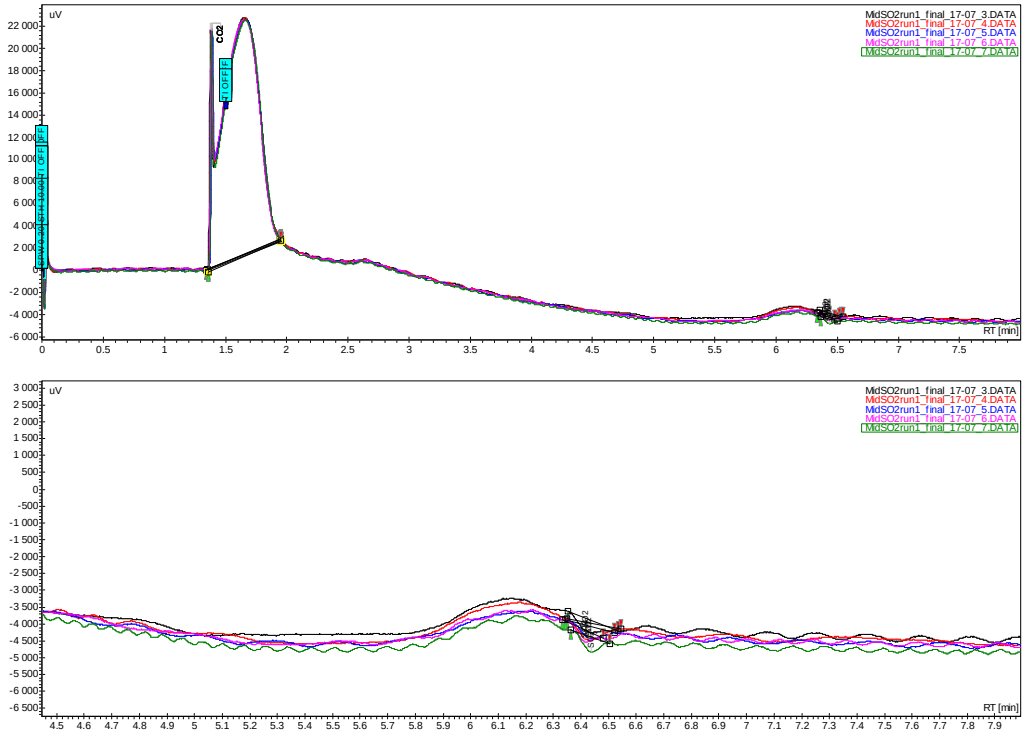


Figure D.44: Chromatograms of five gas sample runs of a CO_2-SO_2 mixture (Low SO_2 - Mixture 2) after sorption. The entire chromatogram (top) and SO_2 peak close-up (bottom) are shown.

Table D.19: Summarised average results table for final concentration of Low SO_2 - Mixture 2

	Name	Time [Min]	Quantity [% Area]	Area [uV.Min]	Area % [%]	Concentration Calculated (mol%)
AVERAGE	CO_2	1.39	99.58	7618.64	99.58	99.775
	SO_2	6.43	0.42	32.44	0.42	0.225
STD DEV	CO_2	0.01	0.13	41.43	0.14	
	SO_2	0.01	0.13	10.52	0.14	

Comparison

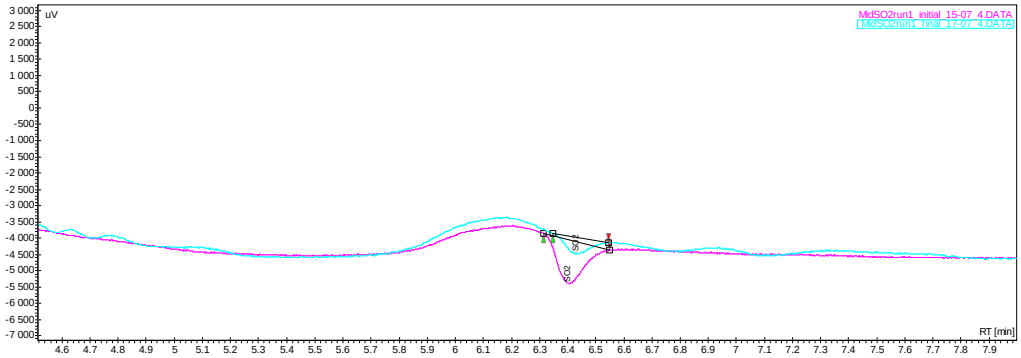


Figure D.45: Comparison of representative SO_2 peaks before and after sorption. Low SO_2 - Mixture 2.

Low SO_2: Mixture 1

Before Sorption

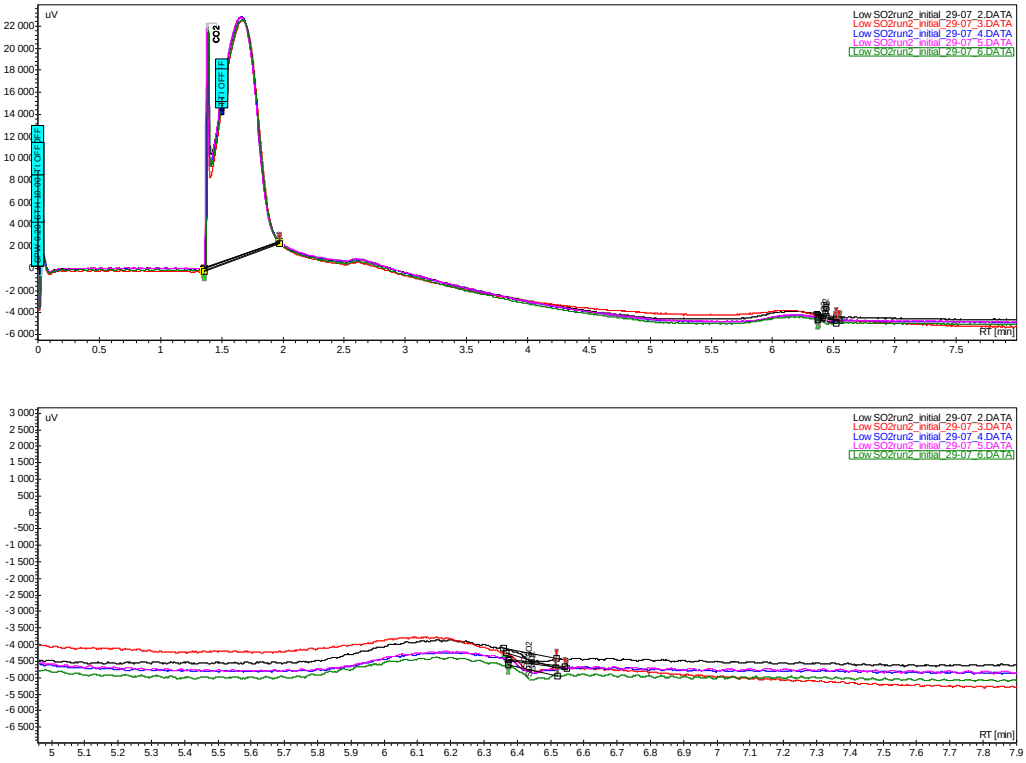


Figure D.46: Chromatograms of four gas sample runs of a CO_2-SO_2 mixture with a low level of SO_2 (Low SO_2 - Mixture 1) before sorption. The entire chromatogram (top) and SO_2 peak close-up (bottom) are shown.

Table D.20: Summarised average results table for initial concentration of Low SO_2 - Mixture 1

	Name	Time [Min]	Quantity [% Area]	Area [uV.Min]	Area % [%]	Concentration Calculated (mol%)
AVERAGE	CO_2	1.38	99.71	7815.42	99.70	99.839
	SO_2	6.44	0.29	23.16	0.30	0.161
STD DEV	CO_2	0.01	0.05	22.23	0.05	
	SO_2	0.01	0.05	3.91	0.05	

After Sorption

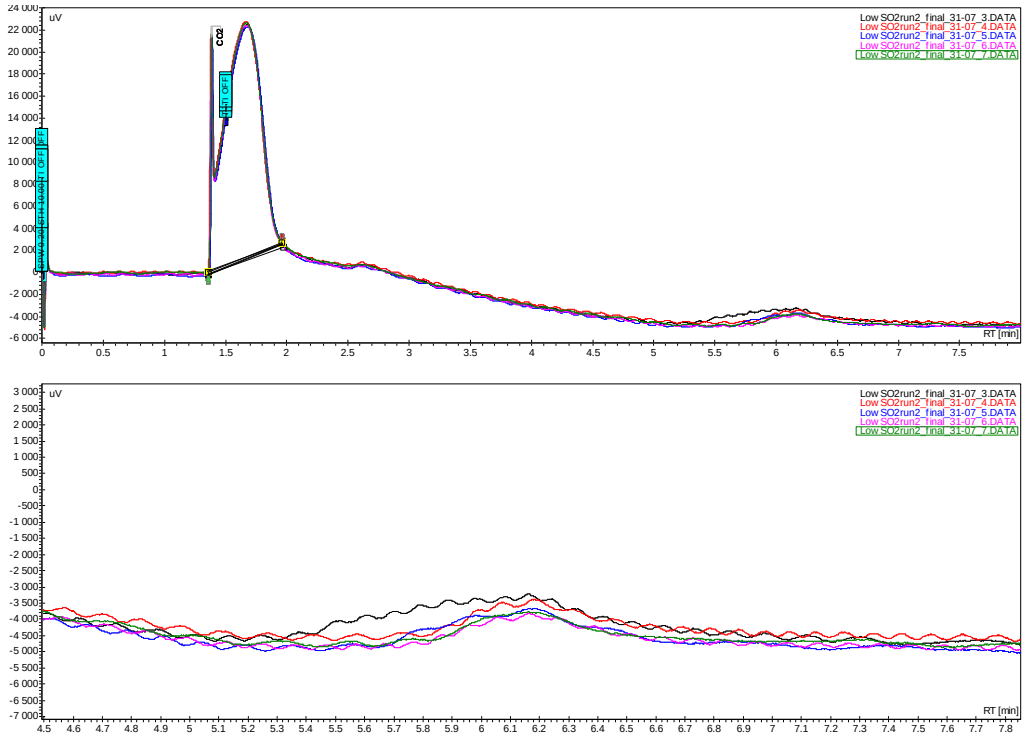


Figure D.47: Chromatograms of five gas sample runs of a CO_2-SO_2 mixture (Low SO_2 - Mixture 1) after sorption. The entire chromatogram (top) and SO_2 peak close-up (bottom) are shown.

Table D.21: Summarised average results table for final concentration of Low SO_2 - Mixture 1

	Name	Time [Min]	Quantity [% Area]	Area [uV.Min]	Area % [%]	Concentration Calculated (mol%)
AVERAGE	CO_2	1.38	100.00	7687.30	100.00	100
	SO_2	-	-	-	-	0
STD DEV	CO_2	0.01	0.00	45.50	0.00	
	SO_2	-	-	-	-	

Comparison

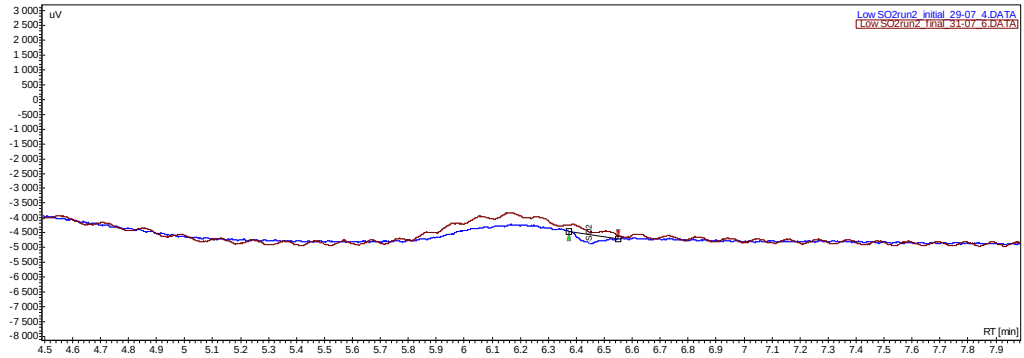


Figure D.48: Comparison of representative SO_2 peaks before and after sorption. Low SO_2 - Mixture 1.

D.5 Adsorption Modelling

In this Appendix, attempts were made to model the experimentally determined excess sorption of CO_2 as a function of the CO_2 concentration in a SO_2-CO_2 mixture using several adsorption theory models. The models considered were the Langmuir, Freundlich and Dubinin-Radushkevich (DR) isotherm models. These isotherms are described below in Table D.22. The equations describing the models were fit to the experimental excess sorption data for CO_2 once the model parameters were known. The model parameters were determined using linear methods; once the linear forms of the models are plotted, the model parameters can be easily calculated from the slope and y-intercept. The linear forms of the isotherms and plotted variables are also presented in Table D.22.

Table D.22: Summary of adsorption isotherm models fit to experimental data (Foo and Hameed (2010))

Isotherm Model	**Non-linear form for N_{sorbed}**	**Linear form**	**Plot**
Langmuir	$\frac{\beta\gamma x}{1+\gamma x}$	$\frac{x}{N_{sorbed}} = \frac{x}{\beta} + \frac{1}{\gamma\beta}$	$\frac{x}{N_{sorbed}}$ vs x
Freundlich	$\delta . x^{1/\zeta}$	$\log(N_{sorbed}) = \frac{1}{\zeta}\log(x) + \log(\delta)$	$\log(N_{sorbed})$ vs $\log(x)$
DR	$\lambda . \exp(-\kappa . e^2)$ Where $e = RTln(1+\frac{1}{x})$	$\ln(N_{sorbed}) = -\kappa . e^2 + \ln(\lambda)$	$\ln(N_{sorbed})$ vs e^2

Symbols: N_{sorbed} and x — Number of moles sorbed, and Mole fraction, respectively
R and T — Universal gas constant, and Absolute temperature, respectively
$\beta, \gamma, \delta, \zeta, \kappa, \lambda$ — Model parameters

Once the variables in the fourth column in Table D.22 were plotted, the MS Excel *trendline* function was used to produce a linear function regressed to the data. Thus, the parameters required for the isotherm models were determined and are presented in Table D.23. The isotherm models are plotted alongside the experimental CO_2 sorption data for comparison in Figure D.49. From Figure D.49 it is evident that the models describe the data poorly.

Table D.23: Sorption isotherm model parameters

Isotherm Model Parameters		
Langmuir	**Freundlich**	**DR**
Linear Form		
y-intercept		
68.45	-0.0494	14.141
Slope		
-66.13	21.916	-4.384E-06
Non-linear form		
β	δ	λ
-0.015	0.892	1.385E+06
γ	ζ	κ
-0.966	0.0456	4.384E-06

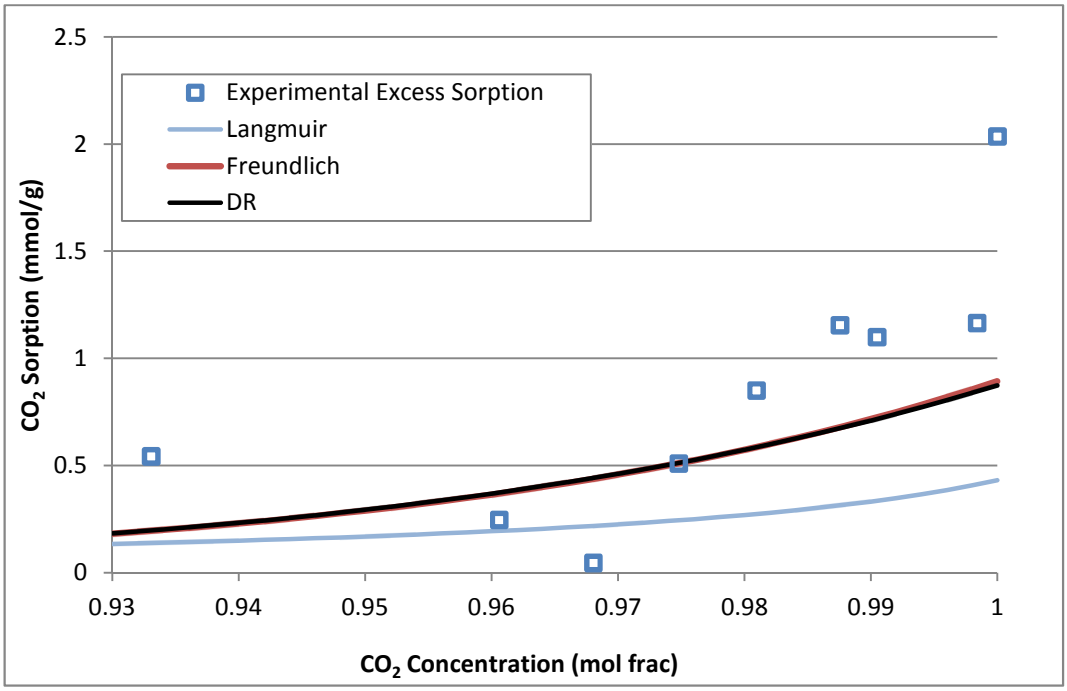


Figure D.49: Comparison of sorption isotherm models fit to CO_2 sorption data

Appendix E: Sample Characterisation

E.1 Sample Volume Calculations

A stereopycnometer run with He is used to determine the volume of the 2 g coal sample used in the sorption experiments. This piece of equipment consists of a sample cell and an expansion cell linked together with a valve as well as a helium source. A schematic diagram of the apparatus is offered in Figure E.1 below.

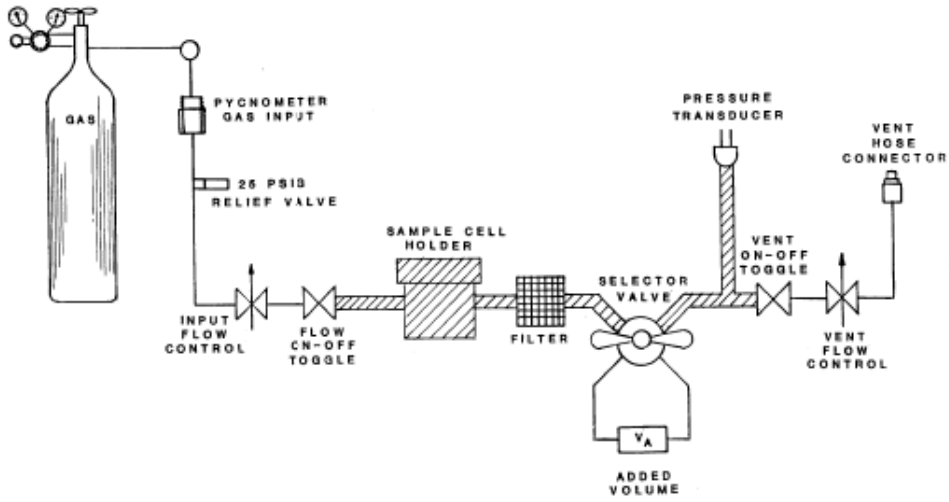


Figure E.1: Schematic diagram of stereopycnometer (Quantachrome Instruments, 2009)

It is necessary to take two pressure readings in order to determine the sample volume. The first pressure reading is when the helium is allowed only to occupy the cell in which the sample is situated, and the second is taken when the helium is allowed to expand to the empty expansion volume. The pressure readings are then inserted where required into Equation E.1 below.

$$v_p = v_c + \frac{v_A}{1 - P_2/P_3} \tag{E.1}$$

The volume of the sample to be calculated is v_p; v_c and v_A are the known volumes of the sample cell and expansion cell respectively; P_2 is the first pressure reading which is taken once only the sample cell has been pressurised; and P_3 is the second pressure reading taken when the helium is expanded to the expansion volume. Equation E.1 is based on the ideal gas assumption and its derivation may be found in Quantachrome Instruments, 2009.

The sample volume can thus be calculated with the results and all readings taken offered in Figure E.2 below. Figure E.2 depicts the working as viewed in a working spreadsheet.

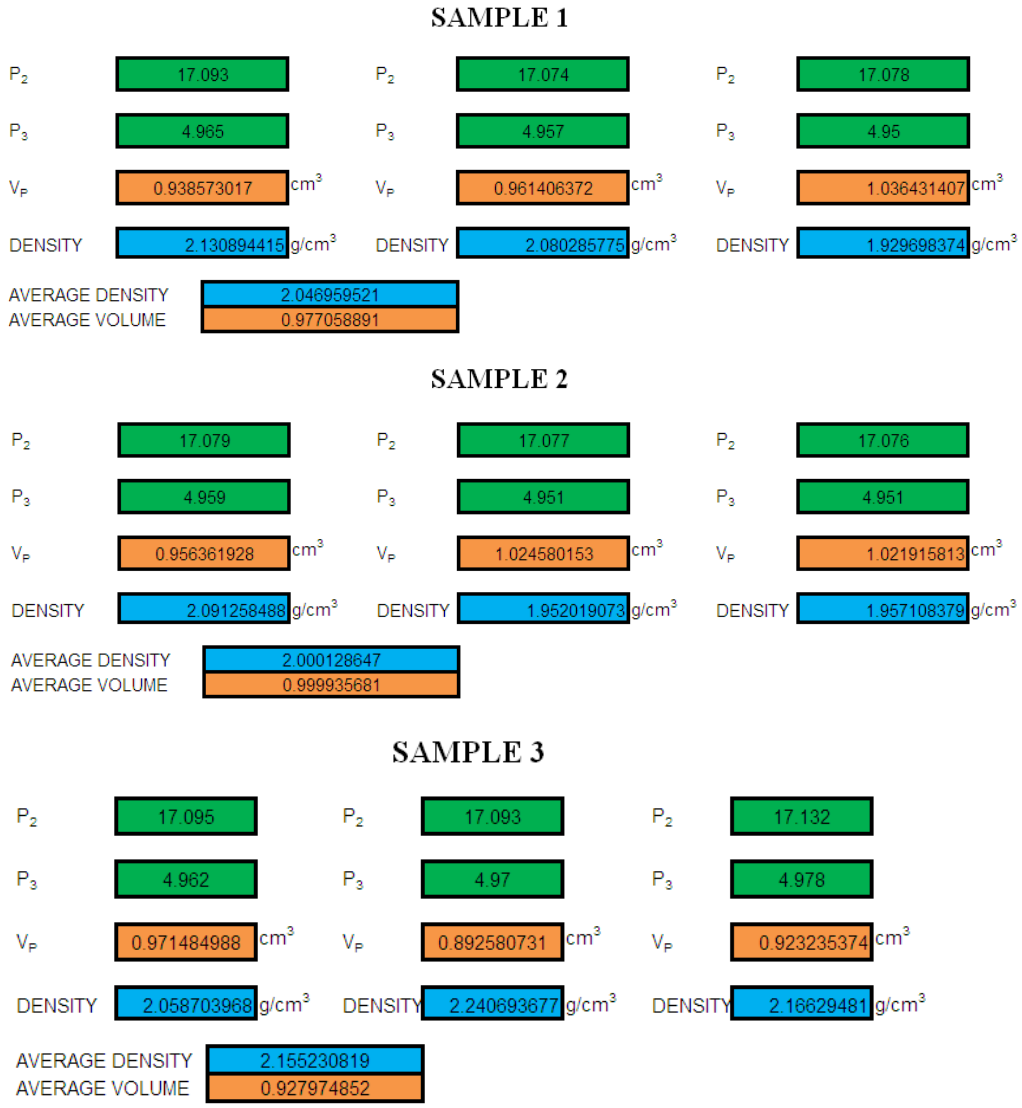


Figure E.2: Complete results and calculations for stereopycnometer sample volume calculations for three identically prepared 2 g coal samples

The average sample volume and density were thus calculated to be 0.968 cm^3 and 2.07 g/cm^3 respectively.

E.2 Petrography Report

Table E.1 below reports the detailed results obtained from the petrographic analysis (Section 3.1.4) performed on the coal samples.

Table E.1: Detailed Petrographic Report

MACERAL ANALYSIS (PERCENT BY VOLUME) & RANK DETERMINATION (%RoVmr)										
CLIENT:	Nicolas Koutsouvelis									
PROJECT:	CO2 adsorption									
DATE:	28-Sep-12									
JOB / SAMPLE NUMBERS:	**Job 1225**									
ANALYST:	Prof NJ Wagner; Coal & Carbon Research Group, School of Chemical & Metallurgical Engineering, University of the Witwatersrand									
ICCP ACCREDITATION:	ICCP/SCAP-056/AB (expires Dec 2012); ICCP/CBAP/056									
THESE RESULTS RELATE ONLY TO THE SAMPLES ANALYSED										
MACERAL ANALYSIS (ISO 7404 PART 3)										
MACERAL GROUP	**MACERAL SUB GROUP**	**SAMPLE NUMBER / ID** sample 1								
		mm inc	**mmf**							
VITRINITE	VITRINITE (collotelinite)	24.8								
	PSEUDOVITRINITE	0.8								
	VITRODETRINITE	7.5								
	CORPOGELINITE	0								
	OTHER VITRINITE	0								
% TOTAL VITRINITE		**33.1**	**0.0**	**0.0**	**0.0**	**0.0**	**0.0**	**0.0**	**0.0**	**0.0**
LIPTINITE	CUTINITE	0.8								
	SPORINITE	4.3								
	RESINITE	0								
	ALGINITE	0								
	LIPTODETRINITE	0								
	OTHER LIPTINITE	0								
% TOTAL LIPTINITE		**5.1**	**0.0**	**0.0**	**0.0**	**0.0**	**0.0**	**0.0**	**0.0**	**0.0**
INERTINITE	R. SEMIFUSINITE	2								
	I. SEMIFUSINITE	9.3								
	FUSINITE	5.3								
	SECRETINITE	0								
	MACRINITE	0								
	MICRINITE	0.5								
	R.INERTODETRINITE	2.3								
	I.INERTODETRINITE	17.3								
	FUNGINITE	0								
% TOTAL INERTINITE		**36.7**	**0.0**	**0.0**	**0.0**	**0.0**	**0.0**	**0.0**	**0.0**	**0.0**
% TOTAL REACTIVE MACERALS		**42.5**	**0.0**	**0.0**	**0.0**	**0.0**	**0.0**	**0.0**	**0.0**	**0.0**
MINERAL MATTER	CLAYS	12.8								
	QUARTZ	10.5								
	PYRITE	0.3								
	CARBONATES	1.5								
	OTHER	0								
% TOTAL MINERAL MATTER		**25.1**	**0.0**	**0.0**	**0.0**	**0.0**	**0.0**	**0.0**	**0.0**	**0.0**
		100								
TABLE 2: RANK DETERMINATION (ISO 7404 - 5, 1994)										
RoVmr% Standard deviation										
Range	**low**									
	high									
RANK CATEGORY	bituminous									
Heat affected	**y / n**	no								
KEY: MACERAL GROUP ANALYSIS Total Reactives = Vitrinite + Liptinite + R.Semifusinite + R. inertodetrinite			**mminc - mineral matter included** **mmf - mineral matter excluded**							

Other vitrinite includes telinite, collodetrinite, gelinite
Other liptinite includes suberinite and exsudatinite

COMMENTS
Typical high ash, inertinite-rich, high volatile bituminous C Witbank coal

E.3 BET Isotherm and Summary Report

Figure E.3 below is the low pressure sorption isotherm produced for BET analysis at facilities at North West University. The data used to produce this plot is manipulated by various different methods to determine the desired values of surface area, pore volume, etc. The values calculated from the BET analysis are depicted by means of a summary report in Table E.3. The conditions under which the BET experiment was performed can be found below in Table E.2.

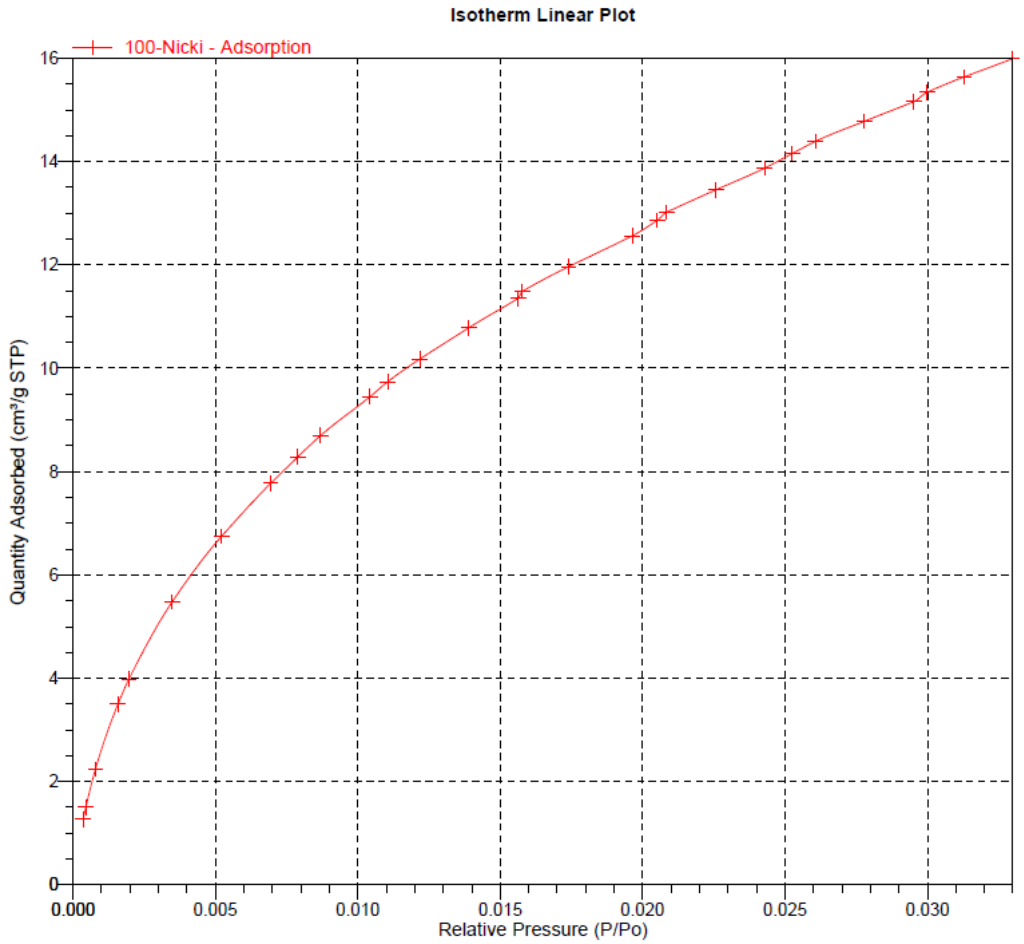


Figure E.3: Low pressure isotherm plot produced for coal parameter calculations

Table E.2: Conditions of BET Experiment

Started:	3/27/2013 11:22:10PM	Analysis Adsorptive:	CO2
Completed:	3/28/2013 7:05:50AM	Analysis Bath Temp.:	0.000 ℃
Report Time:	3/28/2013 7:08:43AM	Thermal Correction:	No
Sample Mass:	0.2080 g	Warm Free Space:	27.0062 cm³ Measured
Cold Free Space:	29.0870 cm³	Equilibration Interval:	30 s
Ambient Temperature:	22.00 ℃	Low Pressure Dose:	3.00 0 cm³/g STP
Automatic Degas:	Yes		

Table E.3: Summary Report of coal parameters calculated by specified numerical methods

Surface Area

Single point surface area at P/Po = 0.032973224:	70.6180 m²/g
BET Surface Area:	81.7103 m²/g
Langmuir Surface Area:	87.3033 m²/g

Horvath-Kawazoe

Maximum pore volume at P/Po = 0.032973224:	0.029264 cm³/g
Median pore width:	0.000 Å

Dubinin-Astakhov

Micropore surface area:	150.908666 m²/g
Limiting micropore volume:	0.063596 cm³/g